A Heuristic Investigation into Methods to Model Medium-term Meso-scale Morphological features in Tidal and Estuarine Environments

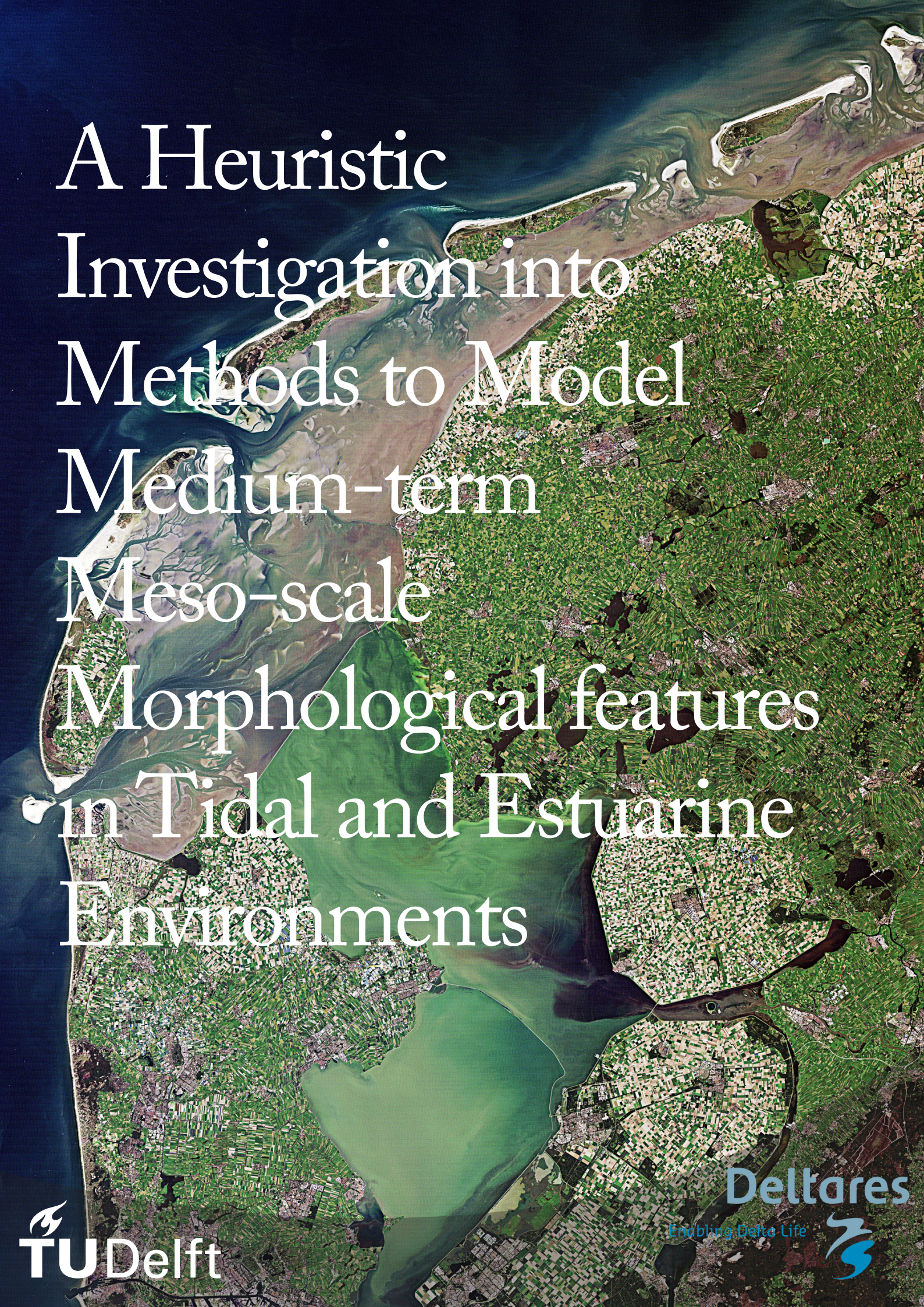

TU Delft

Deltares
Enabling Delta Life

ADDITIONAL THESIS

MEDIUM-TERM MESO-SCALE MORPHODYNAMIC MODELLING IN TIDAL & ESTUARINE ENVIRONMENTS

by

DENZEL VIRGIL HARLEQUIN

Project Duration:	September 14th 2020 - December 21st 2020			
Student Number:	4484207			
Thesis Committee:	Assoc. Prof. dr. ir.	B.C. van Prooijen	TU Delft	chair
	dr. ir.	E.P.L. Elias	Deltares	
	ir.	S.G Pearson	TU Delft & Deltares	

Delft University of Technology
Faculty of Civil Engineering and Geosciences

Medium-Term Meso-scale Morphodynamic Modelling in Tidal & Estuarine Environments

Denzel Virgil Harlequin

December 2020

ACKNOWLEDGMENTS

This additional thesis is proceeded to complement my study towards the degree of Master of Science in Hydraulic Engineering - *specialisation Coastal Engineering* at the Delft University of Technology. This research was conducted at the research institute Deltares, Delft and I have had the owner and utmost privilege to work on this exciting and intricate project in close collaboration with the esteemed colleagues of Deltares.

This study would not have been possible without the support and guidance from my thesis committee. Therefore, I would like to deeply thank the committee members Bram van Prooijen, Edwin Elias, and Stuart Pearson for their guidance during this additional thesis. My sincere gratitude goes to Edwin Elias and Stuart Pearson for giving me the opportunity to work on this wonderful project, the endless motivation, guidance, and witted feedback. Our enlightening discussions, the patience, and support throughout the process and during our weekly meetings has made this period such an exquisite time that went by so fast. My gratitude goes also to my fellow colleagues of Deltares who have given me a warm and open environment that I have been able to call home for the past 4 months - for which my profound gratitude. In particular, I would like to personally thank Victor Chavarrías Borrás, Mick van der Wegen, João Dobrochinski, and Pieter Koen Tonnon for their willingness to contribute to the interviews and the valuable insights that they have given me. Without their effort and time this project would not had reached the latitude that it acquires today. I hope that the reader may find this research insightful, engaging and useful for future (academic) research.

Furthermore, I would like to thank my mother for her endless support, motivation, laughter and care. I will always cherish these moments for old times' sake.

Denzel Virgil Harlequin
Delft, December 2020

ABSTRACT

The overarching aim of this research is to contribute towards a best practice in modelling meso-scale $\mathcal{O}(10km)$, medium-term $\mathcal{O}(5yrs.)$ morphological features in Tidal & Estuarine environments. Therefore, various modelling aspects and stages are reviewed. The first pillar argues the need for numerical models in the Geomorphological Engineering discipline on the basis of a brief overview of the historic advances in numerical modelling. Next, the foundation of a numerical model is considered by means of a concise overview of numerical discretisation techniques and their characteristics. We assess the representation of the typical set of physical processes that one may encounter in present-day morphodynamic models and compare their (mathematical) representation following from their choice of discretisation technique. Hereto, we refrain ourselves to the two commonly used methods - finite element and finite difference method. The second pillar gives an overview of the methods that geomorphologists may employ to reduce the model input, and methods to accelerate morphological computations. The last pillar sheds light on different methods that may be applied by geomorphologists to give more insight into the performance of morphodynamic models. These results can, in turn, be of considerable interest in the pursuit to quantitatively validate model predictions. Lastly, this research is concluded with a set of interviews wherein esteemed *applied morphodynamic* experts were asked about their perception on a possible best practice in modelling skillful meso-scale features in the timeframe of reference. This research hints, therefore, towards an overarching systematic strategy that could be applied by geomorphologists to acquire accurate morphodynamic model predictions on the temporal scale of 5-10 years and for meso-scale features in the order of tens of kilometres.

EXECUTIVE SUMMARY

The place of morphodynamic models in the Coastal Engineering practice has never been as prominent, divers and widely accessible as in the last 3 to 4 decades. Coastal engineers, within the wide range of the geomorphological discipline, apply morphodynamic models to assess the long-term effects of anthropogenic interventions to geomorphological systems in the coastal, estuarine, riverine and/or tidal environment. Meanwhile, starting at the verge of the 21^{st} century, geoscientists apply morphodynamic models not only as a practical engineering tool to evaluate different design options, but also as a research tool to analyse certain (phenomenological) series of events (i.e. breaching of a coastal section, elongation and formation of alluvial deposits in estuaries or deltas, etc.) and their dominant processes. The latter acquires highly detailed morphodynamic models with the ability to compute (i.e. forecast, recast) morphodynamic evolution over a particular timeframe of interest. However, this level of detail comes at the expense of the computational intensity of the model. Therefore, a right balance must be found between computational demand and the level of detail of the physical processes involved. Hence, an assessment of the spatial and temporal scale of the morphological changes may give insight into the required level of detail of the model, the model characteristics and its limitations.

For macro-scale features $\mathcal{O}(100km.)$ and a long-term temporal scale $\mathcal{O}(100yrs.)$, the emphasis is often placed on schematisations of the physical processes (i.e. schematised tide-averaged response of the system) which in turn may be aggregated to efficiently obtain morphological development on the associated time and spatial scale. Formulations describing small-scale $\mathcal{O}(100m)$ hydrodynamic processes provide information on the formation of small-scale features in the long-term setting, however at the expense of the maximum permissible computational demand of the model.

For small-scale features $\mathcal{O}(100m.)$ and a short-term temporal scale $\mathcal{O}(hrs. - dys.)$, the emphasis is placed on small-scale hydrodynamic and morphodynamic processes. The effect of individual wave events on the geomorphological setting and their feedback processes must be captured in great detail. Formulations describing small-scale hydrodynamic processes are therefore required and provide information on the formation of small-scale features in the short-term setting. In light of the shorter timeframe of interest $\mathcal{O}(hrs. - dys.)$, direct computations of the small-scale physical processes allow for highly-detailed computations and is balanced by an acceptable computational time of $\mathcal{O}(1wk)$.

Medium-term $\mathcal{O}(5yrs.)$ Meso-scale $\mathcal{O}(10km.)$ morphodynamic models have the disadvantage that meso-scale behaviour is governed by the interplay between larger scale hydrodynamics and morphodynamics (i.e. shoal formation and migration), and the short-term morphological effects (i.e. onset of small-scale ripples, bar formation and migration). Hence, one is ought to apply a more sophisticated high-resolution morphodynamic model which effectively and efficiently mimics the medium-term changes whilst allowing for small-scale features to interact with the larger morphology (i.e. interaction between migrating shoals and bed ripples). The latter has been observed from previous studies concerning the Ameland Ebb Tidal Delta (ETD) acknowledging that the interaction with small-scale processes is imperative for obtaining a good understanding of the observed morphological behaviour of the ETD. This makes meso-scale medium-term morphodynamic modelling - given its interaction and interdependence with other adjacent temporal and spatial scales - a field of ongoing research.

Given the aforementioned, the aim of this research is to contribute towards a best practice in modelling meso-scale $\mathcal{O}(10km)$, medium-term $\mathcal{O}(5yrs.)$ morphological features in Tidal & Estuarine environments. Therefore, several modelling aspects are discussed throughout 3 proposed pillars. The first pillar argues the need for numerical models in the Geomorphological Engineering discipline on the basis of a brief overview of the historic advances in numerical modelling. Next, the foundation of numerical models is further reviewed. To this end, an assessment is carried out on the implications of

the initial choice of numerical discretisation technique to the final model outcome and their associated characteristics. It is emphasised that irrespective of the choice of numerical discretisation technique, the final numerical results are very much the same. Nonetheless, each of the respective methods have their attractive properties which may be beneficial in later modelling stages, such as the ability to (actively) dampen artificial diffusion (i.e. *finite elements*) and the organised structure in which data is managed in the computational grid (i.e. *finite difference*).

The second pillar outlines the methods that may be employed by geoscientists to reduce the relevant physical processes into (a set of) schematised forcing conditions, and methods to accelerate the morphological computations. The application of input reduction methods is dependent on the geomorphological setting, the temporal & spatial scale over which morphological development is monitored, the relative significance of the observed physical processes, and the possible objective to assess and/or reproduce any observed phenomenological events. Decisions concerning the choice of input reduction methods remain a tailor-made process of recurrent assessments of the geomorphological system at hand. But in general, for medium-term meso-scale morphological features, it is important that the instantaneous interaction between morphodynamics and hydrodynamics is captured appropriately in the model. To do so, the morphodynamic module must be engaged in the flow module. Therefore, it is shown that *online* morphological evolution techniques are best suitable for the aforementioned objective. Moreover, it is seen that the MorMerge approach is an efficient evolution method due to its ability to compute morphology parallelised. The Brute Forcing Merged approach is also reviewed and interpreted as a promising evolution scheme that bears the advantages of the (sequential) online method yet implemented in an efficient *merging* scheme. Consequently, the application of a *Brute Forcing Merge* approach with *seasonal varying wave conditions* and an *astronomical tide decomposition* as schematisation, renders a promising candidate for the model assessment of meso-scale morphological features.

The last pillar provides an overview of the methods that could be employed to quantitatively validate model predictions. It has been shown that the Brier Skill Score (*BSS*) as point-wise metric is prone to the *double penalty effect*. Hereby, the BSS penalises (1) the model predictions for producing morphological features (albeit misplaced), and (2) for the presence of inevitable location errors between the position of the *predicted* and *observed* morphological feature. Model predictions with features (only displaced) are, therefore, under-rewarded compared to the reference prediction of zero morphological change. Inherently, morphologists are, subsequently, encouraged to underestimate morphological variability in order to be rewarded with a larger skill score - which seems odd in the morphologist's intuitive perception of *skill*. Henceforth, it is proposed that Brier Skill Score should be supplemented with a full statistical set of quality parameters describing the overall performance of the model prediction. Incorporation of such quality parameters gives geomorphologists an overview of the model decisions taken to target a certain *skill* or *performance*. Conversely, strong displacement-based error metrics exist that could be applied to assess model performance: (1) the field deformation method and (2) the effective transport difference method. Both methods describe the performance of a model prediction by the amount of work necessary to transform the displacement field into the observational field. Scale-selective accuracy metrics may be considered to quantify the performance of a model on the basis of its ability to produce skillful predictions on each scale within the prediction field.

Lastly, this research is concluded with a set of interviews wherein esteemed *applied morphodynamic* experts were asked about their perception on a possible best practice in modelling skillful meso-scale features in the timeframe of reference. This research hints towards an overarching systematic strategy that could be applied by geomorphologists to acquire accurate model predictions for the scale of 5-10 years.

CONTENTS

Part I

MODELLING TECHNIQUES

1 INTRODUCTION

Worldwide, the coastal environment is in distress by the effects of climate change. Due to relative sea-level rise, the majority of the coastlines are retreating on a fast pace Luijendijk (2019). The appearance of sea level rise in combination with land subsidence due to isostatic changes (i.e. glacial isostasy by offloading of the polar icecap and expansion of the ocean water masses due to increasing temperatures) and local compaction of the Earth's substrate due to anthropogenic activities (i.e. salt, sand, gas mining and ground water extraction) bring extra danger to the coastal systems at large Wong *et al.* (2014).

These coastal systems form the confluence of different functions of which nature, (local) population and economic activities are the largest stakeholders. The presence of large socio-economic development together with an ever-increasing population has enlarged the pressure on coastal systems dramatically. Intensification of and extremities in local rainfall and ocean storms has enhanced these climate-induced pressures on coastal systems making coastlines and deltaic regions prone to flooding. While the climate-induced drivers have limited the extend of coastal systems (i.e. coastline retreat due to SLR), socio-economic drivers are largely expanding and therefore acquiring more space which poses an unprecedented strain on the autonomy of the natural environment Wong *et al.* (2014). Consequently, associated macro-ecological structures (such as salt march environments, coral reefs, wetlands, etc.) and biodiversity may face negative irrevocable effects. The latter circumstances call for hydraulic engineers to find nature-based solutions by means of building with nature principles or soft sandy interventions to answer to societal stakes in such manner that vital ecological structures remain to flourish and flood protection is ensured in the coming decades. In light of the aforementioned, the Dutch Ministry of Infrastructure and Water Management has investigated the flood safety of the Dutch Wadden Sea Barrier Islands in research programmes as the SEAWAD project, Kustgenese 2 but also in National Directives such as the Dutch flood protection programme (Hoogwaterbeschermingsprogramma).

In the Wadden Sea the largest ecological habitat is located which has been designated as UNESCO World Heritage. The Wadden Sea houses one of the largest biodiverse wetland which forms a shelter for many aquatic and terrestrial species that aims to breed and overwinter here Blew *et al.* (2017). A staggering biodiversity of 10 thousand species is found in the flora and fauna of the Wadden Sea of which 2300 different species of phototropic plants - plants which grow in response to light - 2700 marine species and 1300 different macro-fungi are present, making the Wadden Sea the largest pristine household for many ecological inhabitants as the area is remotely influenced by human interference giving nature free reign to grow. The Wadden Sea is imperative for encompassing breeding and migratory birds, marine mammals and many fish species of which some live their whole life within these tidal areas.

It has been found by Elias *et al.* (2019) that the back-barrier basins of the Wadden Sea are drowning since they cannot keep up with the relative sea level rise and the sediment availability within the system runs behind the ever-increasing sediment demand of the basin Van der Spek and Beets (1992). As a consequence to the latter insufficient sediment supply the tidal basin seems to be unequipped to balance with relative sea level rise, coastal anthropogenic interventions may be necessary to guarantee the hydraulic and ecological resilience of the Wadden Sea and its adjacent shorelines. Therefore, further investigations into the behaviour of the Ameland back-barrier basin and the associated ebb-tidal delta is eminent in gaining better understanding in the adaptive capacity of the Wadden Sea basin. The Ameland Basin is the most pristine basin with little dependence to manmade interventions – nature is reigning free - making it the perfect case study for better understanding of morphodynamic behaviour in deltaic regions.

In order to strengthen the flood resilience of the Ameland basin with increasing relative sea level rise and to adequately maintain the adjacent shorelines, the possibilities of ebb-tidal nourishments are investigated. To this end, numerical models are created to gain larger insights in the migration and evolution of ebb-tidal shoals and chute-formations. Long-term macro-scale morphodynamic model (i.e. Unibest,ASMITA,LONGMOR,etc.) has proven to give quite accurate results Huisman (2014). Spurious oscillations have thereby the tendency to dampen out in a fraction of the temporal and spatial scale. For these large scale morphodynamic models, often simplified equations for hydrodynamics and sediment transport are used making them suitable to model large scale evolutions and are less dependent on micro-scale physical behaviour. The shoreline evolution is modelled by means of a one-line or multi-line equation that calculates the coastal retreat or advance based on sediment transport differences over the predefined coastal parcels Huisman (2014). Short-term micro-scale morphodynamic models (i.e. XBeach) provide the same advantage.

Medium-term Meso-scale morphodynamic models (i.e. Delft3D) have the disadvantage that the meso-scale behaviour is governed by the dominance of small-scale short- to medium-term morphological effects (i.e. bed ripples and bars) as well as the dominance of hydrodynamics and sediment transport which take place on a larger temporal and spatial scale Lesser (2009) Luijendijk (2019). Hence, a more-detailed sophisticated hydrodynamic mathematical description as well as high-resolution sediment transport model must be considered to effectively mimic the medium-term changes which occurs as a response to small-scale morphological changes (i.e. migration of bed ripples) and the feedback in hydrodynamics. This makes meso-scale medium-term morphodynamic coastal models an intricate field of research where lots of development has been made over the past years Syvitski *et al.* (2010) van der Wegen (2010) Duong *et al.* (2014) and more research is yet to be carried out to improve the model efficiency and accuracy in complex dynamic regions such as tidal inlets.

1.1 Research Question and Objectives

This thesis aims to build a further understanding in the modelling capabilities of meso-scale (tens of km's) medium-term (order of years) morphodynamic models in tidal inlets and estuarine regions whereby the skill and the accuracy of the model is considered. The overarching thesis objective builds upon 4 interrelated pillars, here below defined as the research objectives. These pillars aim to answer the following research questions:

Research Question

- *What is the best modelling strategy to capture the behaviour of an ebb-tidal delta on a medium-term temporal scale (i.e. 5 years) for meso-scale morphological adjustments?*

Sub-Research Questions

1. *Which physical processes are accounted for in the morphodynamic model and how are they to be mathematically described?*
   (a) *How are the physical processes described in morphodynamic models and are there indications for further improvement?*
   (b) *What is (are) the practical implication(s) associated with the choice of model discretisation technique?*
2. Which modelling methodologies exist to accelerate the computations of morphological development in an efficient and accurate manner?
   (a) *How are waves and currents incorporated in the model?*

(b) *Which upscaling methods exist for upscaling wave conditions?*

(c) *Which morphological acceleration methods exist for upscaling bed level changes?*

(d) *And which combination poses as best candidate for modelling meso-scale medium-term morphological adjustments?*

3. How well is the model capable of producing valuable and accurate results?

(a) *What is the skill of the model and which metrics are available to quantitatively discern between various models?*

(b) *Which spatial and temporal step size would provide stable solutions?*

(c) *What is the stability requirement for the numerical model?*

(d) *How long will it take for spurious oscillations to attenuate in the numerical simulation?*

1.2 Historical Advances in Numerical Modelling

The place of morphological models in the current engineering practice has never been as eminent as now for hydraulic modellers which are concerned with estuarine, coastal and riverine environments Lesser *et al.* (2004). For a long time civil engineers were very interested in the long term effects of human interventions to the morphological development of (large scale) coastal features (i.e. beach positioning, coastline profiles, bar formations, erosion and deposition profiles, etc) Wang *et al.* (2020). Before the arrival of such abstract models (i.e. models derived on the basis of theory, mathematical descriptions and relations/without the need of any material replica), civil engineers used physical models - a scaled replica of the *in-situ* situation - to analyse complex hydraulic flows (i.e. flows in river bends, bifurcations, etc.) or the operations of hydraulic structures. *Froude and Reech* were one of the first in the 19^{th} century that performed research on ship flows and currents by means of scale models (i.e. a particular type of physical models) Froude (1861). The first systematic execution of scale model tests proceeded in the late 19^{th} century with the scientific research on fluid mechanics by scholars of the University of Cambridge [Thijse (1948)] such as Reynolds (1887), Gibson and Allen (1963).

In the Netherlands, the first application of scale models started in confluence with mathematical models during the prelude of the 20^{th} century. After the Zuiderzee flood disaster of 1916, there was a general need for an overarching approach to prevent any flooding of such proportion ever again which resulted in the closure project of the Zuiderzee, led by Lorentz as chair of the ***State Commission Zuiderzee*** or ***Committee Lorentz*** in 1918. Therewith, Lorentz established a mathematical model based on the harmonic method to investigate the tidal wave propagation in the *prior* Zuiderzee by partitioning the basin in a network of 1D channels Lorentz *et al.* (1926). In the period leading up to 1960 Dronkers extended the harmonic theory of Lorentz *et al.* (1926) for the case of tidal rivers (Dronkers (1964)) and shallow waters (Dronkers *et al.* (1958)).

These studies by Dronkers and Lorentz were later supplemented with the analogue model of van Veen (1947) wherein the onset of tidal waves was mimicked by electrical currents. His work gave rise to the implementation of the telegraph equations for tidal wave propagation (van Veen (1947)) - a set of *coupled* partial differential equations is transformed into a set of *decoupled* ordinary differential equations (i.e. linearised shallow water equations) - and the construction of the first tidal forecasting computer in 1954 that was able to predict tidal wave propagation. The technique of van Veen is later used in the ***Dutch Delta Committee*** (1964 - 1982) where his tidal forecasts were eminent in the decision-making of the closure of the Southern Dutch Delta after the flood disaster of 1953 (Aten *et al.* (2001)).

Until 1950 all derived models were handled manually so with the arrival of the first computers after 1950 the application of computers accelerated the development and use of computational models in the civil engineering discipline. While the computational power of the computers had increased rapidly over the years following, in 1960 the latter gave rise to the first practical two-dimensional depth

averaged (2DH) shallow water flow model (De Goede (2020)). These flow models were equipped with an ***A**lternative **D**irection **I**mplicit* time integration method following the work of Leendertse (1967). Hereby, the discretised derivatives of the continuity and momentum conservation equations are integrated in two directions alternately. Often, these models were based on a Cartesian coordinate system that considered a rectilinear grid in both the horizontal and vertical plane. In order to simplify the grid composition for complex geometries, the development of more flexible grids was set about (i.e. curvi-linear grid, boundary fitting methods, unstructured grid, etc.) (Labeur (2009)). This derived computational model found by Leendertse (1967) had been composed in a computational code, called **WAQUA**,that was used in the Dutch Delta Closure projects (De Goede (2020)).
By the 90's the River Engineering discipline made use of two-dimensional depth averaged (2DH) shallow water flow models which were complemented with sophisticated (Quasi) 3D extensions to account for spiral flows in bends (Lesser *et al.* (2004)). Such 2DH shallow water flow models were later used in the Coastal Engineering discipline to model the flow and transport of waterborne constituents and sediment under the influence of waves (Nicholson *et al.* (1997)). The increasing complexity of these models - that made use of various (Quasi) 3D extensions in order to capture the three-dimensional (3D) non-linear hydrodynamic processes (i.e. wave asymmetry, bed-slope related transport mechanisms, return flow, wave-induced bed shear stress, etc.) - created a system that was highly sensitive to small perturbations (de Vriend *et al.* (1993)). Quite contradictory, the added complexity/detailed description of processes decreased the coherence of the model due to the presence of inherent model instability and thereby allowed for the onset of irregular patterns in the numerically obtained results compared with the sole 2DH depth-averaged shallow water flow models (de Vriend *et al.* (1993)).
Later advances of Péchon and Teisson (1996) which presented a morphological model based on three-dimensional (3D) flow descriptions also produced less adequate results (Lesser *et al.* (2004)). The model enabled the coupling of the near-bed velocity with the local sediment transport but has partially fell short due the assumption of local equilibrium transport (Lesser *et al.* (2004)).
The state-of-the-art morphological model arrived in 1999 by the work of Gessler *et al.* (1999) wherein the three-dimensional (3D) mobility of the bed was assessed. This three-dimensional (3D) model, also known as *CH3D-SED*, was fully capable to perform three-dimensional (3D) predictions of scour and deposition as a consequence to secondary flows (i.e. spiral flow, Bulle Effect in river diversions, etc.) in open channel flows such as rivers. The model was equipped with separate modules to account for the mix-grain-size bedload transport and suspended sediment transport in all directions with an intermediate bed level update scheme that solved the sediment transport for each individual sediment fraction in the flow considered (Lesser *et al.* (2004)). This - and alike - sophisticated three-dimensional (3D) models were well-equipped for complex 3D river morphological problems, however the application of the latter models in coastal and estuarine regions was rather limited - also due to the previously reviewed added complexity of the flow and transport of sediment in these regions together with the inherent stability challenge in such process models (de Vriend *et al.* (1993) & Gessler *et al.* (1999)).
Two-dimensional depth averaged (2DH) morphological models (based on the shallow water equations) became the standard practice in the Coastal Engineering discipline around the 2000's and were often used to predict the morphological changes for medium to large scale coastal features (i.e. bar and shoal formations in estuarine regions, channel formations, etc.) on different temporal scales. In the wake of the 20^{th} century and the beginning of the 21^{st} century the urge prevailed within the Coastal Engineering discipline to have a fully comprehensive three-dimensional (3D) model that was able to assess (different combinations of) non-linear hydrodynamic processes in order to obtain high-resolution morphological (bed level) changes (de Vriend *et al.* (1993), Lesser *et al.* (2004) & De Goede (2020)). This gave rise to the ongoing development of various two-/three-dimensional (3D) *process-based* models such as (1) Delft3D of which the development started in 1985 by Deltares (former Delft Hydraulics), (2) several two-dimensional (2D) flow schemes (i.e. WAQUA, SIMONA) and (3) three-dimensional (3D) flow schemes (i.e TRIWAQ and SIMONA) giving a total of 5 largely coherent models by 2011 in the Netherlands (De Goede (2020)). Starting from 2015, Deltares has set the goal to merge these models into one coherent *unstructured grid* model, called ***Delft3D Flexible Mesh***, that is able to perform calculations on 1D (i.e. line models), 2D (i.e. 2DH depth-averaged, 2DV averaged in a vertical plane) or 3D (i.e. flow structures).

Alongside these ***finite difference*** models, a parallel stream has been apparent of two-/three-dimensional (3D) ***finite element*** process-based models such as FINEL2D/-3D which provided an added flexibility to the generation process of complex computational grids for complex geometries (De Goede (2020)).

1.3 The choice of Numerical Discretisations

This section is adopted on the work of Logan (2017), Grossmann et al. *(2007) and Labeur (2009).*

The hereinabove outlined three-dimensional (3D) models describe the flow and transport of constituents (i.e. sediment, biological compounds) as well as the transport of dissolved and suspended waterborne substances in arbitrary basins & channels (i.e. estuary, lake, river, etc.). In order to numerically model the transport and flow of these constituents, the Navier Stokes equation - and associated transport equations - must be therewith discretised to a set of algebraic equations able to be processed by a computer (i.e. a set of recurrence relations in a computer *algorithm*). This discrete set of variables is subsequently updated in time to account for the evolution of the considered constituents over time. Therefore, various discretisation methods prevail of which the most encountered are reviewed in this section. It should be noted that the choice of discretisation solely constitutes different systems of mathematical equations that all solve for the same overarching Navier-Stokes Equations. Hence, it is emphasised that irrespective of the choice of discretisation method the final numerical results should be very much the same.

Finite Difference Method

The finite difference method is predominantly suitable for boundary value problems (Grossmann *et al.* (2007)). Finite difference schemes discretise the computational domain in a set of discrete *grid points*. The flow and transport equations are therewith approximated by a *grid function* - a function defined at these discrete points solely. All derivatives are approximated by means of finite differences in the respective *grid points* applying discrete gradients between the adjacent *grid points*. The variables describing the flow are defined at the respective grid points $\mathbf{x}^i$ in the flow field by a discrete value $\mathbf{f}^i$ (Labeur (2009)).

Examples of models which are derived on the basis of finite difference schemes are WAQUA, TRIWAQ, Delft3D-*Structured grid* (also known as Delft3D-4) (de Vriend *et al.* (1993) & De Goede (2020)).

Advantages of Finite Difference Methods

The advantages proposed by Grossmann *et al.* (2007) and Labeur (2009) of models using finite difference are:

- The presence of relatively simple stencils that can be applied for the discretisation (Grossmann *et al.* (2007)).
- The associated *structured grid* has the advantage that structured ordering of data is evident (i.e. data is allocated as such that the set of *ordered* data is always maintained in each grid cell) (Labeur (2009)).
- The ordered data maintenance property in grid cells is highly useful for maintaining large sets of data (i.e. large computational domain and/or an abundance of computational nodes)
- Finite difference methods are suitable for large systems

Finite Volume Method

The finite volume method partitions the computational domain in *discrete volume parcels*, referred to as ***control volumes***. These *control volumes* describe the state of the flow in each *discretised* region (Labeur (2009)). The governing equations describing the flow and transport are found by conservation of mass

and momentum that is integrated over the respective *local control volumes*. The boundary fluxes between the respective *control volumes* are coupled (i.e. the fluxes between the *control volumes* dictate the rate of change of the state of the flow within each respective *control volume*). Hence, ones included in the discretisation of the computational grid, the local conservation of mass and momentum between the *discrete volume parcels* is met such that *global* mass and momentum is *strictly conserved* (Grossmann *et al.* (2007)).

Finite Element Method

In the finite element method the computational grid is partitioned in *discrete parcels* called *elements* (Logan (2017)). The governing equations for the flow and transport which are defined over the entire computational domain are discretised in sets of algebraic equations - also referred to as *basis functions* - by means of *weak formulations* of the smoothness assumption (Labeur (2009)). These *basis functions* describe the flow state (i.e. the value of each flow variable) at each respective element in the computational domain. Different types of *elements* are available to partition the computational domain. Therefore, it is said that these *elements* are arbitrary in size and shape which ease the generation of complex geometric grids (Labeur (2009)) - although some scientific debate prevails on the presumed added flexibility of *finite element methods* *Elias [in personal communique September 23rd]* (2020).

Examples of models which are derived on the basis of finite element schemes are Swasêk Finel2D/3D (Dam *et al.* (2016) & (Talstra et al. (2016)) and Delft3D-*Unstructured grid* (also known as Delft3D Flexible Mesh) (De Goede (2020)).

Advantages of Finite Element Methods

The (dis)advantages proposed by Grossmann *et al.* (2007) and Labeur (2009) of models using finite element methods are:

- Only strictly conservative schemes must be applied for the discretisation of the governing equations to make sure that the global energy, momentum, and mass is conserved on a local level (i.e. between the defined *elements*) as well as on global level (i.e. over the boundaries of the entire computational domain) (Grossmann *et al.* (2007)).
- The unstructured mesh gives (ample) flexibility to define the computational grid for complex topographies (Labeur (2009)).
- Computations on the basis of finite element method tends to be computationally intensive.
- It is claimed by Labeur (2009) that finite element schemes proof to be suitable for quick assessment of various design options, given the flexibility of the grid generation.

2 THREE-DIMENSIONAL (3D) MORPHOLOGICAL MODELS

An investigation is proceeded in the numerical modelling capabilities of present *state-of-the-art* morphological models for the application in mid-term meso-scale morphological assessments. The later domain of interest is characterised by the inherit challenge to obey the relatively small-scale morphodynamic processes (i.e. bed ripples, bar formation & migration, secondary flow patterns) while providing solutions for a much larger spatial scale (i.e. shoal formations, channel formations in estuaries, tidal flats, etc.). An extra level of complexity arises when the inherent instability - provided by the diffusive character of the solution - is considered of the set of differential equations describing the flow and transport of flow constituents (i.e. sediment). Hereby small perturbations at the undisturbed bed give rise to significant production of numerical diffusion (de Vriend *et al.* (1993)). In combination with the non-linear character of the hydrodynamic processes (i.e. wave asymmetry, short wave propagation), these numerical instabilities may grow exponentially (de Vriend *et al.* (1993)). In order to find an overarching approach of dealing with this practical and theoretical limitations, a brief elaboration is presented of two different models which are used quite frequently in the Netherlands - Delft3D and Finel3D. The findings of the latter research will later be used to update the current *state-of-the-art* Delft3D morphological models by investigating the function and application of these models.

2.1 Finite Difference Method - Delft3D-4 (Structured Grid)

This section is adopted on the work of de Vriend *et al.* (1993) Lesser *et al.* (2004), Roelvink (2006), & Deltares (2020)

In the urge to find a fully three-dimensional (3D) model that was able to assess (different combinations of) non-linear hydrodynamic processes in order to obtain high-resolution morphological (bed level) changes, Delft3D was created around 1980 and later updated by Lesser *et al.* (2004) & Roelvink (2006) to account for *online* calculations of the transport of sediment and other waterborne constituents. This modelling system aims to solve for the unsteady shallow water wave equations in the depth-averaged (2D) situation as well as the three-dimensional (3D) case by means of different modules that together capture the total hydrodynamic flow behaviour alongside the transport of various constituents. The *online* modelling approach in Delft3D-FLOW enables the module to incorporate, amongst other:

- Transport of constituents
- Short Wave Generation and Propagation
- Sediment Transport (Bedload Transport and Suspended Sediment Transport)
- Morphological Changes/ Bed Level Changes
- Water Quality Parameters

FLOW MODULE

Coordinate System

Delft3D may be used to assess flows in shallow waters (i.e. coastal, estuarine & riverine areas, lagoons, lakes, etc.). In all of these cases, the domain of interest is partitioned in smaller *grid cells* for which the discretised governing equations are evaluated for each *grid cell*. This discretisation may occur along a set of axes defined in an arbitrary coordinate system. In Delft3D-4, the user may choose for the following coordinate systems:

- (x, y, z) - Cartesian Coordinate Grid (*Rectangular Grid*)
- Orthogonal Curvilinear Grid (*Boundary Fitting Grid*)
- Spherical Coordinate Grid

The vertical (z-)coordinate is represented by a set of vertical σ-planes that portions the water column in equidistant layers or layers with an arbitrary thickness. σ is here defined as,

$$\sigma = \frac{z - \zeta}{h} \tag{1}$$

Generalised Lagrangian Mean Reference Frame

In the shallow water equations used to describe the flow and transport of fluid parcels, the Eulerian velocity components (u, v, w) are used in simulations wherein solely currents are considered. However, in the case of waves, the Eulerian frame of reference does not provide an accurate description of the three-dimensional (3D) velocity components. Therefore, a Lagrangian frame of reference is applied wherein the wave-related currents & mass transport averaged over the wave cycle (i.e. Stokes' Drift, bottom streaming) are better described. To this end, the following velocity relation is considered in the Delft3D FLOW Module,

$$U = u_{euler} + u_s \tag{2}$$

Governing Equations

Delft3D-FLOW uses a hydrostatic solver for the numerical computations of the hydrodynamic flow (Lesser *et al.* (2004)). It should be noted that a separate (non-hydrostatic) solver exists that may update the hydrostatic results with non-hydrostatic corrections if the deviation between the two computations becomes large.

The system of equations used in the FLOW-Module is composed of:

- ***Horizontal Momentum Equations (u,v)***

$$\frac{\partial U}{\partial t} + U\frac{\partial U}{\partial x} + V\frac{\partial U}{\partial y} + \frac{\omega}{h}\frac{\partial U}{\partial \sigma} - fV = -\frac{1}{\rho_0}P_x + \nu_H\left\{\frac{\partial^2 U}{\partial x^2} + \frac{\partial^2 U}{\partial y^2}\right\} + \frac{1}{h^2}\frac{\partial}{\partial \sigma}\left\{\nu_V\frac{\partial u}{\partial \sigma}\right\} + \frac{F_x}{\rho} \tag{3}$$

$$\frac{\partial V}{\partial t} + V\frac{\partial U}{\partial x} + V\frac{\partial V}{\partial y} + \frac{\omega}{h}\frac{\partial V}{\partial \sigma} + fU = -\frac{1}{\rho_0}P_y + \nu_H\left\{\frac{\partial^2 V}{\partial x^2} + \frac{\partial^2 V}{\partial y^2}\right\} + \frac{1}{h^2}\frac{\partial}{\partial \sigma}\left\{\nu_V\frac{\partial v}{\partial \sigma}\right\} + \frac{F_y}{\rho} \tag{4}$$

- ***Vertical Momentum Equation***
  note that a hydrostatic pressure distribution is assumed.

$$\frac{\partial P}{\partial \sigma} = -\rho g h \tag{5}$$

- ***Continuity Equation***
  The Boussinesq Approximation is considered such that the incompressibility criterion holds.

$$\frac{\partial \zeta}{\partial t} + \frac{\partial h\overline{U}}{\partial x} + \frac{\partial h\overline{V}}{\partial y} = S \tag{6}$$

wherein S represents the added discharge or withdrawal of water.

- ***Transport Equation for waterborne substances***

$$\frac{\partial hc}{\partial t} + \frac{\partial U(hc)}{\partial x} + \frac{\partial V(hc)}{\partial y} + \frac{\partial(\omega c)}{\partial \sigma} = h\left\{\frac{\partial}{x}\left(D_H \frac{\partial c}{\partial x}\right) + \frac{\partial}{\partial y}\left(D_H \frac{\partial c}{\partial y}\right)\right\} + \frac{1}{h}\frac{\partial}{\partial \sigma}\left\{D_V \frac{\partial c}{\partial \sigma}\right\} + hS \tag{7}$$

wherein S represents the sources and sinks of a waterborne constituent in the computational domain.
The vertical eddy ***diffusivity*** D_V is here proportional to the vertical eddy ***viscosity***, which follows from equation(8),

$$D_V = \frac{\nu_V}{\sigma_c} \tag{8}$$

wherein σ_c is related to the stability of the stratification of the flow (i.e. Richardson Number) and defined as,

$$\sigma_c = \sigma_{c0} * F_\sigma(R_i) \tag{9}$$

- ***An Appropriate Turbulence Closure Model***
  to relate the smaller scale turbulent motion with the turbulent motion at the scale of the mean flow by application of the Boussinesq hypothesis (i.e. $\kappa - \varepsilon$ model).

Lesser *et al.* (2004) proposed two turbulence models in which the eddy viscosity has the following shape:

$$\nu_v = c_\mu{}' L\sqrt{\kappa} \tag{10}$$

wherein L is the Prandtl' Mixing Length and κ the turbulent kinetic energy.

1. ***Algebraic Turbulence Model***
   In the algebraic turbulence model, algebraic formulae are used to determine the turbulent kinetic energy κ, the mixing length L and the vertical eddy viscosity ν_V.

2. $\kappa - \varepsilon$ ***Turbulence Model***
   When a $(\kappa - \varepsilon)$-turbulence model is considered, turbulence induced vertical transport of kinetic energy is determined by taking into account the rate of change of the kinetic energy κ in relation to the rate of dissipation of kinetic energy ε over the vertical layers. Hereby, the following conservation balances are applied:

$$\frac{\partial \rho\kappa}{\partial t} + \nabla\left(\rho\kappa\vec{\mathbf{u}}\right) = \nabla_i\left(\frac{\nu_V}{\sigma}\nabla_i(\kappa)\right) + \left(P_\kappa - D_\kappa\right) \tag{11}$$

$$\frac{\partial \rho\varepsilon}{\partial t} + \nabla\left(\rho\varepsilon\vec{\mathbf{u}}\right) = \nabla_i\left(\frac{\nu_V}{\sigma}\nabla_i(\varepsilon)\right) + \left(P_\varepsilon - D_\varepsilon\right) \tag{12}$$

Wherein P_κ and P_ε represent the production of kinetic energy and production of dissipation (i.e. increasing rate of dissipation) respectively. D_κ and D_ε describe the dissipation of kinetic energy and decay of dissipation of kinetic energy (i.e. decreasing rate of dissipation) conversely.
The mixing length is here found by application of the varying value of the turbulent kinetic energy κ and the dissipation of kinetic energy ε, which is described as follows:

$$L = C_D\frac{\kappa\sqrt{\kappa}}{\varepsilon} \tag{13}$$

Wherein C_D is a calibration parameter that may be adjusted by the user.

Delft3D Solution Procedure

Alternating Direction Implicit Method

The user-specified grid (i.e. rectangular, boundary fitted or spherical) discretises the computational domain in grid cells of arbitrary size. In the latter obtained computational grid, the flow variables are allocated in a staggered grid - the Arrakawa C Grid approach. Here, the water level and bedload transport are defined in a point at the centre of each grid cell, whereas the velocity point is found at the centre of the boundaries forming the periphery of the grid cells. Hereby, the *Alternating Direction Implicit Method* (ADI) method according to Leendertse (1967) is adopted to solve the set of discretised governing equations in each grid cell. The *Alternating Direction Implicit Method* is characteristic for integrating the governing equations in two directions alternately to accommodate the coupled character of the velocity and water level point. Consequently, a relatively simple numerical stencil may be acquired to solve the system of equations. The bedload transport is, in this method, calculated in the water level points and *upshifted* to the adjacent grid cell boundary in the integration direction (i.e. the velocity point) where the volume of the grid cell is controlled.

Cyclic Method

An extended case of the Alternating Direction Implicit method is the method described in the work of Leendertse (1967) which is the *cyclic method*. In the *Cyclic method* the horizontal advection terms - which were discretised by a 3^{rd} order accurate upwind finite difference scheme - were split into (1) a 1^{st} order accurate upwind scheme and (2) a 2^{nd} order accurate central difference scheme. Consequently, these split advection schemes are to be assessed in both directions within the integration process on each time level. The advantage of such a partition is that the FLOW scheme becomes less computationally intensive, yet however at the expense of the 3^{rd} order accuracy which is replace by 2^{nd} order accurate solutions. Thereby, the stability of the scheme may be maintained for courant numbers up to 10. It should be noted that the transport equation for bedload, dissolved & suspended sediment is solved by means of the *cyclic method*. In order to maintain the monotonicity of the solution, a flux limiting function - known as the *Forrester Filter* - is hereby applied to attenuate any negative concentration in the flow and to ensure conservation of mass.

WAVE MODULE

Delft3D has a separate solver that accounts for wave-induced forces and currents. In this respect the following processes are included:

1. **Wave forcing due to wave breaking**
   The dissipation of kinetic energy due to wave breaking is decomposed in:
   - a wave-related shear stress component at the bed
   - a wave-related shear stress component at the surface due to the presence of a turbulent surface roller
2. **Enhanced bed shear stresses due to wave-current interaction**
3. **Wave-induced mass transport due to residual motion (i.e. Stokes' Drift)**
4. **Streaming**
   Wave-induced currents - **Streaming** - in the wave boundary layer.
5. **Additional Dissipation**
   The $(\kappa - \varepsilon)$-turbulence model as described in eqs.(11) and (12) is updated with source and sink terms accounting for the added dissipation of turbulent kinetic energy due to wave-related bed shear stress and wave-related surface shear due to White-Capping and Depth-Induced Breaking.

Wave forcing due to wave breaking

The wave-induced forcing due to wave breaking is schematised as a shear stress at the water surface using *Radiation Stress gradients*. These gradients are incorporated in the model and written in the following form:

$$\vec{\mathbf{M}} = \frac{D}{\omega}\vec{\mathbf{k}} \tag{14}$$

wherein:

- $\vec{\mathbf{M}}$: represents the wave-induced forcing due to wave-breaking and is a function of the radiation stress gradients (in N/m^2).
- D: represents the dissipation of kinetic energy at the free surface (in W/m^2).
- ω: represents the angular wave frequency (in rad/s)
- $\vec{\mathbf{k}}$: represents the wave number (in rad/m)

The wave-related driving force, due to an asymmetry in the orbital velocity under the crest and trough of the wave respectively, may be obtained from a velocity decomposition for the horizontal momentum equations (eqs. (3) & (4)) in the (**GLM**) *Generalised Lagrangian Mean Frame of Reference*. It should be noted that the velocity gradients accounting for the viscous forcing are replaced by Reynolds averaged shear stresses while upholding the *Boussinesq approximation*.

$$\frac{\partial \overline{u}^L}{\partial t} + \overline{u}^L\frac{\partial \overline{u}^L}{\partial x} + \overline{v}^L\frac{\partial \overline{u}^L}{\partial y} + \overline{w}^L\frac{\partial \overline{u}^L}{\partial z} + g\frac{\partial \overline{\zeta}^L}{\partial x} - f\overline{v}^L - \frac{1}{\rho_0}\left\{\frac{\partial \overline{\tau_{xx}}^L}{\partial x} + \frac{\partial \overline{\tau_{xy}}^L}{\partial y} + \frac{\partial \overline{\tau_{xz}}^L}{\partial z}\right\} = \frac{F_x}{\rho_0} \tag{15}$$

$$\frac{\partial \overline{v}^L}{\partial t} + \overline{u}^L\frac{\partial \overline{v}^L}{\partial x} + \overline{v}^L\frac{\partial \overline{v}^L}{\partial y} + \overline{w}^L\frac{\partial \overline{v}^L}{\partial z} + g\frac{\partial \overline{\zeta}^L}{\partial y} + f\overline{u}^L - \frac{1}{\rho_0}\left\{\frac{\partial \overline{\tau_{yx}}^L}{\partial x} + \frac{\partial \overline{\tau_{yy}}^L}{\partial y} + \frac{\partial \overline{\tau_{yz}}^L}{\partial z}\right\} = \frac{F_y}{\rho_0} \tag{16}$$

By application of the work of Groeneweg (1999), the *wave-induced driving forces* - as function of the Radian Stresses - in the x-direction F_x and y-direction F_y respectively may be defined as,

$$\frac{F_x}{\rho_0} = -\frac{1}{\rho_0}\left\{\frac{\partial \overline{\tau_{xx}}^s}{\partial x} + \frac{\partial \overline{\tau_{xy}}^s}{\partial y} + \frac{\overline{\tau_{xz}}^s}{\partial z}\right\} - \left\{\frac{\partial \overline{\tilde{u}\tilde{u}}}{\partial x} + \frac{\partial \overline{\tilde{u}\tilde{v}}}{\partial y} + \frac{\partial \overline{\tilde{u}\tilde{w}}}{\partial z}\right\} + O\left(|\zeta|^3\right) \tag{17}$$

$$\frac{F_y}{\rho_0} = -\frac{1}{\rho_0}\left\{\frac{\partial \overline{\tau_{yx}}^s}{\partial x} + \frac{\partial \overline{\tau_{yy}}^s}{\partial y} + \frac{\overline{\tau_{yz}}^s}{\partial z}\right\} - \left\{\frac{\partial \overline{\tilde{v}\tilde{u}}}{\partial x} + \frac{\partial \overline{\tilde{v}\tilde{v}}}{\partial y} + \frac{\partial \overline{\tilde{v}\tilde{w}}}{\partial z}\right\} + O\left(|\zeta|^3\right) \tag{18}$$

wherein the first term represents the Stokes' correction in the radiation stress and the second term accounts for the forcing due to wave-induced shear stresses (Deltares (2020) & Lesser *et al.* (2004)). When rewriting the wave-related driving forces (eqs. (17) & (18)) in terms of radiation stresses, the forces causing wave-related (depth-averaged) streaming in the wave boundary layer and the (depth-averaged) wave forces become prevalent (see eqs. (19) & (20)).

$$F_x = \underbrace{-\left\{\left(\frac{\partial \overline{\tilde{u}\tilde{v}}}{\partial x} + \frac{\overline{p_{wave}}}{\partial x}\right) + \frac{\partial \overline{\tau_{xy}}^s}{\partial y}\right\}}_{\text{Wave Driving Force } M_x = -\left\{\frac{\partial S_{xx}}{\partial x} + \frac{\partial S_{xy}}{\partial y}\right\}} + \underbrace{\frac{\partial \overline{\tilde{u}\tilde{w}}}{\partial z}}_{\text{Longuet-Higgins Streaming in wave boundary layer}} + \{...\} \tag{19}$$

$$F_y = \underbrace{-\left\{\left(\frac{\partial \overline{\tilde{v}\tilde{u}}}{\partial y} + \frac{\overline{p_{wave}}}{\partial y}\right) + \frac{\partial \overline{\tau_{yx}}^s}{\partial x}\right\}}_{\text{Wave Driving Force } M_y = -\left\{\frac{\partial S_{yy}}{\partial y} + \frac{\partial S_{yx}}{\partial x}\right\}} + \underbrace{\frac{\partial \overline{\tilde{v}\tilde{w}}}{\partial z}}_{\text{Longuet-Higgins Streaming in wave boundary layer}} + \{...\} \tag{20}$$

Furthermore, as mentioned by Deltares (2020), using radiation stresses in numerical models may result in spurious currents. To overcome this, Dingemans (1994) proposed the parameterisation of the

energy dissipation (eqs. (21) & (22)) due to wave breaking by means of a function which is entirely described by the wave characteristics (see also eq. (14)). The latter characteristics may be calculated by means of a wave generation model (i.e. SWAN),

$$M_x = \frac{Dk_x}{\omega} \tag{21}$$

$$M_y = \frac{Dk_y}{\omega} \tag{22}$$

Streaming in wave boundary layer

The wave-induced current in the wave boundary layer - Longuet-Higgins streaming - is derived from the momentum equations and presented in equations eqs. (19) & (20). The wave-induced streaming is modelled as shear stress acting on the bed and by the findings of Fredsøe and Deigaard (1992) assumed to be linearly decreasing to zero at height of the wave boundary thickness δ. Fredsøe and Deigaard (1992) give the following approximation for the streaming which is written as function of the wave bottom shear dissipation,

$$-\frac{\partial \overline{\tilde{u}\tilde{w}}}{\partial z} = \frac{D_f k \cos\phi}{\rho_0 \omega \delta}\left(1 - \frac{d+\zeta-z'}{\delta}\right), \text{for } d+\zeta-\delta \leq z' \leq d+\zeta \tag{23}$$

$$-\frac{\partial \overline{\tilde{v}\tilde{w}}}{\partial z} = \frac{D_f k \sin\phi}{\rho_0 \omega \delta}\left(1 - \frac{d+\zeta-z'}{\delta}\right), \text{for } d+\zeta-\delta \leq z' \leq d+\zeta \tag{24}$$

wherein:

- D_f: represents the wave bottom shear dissipation and is given by,

$$D_f = \frac{1}{2\sqrt{\pi}} \rho_0 f_w {u_{orb}}^3 \tag{25}$$

- f_w: is a wave-related bottom friction factor proposed by Soulsby *et al.* (1993):

$$f_w = \min\left\{0.3, 1.39\left(\frac{\frac{u_{orb}}{\omega}}{z_0}\right)^{-0.52}\right\} \tag{26}$$

- u_{orb}: is the orbital velocity and may be defined - on the basis of linear wave theory - as,

$$u_{orb} = \frac{1}{4}\sqrt{\pi}\frac{H_{rms}\omega}{\sinh kh} \tag{27}$$

- δ: is the thickness of the wave boundary layer given by,

$$\delta = h \min\left[0.5, 20 \max\left\{\frac{ez_0}{h}, 0.09\frac{k_s}{h}\left(\frac{\frac{u_{orb}}{\omega}}{k_s}\right)^{0.82}\right\}\right] \tag{28}$$

Wave-induced breaking and Dissipation of Wave Energy

When waves break in the surf zone, kinetic energy stored in the wave motion is dissipated by means of (1) turbulent energy transferal at the free surface and (2) wave-induced shear stresses at the bottom (see Figure 1). Henceforth, these processes shall be reviewed separately in the following section.

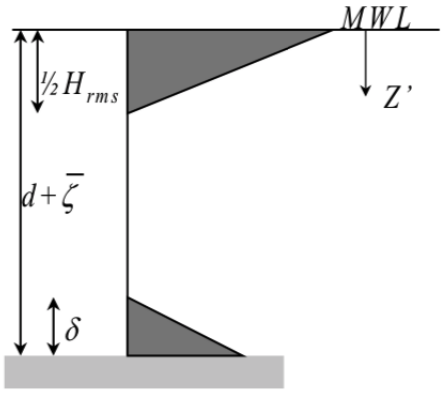

Figure 1: Vertical Distribution of Turbulent Kinetic Energy Production. (From Deltares (2020)-*page(225) Figure(9.8)*)

1. **Wave Breaking and free surface dissipation**

   Turbulent vortices at the free surface - free surface rollers - transfer kinetic energy to the smaller turbulent scale where viscous shear stresses become dominant (i.e. energy cascade at free surface). Adopted on the work of Deigaard *et al.* (1986), the energy dissipation at the free surface is represented by (extra) sink and source terms in the turbulence closure model (i.e. $(\kappa - \varepsilon)$-turbulence model). The *Production* and the *Decay* of turbulent kinetic energy, $P_{\kappa w}$ respectively $P_{\varepsilon w}$, is defined by Deigaard *et al.* (1986) (also see Walstra *et al.* (2000) and Deltares (2020)) as,

$$P_{\kappa w}(z') = \frac{4D_w}{\rho_w H_{rms}} \left(1 - \frac{2z'}{H_{rms}}\right), \text{for } 0 \leq z' \leq \frac{1}{2} H_{rms} \tag{29}$$

   The decay of turbulent kinetic energy $P_{\varepsilon w}$ is here coupled to the production term of kinetic energy $P_{\kappa w}$ and defined as,

$$P_{\varepsilon w}(z') = \underbrace{c_{1\varepsilon}}_{\text{calibration constant = 1.44}} \frac{\varepsilon}{\kappa} P_{\kappa w}(z') \tag{30}$$

   The wave breaking dissipation rate D_w is hereby calculated by a wave generation model (i.e. SWAN) and used as input for the calculation of the sink and source terms in eqs. (29) and (30).

2. **Wave-induced bottom shear stress and energy dissipation**

   Kinetic energy stored in the wave motion is also dissipated through wave-related bottom friction. The wave-related orbital motion at the bed and its associated gradient near the bed (i.e. Longuet-Higgins Streaming) produce wave-induced shear stresses in the wave boundary layer which, by means of energy cascades, set about energy dissipation. The dissipation of wave kinetic energy due to bottom friction is modelled as a *source term/production* of turbulent kinetic energy $P_{\kappa w}$ in the turbulence closure model (i.e. $\kappa - \varepsilon$ model). This results in the following formulation as proposed by Deigaard *et al.* (1986) (and seen in Deltares (2020) and Walstra *et al.* (2000)). It should be noted that the wave-related dissipation rate due to bottom friction D_f may be computed by application of eq.(25).

$$P_{\kappa w}(z') = \frac{2D_f}{\rho_0 \delta} \left(1 - \frac{d + \zeta - z'}{\delta}\right), \text{for } d + \zeta - \delta \leq z' \leq d + \zeta \tag{31}$$

Wave-Current Interaction and enhanced bottom shear stress

The presence of both a wave boundary layer and a current boundary layer at the bed creates an increase of the *total* bed shear stress acting on the bed. It is noted by Soulsby *et al.* (1993) that the interaction between the current and wave-related shear does not prevail linearly. Instead, the presence of the wave-related shear and the wave-related turbulent mixing at the bed constitute to an enhancement of the current-related bed shear stress which could be seen as *virtual added bed roughness*.

The representation of the combined current-wave bed shear stress $\vec{\tau_m}$ and the maximum bed shear stress $\vec{\tau_{max}}$ depends on the applied wave-current interaction model, as found by Soulsby *et al.* (1993). The latter shear stresses ($\vec{\tau_m}$ and $\vec{\tau_{max}}$) are parameterised by Soulsby *et al.* (1993) for various wave-current interaction models whereby $\vec{\tau_m}$ and $\vec{\tau_{max}}$ are defined as such that they acquire the following form,

$$|\vec{\tau_m}| = Y\left(|\vec{\tau_c}| + |\vec{\tau_w}|\right) \tag{32}$$

$$|\vec{\tau_{max}}| = Z\left(|\vec{\tau_c}| + |\vec{\tau_w}|\right) \tag{33}$$

with parameterisation parameters X, Y, Z, a, b, p & q which are uniquely stated for each wave-current interaction model of choice. The values for the latter parameters in various wave-current interaction models are defined in Soulsby *et al.* (1993) and Deltares (2020)).

$$Y = X\left\{1 + bX^p(1-X)^q\right\} \tag{34}$$

$$Z = X\left\{1 + aX^m(1-X)^n\right\} \tag{35}$$

$$X = \frac{|\vec{\tau_c}|}{\left(|\vec{\tau_c}| + |\vec{\tau_w}|\right)} \tag{36}$$

Next, the current-related and wave-related bed shear stresses $\vec{\tau_c}$ respectively $\vec{\tau_w}$ are defined as,

$$|\vec{\tau_c}| = \frac{\rho_0 g U \left|\vec{U}\right|}{C^2} \tag{37}$$

$$|\vec{\tau_w}| = \frac{1}{2}\rho_0 f_w {u_{orb}}^2 \tag{38}$$

Moreover, the formulation of the wave friction parameter accounting for a rough bed and turbulent flow is adopted on the work of Swart (1974) and proposed the following expression,

$$f_w = \begin{cases} 0.00251 \exp\left[5.21\left(\frac{u_{orb}}{\omega k_s}\right)^{-0.19}\right], & \frac{u_{orb}}{\omega k_s} > \frac{\pi}{2}, \\ 0.3, & \frac{u_{orb}}{\omega k_s} \leq \frac{\pi}{2} \end{cases} \tag{39}$$

Overall, it is worthwhile to state that he choice of wave-current interaction model is critical as its dictates the way that the non-linear interaction between waves and currents in the bed shear stress is considered in Delft3D - which may be vital for the determination of the sediment transport in Delft3D. Soulsby *et al.* (1993) compared the effects of non-linear wave-current interactions with the case of linear superposition of wave and current-related bed shear stresses for various wave-current interaction models. The latter is shown in figure 2.

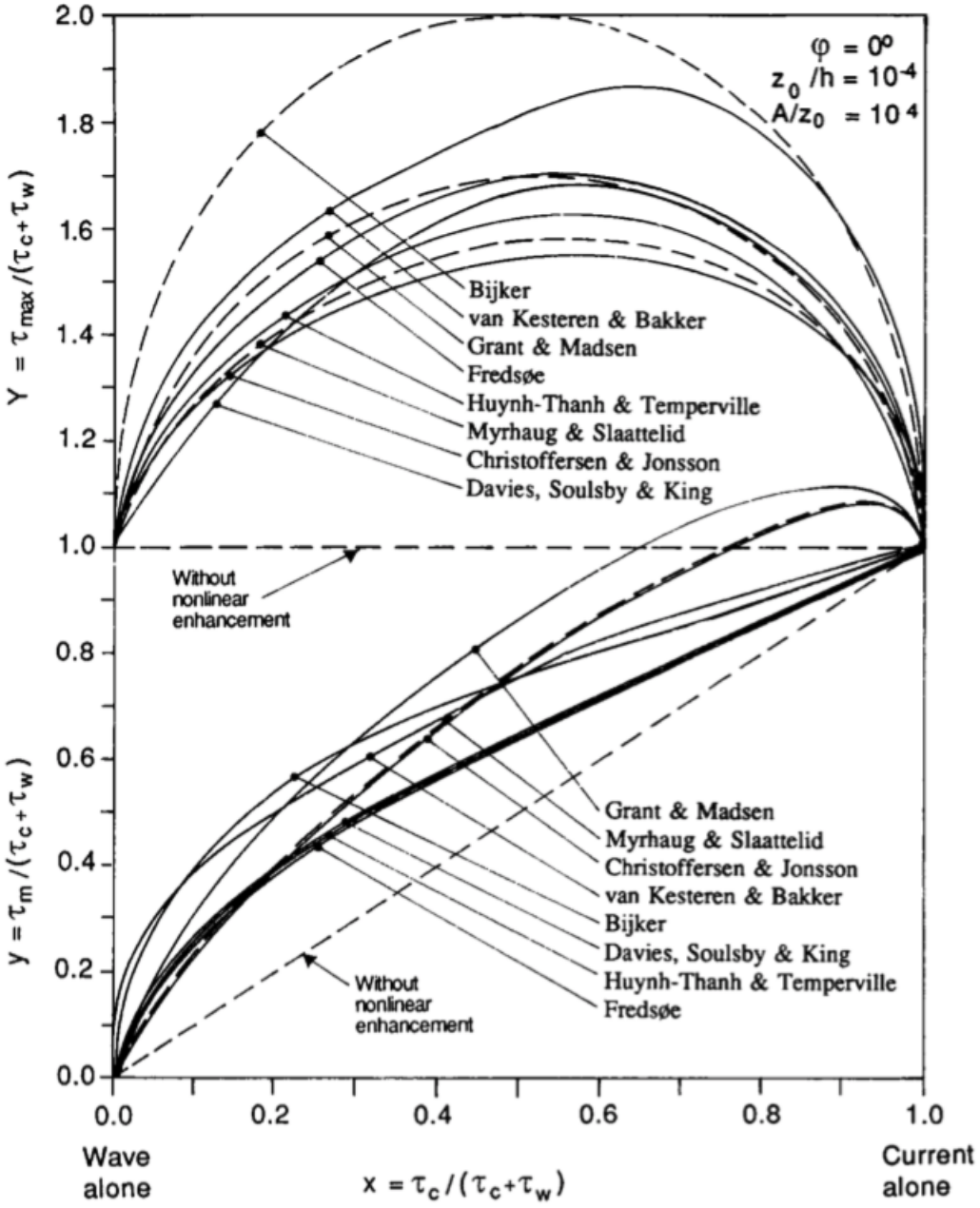

Fig. 7. Intercomparison of WCI models of Bijker (1967), Christoffersen and Jonsson (1985), Davies et al. (1988), Fredsøe (1984), Grant and Madsen (1979), Huynh-Thanh and Temperville (1991), Myrhaug and Slaattelid (1990), and Van Kesteren and Bakker (1984).

Figure 2: Intercomparison between various wave-current interaction models of (1) Bijker, (2) Christoffersen and Jonsson, (3) Davies Soulsby & King, (4) Fredsøe, (5) Grant & Madsen, (6) Huynh-Thanh & Temperville, (7) Myrhaug & Slaattelid, and (8) van Kesteren & Bakker. (From Soulsby *et al.* (1993) - *page(55) Figure(7)*)

Residual motion

The origin of the wave-related mass transport due to Stokes' drift becomes apparent when a derivation is proceeded for the continuity equation in the (**GLM**) *Generalised Lagrangian Mean Frame of Reference*. To this end, the conservation equation described in eq.(6) is revisited. Local accumulation or withdrawal of mass due discharges and/or evapotranspiration (sink and source terms) are temporarily omitted.

$$\frac{\partial \zeta}{\partial t} + \frac{\partial hu}{\partial x} + \frac{\partial hv}{\partial y} = 0$$

The velocity components in eq.(6) are decomposed by application of eq.(2) after which depth-integration is proceeded such that the right hand side of eq.(6) entails a description of the depth-averaged mass flux due to wave orbital motion F_c, viz. eq.(40).

$$\frac{\partial \overline{\zeta}^L}{\partial t} + \frac{\partial}{\partial x}\left\{\int_{-h}^{\overline{\zeta}^L} \overline{u}^L \, dz\right\} + \frac{\partial}{\partial y}\left\{\int_{-h}^{\overline{\zeta}^L} \overline{v}^L \, dz\right\} = F_c \tag{40}$$

Consequently, since F_c is the *wave-induced volume transport*, by application of the Boussinesq approximation, the *wave-induced mass transport* $\rho_0 F_c$ may be defined as,

$$\begin{aligned} \rho_0 F_c &= \frac{\partial}{\partial x}\left\{\int_{-h}^{\overline{\zeta}^L} \rho_0 \overline{u}^s \, dz\right\} + \frac{\partial}{\partial y}\left\{\int_{-h}^{\overline{\zeta}^L} \rho_0 \overline{v}^s \, dz\right\} \\ &= \frac{E}{\omega}\kappa_x + \frac{E}{\omega}\kappa_y \end{aligned} \tag{41}$$

$$E = \frac{1}{8}\rho g {H_{rms}}^2 \tag{42}$$

wherein:

- E: represents the time-averaged wave-induced energy per unit of the horizontal area (sum of potential and kinetic energy) (in J/m^2).
- H_{rms}: represents the root mean squared wave height which is equal to $\sqrt{8m_0}$ (in m).
- ω: represents the angular wave frequency (in rad/s)
- $\vec{\mathbf{k}}$: represents the wave number in the respective coordinate direction (in rad/m)

SUSPENDED SEDIMENT MODULE

The separate suspended sediment module has a solver that, in the *online* approach, solves the transport equation (eq.(7)) for each sediment fraction simultaneously with the equations describing the hydrodynamic flow (eqs.(3), (4), (5), (11) & (12)). Here, the suspended sediment transport is added as *transported constituent* in the FLOW module, whereby up to 5 sediment fractions may be included in the computations. The suspended sediment transport equation for each of these fractions is modified based on the *user-specified* classification of the type of sediment fraction (i.e. sand or mud) to account for the difference in bed exchange processes and settling velocity (Deltares (2020) & Lesser *et al.* (2004)).

In the suspended sediment transport module, the entrainment and deposition of suspended sediment particles is represented by sink and source terms in the transport equation (eq.(7)) based on a theoretical concentration distribution profile (i.e. Rouse profile) for which a theoretical bed concentration c_a is considered as bottom boundary condition for the profile. As such, the following processes are reviewed:

- Suspended sediment transport equation
- Density Effects
- Sediment exchange with the bed
- Correction Factor to account for excess computed suspended sediment transport

Suspended Sediment Transport Equation

The suspended sediment transport for each sediment fraction l is - as presented in Lesser *et al.* (2004) & Deltares (2020) - defined by eq.(43) below,

$$\frac{\partial c^{(l)}}{\partial t} + \frac{\partial u c^{(l)}}{\partial x} + \frac{\partial v c^{(l)}}{\partial y} + \frac{\partial \left(\omega - {\omega_s}^{(l)}\right) c^{(l)}}{\partial \sigma} - \frac{\partial}{\partial x}\left(D_H \frac{\partial c^{(l)}}{\partial x}\right) - \frac{\partial}{\partial y}\left(D_H \frac{\partial c^{(l)}}{\partial y}\right) - \frac{\partial}{\partial \sigma}\left(D_V \frac{\partial c^{(l)}}{\partial \sigma}\right) = S \quad (43)$$

Wherein S represents the sinks and sources of suspended sediment fractions in the flow.

Vertical eddy diffusivity

As proposed by Lesser *et al.* (2004), the vertical eddy ***diffusivity*** D_V is considered to be proportional to the vertical eddy ***viscosity*** ν_V and obtained from the chosen turbulence closure model. Here, the eddy viscosity ν_V is assumed to obey the *eddy viscosity concept* such that the ν_V is found in the following form:

$$\nu_V = c'_\mu L \sqrt{\kappa} \quad (44)$$

wherein:

- c'_μ: represents a user-specified calibration parameter (default $c'_\mu = 1$)
- L: represents the mixing length
- κ: represents the turbulent kinetic energy.

1. **Formulation in the case of solely currents - *($\kappa - \epsilon$)-Turbulence closure model***

   The vertical eddy diffusivity D_V may be calculated by application of eqs.(8) & (9), with the small modification proposed by van Rijn (1993) accounting for the difference in vertical diffusion between a fluid parcel and a (fine) sediment grain. To this end, the vertical eddy diffusion is defined as,

   $$D_V = \frac{\nu_V \beta}{\sigma_c}, \quad \beta = 1 + 2\left\{\frac{w_s}{u_{*,c}}\right\}^2 \quad (45)$$

   σ_c is related to the stability of the stratification of the flow (i.e. Richardson Number) and may be calculated by application of eq.(9)- here below stated for brevity,

   $$\sigma_c = \sigma_{c0} * F_\sigma(R_i)$$

   It should be noted that in the case of solely current-action (i.e. *no waves*) σ_{c0} is set to 1.

2. **Formulation in the case of currents and waves - *($\kappa - \epsilon$)-Turbulence closure model***

   In the presence of both waves and currents, the diffusion factor β proposed by van Rijn (1993) is changed to account for the enhanced bed shear stresses as a consequence to wave-current interaction. Instead of β, the *effective* diffusion factor β_{eff} must be applied in equation eq.(45), and may be calculated using eq.(46) below,

   $$\beta_{eff} = 1 + \{\beta - 1\} \frac{\tau_c}{\tau_w + \tau_c} \quad (46)$$

3. **Formulation in the case of currents and waves -** ***Algebraic or*** $(\kappa - L)$***-Turbulence closure model***

In the case of an algebraic turbulence closure model - or a $(\kappa - L)$-turbulence closure model - the vertical eddy diffusivity D_V is found using the *analytical* expressions stated by van Rijn (1993) for both currents and waves-related turbulent mixing. Each part is individually assessed and superposed to find the *total* vertical eddy diffusivity D_V.

The current-related part results from equation eq.(47),

$$D_{V,c} = \begin{cases} \kappa\beta u_{*,c} * z(1 - \frac{z}{h}), & \text{for } z \leq 0.5h \\ 0.25\kappa\beta u_{*,c} h & \text{for } z \geq 0.5h \end{cases} \tag{47}$$

And the wave-related part is defined by equation eq.(48),

$$D_{V,w} = \begin{cases} D_{V,w} = D_{V,bed} = 0.004 D_* \delta_s \hat{u}_\delta, & \text{for } z \leq \delta_s \\ D_{V,w} = D_{V,bed} + [D_{V,max} - D_{V,bed}] \left[\frac{z-\delta_s}{0.5h-\delta_s}\right] & \text{for } \delta_s \leq z \leq 0.5h \\ D_{V,w} = D_{V,max} = 0.035 h \left(\frac{H_s}{T_p}\right), & \text{for } z \geq 0.5h \end{cases} \tag{48}$$

Wherein:

- δ_s: represents the thickness of the wave boundary layer where sediment mixing is apparent and as proposed in Deltares (2020) defined as,

$$\delta_s^{(l)} = \min\left[0.5, \max\left\{0.1, \max\left(5\gamma_{br}\delta_w, 10\gamma_{br}k_{s,w}\right)\right\}\right] \tag{49}$$

with,

$$\delta_w = 0.072\hat{A}_\delta \left(\frac{\hat{A}_\delta}{k_{s,w}}\right)^{-0.25}, \qquad \gamma_{br} = \begin{cases} 1 + \left(\frac{H_s}{h} - 0.4\right)^{0.5}, & \text{for } \frac{H_s}{h} > 0.4 \\ 1, & \text{for } \frac{H_s}{h} \leq 0.4 \end{cases} \tag{50}$$

- $\hat{u}_\delta$: represents the peak wave orbital velocity at the edge of the wave boundary layer
The total vertical eddy diffusivity follows from the *modulus* of the wave and current component and is subsequently used in the computations of the suspended sediment transport.

$$D_V = \sqrt{D_{V,c}^2 + D_{V,w}^2} \tag{51}$$

Horizontal eddy diffusivity

The horizontal eddy diffusivity D_H is not included in the advection dominated suspended sediment transport and must be added as *background diffusion* to the model. The user may specify the associated value as constant throughout the computational domain or by means of an *input file* wherein the spatial distribution of horizontal eddy diffusivity D_H is prompted.

Density effects

Density differences may have influence on the flow and occurs due to differences in temperature, salinity and other dissolved/suspended constituents which is noted by Eckart (1958). In light of the presence of suspended sediment transport, the density of the fluid must also account for changes in the

concentration of sediment fractions in the flow. Therefore, the density of the fluid is updated by means of the following equation (eq.(52)) taking into consideration all sediment fractions $LSED$,

$$\rho = \rho_w + \sum_{l=1}^{LSED} c_s^{(l)} \left(\rho_s^{(l)} - \rho_w \right) \tag{52}$$

Settling Velocities

van Rijn (1993) proposed that the settling velocity for non-cohesive sediment is related to the nominal diameter of the sediment fraction and its relative density which resulted in the following formulation eq.(53) below,

$$w_{s,0}^{(l)} = \begin{cases} \frac{(s^{(l)}-1)g(D_s^{(l)})^2}{18\nu}, & 65\mu m < D_s \leq 100\mu m \\ \frac{10\nu}{D_s}\left(\sqrt{1+\frac{0.01(s^{(l)}-1)g{D_s^{(l)}}^3}{\nu^2}}-1\right), & 100\mu m < D_s \leq 1000\mu m \\ 1.1\sqrt{(s^{(l)}-1)gD_s^{(l)}}, & 1000\mu m < D_s \end{cases} \tag{53}$$

wherein the following parameters are included:

- $s^{(l)}$: represents the relative density $\rho_s^{(l)}/\rho_w$ of each sediment fraction l
- $D_s^{(l)}$: is the representative diameter of each sediment fraction l
- ν: represents the kinematic viscosity of water

Sediment Exchange with the bed

The erosion and deposition of non-cohesive sediment fraction are modelled by means of local sinks and sources at a layer near the bottom (i.e. Deltares (2020) & Lesser *et al.* (2004)). For each fraction, a separate pair of sinks and sources is taken into consideration. The placement of the sources and sinks for non-cohesive sediment is shown in figure 3. Based on the research of van Rijn (1993), a reference height a is defined as such that - depending on the layer thickness of the computational cells - the sediment sinks and sources are placed at the surface of the computational cell that is in its entirety above the reference height.

The sediment concentration c_a at this theoretical height - called the reference concentration - is assumed and calculated by means of van Rijn (1984a)'s equation eq.(54) below.

$$c_a = f_{sus}\eta 0.015\rho_s \frac{d_{50}}{a} \frac{{T_a}^{1.5}}{{D_*}^{0.3}} \tag{54}$$

wherein:

- f_{sus}: is a user-specified calibration constant (Default 1.0)
- η: represents the relative availability of sediment fractions at the bed
- d_{50}: is the representative diameter of each sediment fraction at the bed for which 50% of the grains in the sieving distribution exceeds this value.
- T_a: is the dimensionless parameter accounting for the bed shear stress at the reference height a
- D_*: is a dimensionless parameter accounting for the particle diameter of each (individual) sediment fraction

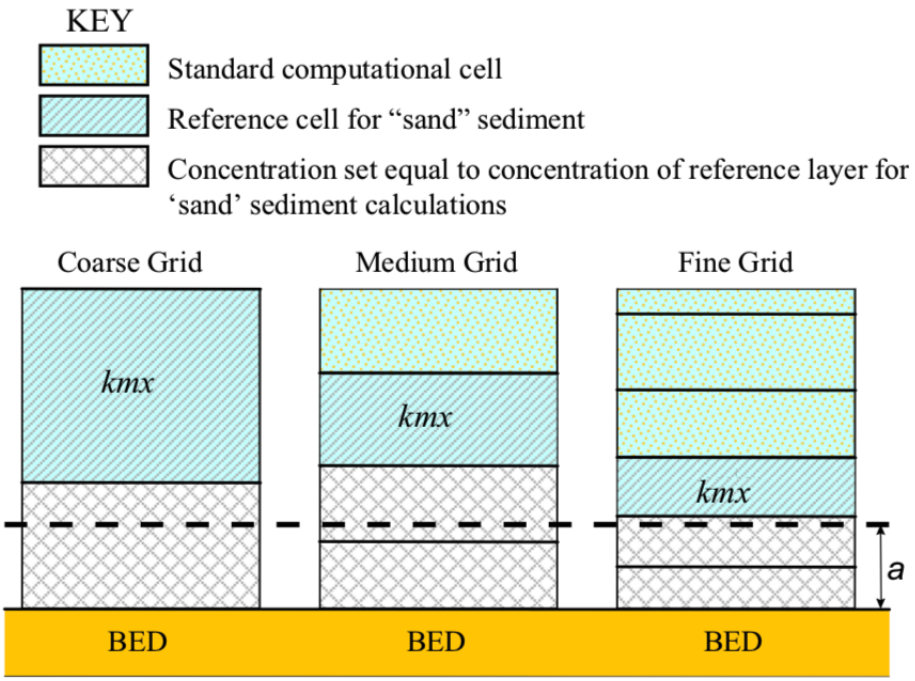

Figure 11.2: *Selection of the kmx layer; where a is Van Rijn's reference height*

Figure 3: Allocation of non-cohesive sediment fraction sinks and sources on a near-bed reference layer. (As presented in Deltares (2020)-*page(323) Figure(11.2)*)

In order to define the sink and source terms at the surface of the computational cells directly above the reference height a, the concentration at the kmx layer $c_{kmx,bot}$ should be known. The latter concentration can only be defined when the vertical distribution profile of the suspended sediment is specified. Therefore, the concentration at the bottom of the kmx layer $c_{kmx,bot}$ is approximated by application of a rouse profile eq.(55), between the reference height a and the bottom of the kmx layer.

$$c^{(l)} = c_a^{(l)} \left[\frac{a(h-z)}{z(h-a)} \right]^{A^{(l)}} \tag{55}$$

It is, thereby, assumed that a linear gradient prevails between the concentration in the reference layer c_a and the concentration in the kmx layer c_{kmx}.

By evaluation of the Rouse profile at the centre of the kmx layer - where the concentration is known - a value for the Rouse number $A^{(l)}$ is to be defined as is proceeded in eq. (56).

$$c_{kmx}^{(l)} = c_a^{(l)} \left[\frac{a(h-z_{kmx})}{z_{kmx}(h-a)} \right]^{A^{(l)}} \quad \rightarrow A^{(l)} = \frac{\ln\left(\frac{c_{kmx}}{c_a}\right)}{\ln\left(\frac{a(h-z_{kmx})}{z_{kmx}(h-a)}\right)} \tag{56}$$

Consequently, the concentration at the bottom of the kmx layer $c_{kmx,bot}$ may be derived by evaluation of the Rouse profile at the bottom of the kmx layer.

$$c_{kmx,bot}^{(l)} = c_a^{(l)} \left[\frac{a(h-z_{kmx,bot})}{z_{kmx,bot}(h-a)} \right]^{A^{(l)}} \tag{57}$$

Table 11.1: *Additional transport relations*

Formula	Bedload	Waves
11.5.1, Van Rijn (2007)	Bedload + suspended	Yes
11.5.2, SANTOSS	Bedload + suspended	Yes
11.5.3, Van Rijn (1993)	Bedload + suspended	Yes
11.5.4, Engelund-Hansen (1967)	Total transport	No
11.5.5, Meyer-Peter-Muller (1948)	Total transport	No
11.5.6, General formula	Total transport	No
11.5.7, Bijker (1971)	Bedload + suspended	Yes
11.5.8, Van Rijn (1984)	Bedload + suspended	No
11.5.9, Soulsby/Van Rijn	Bedload + suspended	Yes
11.5.10, Soulsby	Bedload + suspended	Yes
11.5.11, Ashida–Michiue (1974)	Total transport	No
11.5.12, Wilcock–Crowe (2003)	Bedload	No
11.5.13, Gaeuman et al. (2009) laboratory calibration	Bedload	No
11.5.14, Gaeuman et al. (2009) Trinity River calibration	Bedload	No

Figure 4: Additional options for bedload transport relations. (As presented in Deltares (2020)-*page(334) Table(11.1)*)

Lastly, the sediment sinks and sources for each sediment fraction follows from eqs.(58) & (59) below (as seen in Lesser *et al.* (2004) and adopted by Deltares (2020)),

$$Sinks = E^{(l)} = c_{kmx}^{(l)} \left(\frac{D_V^{(l)}}{\Delta z} \alpha_2^{(l)} + w_s^{(l)} \alpha_1^{(l)} \right) \tag{58}$$

$$Sources = D^{(l)} = \alpha_2^{(l)} c_a^{(l)} \left(\frac{D_V^{(l)}}{\Delta z} \right) \tag{59}$$

In combination with eq.(60), these equations (eqs.(58) & (59)) form the boundary condition at the bed for the timely calculation of the suspended sediment transport.

$$-w_s^{(l)} c^{(l)} - D_V^{(l)} \frac{\partial c^{(l)}}{\partial z} = \begin{cases} 0, & \text{for } z = \zeta \\ D^{(l)} - E^{(l)} & \text{for } z = z_b \end{cases} \tag{60}$$

BEDLOAD SEDIMENT TRANSPORT MODULE

The bedload transport module is a separate solver of Delft3D wherein the bedload transport is calculated on the basis of a bedload transport formulation. Figure 4 gives an overview of the formulations that may be prompted by the user. In this report, the bedload transport formulation on the basis of van Rijn (1993) is considered.

van Rijn (1993) - Solution Procedure

In the sediment transport formulation of van Rijn (1993), the total transport of sediment is split in (1) bedload transport in the computational reference cell below the reference height a and (2) a suspended sediment transport above the reference cell throughout the water column. The solution procedure for the suspended sediment module is hereinabove discussed. Here, the bedload transport formulation

shall be assessed. It is thereby argued by van Rijn (1993) that the magnitude and direction of the bedload transport depends on the occurrence of waves in the computational domain. Therefore, the case of currents-only and the case of combined wave-current effects is separately discussed below.

Bedload transport magnitude and direction - currents-only

In Lesser *et al.* (2004), a formulation is proposed for the magnitude of the bedload transport in the case of solely current effects and is presented here below in equation eq.(61),

$$|S_b| = f_{bed}\eta 0.5\rho_s d_{50} u'_* D_*^{-0.3T} \tag{61}$$

wherein the following parameters are defined:

- f_{bed}: is a user-specified calibration constant (Default 1.0)
- η: represents the relative availability of sediment fractions at the bed
- u'_*: represents the effective bed shear stress velocity based on the computed velocities in the computational layer below the reference height a
- D_*: is a dimensionless parameter accounting for the particle diameter of each (individual) sediment fraction
- T: is the dimensionless parameter accounting for the bed shear stress at the reference height a

Next, the direction of the bedload transport must be defined. As stated by van Rijn (1993), the direction of the (flatbed) bedload transport is assumed to be parallel to the flow in the bottom reference layer. Therefore, the direction of the bedload transport eq.(64) is found by calculation of the separate u- and v-component of the bedload transport $S_{b,u}$ (eq.(62)) & $S_{b,v}$ (eq.(63)) respectively, and the magnitude of the local bed velocities (eq.(64)).

$$S_{b,u} = \frac{u_{b,u}}{|u_b|}|S_b| \tag{62}$$

$$S_{b,v} = \frac{u_{b,v}}{|u_b|}|S_b| \tag{63}$$

$$|u_b| = \sqrt{u_{b,u}^2 + u_{b,v}^2} \tag{64}$$

Bedload transport magnitude and direction - waves & currents combined

In the case of both current and wave-related effects, the magnitude and direction of the bedload transport follows from an approximate method as stated in Lesser *et al.* (2004). The magnitude of the bedload transport under wave and current-effect is defined as,

$$|S_b| = \eta 0.006\rho_s w_s M^{0.5} M_e^{0.7} \tag{65}$$

wherein:

- M: represents the mobility parameter of the bed sediment particles under wave and current effect.

$$M = \frac{v_{eff}^2}{(s-1)gd_{50}} \tag{66}$$

- M_e: describes the *excess* mobility parameter of the bed sediment particles under wave and current effect. That is, the relative mobility of the bed sediment with respect to the critical condition for incipient motion.

$$M_e = \frac{(v_{eff} - v_{cr})^2}{(s-1)gd_{50}} \tag{67}$$

- v_{eff}: represents the effective velocity at the bed found by a superposition of the equivalent depth-averaged velocity at the bed v_R and the peak near-bed velocity U_{on} in the case that the effect of short wave asymmetry on the orbital motion is considered.

$$v_{eff} = \sqrt{v_R^2 + U_{on}^2} \tag{68}$$

The direction of the bedload transport under wave and current-effects is considered to be composed of two components ($S_{b,c}$ and $S_{b,w}$) - hereby individually accounting for each of the latter effects (Lesser *et al.* (2004)):

- $S_{b,c}$ is related to the bedload transport in the direction of the near-bed currents
- $S_{b,w}$ describes the bedload transport in the direction of the (shallow water) wave propagation

The magnitude of these components are defined by application of equations eqs.(69) and (70) below,

$$\mid S_{b,c} \mid = \frac{|S_b|}{\sqrt{1 + r^2 + 2\,|r| \cos\varphi}} \tag{69}$$

$$\mid S_{b,w} \mid = r \mid S_{b,c} \mid , \qquad \text{with } r = \frac{(|u_{on}| - v_{cr})^3}{(|v_R| - v_{cr})^3} \tag{70}$$

wherein the following parameters are included:

- r: represents the relative importance of the non-linear wave effects (i.e. wave skewness) on the otherwise logarithmic profile. That is, the relative significance of the near-bed orbital motion on the depth-averaged velocity.
- φ: represents the angle between the current and the wave direction.

The above described magnitudes of the current-related and wave-related bedload transport are (unfortunately) defined in the direction of the current and wave propagation. Therefore, a transformation is proceeded such that the bedload transport components ($S_{b,w}$ & $S_{b,c}$) are defined in the direction of the cartesian axes. Hereby, careful considerations are taken into (1) the non-linear wave effects as well as (2) the effect of short wave stirring on the suspended sediment transport in the vicinity of the bed (Lesser *et al.* (2004)). The magnitude of these components is approximated as proposed by van Rijn (2001) on the basis of the formulation described in eq.(71) below,

$$|S_{s,w}| = \gamma U_A L_T \tag{71}$$

wherein:

- γ: represents the phase lag in the orbital motion in the form of a phase lag coefficient (Default 0.2)
- U_A: represents the relative effect of the shape of the wave on the bedload transport in the form of a *velocity asymmetry value* which may be computed by application of eq.(72):

$$U_A = \frac{\left(U_{on}^4 - U_{off}^4\right)}{\left(U_{on}^3 + U_{off}^3\right)} \tag{72}$$

Consequently, the bedload transport components are defined by equations eqs.(73) & (74) respectively as stated below.

$$S_{b,u} = f_{BED}\left[\frac{u_b}{|\vec{u_b}|} \mid S_{b,c} \mid + (f_{BEDW} S_{b,w} + f_{SUSW} S_{s,w}) \cos\varphi\right] \tag{73}$$

$$S_{b,v} = f_{BED}\left[\frac{u_b}{|\vec{u_b}|} \mid S_{b,c} \mid + (f_{BEDW} S_{b,w} + f_{SUSW} S_{s,w}) \sin\varphi\right] \tag{74}$$

wherein:

- f_{BED}: is a user-specified calibration constant (default 1.0)
- f_{BEDW}: is a user-specified calibration constant (default 1.0)
- f_{SUSW}: is a user-specified calibration constant (0.5 for field cases, 1.0 for flumes)
- φ: represents the relative angle between the wave propagation direction and the computational grid

Bedslope Effects

As stated in Lesser *et al.* (2004), the direction and magnitude of the bedload transport is depended on the slope of the bed as the sediment transport is assumed to be largely contacted with the bed. Therefore, the effect of bed slopes on the direction and magnitude of the bedload transport shall be reviewed.

1. **Longitudinal bed slope effects**

   Based on the work of Bagnold (1966), a longitudinal slope in the direction of the bedload transport may be related to a magnitude adjustment of the bedload transport components in their respective directions. Consequently, Bagnold (1966) proposed the following equations, here stated as eqs. (75), (76) & (77).

$$S_{b,uu} = \alpha_s S_{b,u} \tag{75}$$

$$S_{b,vv} = \alpha_s S_{b,v} \tag{76}$$

$$\alpha_s = 1 + f_{ALFABS}\left[\frac{\tan\phi}{\cos\left(\arctan\left(\frac{\partial z}{\partial s}\right)\right)\left(\tan\left(\phi\right) - \frac{\partial z}{\partial s}\right)} - 1\right] \tag{77}$$

   wherein:

   - f_{ALFABS}: is a user-specified calibration constant (default 1.0)
   - α_s: is a reduction factor accounting for the *longitudinal* bed slope effects on the bedload transport.

2. **Transverse bed slope effects**

   For transverse bed slopes perpendicular (or obliquely) from the direction of the bedload transport, Ikeda (1982) stated that such bed slope constitutes to direction adjustments. Hence, the following equations eqs.(78), (79) & 80 are considered for transverse bed slope effects.

$$S_{b,uu} = S_{b,uu} - \alpha_n S_{b,vv} \tag{78}$$

$$S_{b,vv} = S_{b,vv} + \alpha_n S_{b,uu} \tag{79}$$

$$\alpha_n = f_{ALFABN}\left(\frac{\tau_{b,cr}}{\tau_{b,cw}}\right)^{0.5}\frac{\partial z}{\partial n} \tag{80}$$

   wherein:

- f_{ALFABN}: is a user-specified calibration constant (default 1.5)
- α_n: is a reduction factor accounting for the *transverse* bed slope effects on the bedload transport.

MORPHODYNAMICS MODULE

The Morphodynamic module concludes the full calculation cycle, as the information originating from the WAVE Module, FLOW Module and associated SUSpended Sediment Module & Bedload Transport Module are used here to make a prediction on the magnitude of the bed level adjustment in each time step for all *computational cells* in the computational domain. It should be noted that the quantity of the (suspended) sediment fractions is calculated for each half time step due to the upshifting procedure of the sediment transport point to the velocity point in the *ADI* method.

The bed level changes are calculated based on the contributions of the following sediment transport components:

- Suspended Sediment transport ΔS_{sus}
- Correction Factor for double counting suspended sediment ΔS_{cor}
- Bedload Transport ΔS_{bed}
- Morphological Acceleration Factor f_{MOR}

Morphological Acceleration Factor f_{MOR}

The morphological acceleration factor f_{MOR} is a measure that coastal modellers may apply to overcome the differences between (1) the temporal scale wherein the hydrodynamic development prevails and (2) the temporal scale wherein the morphodynamic adjustment sets about. The associated parameter f_{MOR} enables the modeller to arbitrarily extend the considered time step $\Delta t_{morphology}$ wherein the morphodynamic computations are proceeded with respect to the time step $\Delta t_{hydrodynamic}$ wherein the hydrodynamic development is computed - as may be seen in eq.(81) and proposed by Roelvink (2006). The advantage of such *accelerations* is that, in an efficient manner, long-term morphodynamic computations may be proceeded with just a fraction of the total set of hydrodynamic input data. Depending on the situation at hand (i.e. the location characteristics), there is a limitation in the extend at which the morphological changes may be *accelerated*. However, a sensible factor is solely to be found by means of sensitivity analysis and expert judgement. Numerical simulations based on morphological acceleration techniques are often provided with a Total Variation Diminishing *TVD* function - in Delft3D a Forrester Flux limiting Function - to prevent that the sediment availability at the bed becomes negative or zero (Lesser *et al.* (2004) & Roelvink (2006)).

$$\Delta t_{morphology} = f_{MOR} \Delta t_{hydrodynamics} \tag{81}$$

Suspended Sediment transport

The total change in bed sediment availability due to suspended sediment transport is defined as in eq.(82) below. Note that due to the *upwind shifting technique* in the *ADI* method, the computational time step Δt_{sus} of the suspended sediment transport is halved. Furthermore, the associated sinks and sources in the latter computations are found using the expressions eqs.(58) & (59).

$$\Delta S_{sus}^{(m,n)} = f_{MOR} \left(\underbrace{E^{(l)}}_{\text{Sinks}} - \underbrace{D^{(l)}}_{\text{Sources}} \right) \Delta t_{sus} \tag{82}$$

Correction Factor

The Delft3D FLOW module calculates the suspended sediment transport over the entire water column by means of eqs.(43), (60), (58) & (59). However van Rijn (1993) suggested that the suspended sediment transport below a certain height a above the bed (i.e. the reference height a) should no longer be counted for suspended sediment transport as in this layer the sediment particles appear to have frequent contact with the bed and should be therefore accounted as *bedload* transport.
The complication of the above is that the sediment transport is double counted in the reference layer where the bedload transport is calculated in the FLOW module. To overcome and prevent double counting of the sediment transport near the bed, the FLOW module approximates at each time step the suspended sediment transport in the reference layer by means of a 2^{nd} order central difference scheme. The results are written, as correction vectors $\vec{S_{cor,uu}}$ and $\vec{S_{cor,vv}}$ to a *communication file* that will be used in the MORPH Module to correct the nett calculated bed level change. The total correction in each *computational cell* with area $A^{(m,n)}$ is then defined by means of the spatial gradients of the correction vectors $\vec{S_{cor,uu}}$ & $\vec{S_{cor,vv}}$ as presented in eq.(83),

$$\Delta S_{cor}^{(\mathbf{m},\mathbf{n})} = f_{MOR} \left\{ \begin{array}{l} S_{cor,uu}^{(\mathbf{m-1}),\mathbf{n}} \Delta y^{(\mathbf{m-1}),\mathbf{n}} - S_{cor,uu}^{(\mathbf{m},\mathbf{n})} \Delta y^{(\mathbf{m},\mathbf{n})} + \\ S_{cor,vv}^{\mathbf{m},(\mathbf{n-1})} \Delta x^{\mathbf{m},(\mathbf{n-1})} - S_{cor,vv}^{(\mathbf{m},\mathbf{n})} \Delta x^{(\mathbf{m},\mathbf{n})} \end{array} \right\} \frac{\Delta t}{A^{(\mathbf{m},\mathbf{n})}} \tag{83}$$

Bedload Sediment transport

Changes in the sediment availability due bedload transport are calculated by application of eq.(84) below and the expressions for the bedload transport magnitudes under slope effects $S_{b,uu}$ eq.(78) and $S_{b,vv}$ eq.(79) respectively.

$$\Delta S_{bed}^{(\mathbf{m},\mathbf{n})} = f_{MOR} \left\{ \begin{array}{l} S_{b,uu}^{(\mathbf{m-1}),\mathbf{n}} \Delta y^{(\mathbf{m-1}),\mathbf{n}} - S_{b,uu}^{(\mathbf{m},\mathbf{n})} \Delta y^{(\mathbf{m},\mathbf{n})} + \\ S_{b,vv}^{\mathbf{m},(\mathbf{n-1})} \Delta x^{\mathbf{m},(\mathbf{n-1})} - S_{b,vv}^{(\mathbf{m},\mathbf{n})} \Delta x^{(\mathbf{m},\mathbf{n})} \end{array} \right\} \frac{\Delta t}{A^{(\mathbf{m},\mathbf{n})}} \tag{84}$$

Total Sediment Changes

Lastly, the total sediment change - for each fraction - at the bed as a response to the changes in the sediment availability due to (1) the suspended sediment transport and (2) the bedload transport follows from superposition of the latter effects as stated in eq.(85) which concludes the *computational procedure* applied in each *computational cycle*.

$$\Delta S_{tot}^{(\mathbf{m},\mathbf{n})} = \Delta S_{sus}^{(\mathbf{m},\mathbf{n})} + \Delta S_{cor}^{(\mathbf{m},\mathbf{n})} + \Delta S_{bed}^{(\mathbf{m},\mathbf{n})} \tag{85}$$

2.2 Finite Element Method - Swasêk Finel3D (Unstructured Grid)

This section is adopted on the work of Labeur and Wells (2007), Labeur (2009) & Dam *et al.* (2016)

A finite element method such as FINEL3D uses the three-dimensional (3D) Navier-Stokes (NS) equations for non-hydrostatic flows in the numerical computations of hydrodynamic flows (Labeur (2009)).

Governing Equations

system of equations

The system of equations used in the flow module is based on the TRIWAQ flow scheme and composed of (1) the momentum equations, (2) the continuity equation, (3) the transport equation for (suspended)

particles and (4) a turbulence closure model. Note that the setup of the governing equation is precisely the same as in the the Delft3D-4 model be it that the equations are written in vector form to compress the relevant information. One minor difference prevails itself in the notation of the momentum equation. Hereby, the vertical advection terms are connsidered in the vertical momentum equation as opposed to the Delft3d-4 hydrostatic solver which solves for hydrostatic flow and applies a separate non-hydrostatic solver to account for non-hydrostatic variations in the flow at location where this condition does not hold anymore.

- ***3D Momentum Equations (NS)*** [1]

$$\frac{\partial \rho \vec{\mathbf{u}}}{\partial t} + \nabla \cdot (\rho \vec{\mathbf{u}} \otimes \vec{\mathbf{u}}) + \nabla p - \nabla \cdot (2\mu \nabla^s \vec{\mathbf{u}}) = \vec{\mathbf{f}} \tag{86}$$

- ***Continuity Equation***

$$\frac{\partial \rho}{\partial t} + \vec{\mathbf{u}} \cdot \nabla \rho = 0 \tag{87}$$

- ***Transport Equation for waterborne substances***
  wherein the transport is considered for each fraction $\varphi_i = \frac{\rho_i}{\rho}$ *individually.*

$$\frac{\partial \varphi_i}{\partial t} + \vec{\mathbf{u}} \cdot \nabla \varphi_i - \nabla \cdot (\kappa_V \nabla \varphi_i) = \vec{\mathbf{f}}_i \tag{88}$$

- ***An Appropriate Turbulence Closure Model***
  to relate the smaller scale turbulent motion with the turbulent motion at the scale of the mean flow by application of the Boussinesq hypothesis (i.e. $\kappa - \varepsilon$ *model).*

FINEL 3D Solution Procedure

The finite element method in FINEL3D as proposed by Labeur (2009) uses a combination of a continuous and discontinuous Galerkin method to discretise the computational domain. The Galerkin method is a numerical method that converts (i.e. discretises) continuous operators - such as basis equations - to discrete sets of operators which describe the state of the flow for each *computational element*. The discretised sets of operators are here characterised by a weak formulation of the smoothness criteria of the equation.
Hence, the ***continuous*** Galerkin method approximates the set of operators eqs.(86), (87) & (88) by means of a *continuous* function space, whereas the ***discontinuous*** Galerkin method approximates the set of operators by means of a *discontinuous/broken* function space. In the case of the ***discontinuous*** Galerkin method it is suggested in Labeur (2009) that weaker continuity requirements may constitute more accurate solutions.

Spatial Discretisation - Computational Domain

The discretisation process for a finite element model, starts with the definition of the computational domain and the associated boundaries. To this end, the computational domain Ω is sectioned in element spaces Ω_e with local boundaries Γ_e.
For the piecewise defined functions describing the flow state in each element, a function space $\mathbf{V}$ is considered containing functions $\vec{v}$ which depend on the flow variables $\vec{u}$. Hence $\vec{v} \subseteq \mathbf{V}$.
The boundary is given by a *boundary function* Γ for which at an arbitrary section of an element boundary - denoted by Γ_g - the boundary condition is set,

$$L^2(\Omega, \Gamma_g) = \left\{ u \subseteq L^2(\Omega) : u = \mathrm{g} \text{ on } \Gamma_g \subset \partial\Omega \right\}. \tag{89}$$

[1] Note that $\otimes$ describes the tensor product of two tensors which is the multiplication of the scalar components of first vector $\rho\vec{u}$ x the second vector $\vec{\mathbf{u}}$ (i.e. $\rho u \begin{pmatrix} u \\ v \end{pmatrix}$ and $\rho v \begin{pmatrix} u \\ v \end{pmatrix}$)

Otherwise stated, $u_i = g_i$ is enforced at each arbitrary section of the element boundary Γ_g. In between the element boundaries - where the element space $\tilde{\Omega}_e$ is defined for element Ω_e - the discretised functions in the function space $\vec{v} \subseteq \mathbf{V}$ are defined as such that variation in the quantities of the unknown variables is possible.
A weak formulation of the exact problem (eqs.(86), (87) & (88)) arises when instead of the exact problem (solving for the exact quantities u_n), the *discretised* problem is solved (for the element values u_e).
The obtained error between the exact solution u_n and the value in the discretised element u_e is characterised by the *Galerkin Orthogonality Principle* which states that (1) the error between the two variables following from a minimisation problem of an arbitrary functional[2] - the variational formulation - should equal zero,

$$\int_{\Omega} \left(\vec{e_n} - \nabla e_\phi\right) \cdot \vec{v}\, d\Omega = 0, \qquad \forall \vec{v} \subseteq \mathbf{V} \tag{90}$$

And (2) that the error following from the discretisation of the exact formulations to the discrete formulations should constitute conservation, viz. for a potential flow problem.

$$\int_{\Omega} \nabla \cdot \vec{e}_u q\, d\Omega - \int_{\Gamma_h} \vec{e_n} \cdot \vec{n} q\, d\Gamma = 0, \qquad \forall q \subseteq Q \tag{91}$$

wherein:

- Q is equal to the set of non-trivial functions q ($q \subseteq Q$) - the basis functions
- $\vec{e_u}$ is the discrete error vector equal to the difference between the actual value and the discrete value

$$\vec{e_u} = u_n - u_e$$

- ∇e_ϕ is the discrete error vector (gradient) equal to the difference between the actual velocity potential and the velocity potential of the discrete set of equations

$$\nabla e_\phi = \nabla(\phi_n - \phi_e)$$

Consequently, given a proper selection of discretised functions in function space $\mathbf{V}$ and non-trivial solution space Q, the discrete solution converges to the exact solution if the *LBB* condition (here below) is met,

$$\sup_{\vec{v} \subseteq \mathbf{V}} \frac{(\nabla q, \vec{v})}{\|\vec{v}\|_2} \geq \gamma \|\nabla q\|_2 \qquad \forall q \subseteq Q \tag{92}$$

Herein is γ the mesh-independent constant ($geq0$) which suggests an higher resolution of the computational grid for an arbitrary problem statement.

Spatial Discretisation - Galerkin Continuous Method

The spatial discretisation of the computational domain in discrete elements also involves a discretisation of the governing equation for the respective elements. This may be proceeded with the *Continuous Galerkin Method*. In the Continuous Galerkin Method, the governing equations are approximated as piecewise defined continuous functions $\vec{v}$ in each element Ω_e. The flow field in the computational domain is, thereby, characterised by a *continuous* representation of the flow variables (i.e. velocity potential ϕ). As proposed by Labeur (2009), geophysical flows can be solved by means of the *variational principle*. This method considers small deviations in the functions and functionals [3] $\vec{v} \subseteq \mathbf{V}$ and aims to

[2] for a set of variables describing the flow, the smallest value is sough after to solve for the functionals of the flow such as the total turbulent kinetic energy, potential energy, pressure, etc.
[3] mathematical description of underlying variables used to define the functions in $\mathbf{V}$

find a function that minimises the functional describing the flow (i.e. flow state variables).
For a potential flow, the variational problem may be defined is,

$$\int_{\Omega} (\vec{u} - \nabla\phi) \cdot \vec{v}\, d\Omega + \int_{\Omega} (\nabla \cdot \vec{u} - f)\, q\, d\Omega - \int_{\Gamma_h} (\vec{u} \cdot \vec{n} - h)\, q\, d\Gamma = 0 \qquad \forall\ \vec{v} \subseteq \mathbf{V}\ \&\ \forall\ q \subseteq \mathbf{Q} \tag{93}$$

where the first two terms describe the fluxes over the boundary $d\Omega$ and the last term describes the net transport at the boundary $d\Gamma$. This may be further reduced if $\vec{u} = \nabla\phi$ is substituted in eq.(93),

$$\int_{\Omega} \left(\nabla^2\phi - f\right) q\, d\Omega - \int_{\Gamma_h} (\nabla\phi \cdot \vec{n} - h)\, q\, d\Gamma = 0 \qquad \forall\ q \subseteq \mathbf{Q} \tag{94}$$

The error that this discrete formulation produces with respect to the exact solution may be found by means of construction of the minimisation problem for some functional J, describing the potential flow.

$$\min_{\phi \subseteq Q_g} J = \int_{\tilde{\Omega}} \frac{1}{2} \nabla\phi \cdot \nabla\phi\, d\Omega + \int_{\tilde{\Omega}} f\phi\, d\Omega - \int_{\Gamma_h} h\phi\, d\Gamma \tag{95}$$

A comparison between the functional of the exact solution and the functional obtained from the discrete solution reveals an associated remainder (i.e. error) resulting from such discretisation.

$$J(\phi) - J(\phi_e) = \int_{\tilde{\Omega}} \frac{1}{2} \nabla e \cdot \nabla e\, d\Omega \tag{96}$$

Considering solely minimised equations, the latter would entail that for every function space the error as described in eq.(96) are minimised. An approximation of this error is given by Labeur (2009) and may be computed by forehand using the equation below,

$$\|e\|_m \leq C h_e^{k+1-m} \|\phi\|_{k+1} \tag{97}$$

wherein:

- C is constant depending on the shape of the elements
- h_e is a factor related to the size of the element,

$$h_e = diag(\Omega_e)$$

- ϕ is the velocity potential
- m is the order of the norm
- k is the order of the (discretisation) polynomial

For *variables* described by a L^2 norm an error may be found, given $k = 1$ & $m = 2$,

$$\|e\|_2 \leq C h_e^2 \left\| \nabla^2\phi \right\|_2 \tag{98}$$

For *partial derivatives* described by a H^1 norm an error may be found, given $k = 1$ & $m = 1$,

$$\|e\|_1 \leq C h_e \left\| \nabla^2\phi \right\|_2 \tag{99}$$

Spatial Discretisation - Galerkin Discontinuous Method

When the governing equations are discretised by application of the Galerkin Discontinuous method the functions in the function space **V** describing the flow are approximated by means of *broken* function spaces. Hereby, the broken function spaces are allowed to be discontinuous at the boundaries of the elements. At the boundary, an interface function is described to prescribe the local transport over the boundary (i.e. Neumann Boundary condition, Direchlet boundary). Consequently, the number of unknown variables and the amount of degrees of freedom are larger than in the case of a Continuous Galerkin method - which may constitute more intensive computations. Strict boundary conditions should be sufficiently smooth such that the derivatives at the boundary exist. In the Discontinuous Galerkin method a weaker formulation is adopted for the boundary condition giving the method added advantages when dealing with *advection-diffusion problems*. If the DG method for the potential flow is considered (as example), the variational problem may be defined for interface functions $\overline{\phi}$ & $\vec{\overline{u}}$ and the in-the-element-space-defined velocity potential ϕ, viz.

$$\int_{\tilde{\Omega}} \vec{u} \cdot \vec{v}\, d\Omega + \int_{\tilde{\Omega}} \phi \nabla \cdot \vec{v}\, d\Omega - \sum_e \int_{\partial\Omega_e} \overline{\phi}\vec{n} \cdot \vec{v}\, d\Gamma \\ - \int_{\overline{\Omega}} \vec{u} \cdot \nabla q\, d\Omega + \sum_e \int_{\partial\Omega_e} \vec{u} \cdot \vec{n} q d\Gamma - \int_{\tilde{\Omega}} f q\, d\Omega = 0 \qquad \forall\, \vec{v} \subseteq \mathbf{V}\ \&\ \forall\, q \subseteq \mathbf{Q} \quad (100)$$

The variational problem may be further reduced by substitution of the velocity potential description in eq.(100) resulting in,

$$\int_{\tilde{\Omega}} \nabla\phi \cdot \nabla q\, d\Omega + \sum_e \int_{\partial\Omega_e} \left(\overline{\phi} - \phi\right) \vec{n} \cdot \nabla q\, d\Gamma \\ - \sum_e \int_{\partial\Omega_e} \vec{\overline{u}} \cdot \vec{n} q d\Gamma + \int_{\tilde{\Omega}} f q\, d\Omega = 0 \qquad \forall\, q \subseteq \mathbf{Q} \quad (101)$$

Linking the interface variables to the local element spaces, and guaranteeing consistency and conservation of the variational problem by means of an *interior penalty method* prescribing,

$$\overline{\phi} = \{\phi\} \qquad \vec{\overline{u}} = \{\nabla\phi\} - \frac{\alpha}{h_e} \|\phi\| \quad (102)$$

A threshold parameter α prevails for which the penalty holds. The importance of this penalty parameter becomes evident when the minimisation problem of the DG-IP method is evaluated as done in eq. (103) below.

$$\min_{\phi \subseteq Q_g} J(\phi) - J(\phi_e) = \min_{\phi \subseteq Q_g} \int_{\tilde{\Omega}} \frac{1}{2} \nabla e_\phi \cdot \nabla e_\phi\, d\Omega - \int_{\tilde{\Gamma}} \|e_\phi\| \cdot \{\nabla e_\phi\}\, d\Gamma + \int_{\tilde{\Gamma}} \frac{1}{2} \frac{\alpha}{h_e} \|e_\phi\| \cdot \|e_\phi\|\, d\Gamma \quad (103)$$

Here, it may be seen that the third term of the minimisation problem prohibits the error functional of becoming negative. For constant values of α the convergence of the created error reduces to the error obtained when applying a Continuous Galerkin Method eq.(97),(98) & (99).

Notice the difference between the error functional of the CG method and the functional of the DG method. The DG shows extra terms to ensure non-negative errors.

$$\min_{\phi \subseteq Q_g} J(\phi) - J(\phi_e) = \min_{\phi \subseteq Q_g} \int_{\tilde{\Omega}} \frac{1}{2} \nabla e_\phi \cdot \nabla e_\phi\, d\Omega$$

$$\min_{\phi \subseteq Q_g} J(\phi) - J(\phi_e) = \min_{\phi \subseteq Q_g} \int_{\tilde{\Omega}} \frac{1}{2} \nabla e_\phi \cdot \nabla e_\phi\, d\Omega - \int_{\tilde{\Gamma}} \|e_\phi\| \cdot \{\nabla e_\phi\}\, d\Gamma + \int_{\tilde{\Gamma}} \frac{1}{2} \frac{\alpha}{h_e} \|e_\phi\| \cdot \|e_\phi\|\, d\Gamma$$

Spatial Discretisation - Galerkin Interface Stabilisation Method

The *Galerkin Interface Stabilisation Method* proposed by Labeur (2009) - shorthand GIS method - is the confluence of the *continuous* and *discontinuous* Galerkin methods. The starting point is the Discontinuous Galerkin method wherein the interface function $\overline{\phi}$ and interface flux $\overline{\mathbf{u}}$ are defined as functions of the element space. The latter comprises the presence of relatively more degrees of freedom at the boundaries of the element spaces than in the case of the CG-method. Therefore, to overcome the abundance of computational point at the boundary - while having the attractive characteristics of the DG-method - the GIS-method is defined. The interface fluxes $\mathbf{u}$ are defined in terms of the interface functions $\overline{\phi}$ to reduce the degrees of freedom to the level considered in the continuous Galerkin method. Consequently, the GIS-method is characterised by its computational efficiency (i.e. degrees of freedom) while pertaining the interesting properties of the DG-method (i.e. interior penalty parameter α at the boundary enables stabilisation of the flow and reduces the generation of artificial dissipation).

To this end, if the GIS method for potential flow is considered, the variational problem may be defined for the interface functions $\overline{\phi}$ - which are independent of the local element spaces (i.e. the neighbouring elements) - and the interface fluxes $\vec{\overline{u}}$ as stated in eq.(104).

$$\int_{\tilde{\Omega}} \nabla\phi \cdot \nabla q \, d\Omega + \sum_e \int_{\partial\Omega_e} (\overline{\phi} - \phi)\, \vec{n} \cdot \nabla q \, d\Gamma + \sum_e \int_{\partial\Omega_e} \nabla\phi \cdot \vec{n}(\overline{q} - q) d\Gamma + \sum_e \int_{\partial\Omega_e} \frac{\alpha}{h_e}(\overline{\phi} - \phi)(\overline{q} - q)\, d\Gamma + \int_{\tilde{\Omega}} f q \, d\Omega = \int_{\Gamma_h} h\overline{q}\, d\Gamma \qquad \forall\, q \subseteq \mathbf{Q},\ \forall\, \overline{q} \subseteq \overline{\mathbf{Q}} \tag{104}$$

Using the relation of the interface fluxes which are related to the interface functions and the particular variables describing the flow in the neighbouring elements,

$$\overline{\phi} = \{\nabla\phi\} \qquad \overline{\mathbf{u}} = \{\nabla\phi\} + \frac{\alpha}{h_e}\left(\overline{\phi} - \phi\right)\mathbf{n} \tag{105}$$

for $\overline{q} = 0$ a set of local problems Ω_e prevails - in almost resemblance with the DG-method - for which the following minimisation problem holds,

$$\min_{\phi \subseteq Q_g} J = \min_{\phi \subseteq Q_g} \int_{\tilde{\Omega}} \frac{1}{2} \nabla e_\phi \cdot \nabla e_\phi \, d\Omega + \sum_e \int_{\partial\Gamma_e} (\overline{\phi} - \phi)\vec{n} \cdot \nabla\phi \, d\Gamma + \sum_e \int_{\partial\Gamma_e} \frac{1}{2}\frac{\alpha}{h_e}(\overline{\phi} - \phi)^2 \, d\Gamma + \int_{\tilde{\Omega}} f\phi \, d\Omega - \int_{\Gamma_h} h\overline{\phi}\, d\Gamma \tag{106}$$

The variational form and the minimisation problem attests to have the similar form as the CG-method while being supplemented with terms from the DG-method accounting for the properties of the discontinuous Galerkin Method that inherently stabilise discretised equations (i.e. the presence of stabilisation term α). This combination will serve the computations of advection-diffusion problems.

Time Integration Method

For the time integration using a finite element method, the dimension of the space must be considered. The element spaces Ω_e in the computational domain create a 2D/3D space - depending on the modelling approach - such that time integration over the respective element would increase the dimension of the solution space $\mathbf{V}$. The latter has significant consequences on the computational performance of the time integration procedure and subsequent calculations. Therefore, a sequential procedure is considered wherein:

- **First, the time integration is proceeded over the entire computational domain:**
  Take as example the temporal gradient of the velocity potential,

$$\frac{\partial\phi}{\partial t} u$$

Time integration over a time domain I with time element spaces I_n for each time step $\Delta t = N/n$ yields,

$$\frac{\phi_{n+\theta} - \phi_n}{\theta \Delta t} u$$

depending on the θ-method assigned for time integration, i.e. $\theta \in \left[\frac{1}{2}, 1\right]$.

- **Next, the discretisation is proceeded accounting for the partitioning of the computational domain in element spaces Ω_e:**

$$\int_\Omega \frac{\phi_{n+\theta} - \phi_n}{\theta \Delta t} u d\Omega$$

- **Lastly, the solution at time level $n+1$ is found by application of a forward Euler step,**

$$\phi_{n+1} = \phi_n + \frac{\phi_{n+\theta} - \phi_n}{\theta}$$

An application of the θ-method that combines that properties of the Crank-Nicholson method and the Implicit Euler - 2^{nd} order accurate solutions and unconditional stability - is the fractional time stepping method. In this method, the sequential time stepping procedure is split in three sub-time steps per time level. That is, a time stepping from $t_n \rightarrow t_{n+1}$ is split in substeps $\mathbf{t_n} \rightarrow t_{n+\alpha} \rightarrow t_{n+(1-\alpha)} \rightarrow \mathbf{t_{n+1}}$ for $\alpha = 1 - \frac{1}{\sqrt{2}}$. The stepping procedure ensures higher accuracy while pertaining strong stability.

Sediment transport

Firstly, it should be noted that the 3D-implementation of the sediment transport and the morphology module in FINEL3D is currently not operational. Nevertheless, the applied mathematical solution procedure is in line with Labeur (2009).

In the analogy of the variational problem of the potential flow, the sediment transport (i.e. suspended sediment, dissolved sediment transport) is described - in close resemblance with eq.(88) - as,

$$\frac{\partial \varphi}{\partial t} + \nabla \cdot \vec{\sigma} = f \qquad \text{with} , \quad \vec{\sigma} = \vec{\mathbf{a}} \phi - \kappa \nabla \phi \tag{107}$$

wherein:

- φ: represents the mass fraction of the transported sediment parcel l (ρ^l / ρ)
- $\vec{\sigma}$: represents the associated advection and diffusion of the transported sediment parcels
- $\mathbf{a}$: represents the acceleration of the flow

The variational problem for the sediment transport is then defined as given in eq.(108),

$$\int_{\tilde{\Omega}} \frac{\partial \varphi}{\partial t} v \, d\Omega - \int_{\tilde{\Omega}} \vec{\sigma} \cdot \nabla v \, d\Omega + \sum_e \int_{\partial \Omega_e} \vec{\bar{\sigma}} \cdot \vec{n} v \, d\Gamma + \sum_e \int_{\partial \Omega_e} \kappa \left(\overline{\varphi} - \varphi \right) \vec{n} \cdot \vec{w} d\Gamma$$
$$= \int_{\tilde{\Omega}} f v \, d\Omega \qquad \forall \, v \subseteq \mathbf{V} \;\; \& \;\; \forall \, w \subseteq \mathbf{W} \tag{108}$$

wherein:

- v: represents the discretised functions describing the flow state in the element spaces Ω_e and is part of the function space $\mathbf{V}$
- w: represents the flux at the element interfaces Γ_e and is part of the interface space $\mathbf{W}$

To obtain the variation problem for the Galerkin Interface Stabilisation Method (GIS), the Neumann boundary condition is substituted which, results in the following equation

$$\int_{\tilde{\Omega}} \frac{\partial \varphi}{\partial t} v \, d\Omega - \int_{\tilde{\Omega}} \vec{\sigma} \cdot \nabla v \, d\Omega - \sum_e \int_{\partial\Omega_e} \vec{\bar{\sigma}} \cdot \vec{n} (\bar{v} - v) \, d\Gamma + \sum_e \int_{\partial\Omega_e} \kappa \, (\bar{\varphi} - \varphi) \, \vec{n} \cdot \nabla v d\Gamma$$
$$+ \int_{\Gamma_h} (1-\gamma) \vec{a} \cdot \vec{n} \bar{\phi} \bar{v} \, d\Gamma = \int_{\tilde{\Omega}} f v \, d\Omega - \int_{\Gamma_h} h \bar{v} \, d\Gamma \qquad \forall \, v \subseteq \mathbf{V} \;\; \& \;\; \forall \, \bar{v} \subseteq \overline{\mathbf{V}} \tag{109}$$

Schematisation of the morphological model in 2DH mode - FINEL2D

In the 2DH depth-averaged shallow water flow models as used in FINEL2D, the following momentum equations and continuity equations are considered,

$$\frac{\partial h}{\partial t} + \frac{\partial uD}{\partial x} + \frac{\partial vD}{\partial y} = 0 \tag{110}$$

$$\frac{Du}{\partial t} + \frac{Du^2}{\partial x} + \frac{Duv}{\partial y} - f_c Dv + gD\frac{\partial h}{\partial x} - \frac{1}{\rho}\tau_{x,b} + \frac{1}{\rho}\tau_{x,w} + \frac{1}{\rho}\tau_{x,r} = 0 \tag{111}$$

$$\frac{Dv}{\partial t} + \frac{Duv}{\partial x} + \frac{Dv^2}{\partial y} + f_c Du + gD\frac{\partial h}{\partial y} - \frac{1}{\rho}\tau_{x,b} + \frac{1}{\rho}\tau_{x,w} + \frac{1}{\rho}\tau_{x,r} = 0 \tag{112}$$

wherein is considered:

- D: The water depth
- f_c: which represents the coriolis force
- τ_b: The bed shear stress
- τ_w: The wave-induced bed shear stress
- τ_r: The wave-induced Radiation stresses

The solution method considered is the Discontinuous Galerkin method as shown in eqs.(100) & (103)
In line with the system of equations describing the 2DH (depth-averaged) flow as stated in eqs.(110),(111) & (112) the latter system may be converted in a matrix-vector problem which is shown in eq. (113) below,

$$\frac{\partial \mathbf{U}}{\partial t} + \nabla \cdot \mathbf{F} = \mathbf{H} \tag{113}$$

Wherein is considered:

- **U**: which is the inertial vector representing the accretion and/or regression of mass and momentum in the element space

$$\mathbf{U} = \begin{pmatrix} h \\ uD \\ vD \end{pmatrix} \tag{114}$$

- **F**: which is the advective flux tensor and describes the flux of mass and momentum over the boundaries of the element space

$$\mathbf{F} = \begin{pmatrix} uD & vD \\ u^2D + \frac{1}{2}gh^2 & uvD \\ uvD & v^2D + \frac{1}{2}gh^2 \end{pmatrix} \tag{115}$$

- **H**: which is the force tensor and represents the excitation of the system as a consequence to external forces

$$\mathbf{H} = \begin{pmatrix} 0 \\ \frac{1}{\rho}\tau_{x,tot} + f_c v D - g D i_{b,x} \\ \frac{1}{\rho}\tau_{y,tot} - f_c u D - g D i_{b,y} \end{pmatrix} \tag{116}$$

Time integration and spatial discretisation of the latter system of equations entails,

$$\frac{d}{dt}\int_{\Omega_e} \mathbf{U} d\Omega + \int_{\Gamma_e} \mathbf{F}\ \mathbf{n}\, d\Gamma = \int_{\Omega_e} \mathbf{H}\, d\Omega \tag{117}$$

Taking into consideration that the Discontinuous Galkerkin method is applied in combination with a θ-time integration method this would involve the following problem,

$$\int_{\Omega_e} \frac{\mathbf{U}_{n+\theta} - \mathbf{U}_n}{\theta \Delta t} d\Omega + \int_{\Gamma_e} \mathbf{F}\ \mathbf{n}\, d\Gamma = \int_{\Omega_e} \mathbf{H}\, d\Omega \quad \text{with,} \quad \theta \in \left[\frac{1}{2}, 1\right] \tag{118}$$

Sediment transport and Bed Level Changes

For the sediment transport, a total transport formulation is considered in line with the work of Engelund and Hansen (1967). The formulation considers the transport of sediment and does not discriminate between suspended and bedload transport. Thereby should be noted that this formulation also omits the presence of wave-driven sediment transport (see also Figure (4)). As such the bed level changes are defined using the Exner equation,

$$\frac{\partial z_b}{\partial t} + \frac{\partial q_x}{\partial x} + \frac{\partial q_y}{\partial y} = 0 \tag{119}$$

wherein:

- q_x: represents the total sediment transport in x-direction

$$q_x = S * \cos\alpha$$

- q_y: represents the total sediment transport in y-direction

$$q_y = S * \sin\alpha$$

- S: represents the equilibrium transport which quantity depends on the sediment transport formulation chosen. The sediment transport as proposed by Engelund and Hansen (1967) is hereby defined as,

$$S = m u^n \quad \text{with,} \quad n = 3 \rightarrow EH \tag{120}$$

- z_b: represents the bed level aggradation or degredation in time

Suspended transport

The suspended transport in 2DH (depth-averaged) form may be described as follows,

$$D\left(\frac{\partial c}{\partial t} + u\frac{\partial c}{\partial x} + v\frac{\partial c}{\partial y}\right) = \frac{1}{T_A}\left[c_e(t) - c(t)\right] \tag{121}$$

wherein is considered:

- c: The suspended sediment concentration in the water column

- c_e: The (theoretical) equilibrium concentration in the water column which could be defined as function of the equilibrium transport S if the conveyed sediment parcels are predominantly in suspension. Hence, by application of the work of (Galappatti and Vreugdenhil (1983)) the following expression is adopted in the 2DH model,

$$c_e = \frac{S}{D\sqrt{u^2 + v^2}} \tag{122}$$

- D: The water depth
- T_A: is the time scale of settlement of the suspended sediment particle

Energy Dissipation

Lastly, the energy dissipation is considered in the FINEL2D model. Here, the total energy dissipation is computed per element Ω_e over a fortnightly period and subsequently summed to obtain a gross quantity of dissipation of the entire computational domain,

$$\sum_{\Omega_e} P_e = \sum_{\Omega_e} \sum_{t}^{14dys} c_w \rho_w |u|^3 A_{\Omega_e} \quad \forall t \in \{15min, 30min, 45min, ..., N = 14dys\} \tag{123}$$

wherein:

- P_e: represents the energy dissipation in each element Ω_e
- c_w: is the friction coefficient accounting for the gross effect of frictional forces in the flow
- A: represents the surface area of each element Ω_e

The time resolution within the spring-neap cycle is 15 minutes.

3 CASE STUDIES - NUMERICAL EXAMPLES

In this chapters, several case studies will be reviewed in order to get a better understanding in the practical influence on model decisions to the overarching model results. In this regard, closer look will be given to:

- Location-specific and Environmental conditions
- The scope of project and the model setup
  - Input reduction methods (i.e. clever statement of the high-frequency data in representative forcing conditions to increase the efficiency of the model)
  - Model reduction methods (i.e. what processes are considered to mimic the real morphodynamic behaviour)
- The results
- The skill and performance of the model

3.1 Case Study - Western Scheldt Estuary - *Dam et al. 2016*

This section elaborates on the findings of Dam et al. (2016) on the long-term morphodynamic activity of the Western Scheldt Estuary by means of a 2DH morphodynamic model.

Western Scheldt

The Western Scheldt Estuary (Figure 5) is a mesoscale tide-dominated coastal system acquiring a length of 50 kilometres and a width of 5 kilometres Dam *et al.* (2016). It is located in Zeeland at the southwest region of the Netherlands and is a subregion of the greater Scheldt Estuary which finds its origin also partially in Belgium. The Estuary is comprised of various braiding channels which migrates freely between the embankments of the system. Periodic cut-offs and reconnections are apparent creating oxbow lakes and connections between secondary channels. Hence, the Western Scheldt Estuary is a multichannel system with distinct ebb- and flood-channels. The Western Scheldt forms the entrance channel to the Port of Antwerp. Hence, an extensive collection of over a century of bed level data is available for the study of the morphodynamic adjustment of the Western Estuary. The Estuary is comprised of erosion-resistant layers in the form of clay and peat layers - some are located at the bed surface, some are embedded. The river inflow and fluvial transport to the Western Scheldt Estuary is rather nil as is comprised only 0.6% of the tidal prism. Negligible stratification is thereby observed in the system as the flow is predominantly well-mixed.

Historic overview of Estuary and its Anthropogenic Adjustments

The Estuary find its origin in the early Middle Ages when the tidal inlet *Honte* connected to the Scheldt River Dam *et al.* (2016). Due to human interventions (i.e. flooding and deliberate inundation) the system perished in surface area, primarily as a consequence to retreat of the intertidal flats (Table 1). The latter saw a drastic change over the course of the 17^{th} century onwards to the late 20^{th} centuries (see Table 2).

In the 17^{th} century the Western Scheldt had the largest (natural) extend with free reigning secondary/side channels, braiding main channels as well as fast connections with the Eastern Scheldt

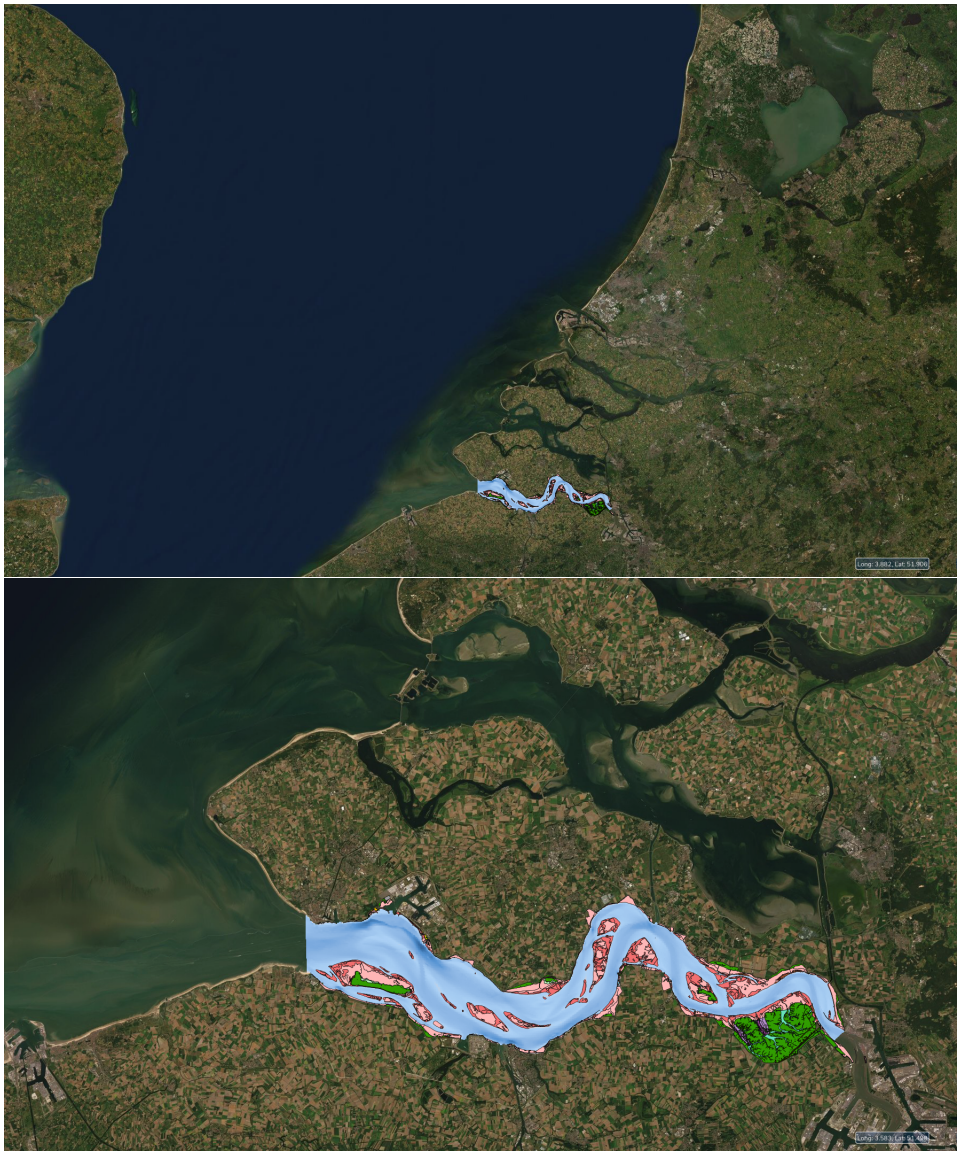

Figure 5: Bathymetry (based on 2019 data) and (based on 2018 data) geomorphological map superposed on an ESRI Worldimagery topography Scheldemonitor

Decrease of Surface Area of Western Scheldt due to Land Reclamation (in m^2)		
1650	$\rightarrow$	$410km^2$
> 1970	$\rightarrow$	$323km^2$

Table 1: System area in the period of 1600 - 1970 (Dam *et al.* (2016))

Decrease of Intertidal Storage Area due to Land Reclamation (in m^2)		
1650	$\rightarrow$	$295km^2$
1800	$\rightarrow$	$196km^2$
> 1970	$\rightarrow$	$104km^2$

Table 2: Intertidal Storage area in the period of 1600 - 1970 (Dam *et al.* (2016))

Estuary. These side channels silted up later due to large mud deposits after which was chosen that these channels had to be dammed. The faith of the connections was thereby largely correlated resulting in the siltation and closure of the connections between the Eastern and Western Scheldt Estuary over the course of 1867 - 1871.

After the 19^{th} century - around 1860 - the braiding channel patterns were still quite evident prevailing traces of (1) main channel migration and (2) shoal deposition & erosion cycles. Thereby, secondary channels were issued periodically as well as the cut-off of the latter channels. It is apparent that the system did not found itself in an equilibrium condition in 1860 Dam *et al.* (2016). Starting from 1970, the main channels were deepened by means of perpetual dredging works in order to maintain the navigability of the Western Scheldt for maritime ships.

Considering the more or less constant external forcing - given that (1) the tidal forcing appeared to be rather constant and (2) the absolute sea level rise was rather limited (15 cm/ century) - the large changes in morphodynamic activity over the course of 1860 - 1970 could be only ascribed to the anthropogenic interventions which changed the system area drastically. This issued the morphodynamic adjustment process of the Western Scheldt Estuary to a new equilibrium condition. As a consequence of negative feedback processes, it may be argued that - in an attempt to reduce the channel length and the associated amount of energy dissipation by bed friction - the system is marching towards a planform wherein the energy dissipation is minimised.

Model Assumptions

In this research performed by Dam *et al.* (2016), the objective was:

- to measure the performance of morphodynamic process-based models in a relatively **undisturbed** system as the skill of the latter is currently not comprehensively understood.
  - **The analysis is limited to a period onto 1970**
    This means that the natural behaviour of the system is aimed to be modelled whilst omitting the effect of large changes in the sediment availability due to human interventions (i.e. dredging works).
- Thereby, the skill of the model on a centennial time span is investigated.
  - A cut-off is made in the simulation period, reviewing the 1860 - 1970 period initially.
  - Afterwards, the model performance is considered on a centennial time span onwards to 2110.
- The bathymetry of 1871 is used as initial condition (i.e. starting point) for the numerical simulations encompassing the time span of 1860 - 1970. It is hypothesized in this report that this procedure is undertaken in light of the recent siltation of the connections to the Eastern Scheldt which ended around 1871, thereby considering the natural response of the Western Scheldt Estuary solely.
- Only sand fractions are considered given the interest of Dam *et al.* (2016) to the main morphodynamic adjustment of the estuarine bed - which is comprised of fine sand primarily.
- An absolute sea level rise of 15 centimetres per century is included in the simulations.

Model Setup

The following aspects where considered in schematisation of the Western Scheldt Estuary:

Numerical Model - FINEL2D

A 2DH depth-averaged process-based (morphodynamic) model is acquired for this research. The description of the physical processes is in line with the proceedings reviewed in chapter 2:

- *Representation of a 2DH Flow model: eqs.* (113) ,(114), (116) & (115)
- *Representation of the fine sediment transport: eqs.* (121) & (120)
- *Representation of the energy dissipation due to bed friction: eq.* (123)

Physical Processes

- The astronomical tide is schematised by means of a representative morphological tide obeying a wave period of approximately one year (365.31 days).
- Fresh water inflow from the upstream rivers is included in the model, be it that the inflow does not cater any significant stratification (i.e. the inflow amounts to approximately 0.6 % of the tidal prism).
- Spiral flow is included and parameterised to account for the curvature in the current and subsequent sediment transport direction.
- Waves are not included the computations.

Computational Domain

The computational domain comprises an area of approximately 80 km x 40 km. This area is partitioned in triangular elements which change in element size from 1.1 ha in the North Sea to 2.5 km^2 in the Western Scheldt Estuary. Figure 6 gives an overview of the grid composition.

Sediment Transport

- The equilibrium bulk transport formulation of Engelund and Hansen (1967) is applied.
- Only fine sand fractions are considered to predict the planform changes of the estuarine system.
- No mud fractions are included in the computations since mud is mostly found at the intertidal flats of the estuary and thereby does not cater large changes in the planform of the main channel.

Initial Condition

- An initial bathymetry is composed based on the bathymetric dataset available from 1871.
- Erosion-resistant layers are hereby included in the model (see Figure 7).

Boundary Conditions

- **A constant annual river discharge is considered at the eastern boundary of the estuary over the simulation time span, viz.**
  - A boundary condition representing the discharge of the Scheldt river (and tributaries) into the Western Scheldt Estuary is amounted to 50 m^3/s in the summer period.
  - A boundary condition representing the discharge of the Scheldt river (and tributaries) into the Western Scheldt Estuary is amounted to 180 m^3/s in the winter period.
- **Nested Grid & Boundary conditions**
  The sea boundary is placed at a distance of 40 kilometres away from the adjacent coastline such that the wave and tidal conditions could be adopted from existing models (Dam *et al.* (2008)) - The North Sea basin model.

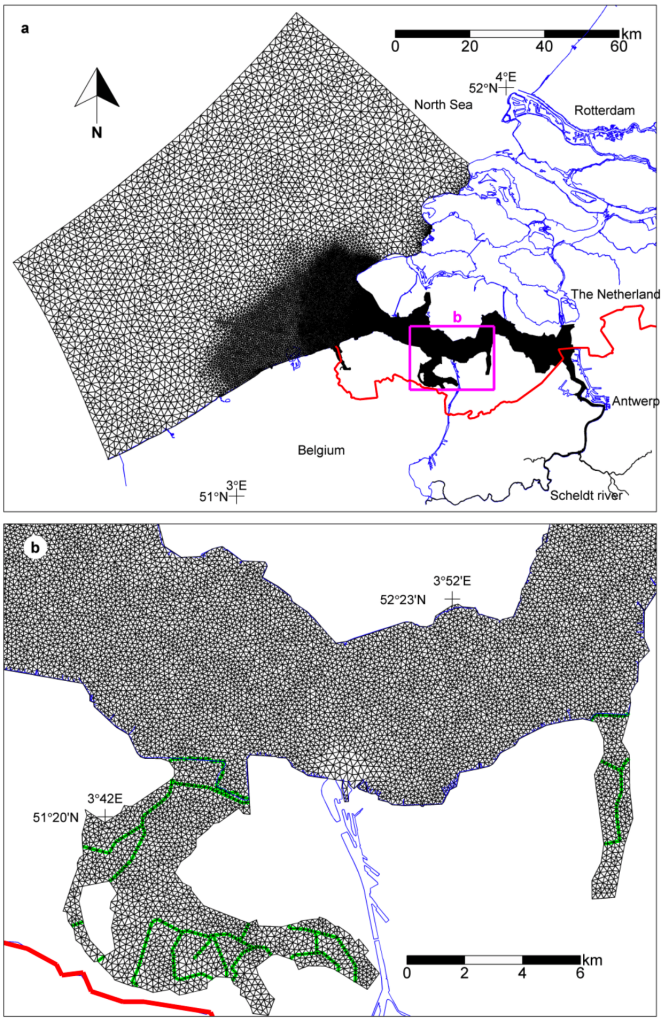

Figure 6: Figure(S1): Computational Mesh of FINEL2D model. (From Dam *et al.* (2016))

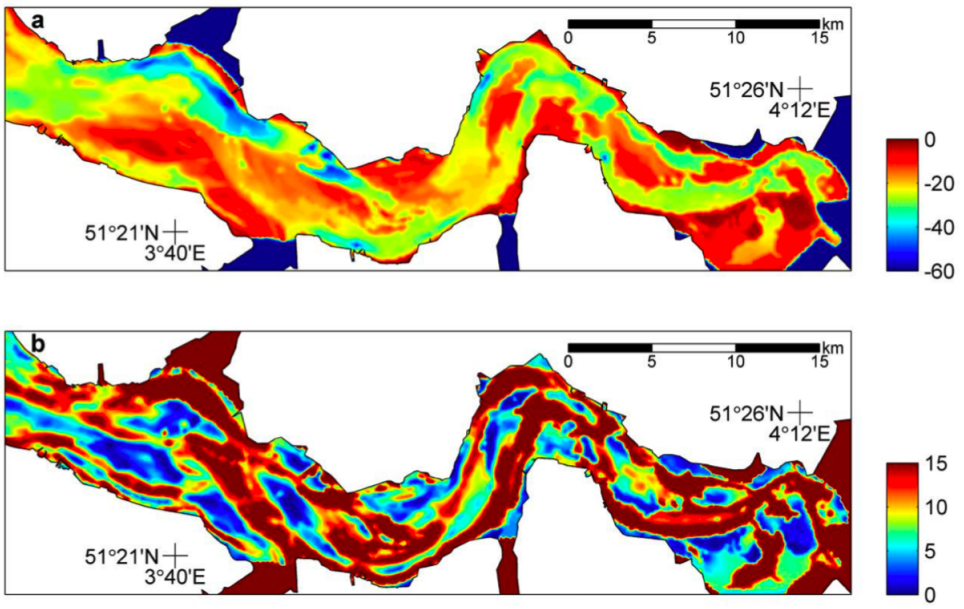

Figure 7: Erosion resistant layer. (a) Height of the erosion resistant layer [m MSL]. (b) Sediment layer thickness above erosion resistant layer in 1860 [m]. (From Dam *et al.* (2016))- *Figure(S2)*

Morphodynamics

- The astronomical tide is accelerated by means of a morphological acceleration factor - hereafter referred to as *MORFAC* - of 24.75, upscaling the spring-neap tidal cycle of 14.76 days (synodic month) to an annual tide cycle of approximately 365.31 days. Hereby, the error in the erosion and sedimentation volumes is measured to be less than 15 % as stated by Dam *et al.* (2008).

Results

Methodology of measuring the skill of the model - Brier Score

The performance of the model is quantitatively and qualitatively defined. For the quantitative assessment the Brier Score is applied, which ascribes the skill of the model to the ratio between (1) the squared error of the model results with respect to the measured data, and (2) the squared error of the model results with respect to the initial bathymetry (see eq.(124)),

$$\frac{\langle Y - X \rangle^2}{\langle B - X \rangle^2} \tag{124}$$

herein is considered:

- B: the initial bathymetry in the computational domain
- X: the modelled bed in the computational domain
- Y: the measured bed level in the computational domain

An *averaged* value of the model skill could be acquired when for each respective point the Brier Score is defined and subsequently averaged over the entire computational domain.

The performance of the model may also be reviewed by means of a qualitative comparison between the modelled bed level and the measured bed level over the course of the simulation. Both measures are considered in this research to investigate the skill of the model.

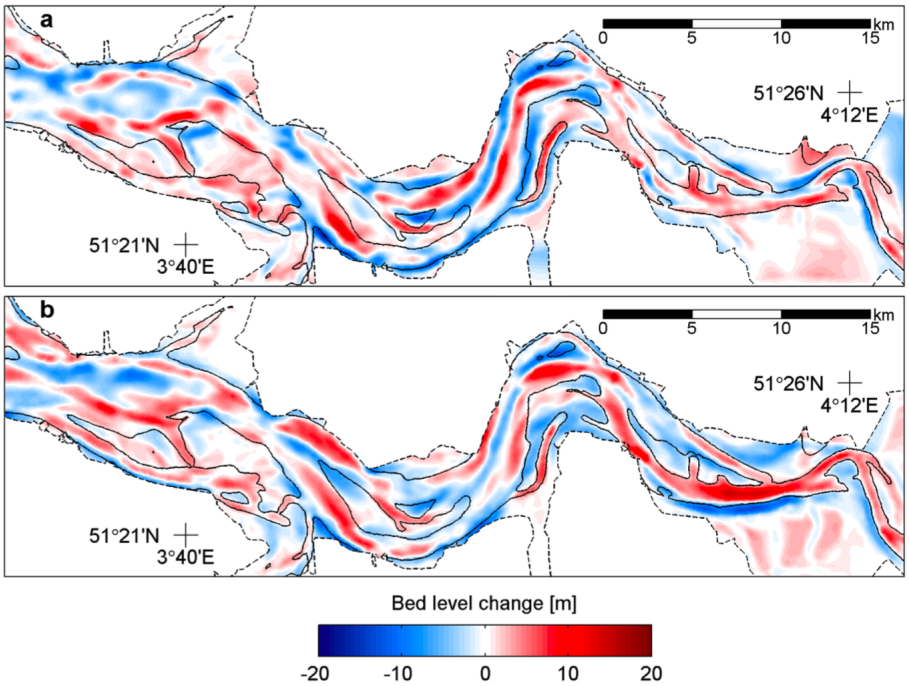

Figure 8: Erosion and Sedimentation patterns over the 1860-1878 period. (a) Measured. (b) Modeled. Black dashed line indicates the 1860 plan form. Black solid line indicates the - 5m contour line of the 1860 bed. (From Dam *et al.* (2016)- *Figure(S3)*)

Visual Observations

This section gives a summary of the findings described in Dam *et al.* (2016)

It is stated by the author that the model results deviate considerably from reality (i.e. measured data) in the first decades of the model simulation (see Figures 8 & 9) although it may be seen that on the basis of a visual observation the results look very promising.

The meandering strength of the main channels is clearly visible indicated by the deep curved channels in blue. The location of the scour and deposition of the bed appears hereby to be close to the measured location albeit that the magnitudes of the scour & deposition and specific treats of the bed topography are somewhat merged.

This remains from a visual perspective the main subject after a simulation time of approximately 40 years (i.e. starting from 1905 - Figure 10). Here, it may be seen that the bed level elevations at the location of *modelled* morphodynamic activity are reasonably in line with the measured morphological development. Yet the specific characteristics of the bed topography remains to be overall acceptably represented although fails to display the detailed particularities of the topography.

After a period of approximately 60 years (i.e. starting from 1931 - Figure 11) the model seems to predict the magnitude of the bathymetric changes significantly better showing thereby also reasonable comparisons between the high-frequency topography changes and the measured data.

It is therefore hypothesised in this report that after approximately 50-60 years (i.e. between 1905 - Figure 10 - and 1931 - Figure 11) the model gives valuable results.

Quantitative Observations

The latter results are largely consistent with the averaged skill of the model at respective time instances hereinabove considered. The quantitative scale along which the results may be compared is adopted following the work of Sutherland *et al.* (2004) and is depicted in Table 3.

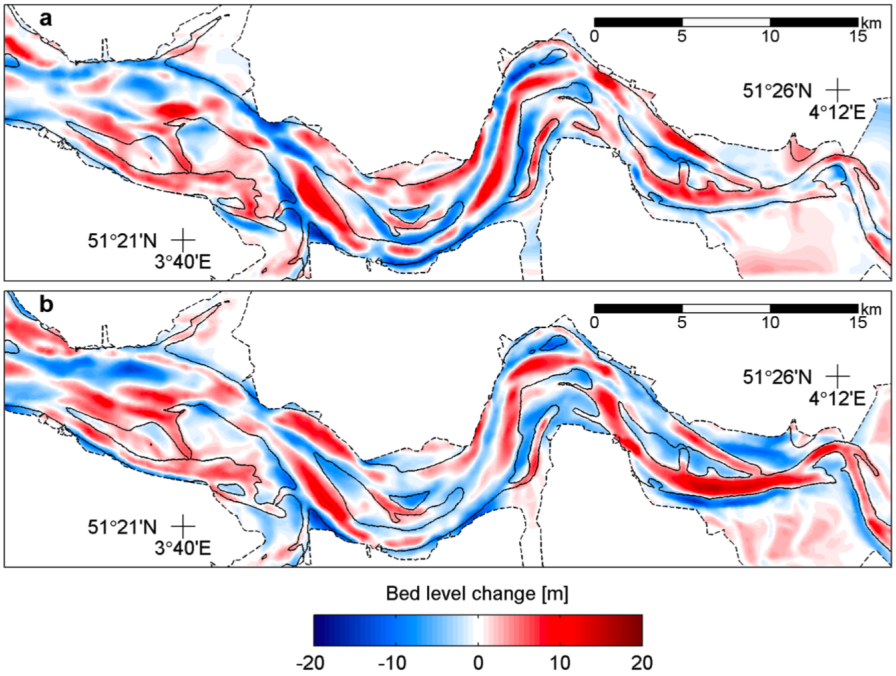

Figure 9: Erosion and Sedimentation patterns over the 1860-1890 period. (a) Measured. (b) Modeled. Black dashed line indicates the 1860 plan form. Black solid line indicates the - 5m contour line of the 1860 bed. (From Dam *et al.* (2016)- *Figure(S4)*)

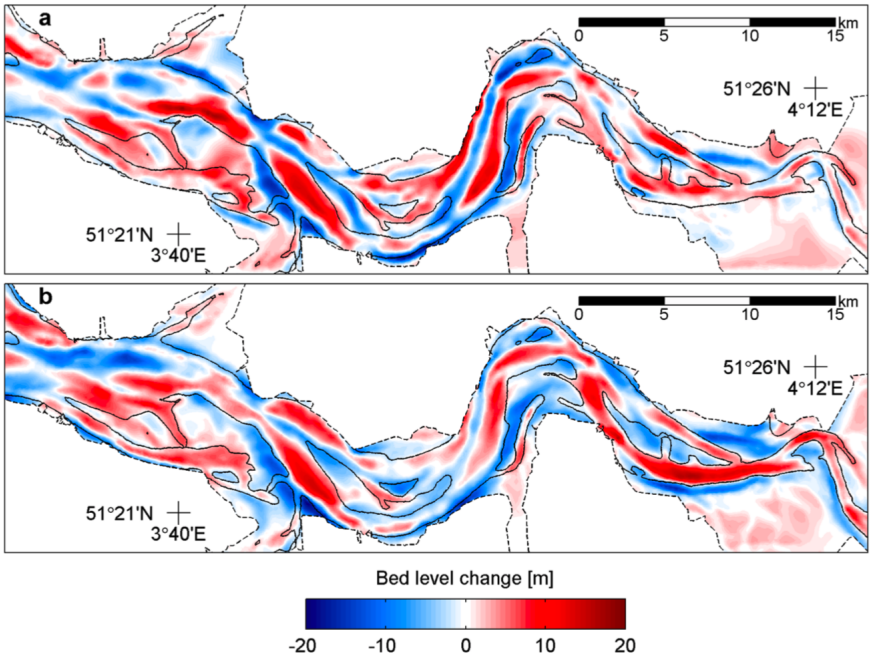

Figure 10: Erosion and Sedimentation patterns over the 1860-1905 period. (a) Measured. (b) Modeled. Black dashed line indicates the 1860 plan form. Black solid line indicates the - 5m contour line of the 1860 bed. (From Dam *et al.* (2016)- *Figure(S5)*)

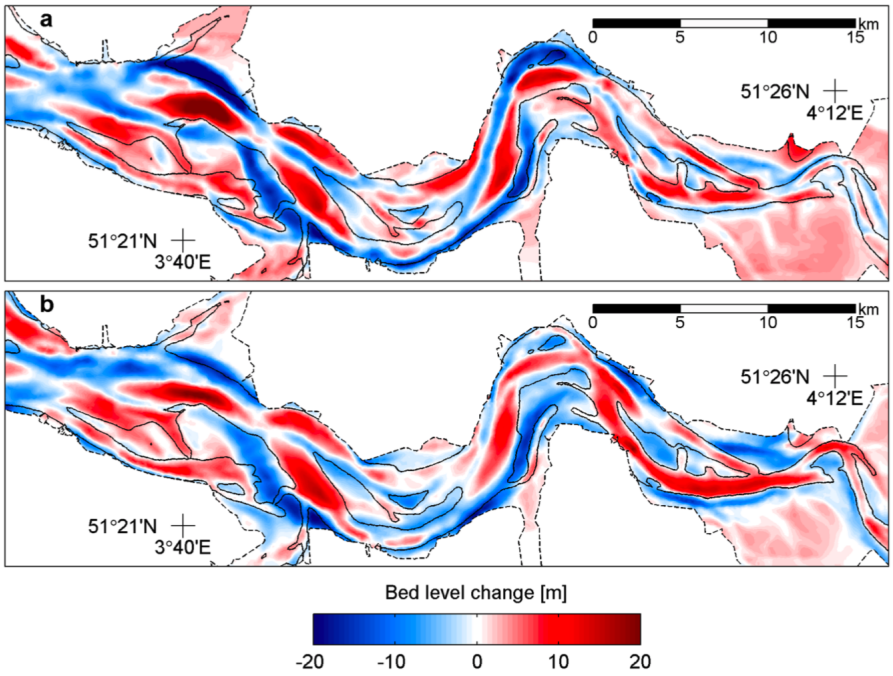

Figure 11: Erosion and Sedimentation patterns over the 1860-1931 period. (a) Measured. (b) Modeled. Black dashed line indicates the 1860 plan form. Black solid line indicates the - 5m contour line of the 1860 bed. (From Dam *et al.* (2016)- *Figure(S6)*)

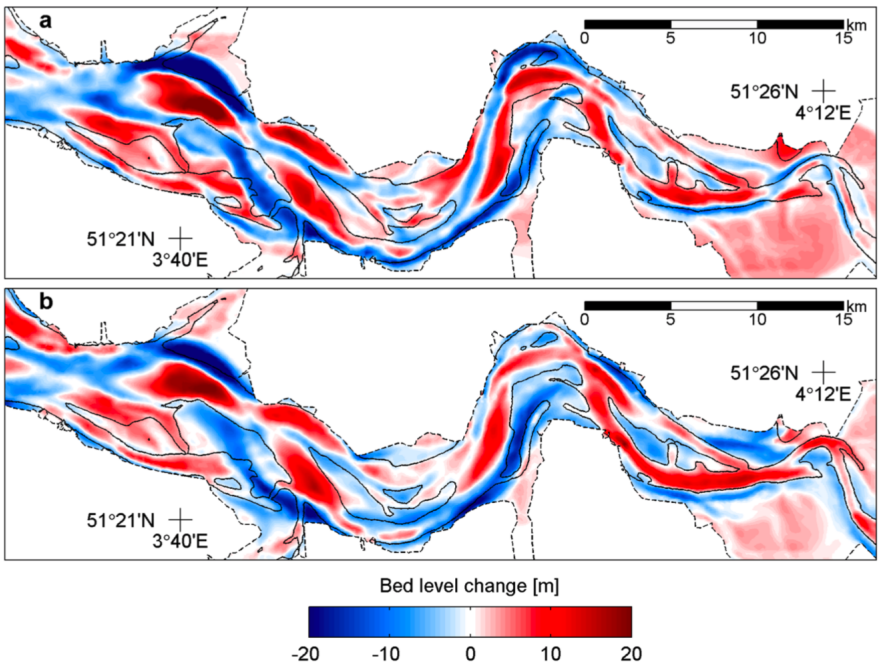

Figure 12: Erosion and Sedimentation patterns over the 1860-1955 period. (a) Measured. (b) Modeled. Black dashed line indicates the 1860 plan form. Black solid line indicates the - 5m contour line of the 1860 bed. (From Dam *et al.* (2016)- *Figure(S7)*)

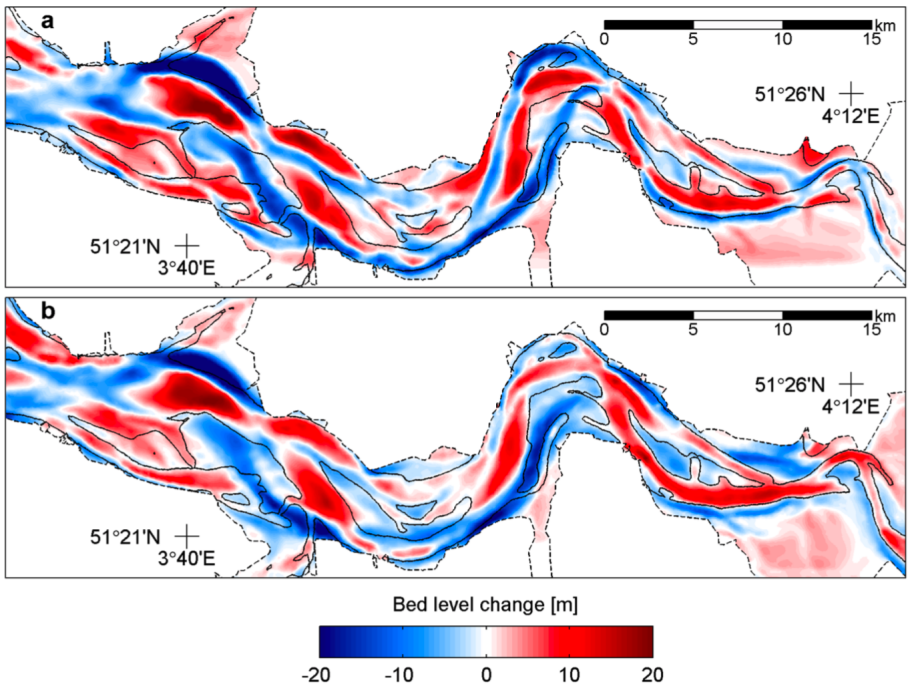

Figure 13: Erosion and Sedimentation patterns over the 1860-1960 period. (a) Measured. (b) Modeled. Black dashed line indicates the 1860 plan form. Black solid line indicates the - 5m contour line of the 1860 bed. (From Dam *et al.* (2016)- *Figure(S8)*)

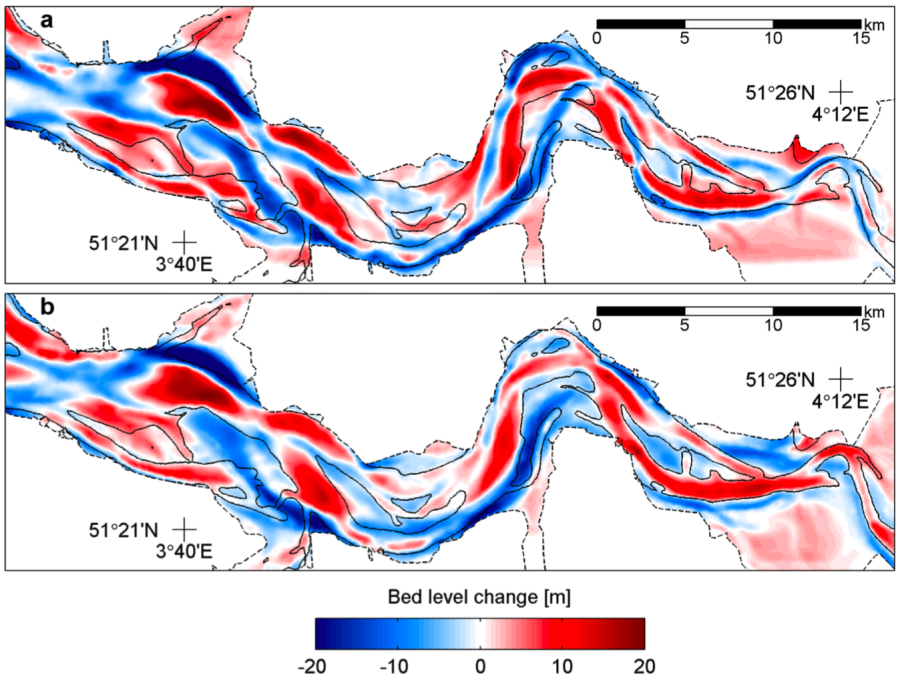

Figure 14: Erosion and Sedimentation patterns over the 1860-1965 period. (a) Measured. (b) Modeled. Black dashed line indicates the 1860 plan form. Black solid line indicates the - 5m contour line of the 1860 bed. (From Dam *et al.* (2016)- *Figure(S9)*)

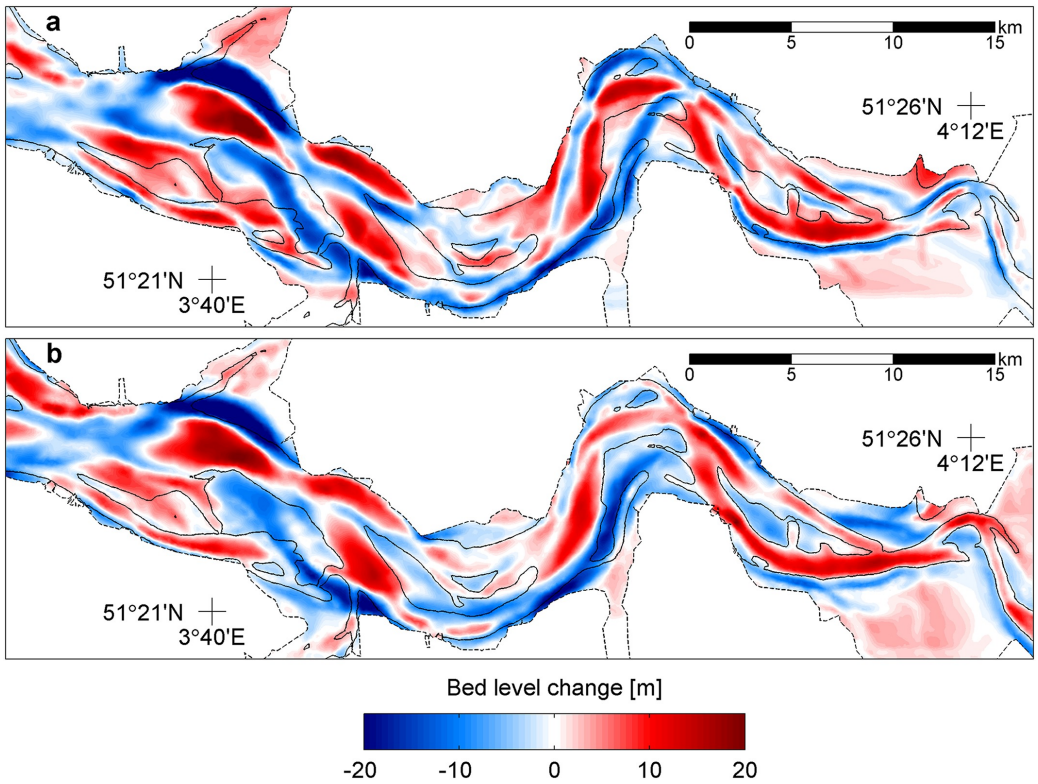

Figure 15: Erosion and Sedimentation patterns over the 1860-1970 period. (a) Measured. (b) Modeled. Black dashed line indicates the 1860 plan form. Black solid line indicates the - 5m contour line of the 1860 bed level. (From Dam *et al.* (2016)- *Figure(2)*)

Brier Skill Classifications and associated score		
Excellent	→	1.0 - 0.5
Good	→	0.5 - 0.2
Reasonable/fair	→	0.2 - 0.1
Poor	→	0.1 - 0
Bad	→	<0

Table 3: Description of quantitative BSS skill of the model

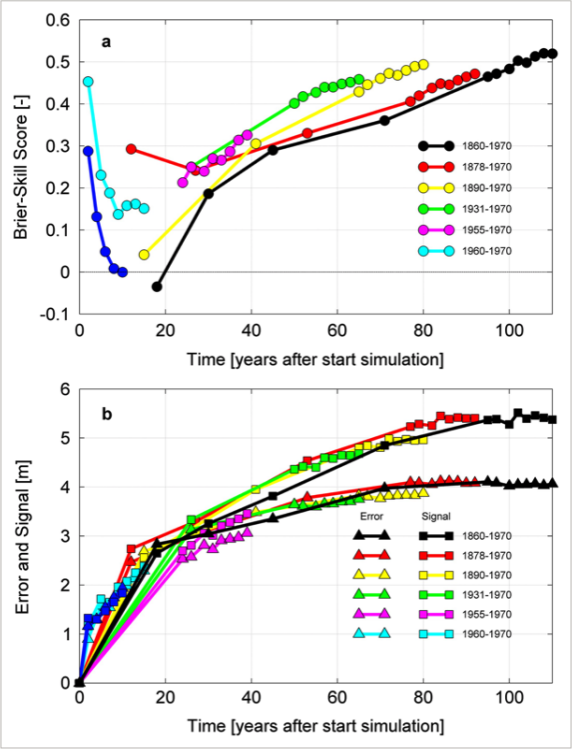

Figure 16: Brier-Skill Score and error versus signal for seven simulations with different start years. (a) BSS. (b) Error and signal. Markers indicate comparisons between model and data; solid lines interpolate between subsequent comparisons. BSS, error, and signal are determined over entire Western Scheldt area. (From Dam *et al.* (2016)- *Figure(3)*)

Initially, at the start of the model simulation, the model results did not fully comply with the measured bathymetry resulting in a negative BSS score (≈ -0.05). It may thereby be seen that the skill of the model increases over time, giving *Good* results after 3 decades (BSS ≈ 0.2)/ 4 decades (BSS ≈ 0.3) of simulation. *Excellent* results prevailed only after 1 century of model simulation. The latter is depicted in Figure 16. In the second panel of Figure 16 the *signal* of the model - a measure for the morphological activity being equal to the denominator of the BSS score following Dam *et al.* (2016) - and *error* of the model - a measure for the obtained error between the modelled and measured data - is displayed. Here, it may be seen that the bed evolution finds its model equilibrium after 80 years of model simulation whereas the deviation between the modelled and measured data increases steadily yet attenuating over the entire simulation interval - both contributing to a higher *skill* of the model.

3.2 Case Study - Western Scheldt Estuary - *van der Wegen 2010*

Morphodynamic Modeling in Alluvial Estuaries
This section is composed based on the findings of van der Wegen (2010)

In the dissertation of van der Wegen (2010), the importance of the geometry of an estuary to the position of the shoals and channel is assessed. To this end, the Western Scheldt estuary is investigated in an attempt to model the channel-shoal formations over the course of 200 years starting from an initial flat bed. Also as seen in the research of Dam *et al.* (2016), the presence and location of erosion-resistant layers formed by peat, clay and/or rocks may have considerable effect on the (local) flow direction and the positioning c.q. migration of the channel formations. The application of varying discharges and erosion-resistant layers and inclusion of dredging gave fairly better results. It is stated by the author that variations in the model parameter settings (i.e. density differences and grain size variations) did not

constitute to significant changes in the model results whereby is theorised that the interaction between the tidal forcing and the geometry appears to be the largest contributing factor to the outcome of the model.

Model Assumptions

Model Setup

Numerical Model - Delft3D 4

A 2DH depth-averaged and a 3D process-based morphodynamic model with 10 sigma layers is applied for this research. The description of the physical processes is in line with the description reviewed in chapter 2:

- *Representation of a 2DH Flow model: eqs.* (3) ,(4), (5) & (6)
- *Representation of the sediment transport: eqs.* (7),(120 - EH formulation) & (65 - van Rijn Formulation)

Physical Processes

- The astronomical M2 tide is schematised by means of a representative morphological tide obeying a wave period of 207 days. Consequently, the latter ensures that 6 months of hydrodynamic simulation accounts for 200 years of bed level evolution.
- Fresh water inflow from the upstream rivers is included in the model, be it that the inflow does not cater any significant stratification.
- Since a 3D simulation is proceeded, secondary flow features such as spiral flow are by default included in the computations.
- Waves are not included the computations.

Computational Domain

The computational domain comprises an area of approximately 80 km x 20 km. This area is partitioned by means of a curvilinear boundary fitted grid changing in element size from $O\left(1km^2\right)$ in the North Sea to 2 km^2 (i.e. 100 m x 200 m) in the Western Scheldt Estuary. Figure 17 gives an overview of the grid composition.

Sediment Transport

- In this case study two sediment transport formulations are separately assessed:
  - The Engelund and Hansen (1967) formulation which accounts for total transport.
  - and the van Rijn (1993) formulation which considers the sediment transport as combination of bedload transport and suspended transport.
- The transverse bed slope reduction factor α_n is set to 10 in 2DH calculations whereby the Engelund and Hansen (1967) formulation is prompted.
- When the van Rijn (1993) formulation is prompted, a transverse bed slope reduction factor α_n is considered with an order of magnitude larger than in the case of the Engelund and Hansen (1967) formulation (i.e. $O\left(10^2\right)$) to ensure realistic results.
- The sediment transport is by default computed using the Engelund and Hansen (1967) formulation in 2DH mode.

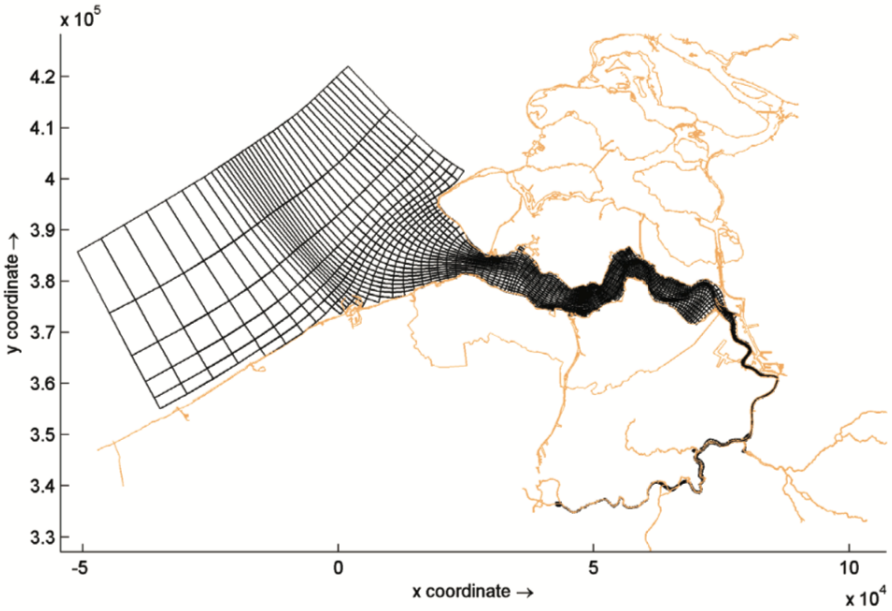

Figure 17: Model grid (black) and land boundary (orange). (From van der Wegen (2010)- *Figure(5.1)*)

Initial Condition

- The bathymetric dataset of 1998 is used as initial bed for the model computations. This bed is considered to have a sediment layer of 50 metres. The 1998 bed topography and the location of the erosion-resistant layers are shown in Figure 18.

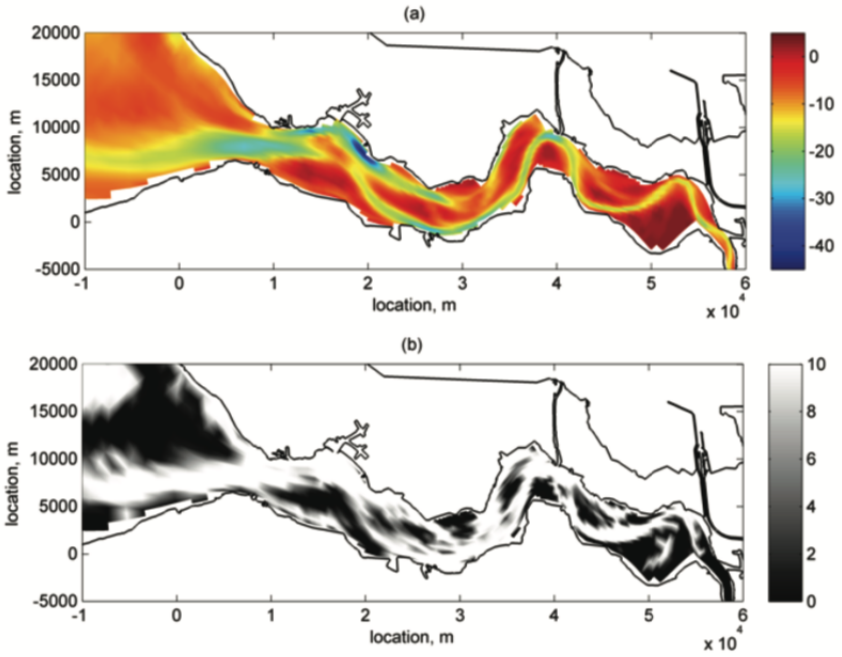

Figure 18: (a) measured 1998 bathymetry; (b) indication of location of non-erodible layers in meters of available sediments. (From van der Wegen (2010)- *Figure(5.3)*)

- A uniform grain size distribution of 200μm is included in the computations.

Boundary Conditions

- A constant annual river inflow of $15m^3/s$ is considered at the eastern boundary of the estuary. In particular simulations, it may be seen that the annual river inflow is set to $500m^3/s$.
- The astronomical semi-diurnal M_2 tide, its overtides M_4 & M_6 and the artificial diurnal component C_1 are imposed at the sea boundary of the computational grid. The wave amplitudes are displayed in Table 4. It has been theorised by the author that this set of tidal constituents give rise to a comparable sediment transport.

Tidal Constituents	
M_2	1.72 m
M_4	0.09 m
M_6	0.05 m
C_1	0.17 m

Table 4: Amplitudes of tidal components imposed at the sea boundary of the computational grid in line with van der Wegen (2010)

Morphodynamics

- The astronomical tide is accelerated with a MORFAC of 400 upscaling the individual tidal cycle of 14.42 hrs. (semi-diurnal lunar M2) to a representative tidal cycle of approximately 207 days.
- The initial geometry of the Western Scheldt Estuary is fixed over the entire model simulation.
- Due to the appearance of erosion-resistant layers (i.e. clay, peat & Pleistocene) in the Western Scheldt Estuary the bed erosion must be adjusted accordingly. The latter is proceeded by changing the sediment availability at the respective grid cells.
- Dredging works are included in the computations by designation areas where a navigable depth of 12.5 metres must be maintained.

Results

This section gives a summary of the findings described in van der Wegen (2010)

van der Wegen (2010) performed various runs for different morphodynamic model settings. The resulting bathymetries may be observed in Figure 19. The upper left plot shows the measured bathymetry of 1998 in the Western Scheldt. Next, model simulations are proceeded to obtain morphological development of the Western Scheldt for 200 years. The author acknowledges the overall resemblances of the model prediction and the measured bathymetry, but also notes the apparent dissimilarities.

The formation of the flood channel is one of the main characteristics that is persistent in all the predicted bathymetries. The exact position of the flood channel and the attainment towards the land boundary of the estuary is only observed in the model run (d) van Rijn (1993)-2D-($\alpha_{BN} = 100$), run (f) Engelund and Hansen (1967)-3D-(w/ only M_2 tidal component), run (g) Engelund and Hansen (1967)-3D (w/ Non Erodible Bed) and for run (h) Engelund and Hansen (1967)-3D-(w/ Non Erodible Bed & Dumping and Dredging Sites).

Note that the majority of the runs that show major resemblance are based on the Engelund and Hansen (1967)formulation for the sediment transport and 3D model runs. The author states that the formation of the channels and the channel curvature is rather straight in 2DH runs whereas more curved bends are seen for 3D runs. It is argued that the latter is the consequence of the secondary flows which where incorporated in the 3D model yet not in the 2DH.

For the 2DH models the transverse bed slope factor is tuned to enable to bank erosion and channel migration. Smaller values for the bed slope parameter created deeper and narrower channel whereas larger values provided the formation of wider channels. The van Rijn (1993)-formulation showed the

development of more diffusive patterns. This is the consequence of the settlement and suspension time lags which are implemented in the formulation to account for the relaxation of the suspended sediment concentration in between boundary forcing. The effect of the bed slope parameter on the net sediment transport (i.e. enhancement of gravitational effects) is also considered as probable cause for the inherent mismatches.

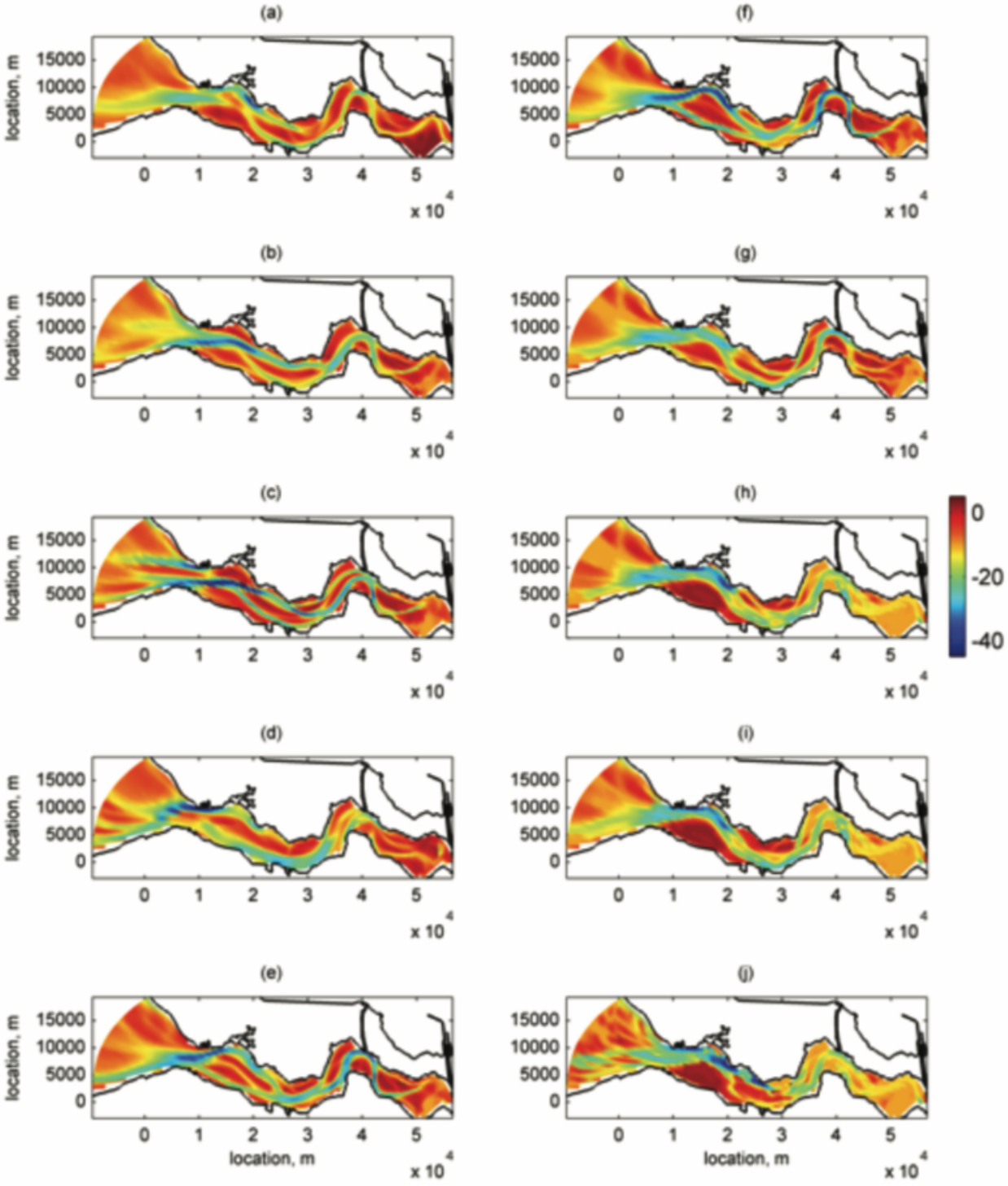

Figure 19: Bed level development after 200 years after starting from a flat bed. (a) measured 1998 bathymetry; (b) Engelund and Hansen (1967)-2D; (c) Engelund and Hansen (1967)-2D-($\alpha_{BN} = 5$); (d) van Rijn (1993)-2D-($\alpha_{BN} = 100$); (e) Engelund and Hansen (1967)-3D; (f) Engelund and Hansen (1967)-3D-(w/ only M_2 tidal component); (g) Engelund and Hansen (1967)-3D (w/ Non Erodible Bed); (h) Engelund and Hansen (1967)-3D-(w/ Non Erodible Bed & Dumping and Dredging Sites); (i) Engelund and Hansen (1967)-3D-(w/ Non Erodible Bed, Dumping and Dredging Sites & $Q = 500m^3/s$); (j) van Rijn (1993)-3D-(w/ Non Erodible Bed, Dumping and Dredging Sites & $\alpha_{BN} = 100$).

Brier Score

The brier skill score is applied as to assess the performance of the model predictions. The results are shown in Figure 20.

In contrast with the visual observations, according to the BSS skill score classification as proposed by Sutherland *et al.* (2004) the model is not performing so well. The best model prediction is given by model run (g) Engelund and Hansen (1967)-3D (w/ Non Erodible Bed). For this model it can be that the performance increases over time to a maximum around the 0.2 (i.e. dotted red line) followed by a slow decay after 200 years. Thereby, all models are producing a large β which means that the model is overestimating the erosion volumes and underestimating the deposition volumes. Also, here model run(g) shows the slowest increase in β over time. Furthermore, the values for α - which gives an indication for the extent to which the model follows observed morphological trends - appears to be slightly increasing for all model runs. Model run(9) shows thereby after 200 years to closest resemblance with the observations (i.e. $\alpha = 0.48$). Nonetheless, this would make still a large difference. Lastly, γ value is shown in the lower panel. As may be seen is that the values all increasing for all model runs. Consequently, this entails that all model runs are systematically overestimating the morphological activity producing larger erosion volumes and larger deposition volumes compared to the observations. Hence, a 3D model on the basis of the Engelund and Hansen (1967)-formulation for the sediment transport and patches of non-erodible bed have shown to give the best predictions for 200 years morphological development in the Western Scheldt Estuary.

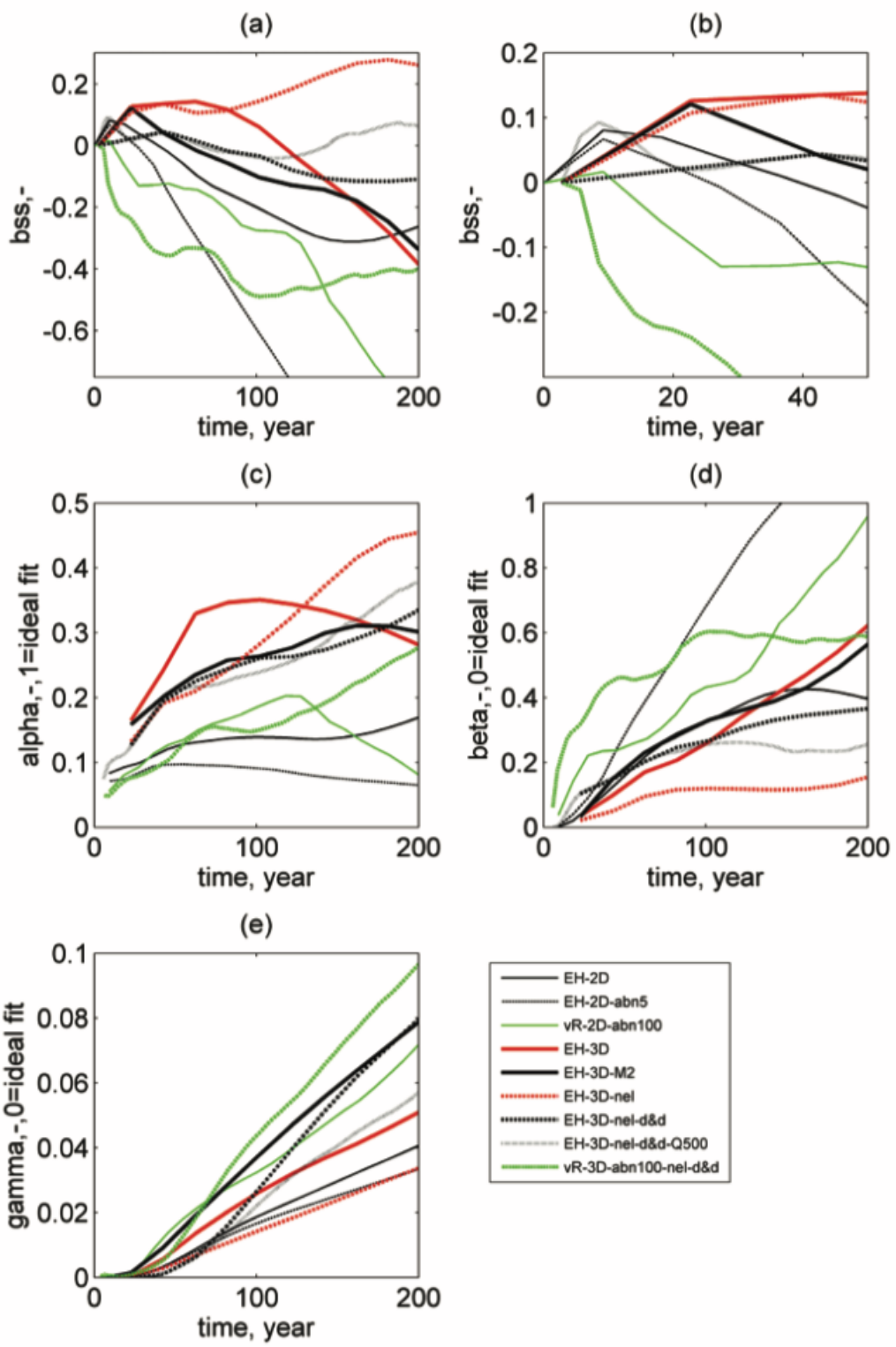

Figure 20: Model results over time for selected runs (a) BSS; (b) detail of (a); (c) α, 1=ideal fit; (d) β, 0=ideal fit; (e) γ, 0=ideal fit; (from van der Wegen (2010))

4 CONCLUSION

The place of morphodynamic models in the present-day engineering practice has never been as eminent as now. Morphologist within the wide range of the geomorphology discipline apply morphodynamic models to assess the long-term effects of anthropogenic interventions to the geomorphological system at hand (e.g. coastal, estuarine and tidal environments). Lately, morphodynamic models are used not only as a practical engineering tool to evaluate different design options, but morphodynamic models are also applied as a research tool whereby research is conducted on the dominant processes that have contributed towards the appearance of certain particular phenomenological events. In this pillar, the context and place of morphodynamic models in the engineering discipline is also further elaborated on through an investigation on the historical advances in numerical models tailored to predict morphological development. This led to the development of process-based models. These models are characteristic for their ability to predict morphological development for a combination of selected physical processes.

To develop such a model, a certain numerical technique must be decided upon to discretise and solve the set of differential equations describing the flow and transport of sediment & waterborne constituents. Therefore, primarily three options are apparent and can be characterised by the following classes of numerical discretisation techniques: (1) finite difference method, (2) finite volume method, and (3) finite element method:

Finite difference method discretises the computational domain in a set of discrete grid points. Hereby, the description of the governing physical processes is discretised using an approximation of the derivatives upon *finite differences*.

Finite volume method partitions the computational domain in discrete volume parcels (i.e. control volumes). The state of the flow is, thereby, described in each control volume and found by solving the local mass and momentum conservation balances.

Finite element method discretises the computational domain in a set of discrete elements. The description of the physical processes is, hereby, discretised in sets of algebraic equations (i.e. basis functions) which express the local state of the flow and transport in each respective element.

It is emphasised that irrespective of the choice of numerical discretisation technique, the final numerical results should be very much the same. Nonetheless, each of the respective methods have attractive properties which may be beneficial in later modelling stages:

Finite Difference Method

- The finite difference method is generally suitable for boundary value problems.
- The presence of relatively simple stencils that can be applied in the updating procedures of the numerical values (e.g. relatively easy sediment transport updating scheme).
- The structured grid has an advantage that structured ordering of data is evident in the computational grid (i.e. information on the numerical flow parameters and transport are stored in each grid point)

Finite Volume Method

- Finite volume method is extremely suitable for fluid dynamic problems - especially if the boundary fluxes are included in the discretisation of the computational domain. (i.e. strictly conservative schemes)

- Ones the finite volume method is applied for elliptical problems which satisfy the boundary maximum conditions, then the discretisation automatically holds for the discrete boundary maximum conditions (i.e. characteristics pertain even after discretisation procedures).

Finite Element Method

- Finite element methods create a strong numerical tools to compute fluid dynamics problems - especially when strictly conservative schemes are considered.
- The unstructured mesh gives flexibility to tailor the computational grid composition for complex geometries.
- Finite element schemes have shown to be quite suitable for quick assessment of various design options, given their flexibility.

Next, the pillar provides an outline on two different *process-based* morphodynamic models that are able to account for complex interactions with many nonlinear processes in order to predict morphological evolution. Firstly, the investigation is proceeded with an analysis on the Delft3D-4 model - hereafter referred to as D3D4[1]. The D3D4 model solves for unsteady shallow water wave equations, and subsequently for the transport of sediment and waterborne constituents. It is shown that the online computations of the sediment transport (and other waterborne constituents) create several advantages with respect to the numerical solution procedure:

- The 3D hydrodynamic processes and the adaptation of non-equilibrium suspended concentration are automatically accounted for in the hydrodynamic module.
- Density effects of the sediment in suspension are accounted for in the hydrodynamic computations
- Changes in the bathymetry are included in the hydrodynamic computations
- The *online* computations create a simple platform for both the hydrodynamics and morphodynamic module due to a shorter and faster intermittent communication between the two modules
- The robust and stable numerical scheme enables the computations of 2^{nd} order accurate solutions with a courant number up to 10.

Furthermore, an investigation is proceeded on the sediment transport formulation and bed level updating scheme of the D3D model using, hereby, the van Rijn (1993)-sediment transport formulation[2]. In the van Rijn (1993)-transport formulation, the bedload transport and suspended sediment transport are considered separately. Upon calibration of the parameters that tailor the relative influence of the wave- and current-related effects on the transport (i.e. $f_{sus(w)}$, $f_{bed(w)}$, α_{BN}), the model can be tuned as such that it aligns with the observations of the selected region of interest.

Another, 3D numerical model that can be applied for the computations of the morphological evolution is the FINEL(2D/3D) model. FINEL3D is based on a finite element scheme that solves directly for the nonhydrostatic[3] Navier-Stokes equation and the transport of sediment & waterborne constituents. FINEL3D uses an unstructured grid which can be composed of many different geometric shapes for the most complex geometries[4]. FINEL may use a combination of discretisation methods to partition the computational domain in respective elements. Here, FINEL3D may use a combination of a continuous and discontinuous Galerkin method to discretise the domain and the governing equations describing the flow. The Galerkin method ensure that the continuous functions of the flow state are transformed into discrete operators - the basis functions. A special case of the Galerkin method - the Galerkin Interface Stabilisation (GIS) method - is shown to be rather suitable for geophysical flow problems given its attractive properties. That is, it is shown that the geophysical flows can also be

[1] The subscript "4" distinguishes here the structured model from its unstructured counterpart Delft3d-FM
[2] Note that other transport formulations are also available in the model
[3] Note that the D3D4 model uses a hydrostatic solver and a separate nonhydrostatic solver (i.e. corrector) that corrects for the hydrostatic computations if the local deviations are too large
[4] It should be noted that the counterpart of the D4D4 - D3D-Flexible Mesh - also holds such characteristics

solved using the *variational principle*. Here, the functions and the functionals which are defined in the euclidean space $\mathbb{R}^3$ are obliged to follow the minimisation problem: *"find, a function that minimises the flow state functional (given a certain minimisation criteria) "*. The application of the *variational principle* in geophysical flows provides an effective strategy to solve the flow state equations in a way that the errors are always minimal. The associated implementation of the GIS method, which poses an interior penalty on the element boundaries, ensures the stabilisation of the numerical scheme and active damping of the artificial diffusion - especially in advection-dominated flows. The latter properties will show to be rather beneficial in the later stages of the conceptualisation of the model (i.e. model calibration).

Part II

MODELLING METHODOLOGIES AND SCHEMATISATION

5 INTRODUCTION

A comprehensive understanding of the physical behaviour of a geomorphological system (e.g. coastal, estuarine, tidal environment) is eminent in the process of translating parts of reality into a model representing a certain set of phenomenological events. Following the process-based approach, wherein the response of the system is analysed by means of the contribution of its underlying physical processes, an attempt is proceeded to investigate the dominant processes that result in (1) the observed bed level evolution and (2) a reasoning towards the cause of particular observed changes (i.e. theorising which forces are underlining the observed phenomenological advances). The latter approach gives rise to computational models that describe the response of a geomorphological system by means of the governing processes whilst reducing the larger physical description to a set of primary processes encompassed in different modules. The reduction of the physical nature of the system to solely a set of governing processes which pertains the same morphological evolution (i.e. input reduction) leads to an efficient model given its reduced computational effort. However, if the phenomenological response of the system is defined by the interaction between its (small-scale) physical processes, the computational effort will increase drastically. Especially, if such small-scale responses are considered in simulations concerning long-term morphological evolution. The latter being rather impractical for long-term macrotidal morphological evolution given its extensive computation time. Several evolution techniques are proposed by Roelvink (2006) to bridge the gap between small-scale hydrodynamic processes and larger scale morphodynamic responses. The latter enables geomorphologists to perform efficient computations for medium- to long-term temporal time scale evolutions. These modelling techniques are described in the following section and may be seen as methods to capture large-scale morphological adjustments within the realm of computational capabilities that a geomorphologist can acquire to obtain valuable model outcomes on the longer run. Hereby, the following evolution techniques are reviewed:

- The tide-averaging approach ("offline approach")
- The parallel tide-averaging approach ("RAM Method")
- The (sequential) online approach ("online morphology")
- The parallel online approach ("MorMerge approach")

Several other morphological evolution techniques are thereby proposed by Luijendijk (2019) which are related to the well-known evolution techniques of Roelvink (2006). These new evolution techniques are an extension to the aforementioned techniques and give geomorphologist the ability to perform efficient numerical computations by application of witted pre-processing procedures (e.g. compressing and filtering of time series data, schematisation of full time series data in seasonal conditions). These evolution techniques will be intermittently discussed in coherence with the well-known evolution techniques of Roelvink (2006):

- *The (sequential) online approach ("online morphology")*
  - Brute Forcing Compressed
  - Brute Forcing Filtered
  - Brute Forcing Filtered & Compressed
- *The parallel online approach ("MorMerge approach")*
  - Brute Forcing Merged

6 MORPHOLOGICAL EVOLUTION TECHNIQUES

This section is composed based on the findings of Roelvink (2006) & Luijendijk (2019)

6.1 Tide Averaging Approach - The Offline Approach

The tide-averaging approach concerns a modelling technique wherein the morphological adjustment is computed on the basis of the tide-averaged flow conditions. Hereby, the sediment transport is found by calculating the transport on several points in the tidal cycle. These values are averaged to obtain the tide-averaged sediment transport. Meanwhile, the bathymetry is kept stationary over the tidal cycle, and the flow *patterns* are assumed not to vary significantly by the presence of small bed level changes such that the *patterns* are pertained within the cycle. Lastly, the (initial) bathymetry is updated by the averaged sediment transport *field* and a continuity correction is considered adjusting the flow *field* within the tidal cycle given that the intermediate bathymetric changes are sufficiently small. Conversely, the flow *field* is updated such that the magnitudes in the flow *field* are adjusted for the respective (averaging) points in the tidal wave cycle. A morphological update of the initial bathymetry based on (1) tide-averaged sediment transport and (2) the described bathymetric changes concludes this morphodynamic cycle. The flow chart of the modelling technique is depicted in Figure 21.

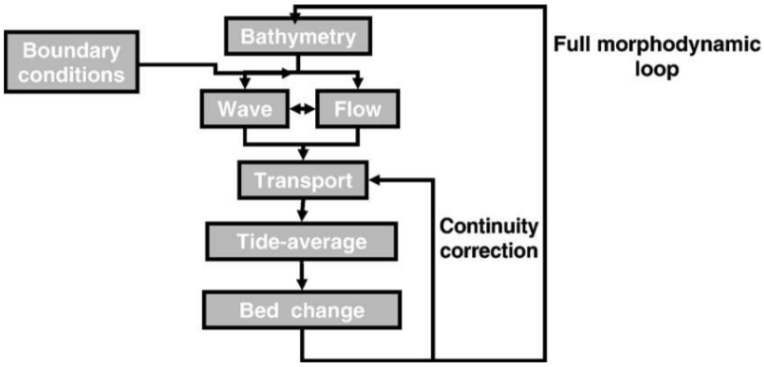

Figure 21: Flow diagram of tide-averaging morphodynamic model setup. (From Roelvink (2006))

Characteristics and Limitations of the offline approach

- The offline approach assumes that the wave and flow *patterns* are stationary within the hydrodynamic cycle, which provides only changes in the flow *field*. The inherit challenge of the latter assumption is that the flow *field* may produce unrealistically large velocities with the changes of the flow depth over a static bed (i.e. drying and flooding). For instance, at shallow locations where flooding and drying may occur, the velocity $\vec{u}$ which may be defined as the ratio of the discharge $\vec{q}$ & the local flow depth h. Viz,

$$\vec{u} = \frac{\vec{q}}{h}$$

  becomes (unrealistically and) increasingly larger with shallower depths within the continuity correction process.

- If in the coastal system the effect of suspended transport is of considerable importance for the formation of the morphological features, then the computation time will increase over a hydrodynamic (tidal) cycle as the morphodynamic time step must be reduced in order to obtain stable solutions. As for linear bed level changes - small perturbations and $F_r << 1$ - the bed wave celerity c_{bed} is defined by as the ratio of the product of the degree of non-linearity b & the sediment transport S and the local flow depth h eq.(125). Viz,

$$c_{bed} = \frac{bS}{h} \tag{125}$$

  bed waves following from finer grains will result in an upper bound for the computational morphodynamic time stepping.

- The offline approach uses an explicit Euler method to update the bed and therefore provides first order accurate bed level changes. Consequently, to increase the accuracy of the computed bed level change, for each hydrodynamic cycle the continuity correction process encompasses in the order of 5 - 20 cycles such that the tide-averaged sediment transport *field* is acceptably converged.

6.2 Parallel Offline Approach (RAM method)

In the parallel offline approach - also known as the *rapid assessment of morphology method* - multiple input conditions are accounted for in addition to the tide-averaging (offline) approach. Analogue to the continuity correction process, the flow *patterns* and bathymetry are kept constant within each morphodynamic cycle while the sediment transport *field* is being computed. The obtained sediment transport *fields* are, next, averaged using a particular weighing scale (i.e. a factor depending on the probability of occurrence for instance) hereby acquiring a *weighted averaged sediment transport*. On the basis of this weighted averaged sediment transport, the bed level change is calculated and subsequently used to update the initial bathymetry. The flow chart of the RAM method is depicted in Figure 22.

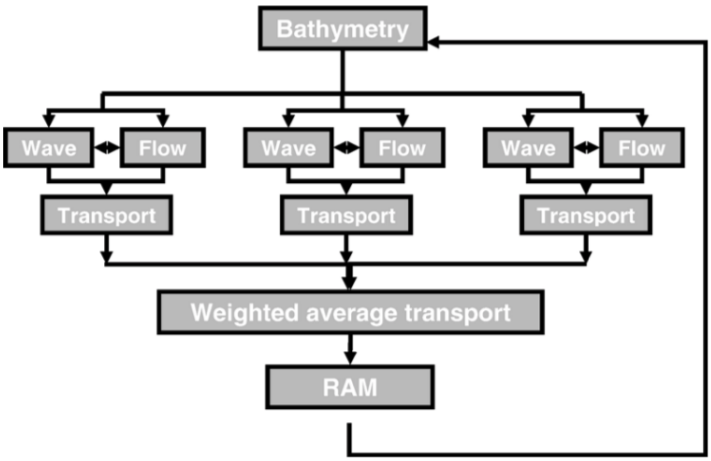

Fig. 2. Flow diagram of RAM approach.

Figure 22: Flow diagram of RAM approach.(From Roelvink (2006))

Characteristics and Limitations of the Parallel Offline approach

- As a rapid assessment tool, the RAM method calculates quickly the effect of varying wave and current conditions on a stationary (initial) bed.

- In dynamic areas such as estuarine and tidal (inlet) environments, this method works very well. However, for large bottom changes more often a full hydrodynamic cycle must be employed to capture the right wave & flow *field* while computing the bed level changes. The latter resulting in larger computation time.
- The essence of the rapid assessment method is that the wave and current *patterns* are considered to be stationary under small bed level changes. The sediment transport is in this case solely a function of the local flow depth which varies in time as such that for the computation of the sediment transport only the changes in the water level are to be accounted for within the hydrodynamic cycle.
  When the bed level changes become too large, however, a full hydrodynamic cycle is necessary to obtain the right wave & current *patterns* before the sediment transport is computed and the bed level is adjusted in the morphological loop.
- The presence of multiple (independent) input conditions inherently favours the application of parallelisation of the morphodynamic scheme enabling the division of the workload over the amount of (independent) processors or (independent) cores. This has the advantage that faster and more efficient computations may be proceeded.
- If in the coastal system the effect of suspended transport is of considerable importance for the formation of the morphological features, then the computation time will increase over a hydrodynamic (tidal) cycle as the morphodynamic time step must be reduced in order to obtain stable solutions. As for linear bed level changes - small perturbations and $F_r << 1$ - the bed wave celerity is defined by eq.(125). Bed waves following from finer grains will provide in an upper bound for the computational morphodynamic time stepping.

6.3 The Online Approach - Brute Forcing Method

The Online approach concerns a morphological modelling technique wherein the morphodynamic changes are computed simultaneously with the hydrodynamics. Depending on the input conditions considered (i.e. tidal conditions, wave climate and non tidal water level variations) the flow and wave *field*s are computed. Thereby, the flow *patterns* are updated in each hydrodynamic step, and the resulting sediment transport *field* - as well as the bed level changes - is embedded in the hydrodynamic cycle. The flow chart of the online approach is depicted in Figure 23.

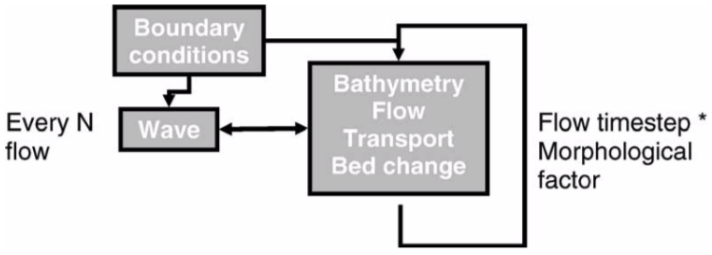

Figure 23: Flow diagram of 'online' morphodynamic model setup.(From Roelvink (2006))

In the Online approach the morphological cycle aligns with the hydrodynamic cycle. For long-term morphological evolution, this may be rather cumbersome as a vast amount of hydrodynamic cycles are to be evaluated for which only a fraction results in bed level changes (i.e. larger simulation time). To overcome this, input conditions following from direct implementation of the forcing conditions (i.e. time series approach) may be reduced to a set of governing schematised forcing conditions that prescribe the same morphological evolution on the long temporal scale. (Input reduction methods will be further investigated in the next chapter). Alongside such schematised forcing conditions, a morphological acceleration factor can be assigned to speed up the morphological computations. The underlying

nature of the efficacy of this morphological acceleration factor - as introduced by Lesser *et al.* (2004) and hereafter referred to as *morfac* - is underpinned by the presence of a gap between the small-scale hydrodynamic action and the large scale morphodynamic response. Hereby, the bed level changes which are calculated within one hydrodynamic cycle are aggregated (i.e. multiplied by the factor of *morfac*) to obtain morphological adjustments on the temporal scale of $morfac * \Delta t$. The latter greatly reduces the computational effort and time of the morphological updating scheme, while pertaining accurate calculations of the hydrodynamics (i.e. wave and flow *patterns*) and morphodynamics (i.e. aggregated sediment erosion & deposition volumes and bed level changes).

Variations of the online approach are also existing as proposed by Luijendijk (2019). Hereby, the wave time series is reduced to solely obtain time series data that contributes to the sediment transport and bed level changes. This method is referred to as the *Brute Forcing Filtered* method.
In the *Brute Forcing Compressed* method, the unaltered wave time series is squeezed in the same fashion as *morfac* to reduce the computation time. Note that the astronomic tidal series cannot be squeezed in inertia dominated areas wherein the tidal filling and emptying cycle is of considerable importance.
The combination between the former and the latter adopted methods results in the *Brute Forcing Compressed and Filtered* method whereby the numerical computations of the reduced time series is accelerated in the same fashion as *morfac*. An overview of the Brute Forcing methods and its characteristics is also depicted in Figure 25.

Characteristics and Limitations of the online approach

- In the offline approach larger time steps are permitted to compute the bed level changes on a longer temporal scale (i.e. larger than the scale of the individual tidal cycle) in comparison with the online approach.
  For instance, in the case that the online approach is prompted and when a semi-diurnal M_2 tide - with a wave period of 12.42 hrs. - is considered with a *morfac* of 60 (i.e. 30-days morphological cycle), the morphodynamic response can be evaluated on a monthly time scale within one whole hydrodynamic tidal cycle (i.e. one tidal cycle represents a monthly bed level change). On a time-step level, this means that with a time step Δt smaller than 1 minute, morphodynamic changes are considered of (smaller than) an hour. In the case that the tide-averaging approach is applied the hydrodynamic time step must increase (i.e. time steps of a month) in order to obtain bed level changes on a monthly temporal scale, given one tidal cycle.

- In the online approach, the small-scale hydrodynamic processes are coupled with the morphodynamics within each hydrodynamic time step Δt. Consequently, the small-scale interactions between the hydrodynamic processes (i.e. current-wave interactions) and the morphodynamic processes (i.e. sediment transport, bed level evolution, bed sloping effects) are captured appropriately in the modelling technique.

- The online approach enables modellers to access the small-scale processes and forcing interactions on the temporal scale of individual wave events (i.e. storm events).

- The online approach may result in larger computation times - especially in the case of complex environments - as every hydrodynamic change (i.e. changes in the flow *patterns* and wave *field*) must be computed on each hydrodynamic time stepping level.

6.4 The Parallel Online Approach - MorMerge Method

In the parallel online approach - also known as the Morphological Merging method - the morphological changes are (in the same analogy as the online approach) computed on the hydrodynamic time scale. However, as opposed to the online approach *using varying input conditions*, in the case of the MorMerge method *using varying input conditions* (i.e. when the effect of a set of combinations of flow & wave

conditions are of considerable interest) the resulting bed level changes following from respective forcing conditions are merged and weight-averaged using a particular weighing scale (i.e. on the basis of the probability of occurrence). Lastly, to conclude the morphological loop the initial (or previous calculated bed) is updated with the latter calculated weight-averaged bed level change which is in turn the starting point for the next morphological cycle.

In absence of any morphological acceleration factors (*morfac*=1), the hydrodynamic time stepping is the same as the morphological time step giving weight-averaged bed level changes on the hydrodynamic temporal scale. However, the latter may be cumbersome for long temporal scales. Conversely, the strength of the MorMerge approach is - in combination with a constant or varying *morfac* - that long-term morphological evolutions may be computed in a very efficient manner. Hereby, the bed level changes are aggregated (i.e. multiplied by the factor of *morfac*), merged, and weight-averaged which is used to update the initial/previously computed bathymetry. The flow chart of the parallel online approach is depicted here below in Figure 24.

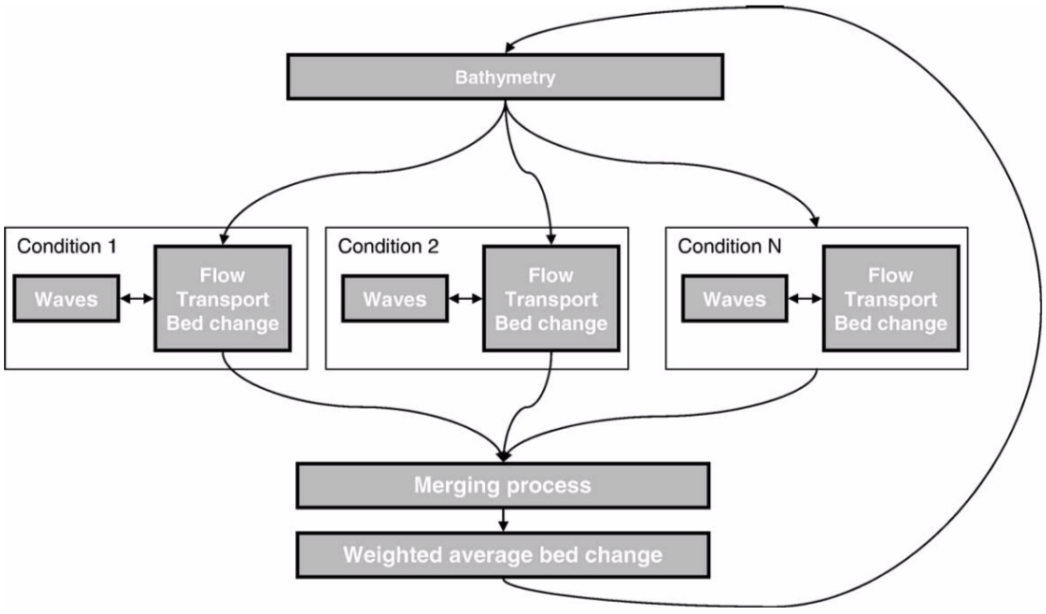

Figure 24: Flow scheme of 'parallel online' approach. (From Roelvink (2006))

Characteristics and Limitations of the parallel online approach

- Parallelisation of the bed level evolution procedure results in faster computations.
- The essence of the MorMerge approach lies in the assumption that - given the difference in time scale between the hydrodynamic action and the morphodynamic response - every hydrodynamic condition that contributes to morphological changes can be computed simultaneously (on the same bathymetry) without violating the physical nature of the system.
- Various combinations of different input conditions can lead to computations wherein larger *morfac* can be assigned especially when the short-term bed level changes are rather small per hydrodynamic time step. Large aggregated bed evolutions are hereby less likely to entirely erode the bed in one timestep such that large *morfac* can be safely applied (i.e. prevention of possible substrate excursion within one hydrodynamic time step).
- The small-scale hydrodynamic processes are coupled with the morphodynamics within each hydrodynamic time step Δt. Consequently, the small-scale interactions between the hydrodynamic

processes (i.e. current-wave interactions) and the morphodynamic processes (i.e. sediment transport, bed level evolution, bed sloping effects) are captured appropriately in the modelling technique.

6.5 The Brute Forcing Merged Approach as proposed by Luijendijk (2019)

The Brute Forcing Merged Method is a new method proposed by Luijendijk (2019) which provide a clever combination between two strong morphological evolution methods: (1) the online morphology approach and (2) the MorMerge approach. The online morphology approach provides the sequential evaluation of various sets of schematised morphological tides and waves (with varying or constant *morfac*), and morphological computations using the time series approach. The above enables the computation of morphology whilst holding paramount to the correlation between forcing conditions, seasonal variations in forcing magnitudes and directions, variations in (gross) transport rates, etc. Due to the monitored changes of the highest waves throughout the computations, the depth of closure could thereby be adequately adjusted (which is important for the littoral drift and the cross-shore profile evolution).
The MorMerge approach caters the application of parallelisation of the forcing conditions such that the relative contributions of the respective wave classes and schematised tides to the weight-averaged bed level changes - starting from the same bathymetry - are simultaneously derived. The combination of the two methods gives the ability to incorporate seasonal variations, chronology of the wave events, correlations between forcing conditions in the realm of parallelised computations. In the Brute Forcing Merged approach, the wave and surge time sequences are divided in sub-sequences of the respective seasons for which schematised conditions are defined. These schematised conditions are defined as such that the associated transport matches the *target* residual transport of the benchmark computations proceeded on the basis of time series analysis. These input conditions are, next, applied in a parallel online updating scheme whereby the individual bed level changes - computed from the same initial bed - are merged and averaged to obtain *weight-averaged bed level changes* using hereby a weighing scale based on the probability of occurrence of the respective wave events. Consequently, the setup of the Brute Forcing Merged method guarantees that the characteristics of the online morphology approach are completely embedded in a MorMerge updating scheme. An overview of the Brute Forcing methods and its characteristics is also depicted in Figure 25.

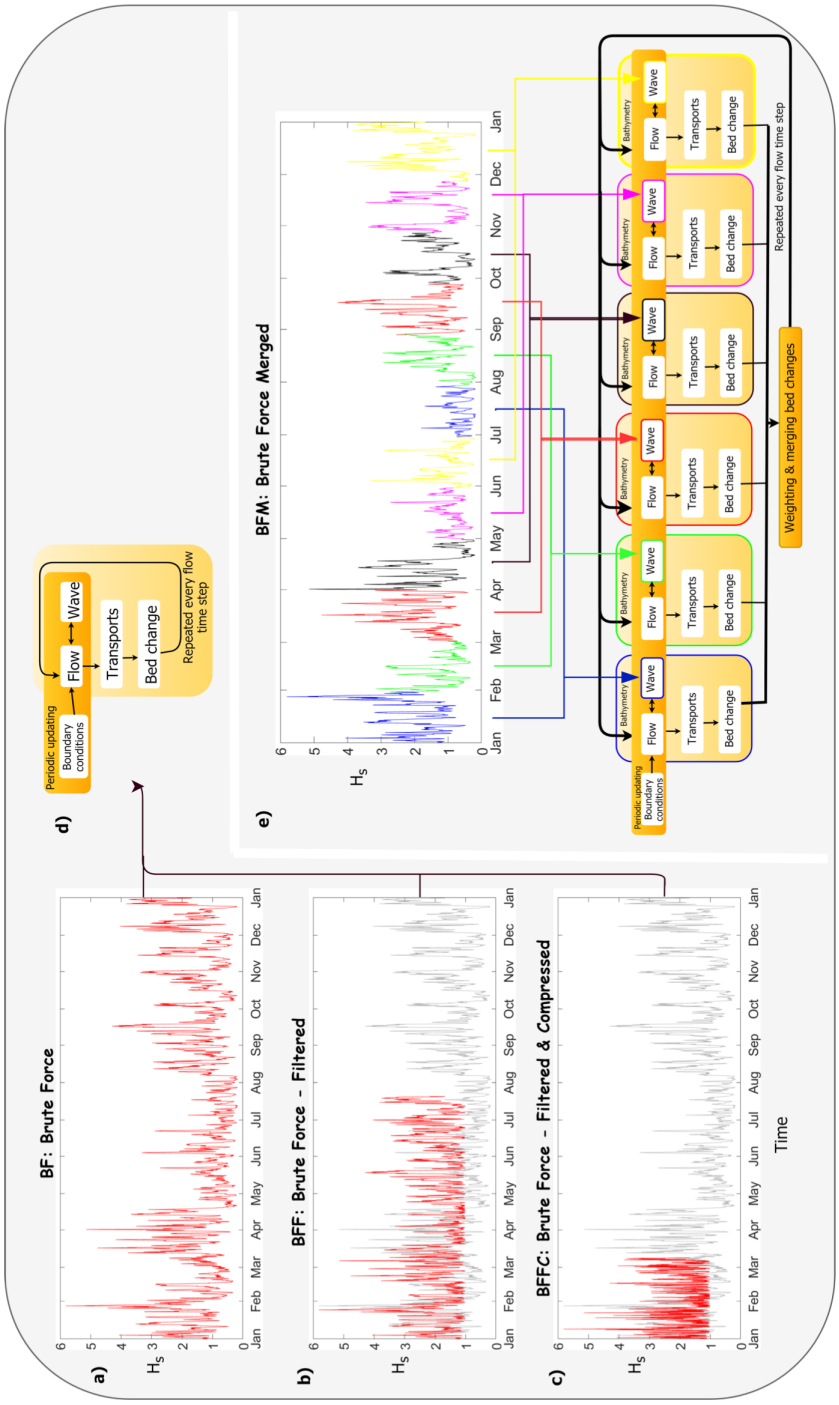

Figure 25: Graphical overview of (a) the non-scaled brute force approach (BF) and the three considered morphodynamic acceleration techniques using brute-force time series: (b) brute force filtered (BFF), (c) brute force-filtered and compressed (BFFC), and (e) brute force merged technique (BFM). (d) shows the basic morphodynamic feedback loop used in BF, BFF, and BFFC. The red wave time series in (a–c) indicate the selected wave time series. (From Luijendijk (2019))

.

7 MODEL SCHEMATISATION

This section is composed based on the findings of Latteux (1995), Lesser (2009) & Luijendijk (2019)

In reality, the coastal system and its associated behaviour depends on the governing physical processes that prevail in the latter region of interest. These physical processes thereby change over time due to a variety of causes such as - amongst others - seasonal variations in the weather conditions, the variability in the availability of sinks and sources due to the presence of storm events, timely variations in the local bathymetry and climate change. These variations are readily observed in historic measurement data comprising information about the local wave climate, water level & velocity data from for instance acoustic doppler current profilers (ADCP) and echosounders.
The time series following from the observed data can be applied in morphological models to prescribe the time varying forcing conditions. Thereby, the time series is a powerful tool to hindcast prior observed morphodynamic changes in so-called *hindcasting models* and are often applied to investigate the most important physical processes that contribute to a particular phenomenological event. After calibration, such models could in turn be used to forecast morphological evolutions. In such *forecasting models* probable morphodynamic changes may be computed over the extend of an arbitrarily distant time span (i.e. near future) with the attempt to, for instance, aid in coastal management decision-making on a medium- to long-term temporal scale or to assess the long-term effect of coastal interventions. Hereby, the forcing conditions that are often taken into consideration are (yet not limited to):

- **Tidal Residual Components**
  - Astronomical tide
- **Non-tidal Residual Components**
  - Storm Surges
  - Wind-generated surface gravity waves
  - Atmospheric tide

These types of forcing conditions are further assessed in the next sections.

7.1 Tide

In morphodynamic models often the effect of tidal motion to the morphodynamic response of a coastal setting is investigated. In such cases, the tidal forcing could be represented in various ways depending on the relative significance of the possible astronomic tidal constituents in the coastal setting.

Astronomical Tide

The Sun and the Moon exert a relative gravitational attraction to the water masses on Earth whereby the associated gravitational pull enables the incipience of tidal motion and the formation of tidal constituents. The origin of these tidal constituents could be ascribed to astronomical phenomenon whereby seasonal variations occur in the declination between the Earth and the sun and the moon, respectively. Also, the elliptical orbit that the moon describes around the Earth gives rise to semi-diurnal and diurnal tidal constituents.
Around the world the tidal character can also vary due to the relative importance of certain (semi-)diurnal tidal constituents and thereby favouring semi-diurnal or diurnal tidal curves in some locations

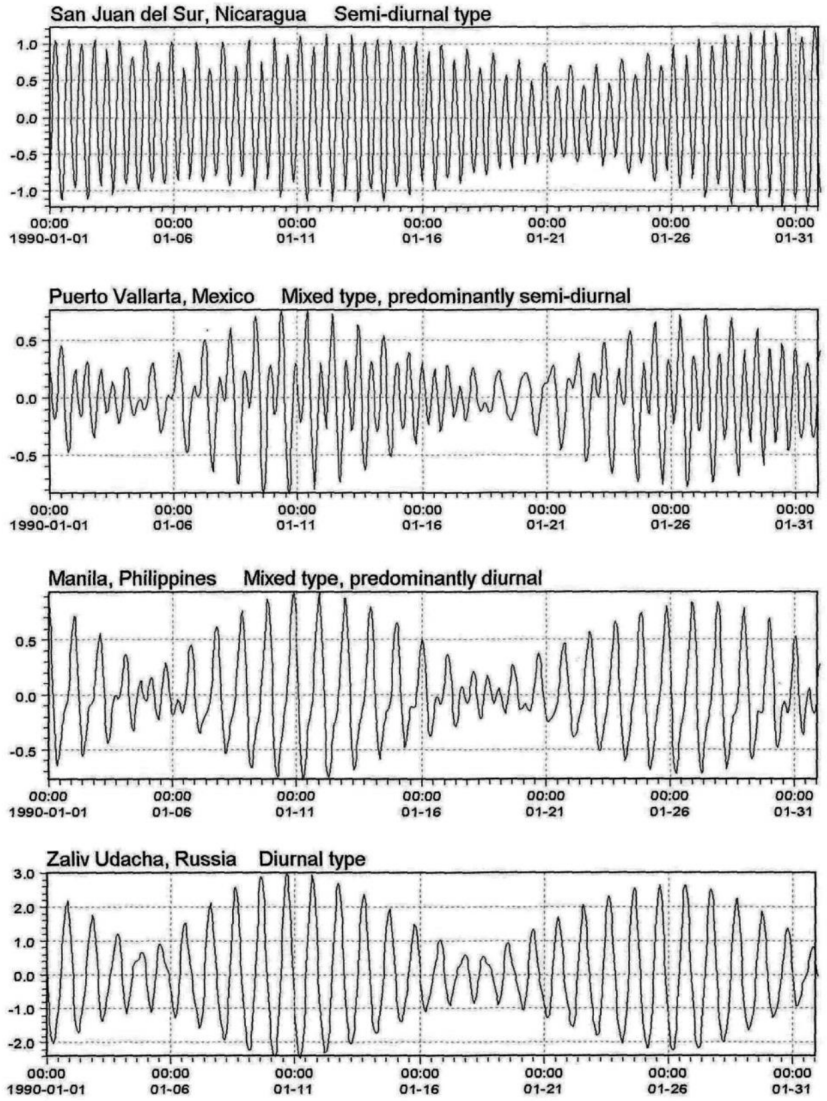

Figure 4-11 Examples of tidal curves showing each of the four tidal characters. From Mangor (2004).

Figure 26: Examples of tidal curves showing each of the four tidal characters. (From Mangor(2004) & Bosboom and Stive (2005))

over mixed-type tidal curves (predominantly, diurnal or semi-diurnal) in other coastal settings. An example of such global variation of astronomical tide could be observed in Figure 26

In coastal settings where the tidal curve is (semi-)diurnal, the tidal residual transport could be readily inferred from a selection of tidal constituents (which may form the basis for a schematised tidal forcing). Conversely, in mixed-tide environments where the relative importance of a vast number of tidal constituents is evident, such tide reduction techniques may not be straightforward. Thereby, the water level time series - filtered for only the tidal response - is adopted aiming to decompose the tidal signal by the governing tidal constituents. An example of such procedure can be seen in Luijendijk *et al.* (2017) - for the case of the Sand Engine, the Netherlands - where the water level time series filtered for solely tidal motion is decomposed in the O_1, K_1, M_2, S_2 constituents and M_2 overtides M_4, MS_4 (see Figure 27 and Figure 28). The resulting components with particular amplitude, phases, frequency and velocity are used as input in further morphodynamic models.

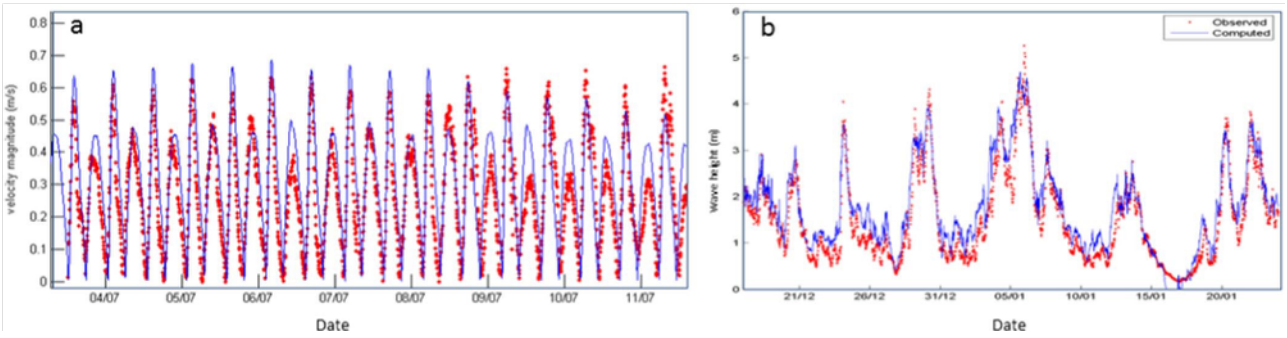

Figure 27: (a) The comparison between computed and observed currents at location F for July 2012 (blue represents the computed currents) and (b) the computed and observed wave heights at the nearshore wave rider buoy for the period 17 December 2011 to 25 January 2012. See locations of the observations in Fig. 2b. (From Luijendijk *et al.* (2017))

Table 3
Results of the statistical tidal analyses of water levels and currents.

Constituents	Water levels at Scheveningen				Constituents	Currents at ADCP F			
	Amplitudes (m/s)		Phases (min)			Amplitudes (m/s)		Phases (min)	
	Obs.	Mod.	Obs.	Mod.		Obs.	Mod.	Obs.	Mod.
O1	0.10	0.11	176	177	MU2	0.03	0.03	119	140
K1	0.09	0.11	338	335	N2	0.04	0.04	325	349
M2	0.78	0.76	68	73	M2	0.29	0.30	40	32
S2	0.17	0.18	136	137	L2	0.05	0.06	113	97
M4	0.22	0.22	103	114	S2	0.08	0.03	115	51
MS4	0.10	0.11	168	174	M4	0.01	0.04	2	81

Figure 28: Results of statistical tidal analysis of water levels and currents.(From Luijendijk *et al.* (2017))

Morphological Tide

Elongated Tide as proposed by Latteux (1995)

Tidal time series may also be reduced to a single "morphological tide" as proposed by Latteux (1995) which he called the *lengthening of the tide* method. Hereby, the morphological response over N consecutive tidal cycles is simulated by *one elongated* tidal wave with a wave period equal to N x the individual tidal cycle.
This procedure encompasses the simulation of the tidal time series for successive tidal cycles over a time span larger than the time scale of the individual tides (i.e. spring-neap cycle for instance). On the scale of the spring-neap cycle, an elongated *representative* tide is constructed with the period of the sum of the successive tidal cycles - here equal to the fortnightly spring-neap duration - for which the mean sediment transport patterns and rates should align with the mean transport patterns observed following from the benchmark time series computations (see Figure 29). Latteux (1995) uses, hereby, the tide-averaging approach and suggests the application of the *continuity correction procedure* to update regularly the transport field within each *elongated* wave cycle.

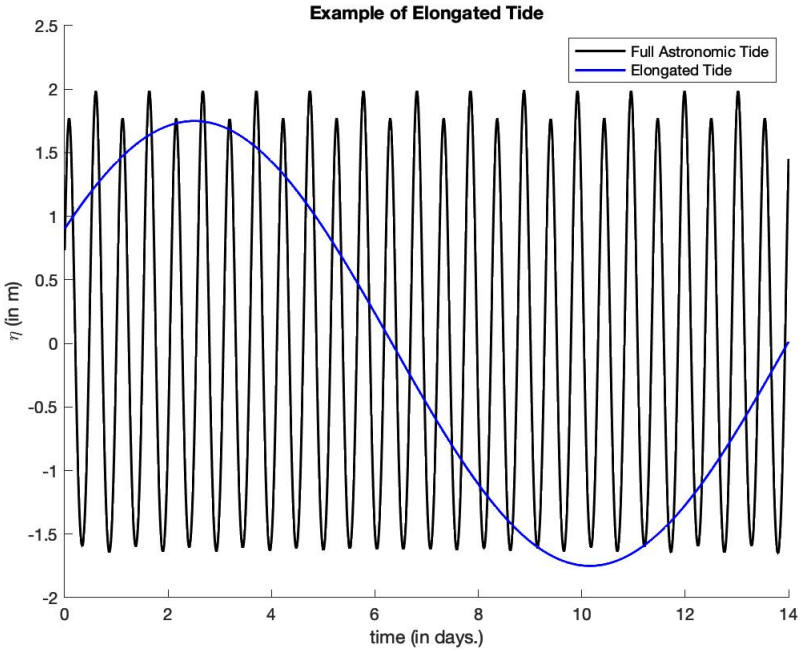

Figure 29: Simple example of elongated tide

An adjusted Morphological Tide as proposed by Latteux (1995)

An adopted method is also described by Latteux (1995). For the astronomical tide, the actual time sequence is simulated over a time span larger than the time scale of the individual tidal cycle (i.e. spring-neap cycle). Here, an individual tidal cycle is *selected* to represent the tidal forcing over the simulation duration (see Figure 30). The subsequent repetition of this individual tidal wave is thereby assumed to give the same mean sediment transport *patterns* as obtained from the benchmark computations with the tidal time sequence.
It could very well be the case that the *mean* transport rates of the *representative* tide may not align with the benchmark observations. The application of a calibration factor to tune the computed rates to the benchmark observations may be an efficient way of dealing with the latter challenge and of subsequently minimising the Root Mean Squared Errors.
As stated by Latteux (1995) and Lesser (2009), applying this adopted method leads to tidal amplitudes which are 7% - 20% larger than the actual tide.

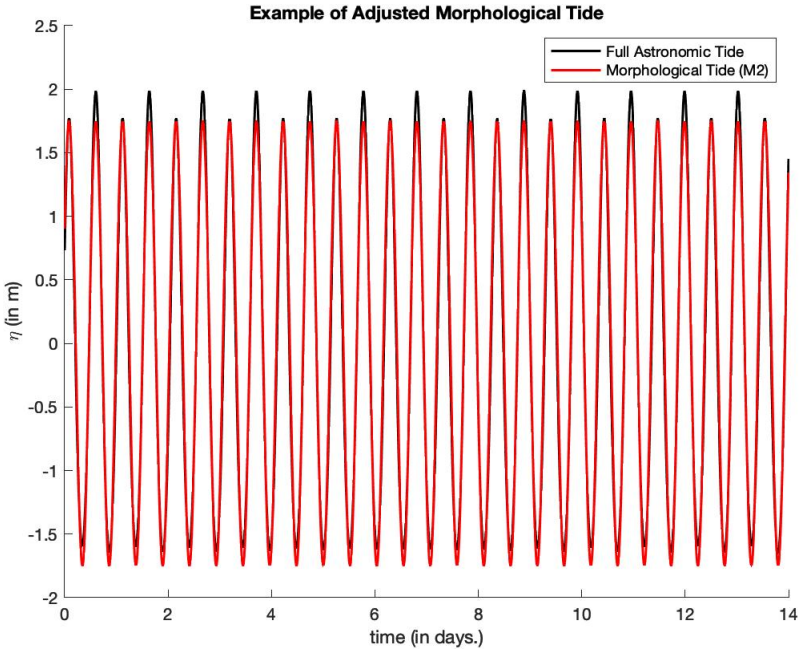

Figure 30: Simple example of Adjusted morphological tide

An improved Morphological Tide as proposed by Lesser (2009)

In the adjusted Morphological Tide as proposed by Latteux (1995), the tidal time sequence is schematised using *one* selected tidal wave (i.e. M_2 for instance) for which the amplitude is adjusted to acquire comparable mean transport rates. The challenge that may occur with such a schematisation is that *all* the important residual transport components may not be adequately represented in such a model. In absence of the missing constituents - especially when the missing constituents are dominant in the region of interest - the interaction between these constituents could contribute to significantly larger residual sediment transport and are unfortunately not incorporated in the model by omission.

As stated by Lesser (2009) an investigation on the Willapa Bay, USA showed that the contribution of just the M_2 component is insufficient to obtain the residual transport of the M_2, O_1 & K_1 constituents which are predominantly prevalent in the Willapa Bay. Prior research had already shown that the M_2, K_1 & O_1 constituents are formed by linear combinations of the two diurnal astronomic frequencies which confluent in such a way that the fortnightly spring-neap tide (period of 13.66 days) prevailed together with daily inequality effects provided by the interaction between the diurnal and semi-diurnal components. The residual transport on the basis of the spring-neap cycle is hereby more significant in comparison with the residual transport based on the semi-diurnal M_2 found by interactions with its overtides.
Furthermore is shown in Lesser (2009) that for harmonic terms the residual transport is found by time-averaged evaluation of the higher-order velocity components, viz. equation (126),

$$\left\langle \left[O_1 cos\left(\omega_{O_1} t - \varphi_{O_1}\right) + K_1 cos\left(\omega_{K_1} t - \varphi_{K_1}\right) + M_2 cos\left(\omega_{M_2} t - \varphi_{M_2}\right) \right]^3 \right\rangle \tag{126}$$

with:

- O_1, K_1 and M_2: The amplitude of the (semi)diurnal tidal wave components (in m)
- ω_{K_1},ω_{O_1} and ω_{M_2}: The frequency of the respective (semi)diurnal tidal wave components (in rad/s)
- φ_{K_1}, φ_{O_1} and φ_{M_2}: The phase shift of the respective (semi)diurnal tidal constituents (in rad/s)
- $\langle U^3 \rangle$: The time-averaged third order velocity component and highlights the net effect of the tidal constituents to the residual transport.

Taking into account that the two diurnal frequencies results in a M_2 semi-diurnal frequency and after some subsequent mathematical simplifications, a description of the residual transport due to the interactions between the M_2, O_1 & K_1 constituents is found as stated in equation eq.(127) below,

$$\left\langle U^3_{O_1K_1M_2} \right\rangle = \frac{3}{2} O_1 K_1 M_2 cos\left(\varphi_{O_1} + \varphi_{K_1} - \varphi_{M_2}\right) \tag{127}$$

In an attempt to capture this nonlinear residual transport in a representative tide, an artificial tidal constituent C_1 is considered with a diurnal frequency $\omega_{C_1} = 0.5\omega_{M_2}$, such that equation eq.(128) now represents the total residual transport,

$$\left\langle \left[C_1 cos\left(\omega_{C_1} t - \varphi_{C_1}\right) + M_2 cos\left(\omega_{M_2} t - \varphi_{M_2}\right)\right]^3 \right\rangle \tag{128}$$

with:

- C_1 and M_2: The amplitude of the (semi)diurnal tidal wave components (in m)
- ω_{C_1}: The frequency of the artificial diurnal tidal wave components (in rad/s)
- φ_{C_1}: The phase shift of the artificial diurnal tidal constituents (in rad/s)

Lesser (2009) finds that a representative morphological tide can be derived with an equivalent residual transport as equation eq.(127) by application of the new artificial diurnal constituent C_1 as follows in equation eq.(129)

$$\left\langle U^3_{C_1M_2} \right\rangle = \frac{3}{4} C_1^2 M_2 cos\left(2\varphi_{C_1} - \varphi_{M_2}\right) \tag{129}$$

with,

$$C_1 = \sqrt{2O_1K_1} \quad \& \quad \varphi_{C_1} = \frac{\varphi_{O_1} + \varphi_{M_2}}{2}$$

Hence the residual transport as a consequence of the nonlinear interaction between the M_2, O_1 & K_1 constituents, is captured by a representative M_2 tide superposed with a diurnal C_1 tidal constituent (see Figure 31).

In the latter derivation the presence of non-tidal mean flow in the region of interest is not considered. Under such circumstances the astronomic tide reduction method is supplemented with a factor f_1 or f_2. For the schematisation of a $(M_2 + C_1)$tide, the sum of the constituents is multiplied by a factor f_1 (i.e. $f_1 * [M_2 + C_1]$) for which the magnitude can be found using equation eq. (130) below,

$$f_1 = \sqrt{\frac{M_2^2 + K_1^2 + O_1^2 + S_2^2 + N_2^2 + ...}{M_2^2 + C_1^2}} \tag{130}$$

An alternative factor may be considered that only tunes M_2 by multiplication of a factor f_2 (i.e. $f_2 * [M_2] + C_1$). The latter factor gives rise to less errors compared to the f_1 factor in the derivation of the residual transport - this error is in the order of the third order moment $\langle f_1^3 \rangle$. f_2 may be found by application of equation eq. (131) below,

$$f_2 = \sqrt{\frac{(M_2^2 + K_1^2 + O_1^2 + S_2^2 + N_2^2 + ...) - C_1^2}{M_2^2}} \tag{131}$$

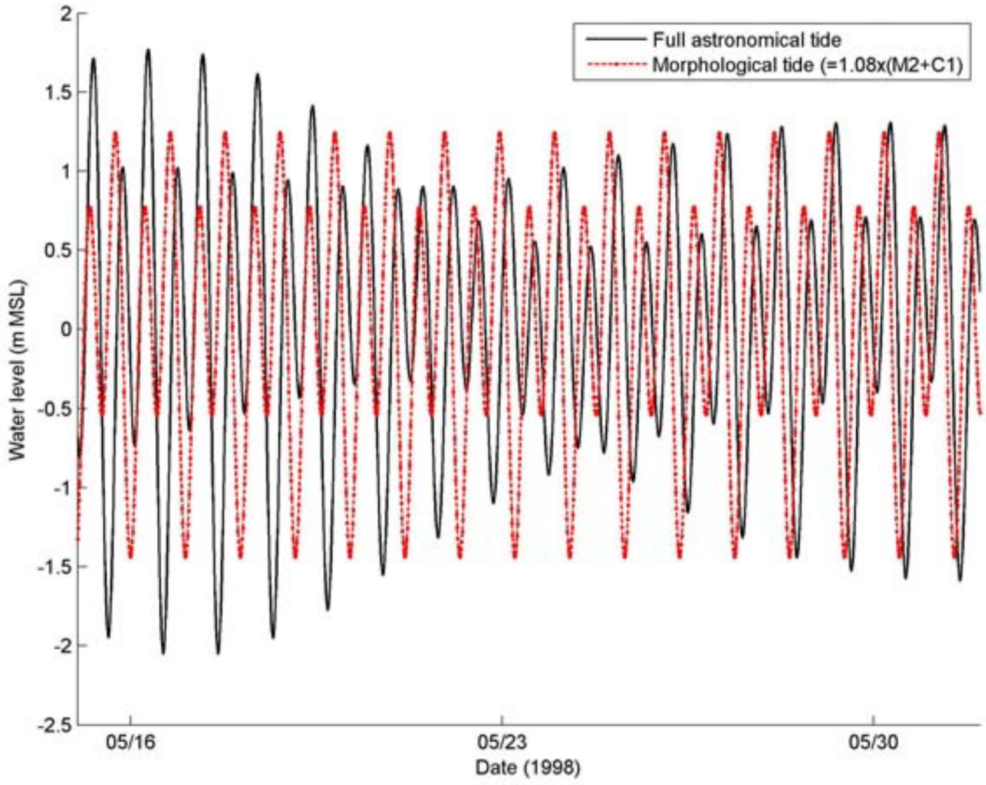

Figure 5.2 *– Full astronomical and simplified morphological tide shown for the duration of one neap-spring tidal cycle.*

Figure 31: Example of an improved morphological tide for the Willapa Bay, Washington (USA). Full astronomical and simplified morphological tide shown for the duration of one neap-spring tidal cycle. (from Lesser (2009))

7.2 Waves

Wave input reduction methods are methods aiming to reduce the wave climate to a set of wave conditions that give the same response (i.e. residual sediment transport) as the benchmark computations with the full wave climate. For input reduction methods wherein wave schematisations are considered, the chronology of wave events may be of certain interest (i.e. when the order in which the respective wave conditions are processed becomes important). An option to overcome this is by application of a *sequential "online morphology"* procedure.

The chronology of wave conditions depends on the coastal setting under investigation. If wave events are present (e.g. storm events) that generate irreversible changes to the coastal setting, then it may be of interest to introduce the chronology of the wave events into the morphodynamic computations. Otherwise, the underlying risk prevails that the actual observed phenomenological events are not reproduced. Conversely, if the geomorphological setting does not show a significant dependence with one particular wave event, then the chronology of the wave event may be disregarded in the computations of the morphological evolution. An indication if a geomorphological setting is dependent on the chronology of wave events may follow from historic data. Here, clear signs may be detected of irreversible system changes. For instance, the occurrence of episodic events that shift the coastal setting back to the highest beach state (i.e. dissipative beach state). Or the occurrence of the breaching of a tidal inlet due to

storm events. Notion of these events, support the decision-making of the geomorphologist to account for chronology of wave events. For meso-scale features, it is known that the small-scale features may influence the behaviour and formation of the larger-scale formations. Here, the *individual* small-scale features have a direct interaction with the development of the larger scale morphological features. The consequence might be that significance of the individual wave conditions that have resulted in the generation of the particular small-scale features becomes more relevant. The chronology of the wave conditions might therefore be necessary to correctly predict the evolution of the geomorphological system at hand. As such, the geomorphologist could try to compute the morphodynamic development on the basis of a model setup that does (not) account for chronological wave events. When the comparison between the two model results, and comparison with the observations show large deviations for one of the two predictions, then the morphologist may be inclined to choose for the model that fits the best to the observations. Hence, a preliminary model assessment may hint if the chronology of the wave events is significant for the geomorphological setting under investigation and further incorporation in the model assessment.

Thereby as theorised by Lesser (2009), the correlation between different forcing processes may influence the schematisation of the wave conditions. In the winter seasons, high wave conditions could very well align with strong winds whereas during the summer season calm wave and wind conditions may be apparent. Hence, it may be important to capture such *seasonality* in the forcing conditions. It is noted by Lesser (2009) that such seasonality were quite important in the numerical modelling procedures concerning the ebb-tidal deltas of the Dutch Wadden Sea.
When forcing conditions are reduced in a model for which the underlying forces are correlated, it should be noted that the correlation between the forcing conditions must also be captured in the schematised forcing conditions as well.

Wave time series may be schematised by manual selection of wave classes based on the offshore wave climate (i.e. weighted class selection approach) or by means of an "optimum" wave selection method which will be further analysed in the next sections.

Wave Class Selection Approach based on Offshore Wave Climate

In the weighted class selection approach, the offshore wave climate is partitioned in wave height and wave direction bins to obtain a discrete set of wave classes. For each class, the weighted-average significant wave height H_s, wave direction ϕ, peak period D_p, and respective probability of occurrence are subsequently computed. Hence, a set of wave classes may be found which provide the same residual transport as the benchmark model simulation.

"Optimum" Wave Class Selection Approach

The "optimum" wave class selection method - hereafter referred to as the "Opti-method" - is a wave schematisation method that aims to reduce the wave time series to a set of wave conditions which focuses on a particular *target* value (i.e. nett longshore transport, gross longshore transport, etc.). This method selects and optimises a discrete set of wave conditions (i.e. $O(10)$) based on the results of a proceeding wave time series benchmark simulation. The outcome of the latter simulation in terms of the *target* value for optimisation is compared with the numerical outcomes in each cycle of wave class reduction wherein the least contributing wave class is discarded. The probability of occurrence of the discarded wave conditions is later added to the closest adjacent wave class. Next, the RMS error, covariance and bias are calculated and monitored throughout the process. A selection of "Optimum" wave classes is thereby proceeded on the basis of the cases for which the RMS error remains within acceptable bounds (i.e. user-specified). Hence, the wave classes which pose as best candidate for swift schematised morphological simulations are hereby taken into account.

The choice of *target* is, lastly, also a factor of the coastal setting at hand as observed by Luijendijk (2019). If coastal interventions are prevalent during the time span of interest (i.e. construction of a

groyne field), having the gross longshore transport as *target* may capture the irreversible changes in the transport field better than a *target* nett longshore transport. In the former, the wave conditions are tuned to provide acceptable results for the individual components of the gross longshore transport, whereas the latter solely considers the nett residual transport.

The limitations of the aforementioned wave class selection methods are proposed by Luijendijk (2019) and depicted in Figure 32 below. Hereby, it may be seen that the varying location of the depth of closure during the morphological computations may not be accurately derived by all wave schematisation methods. The latter is of utmost importance for establishing the cross-shore range of the dynamically active section of the (near-shore) morphology. What is also shown in Figure 32 is that the Brute forcing merged approach seems to be able to capture the most characteristics of the forcing conditions thereby retaining the seasonal variations, the correlation between forces, an accurate description of the timely varying depth of closure and accurate results for both the Gross Longshore and Nett Longshore transport.

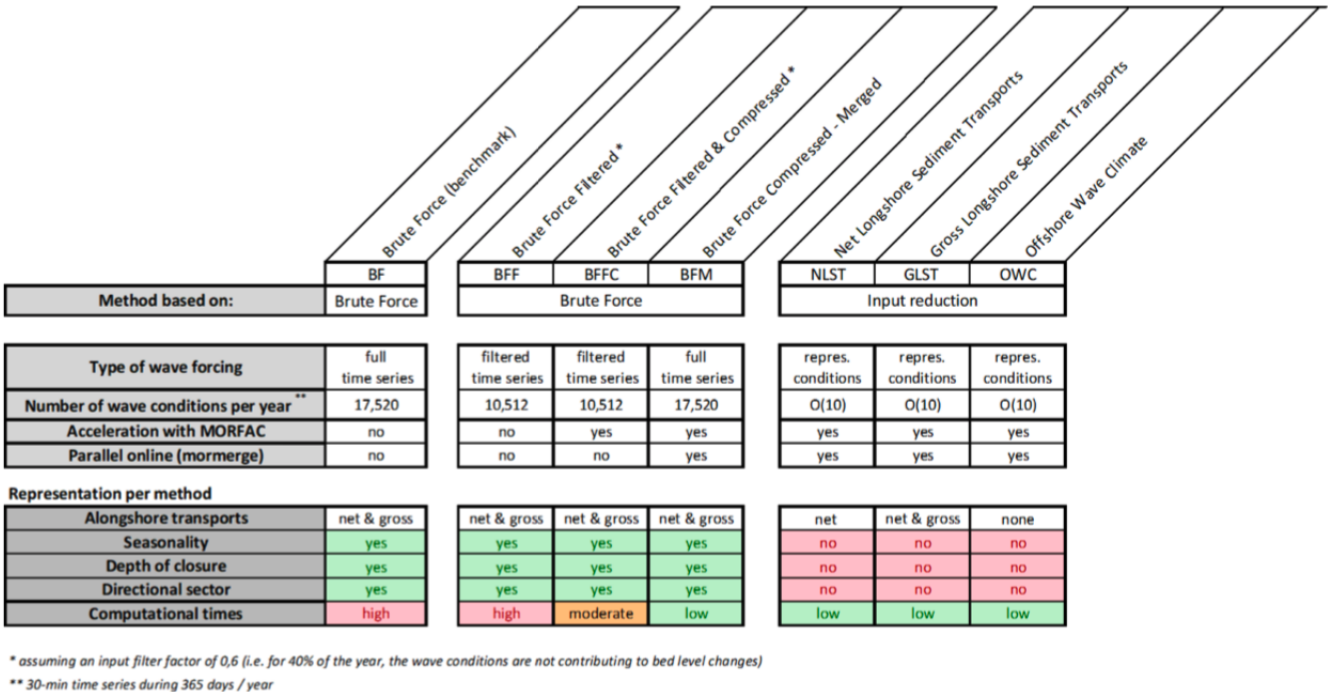

Figure 32: Characteristics of the considered morphodynamic acceleration techniques. (From Luijendijk (2019))

7.3 Morphological Acceleration Factors

The morphological acceleration factor (*morfac*) is a tool to overcome the differences in time scale between the small-scale hydrodynamic processes and the larger scale morphodynamic response. This *morfac* may be beneficial if long-term morphological evolutions without any extensive computational effort are of particular interest. Hereby, the morphodynamic model calculates the bed level changes based on a schematisation of the tides and waves after which the results per hydrodynamic cycle are aggregated by the factor of *morfac*. The magnitude of the *morfac* depends, in essence, on the case at hand. However, since morphological evolution models which enable the use of *morfac* inherently assume linearity within the morphological wave cycle, linear superposition of the computed bed level changes is of categorical importance to the aggregation procedure as noted by de Vriend *et al.* (1993). The latter means that for the bed level changes and its associated residual transports, changes in time are considered to be linear over the hydrodynamic cycle. The maximum *morfac* is thereby largely dependent on the stability and the accuracy of the morphodynamic evolution technique chosen, and on the grid cell resolution. An

overview of the *morfac* restrictions for the modelling techniques considered, is depicted in Figure 33. It should be noted that the factor n concerns here the morphological acceleration factor. What may be seen is that the *morfac* criterion for stability is dependent on the maximum tide-averaged sediment transport, the magnitude of the time step, the local water depth, and the degree of non-linearity[1] of the sediment transport (i.e. b ranges naturally between 3 and 5 Lesser (2009)). Hence, given rather typical conditions for coastal shelf seas - $h = 30m, \quad \Delta x = 500m, \quad U \leq 1m/s, \quad \Delta t \leq 1min. \quad \& \quad b = 3$ - the *morfac* is limited to $O(10)$ for smaller local flow depths (i.e. larger flow velocities), whereas in deeper channels (i.e. smaller velocities) the *morfac* is limited to $O(100)$. It should be noted that in low-energy wave (dominated) environments, the applied *morfac* can be even larger. For example, van der Wegen (2010) proposed a *morfac* of $O(400)$ in the computations of the morphodynamic development of the Western Scheldt Estuary.

Table 1
Overview of criteria for different methods

Method	Numerical stability	Accuracy	Coping with variable input
Tide-averaging	$n < \frac{h\Delta x}{b < S > T}$	$\varepsilon_{\text{rel}} = \frac{1}{2}\frac{b\Delta z_b}{h}$	$n < 700/n_{\text{cond}}$
RAM	$n < \frac{h\Delta x}{b < S > T} n_{\text{RAM}}$	$\varepsilon_{\text{rel}} = \frac{1}{2}\frac{b\Delta z_b}{h}$	No restriction
Online	$n < \frac{h\Delta x}{bS_{\max} dt_{\text{flow}}}$	$\varepsilon_{\text{rel}} = \frac{1}{2}\frac{b}{h}\left(\Delta z_{b,t+nT} - n\Delta z_{b,t+T}\right)$	$n < 700/n_{\text{cond}}$
Parallel online	$n < \frac{h\Delta x}{b < S >_{\max} dt_{\text{flow}}}$	$\varepsilon_{\text{rel}} = \frac{1}{2}\frac{b}{h}\left(\Delta z_{b,t+nT} - n\Delta z_{b,t+T}\right)$	No restriction

Figure 33: Overview of criteria for different methods. (From Roelvink (2006)) Column 1 (left) shows the conditions for which stable numerical computations may be proceeded. As can be seen, an upper bound is apparent for the level at which morphological computations should be accelerated. The magnitude of the *morfac* (n) is highly dependent on the magnitude of the morphological variability for each considered wave condition. If the sediment transport becomes large for a given wave condition, the *morfac* should be reduced to avoid numerical instabilities during the morphodynamic computations (vice versa for smaller sediment transport rates). In the case of instable computations, the numerical scheme produces a relative error in the model outcome. Column 2 (Middle) shows that this error is related with the degree of non-linearity of the sediment transport formulation (b = $3-5$) and the *morfac*. Therefore, *morfac* should be handled with extreme care as it linearly amplifies the numerical errors originating from numerical instabilities.

[1] The degree of non-linearity is equal to the power of the transport formulation (i.e. $S \propto m * S^n$)

Variable *morfac* Conditions

This section is adopted on the findings of Lesser (2009)

Irrespective of the morphological acceleration technique chosen, the application of varying *morfac* throughout the morphodynamic simulation procedure could be rather beneficial. For instance, in cases wherein the seasonality of the wave conditions becomes important and therefore considered in the computations, or when a set of different schematised wave conditions is proceeded. In combination with a constant morphological tide or different morphological tides changing through the simulation (i.e. when combinations of wave, surge and tidal conditions influence the magnitude of the total residual transport such that different morphological tides are to prevail), different *morfac* are to be used to effectively speed up the numerical computations. Consequently, larger *morfac* could be included for the respective input conditions wherein the residual transport and associated bed level changes are rather small. Whereas smaller values of *morfac* should be applied when the set of input conditions generates large residual transports and bed level changes per time step.

Conversely, the seasonal variations in the wave conditions could - in the same analogy - be efficiently assessed by means of a variable *morfac*. If for instance the combination of wave climate and the astronomical tide time series leads to roughly the same mean flow conditions, *one morphological* tide may be taken into account. The wave climate is next, divided into different classes which describe the distinct seasonal wave conditions throughout the time span of particular interest. Computations of the morphological changes should therefore in the same fashion consider the actual seasonal length wherein the wave conditions prevail. When the morphodynamic cycle of the morphological simulation remains constant (i.e. fixed morphological tidal cycle), the latter computations should strictly monitor that the response associated with the respective wave conditions is apparent within the actual season duration and *relative to the scale of the morphological tide*. Thereby, the *morfac* is tailored as such that the changes in seasonal duration over the time span of computations and relative to the morphological tide is incorporated in the description of the varying *morfac*. Furthermore, and especially when an online morphology approach is applied with sequentially varying input conditions, it may be wise to capture the weight-averaged effect of each wave condition to the benchmark morphological changes given the relative occurrence of the respective wave conditions. The latter *morfac* is then again adjusted such that the relative contribution of each wave condition to the observed seasonal morphodynamic changes (i.e. seasonal target for residual transport) is related to the statistical occurrence of the wave conditions in the observed wave climate. As such, the adopted *morfac* varies over time as a function of (1) the probability of occurrence of the wave conditions p_c, (2) the variation in the seasonal duration of each respective wave condition and (3) the time scale of the associated morphological tidal cycle $T_{morph\ tide}$. Equation eq.(132) below gives the mathematical description of the (seasonal) varying *morfac*:

$$morfac = \frac{p_c * \text{seasonal duration}}{T_{\text{morph tide}}} \tag{132}$$

Summarising, when dealing with seasonal varying wave conditions the *morfac* should answer the following questions:

- *Probability of occurrence*
  What is the respective probability of occurrence for the wave conditions derived from the (offshore) wave climate?
- *Seasonal Duration*
  What is the relative duration of the seasonal changes for the respective wave conditions with respect to the morphological tide under consideration?

Varying *morfac* may also be applied in order to align with the changes in the schematisation of the tides and waves over the duration of the morphological assessment. This could be the case if for instance during the chosen time interval coastal interventions are evident which may have irreversible effects on the *target* residual transport patterns and rates over the simulation time span. New morphological

tides should then be proposed for the time span following each intervention. Parallelly, variable *morfac* should be designated which outline the relative contribution of the input conditions to the *target* residual transport as function of its probability of occurrence.
An important notion is that the suspended sediment transport should always be monitored closely during the transition between two states of different *morfac* and input conditions. When switching from one state to another state, the sediment masses in suspension may be overstated in between such transitions whereby consequently larger volume masses (than physically possible) are either brought in suspension or are settling on the bed.

For instance - given a uniform suspended sediment concentration of $5kg/m^2$ - if after the final computations of the first state with *morfac* 20 a suspended sediment volume is calculated of $100kg/m^2$ which settles at the bed, and the *morfac* is adjusted in the second state from 20 $\rightarrow$ 100, the suspended sediment volumes that will be received by the bed increases from $20kg/m^2 \rightarrow$ to $500kg/m^2$. Hence, if in between the two *morfac* states, the morphodynamic simulation is adequately stopped allowing for sufficient relaxation of the suspended sediment and natural reduction of the concentration, the error that is obtained when switching from one state to the other could subsequently be minimised.

When switching from one set of (schematised) input conditions with a particular *morfac* to another, Lesser (2009) proposes the following method to control the switching of *morfac* during a morphodynamic simulation (The derivation starts from an idle simulation):

1. The *morfac* will be set to zero, such that the morphodynamic simulation is halted.
2. Using *slow ramping* over a period of 60 minutes, the new input conditions are prompted. This prevents the model from creating numerical errors due to nonphysical shock waves in the forcing conditions.
3. A(n) (intermediate) relaxation time scale is next considered of 685 minutes to stabilise the hydrodynamics following from the new input conditions. It is hypothesised in this report that Lesser (2009) related the relaxation time interval to the order of the morphological tidal period (i.e. 14900 minutes) giving a relaxation time of approximately half the morphological tidal period.
4. Next, the *morfac* is aligned with the new boundary conditions which restarts the morphological computations.
5. The model computes new hydrodynamic conditions (i.e. flow and wave field, flow patterns, etc.) and new morphodynamic changes (i.e. sediment transport patterns, aggregated bed level changes) throughout precisely one morphological tidal cycle. This guarantees that at identical times the starting and stopping procedure is prompted throughout the simulation, and identical wave conditions are pertained within each morphological tidal loop.
   It should be noted that the transition between conditions can also be aligned with different time instances, such as the time instances wherein slack water is evident. This has the extra advantage that in the latter case the transitional suspended sediment concentrations are minimal.
6. Repeat this procedure for the remainder of the simulation time and input conditions to conclude the numerical computations.

Stark (2012) proposes thereby ,with respect to eq.132, to consider that one wave condition may be simulated over a period longer than one morphological tide. For instance, if the wave conditions of two consecutive, distinct seasons poses almost consistent wave height, wave direction and non-tidal flows then the wave condition of the 1^{st} season can be extended for two morphological tides. To account for the number of morphological tidal cycles that are considered for each wave condition, a factor n is included. Hence, eq.132 becomes then:

$$morfac = \frac{p_c * \text{seasonal duration}}{n * T_{\text{morph tide}}} \tag{133}$$

Moreover, a morphologist may compose a standardised wave climate of schematised wave conditions for a period over which it is readily to assume that the wave conditions does not vary significantly (e.g. 10 years). If this wave climate is extended for an arbitrary period other than a scalar multiple of the considered 10 years - e.g. 7 years - then the factor of *morfac* must be adjusted accordingly. Affirmatively, the morphological development for the 7 years is already sooner observed. To account for the aforementioned, in case of a standardised wave climate, the *morfac* values must be adjusted with a factor of $\frac{7}{10} = 0.7$. More generally speaking, this effect may also be obtained by evaluation of the sum of the weights of the seasonal durations $\sum_i^N p_c * \text{seasonal duration}$ within the considered simulation duration. If the $\sum_i^N \{...\} > 1$, all morfac values should be adjusted with this factor (and vice versa for < 1). Stark (2012) uses hereby as strict upper bound morfac < 100, and also ensure a conservatively low factor of *morfac* in high-energy wave conditions (i.e. designated here to be $H_s > 4m$).

8 CONCLUSION

In Pillar II several methods concerning the efficient computation of morphological evolution have been reviewed and discussed. Hereby, the *offline* methods were discussed.

The tide-averaging approach concerns a modelling technique wherein the morphological adjustments are computed on the basis of tide-averaging flow conditions. The sediment transport is found by computations of the transport on several point in the wave cycle. These values are averaged to obtain the tide-averaged sediment transport which is used to compute the bed level changes and subsequently update the bathymetry.
The parallel-offline approach is an extension to the tide-averaging approach that considers multiple sets of input conditions to compute the bed level changes. During each morphological loop, the flow patterns and bathymetry are kept constant so that the sediment transport only changes with depth-variations. The sediment transport *fields* are weighted to obtain a weighted-averaged sediment transport field after which the bed level changes are computed. These may be used to update the previous bathymetry.

Moreover, another set of updating methods is discussed wherein the morphodynamics are computed simultaneously with the hydrodynamic computations - the *online* methods.
The **Online morphology** approach concerns the modelling technique whereby the morphodynamics is computed simultaneously with the hydrodynamics. Within each hydrodynamic loop, the flow and wave field are computed. The flow patterns are updated, and the sediment transport field is computed such that the bed level changes could be derived to update the bed.

Variations of the online approach are also apparent.
In the **Brute Forcing Filtered (BFF)** method, the time series may be reduced to solely incorporate the time series data that contributes to bed level changes.
In the **Brute Forcing Compressed (BFC)** method, the time series data is squeezed in the same fashion as the factor of *morfac*.
The **Brute forcing Filtered and Compressed (BF-FC)** method, is a combination of the two wherein the filtered time series is squeezed in the same fashion as the factor of *morfac*.

In the **parallel online approach**, the morphodynamic changes are computed on the hydrodynamic time scale Many input conditions are simultaneously proceeded from which the individual transport fields are derived. These are weighted and merged to obtain the weigh-averaged sediment transport. The bathymetry is subsequently updated with the weighted-averaged bed level change.

Variations of the parallel online approach
The **Brute Forcing Merged (BFM)** method is a parallel online approach that caters the sequential evolution of various sets of schematised tide and wave conditions to compute the morphological changes on the bed. In the BFM method the wave and surge time sequences are divided in sub-sequences of the respective seasons for which the schematised conditions are defined. Thereby, the forcing conditions are defined is such a way that the associated residual sediment transport matches with the target residual transport.

Next, Pillar II elaborates on the choices on forcing representation that may be applied for in morphodynamic models. Firstly, considering the tidal residual components, a morphologist may acquire *the astronomical tide*. **The Astronomical tide** is the sea surface variation of the Earth's water masses due. to the attractive forces between the Earth and the Sun and the Moon. The associated gravitational pull

enables the incipience of tidal motion and the formation of tidal constituents.
Conversely a morphologist may apply for a *morphological tide*. **A morphological tide** is a schematised representation of the tidal residual (TR) forces for which holds that the residual transport caters the same morphological changes as the observed astronomical tide. If chosen for the **elongated tide**, the TR time series may be reduced to a single morphological tide. Hereby, a representative tidal wave is cast as such that the *mean* residual transport patterns are consistent with the benchmark computations. Hence, the elongated tidal wave has the same period as N consecutive wave cycles and an amplitude that is defined upon (final) calibration of the predicted sediment transport.
Another type of morphological tide could be applied, which is an **adjusted version of the elongated tide**. Here, an individual tidal wave cycle is selected (out of the TR time series) that matches the observed tidal variation of the free surface while retaining the least squared error with respect to the TR time series. This selected tidal wave is then applied as schematised representation of the tidal forcing over the simulation duration. In order to avoid (large) mismatches in the residual transport, the amplitude of the selected wave is calibrated as such that it aligns with the target transport.
An improved version of the adjusted morphological tide is proposed by Lesser (2009). For the **improved morphological tide**, an individual tidal cycle is selected to represent the TR time series. In order to make sure that the interactions with the relevant and important tidal constituents are captured in the computations of the residual transport, an artificial constituent C is considered. The superposition of the tidal components creates the *improved morphological tide*. After calibration of the amplitude of the tidal constituents with an amplification factor f_1 or f_2, the schematised morphological tide produces a target residual transport that is consistent with the benchmark simulation.

Lastly, the morphologist is inclined to investigate ways to reduce to the non tidal residual components to schematised forcing conditions. Hereby, the **wave class selection based on the offshore wave climate** could be applied. In this weighted class selection approach, the offshore wave climate is partitioned in wave height and wave direction bins to obtain a discrete set of wave classes. Conversely, the **optimum wave class selection method** could be used. Here, the wave climate is reduced into a set of wave conditions for which the target transport (i.e. nett longshore transport, gross longshore transport) retains consistent patterns and rates as observed in the benchmark simulation.
The application of input reduction methods is dependent on the geomorphological setting, the temporal & spatial scale over which morphological development is monitored, the relative significance of the observed physical processes, and the possible objective to assess and/or reproduce any observed phenomenological events. Decision concerning the choice of input reduction methods remains a tailor-made process of recurrent assessments of the geomorphological system at hand.

9 DISCUSSION ON APPLICABILITY OF INPUT REDUCTION METHODS & EVOLUTION TECHNIQUES

Comprehensive understanding of the physical behaviour of a geomorphological system (i.e. estuary, tidal inlet, coast) is eminent when geomorphologists aim to investigate the appearance of a particular phenomenological event (e.g. channel formation and migration, migrating bars, breaching of inlet, formation of shoal platforms). Therefore, a geomorphologist creates morphodynamic models with the objective to recreate the observed morphological development in the model predictions. Such a morphodynamic model requires the specification of a particular set of physical processes for which the observed morphological development may be computed. In coherence with the latter, the morphologist decided upon the right updating scheme for the geomorphological system at hand which allows for efficient and accurate computations within the timeframe of interest. Hence, in Pillar II, methods are discussed which can be applied to create representative forcing conditions for the dominant processes that contributes to the appearance of the observed phenomenological events. Also, morphological evolution techniques are outlined which ensure the swift and efficient computations of morphological development.

In order to capture the behaviour of a geomorphological system, the morphologist must investigate the broad range of physical processes that apply for the geomorphological setting at hand. Measurement campaigns in the region of interest provide a wealth of information about the water level variation, local currents and velocity, wind velocity and directions, observed wave climate, etc. From this broad range of forces and measurements, the morphologist reduces the broad range of physical processes to a set of forcing conditions. For the input reduction, the morphologist must decide upon a method to implement the forcing conditions in the proposed model (i.e. choice of morphological evolution technique).

Furthermore, it is important to consider the characteristic spatial and temporal scale of the morphological features that the model should reproduce. For large-scale features - at a long-term temporal scale - the emphasis is often placed on the tide-averaged response of the system that may be aggregated to efficiently obtain predictions on the long-term morphological development. Formulations describing small-scale hydrodynamic processes will provide information on the formation of small-scale features in the long-term prediction, however at the expense of the allowable computational demand of the model. Hence, for the large-scale morphodynamic computations the morphological updating schemes that may be applied is a (1) **(sequential) "online" morphology with variable *morfac***, and (2) **a Mormerge approach with variable morfac** to efficiently speed up the computations. Multiple schematised forcing conditions may thereby be applied to represent the effect of the dominant physical processes.

For small-scale features - at a short-term temporal scale - the emphasis is placed on the small-scale hydrodynamic and morphodynamic processes. The effect of the individual wave events on the geomorphological setting and the feedback processes must be captured in great detail. Hence, for the small-scale short-term morphodynamic computations a **sequential "online" morphology with variable *morfac*** may be suited. Hereby, the (filtered) time series data (i.e. Brute Forcing Filtered) may be used as forcing condition. Depending on the importance of the chronology of the different wave events, it may be wise to consider here a **sequential updating scheme** with **strict order** of wave event occurrence.

In between the former and the latter, the field of mescoscale medium-term morphodynamic features prevail. Here, the effect of both the small-scale processes and the interaction with the larger scale hydrodynamics and morphodynamics is important in order to predict the observed morphological development in the geomorphological system under consideration. For the Ameland ebb-tidal delta (e.g. Elias *et al.* (2019), Bosboom (2019), Bosboom *et al.* (2014)) it is acknowledged that the interaction between the small-scale processes is imperative to obtain a good understanding of the observed morphological

behaviour of the ebb-tidal system (e.g. Lenstra *et al.* (2019)). Here, a combination of small-scale and large-scale forcing conditions may lead to consistent results. Therefore, the time-series data may be applied to capture the hydrodynamic effects of the individual wave events. Moreover, to reduce the computation time and to ensure efficient computations the revised MorMerge approach is thereby considered (i.e. **Brute Forcing Merged**). It is noted that the tide and wave conditions may be captured in such a way that events, which create the same residual transport, are clustered.

Part III

MODELLING ACCURACY AND EFFICIENCY

10 SKILL METRICS - WAYS TO MEASURE MODEL PERFORMANCE

This section is the work of Bosboom (2019) & Sutherland *et al.* (2004)

The quality of morphodynamic predictions is often indicated by means of a *skill score*, which provides a standardised measure for the relative *accuracy* of a model prediction in comparison with a certain reference prediction (i.e. a prediction which shows zero morphological changes). This standardised measure of *accuracy* is often (yet not solely) related to the Mean-Squared Error (MSE) from which - by means of an overarching classification of *skill classes (levels)* - predictions are discriminated based on their *quality*. Such pointwise accuracy metrics which compare the model predictions and observations on the level of the model *grid points*,(i.e. *Brier Skill Score (BSS)*) seem to be rather trivial in its behaviour yet not entirely understood (misinterpreted) in reality (Bosboom (2019)). The BSS (and other pointwise accuracy metrics) overly penalises misplacements of morphological features (i.e. scour holes, bars, channels, chutes, and shoals) in the model predictions, which is noted by Bougeault (2003) and referred to as the *double penalty effect*. High-resolution models provide better-defined morphological structures and amplitude features whereas their predictions appear to produce *larger* MSEs. On the other hand, smoother topographies following from low-resolution models seem to produce *smaller* MSEs. Hence, the high-resolution model is penalised in twofold: (1) featureless predictions are rewarded over predictions with misplaced features (i.e. rewarding underestimation of morphological changes). And (2) accurate predictions on sedimentation and erosion features (i.e. right amplitude features) yet misplaced does not grant better *skill scores*. It is thereby observed by Bosboom (2019) that producing the right amplitude features (i.e. sediment/erosion), yet not accurately positioned, may not even outperform the reference prediction of zero changes. Furthermore, pointwise accuracy metrics reason rather inconveniently when analysing model predictions of morphological features that vary rapidly and prominently in time and space (i.e. migrating channels, repositioning of shoals and chutes, etc.). Hence, pointwise accuracy metrics fail to take the spatial patterns of the morphological prediction into account and are not quite suitable for highly morphologically active regions. Given the inherent limitations of the pointwise accuracy metrics, other metrics are proposed by Bosboom (2019) to measure the performance of morphodynamic models. Accordingly, Bosboom (2019) proposes three model validation methods that consider the prediction of the magnitude features, spatial patterns, and scale-dependent topography: (1) the field deformation method, (2) the displacement-based error metric, and (3) the scale-selective validation approach. Therefore, this chapter gives a overview of the various ways to measure the performance of morphological models

10.1 Pointwise Accuracy Metrics

Brier Skill Score (BSS or MSESS$_{ini}$)

An often-used grid point measure to classify the performance of morphodynamic models and compare the accuracy of model predictions is the *mean squared error (MSE)*. The Brier Skill Score (BSS) is a Mean Squared Error Skill Score based on the initial predictions giving zero morphological changes (MSESS$_{ini}$). The MSE as tool (metric) in morphological assessments as proposed by Sutherland *et al.* (2004) describes the anomalies between model predictions p and observations o. Often such comparisons proceeds on the basis of a reference observation for which zero morphological changes are considered - a reference bed topography. Hence, the *skillfulness* of a morphodynamic model as a classification measure for the

model performance can be defined by eq.(134) while acknowledging the observations $o' = o - r$ and predictions $p' = p - r$ relative to the reference prediction r, viz.

$$MSESS_{ini} = 1 - \frac{MSE}{MSE_r - MSE_i} \tag{134}$$

with:

- MSE: The mean squared error between relative model predictions p' and observations o'.

$$MSE = \left\langle (p' - o')^2 \right\rangle = \frac{1}{n} \sum_i^n w_i \, (p_i - o_i)^2$$

  - w_i: Weighted factor considering the spatial variation in grid sizes. *For instance,*

$$w_i = \frac{(A_i - \langle A \rangle)^2}{\sigma_A^2}$$

  - p_i: the predicted morphological change in the i^{th} grid cell.
  - o_i: the observed morphological change in the i^{th} grid cell.

- MSE_i: The mean squared error in the presumed "perfect" initial topography.

$$MSE_i = 0 \quad \text{(i.e. no measurement errors)}$$

- MSE_r: The mean squared error in the reference predictions.

$$MSE_r = \left\langle (r - o)^2 \right\rangle = \left\langle o'^2 \right\rangle$$

The skill level (skillfulness) following from the $MSESS_{ini}$ provides thereby a quality measure for the accuracy of the model (performance). Sutherland *et al.* (2004) proposes a classification of the model performance by denoting *skill score classes* which are adopted in Table 5.

		$MSESS_{ini}$
Excellent	→	1.0 - 0.5
Good	→	0.5 - 0.2
Reasonable/fair	→	0.2 - 0.1
Poor	→	0.1 - 0
Bad	→	<0

Table 5: Classification of Brier Skill Score. (From Sutherland *et al.* (2004))

Hence, the characteristics of the Brier Skill score can be summarised as:

- The Brier Skill Score is an accuracy metric which shows the skill of the model within a single-point measure.
- pointwise accuracy metrics - such as the mean squared error skill score - seem to penalise the model performance for their ability to reproduce morphological features albeit with inevitable spatial errors. The metric is prone to produce double penalty effects.
- pointwise accuracy metrics steer intuitively morphologists' in their quality assessment to reduce the predicted morphological variability. The latter being rather contradictory in the eyes of the morphologists' intuition for optimal model performance.
- The initial morphology as reference predictions for model prediction makes it impractical to set about an *absolute* comparison between model prediction and observation, since the intrinsic complexity of the reference prediction is not completely inherited in the relative assessment of the model performance. Hence, the *relative* skill of the model is assessed, not the *absolute* skill.

Murphy-Epstein Decomposition

The aforementioned obstacles in pointwise accuracy metrics can be overcome when the full statistical specification of the morphological model is provided for each model prediction. Hereby morphologists can clearly give insight in the model decisions that they have taken to steer the model predictions towards a specific *target* model performance. To obtain such a set of probabilistic quality measures, Murphy (1988) (e.g. Murphy and Epstein (1989)) proposed a mathematical decomposition of the $MSESS_{ini}$ starting from the expansion of the mean square error (MSE) as shown below in eq. (135),

$$MSE = \sigma_{0'}^2 \sigma_{p'}^2 + 2\sigma_{p'}\sigma_{0'}\rho_{p'o'} + \left(\overline{p'} - \overline{o'}\right)^2 \tag{135}$$

with:

- $\sigma_{p'}$: The standard deviation of the model predictions relative to the reference prediction.
- $\sigma_{0'}$: The standard deviation of the observations relative to the reference prediction.
- $cov(\sigma_{o'}, \sigma_{p'})$: The covariance of the anomaly between the (relative) predictions and observations.
- $\rho_{p'o'}$: The Pearson product-moment correlation coefficient between the (relative) model predictions and observations.
- $\overline{p'}$: The map-mean error [1] of the relative model predictions
- $\overline{o'}$: The map-mean error of the (relative) observations.

The latter can be rewritten into model statistical performance parameters which is proceeded in eq. (136) below,

$$MSE = \sigma_{0'}^2 \left(1 - \alpha + \beta + \gamma\right) \tag{136}$$

with:

- α: The **Coefficient of Determination** which shows the tendency of the model predictions and observations to vary in the same way.
$$\alpha = \left(\rho_{p'o'}\right)^2$$
- β: The **Conditional Bias**, which is mathematically defined as,
$$\beta = \left(\rho_{p'o'} - \frac{\sigma_{p'}}{\sigma_{o'}}\right)^2$$
and shows the tendency of the model predictions to vary in the same (order of) magnitude as the observations in the presence of an arbitrary correlation. Consequently, if the slope b of the regression line in the $\rho_{p'o'}$-graph is given by,
$$b = \frac{\rho_{p'o'}\sigma_{o'}}{\sigma_{p'}} = 1$$
(i.e. β = 0), the magnitude of the *predicted* and *observed* displaced sand volumes, are perfectly aligned. For $b > 1$ and - in absence of systemic bias (i.e. $\gamma = 0$) - larger values in the observations are underestimated whereas smaller values are overestimated (and vice versa for $b < 1$). It should be noted that strictly speaking, β represent *amplitude errors* if the correlation coefficient $\rho_{p'o'}$ is equal to 1.

[1] represents the systemic bias within the model domain.

- γ: The **Systemic Bias** - or also called (normalised) *map-mean error*, which is mathematically defined as,

$$\gamma = \frac{\left(\overline{p'} - \overline{o'}\right)^2}{\sigma_{o'}^2}$$

and shows the natural capability of the model to overestimate (underestimate) model predictions (compared to the observations). It may also be regarded as the *sediment-budget error* as it inherently show the models' tendency the import (export) more sediment from outside the model domain (e.g. Bosboom (2019)).

The mean square error (MSE) can also be written as proceeded in eq. (137) to show that MSE inherently prevails a dependence on the normalisation term ε,

$$MSESS = \frac{\varepsilon + \alpha - \beta - \gamma}{1 + \varepsilon}, \qquad \varepsilon = \left(\frac{\overline{o'}}{\sigma_{o'}}\right)^2 \tag{137}$$

which represents the map-mean error found in the (relative) observations o' normalised with the observed morphological variability $\sigma_{o'}$. ϵ as map-mean error indicates mismatches between the map-mean sediment-budget proposed by the reference prediction and the map-mean sediment-budget found in the observations. A value of $\epsilon > 0$ indicates that the observed morphological trends are reproduced (partially) by the model predictions (i.e. the model predictions become more skillful than the reference predictions). If $\epsilon = 0$, the model predictions do not capture the observed map-mean changes in the sediment-budget.

Quality Assessment on the basis of a Pointwise Accurate Metric

Henceforth, when in future quality assessments, where the performance or *skillfulness* of morphodynamic models is being assessed, it is imperative that the full set of statistical quality parameters (as found by means of the Murphy (1988)-decomposition) is incorporated in the model validation. Incorporation of these parameters gives coastal morphologists an overview of the model decisions proceeded to obtain *skillful* model predictions and notwithstanding the opportunity to employ transparent comparisons between the *skill* of different models in future assessments.

In light of the aforementioned, a framework is provided which may be used as guideline when pointwise accuracy metrics are applied for model quality assessments and is summarised in Table 6.

10.2 Displacement-Based Accuracy Metrics

Another metric that may be employed to measure the performance of morphological models is the displacement-based accuracy metric. These metrics are evaluating the (dis)agreements in spatial morphological patterns between the model predictions and the observations. Often by recreation of a *common footprint*, the *smoothed* displacement field services as basis of comparison to obtain valuable information about the structural resemblance between model predictions and observations. It is noted by Bosboom (2019) that displacement-based (and alike) metrics align better with the coastal morphologists' qualitative (intuitive) sense to accuracy with results in a fair metric that awards the models' ability to produce morphological features rather than penalising. On the contrary, pointwise accuracy metrics lack the capability to assess the quality of model prediction - especially in the case of large observed morphological variability - with the *double-penalty effect* as clear example. High-quality validation requires a suiting validation technique that focuses on the spatial structures within the (timely) morphological evolution. In the following sections, two methods are reviewed: (1) the field deformation method, and (2) the effective transport difference method. Both methods avoid double-penalty effects by evaluating the (dis)agreements in structure and amplitude while inevitable location errors are disregarded.

Case	**Description**	$MSESS_{ini}$	MSE	MSE_r	α'	$1-\alpha'$	β'	b'	γ'	ϵ'	$\rho_{p'o'}$	$\sigma_{p'}/\sigma_{o'}$
-	-	-	-	-	-	-	-	-	-	-	-	-
-	-	-	-	-	-	-	-	-	-	-	-	-

Metric Table for Quality Parameters in comparison with the reference prediction	
$MSESS_{ini}$:	The skill score of a particular model prediction
MSE:	Errors in the model predictions (compared to the observations)
MSE_r:	Errors in the reference predictions (compared to the observations)
α':	**Coefficient of Determination** Tendency of the model prediction and observation to vary coherently
$1-\alpha'$:	**Phase error** An indication of the extent to which the model prediction shows signs of sediment volume misplacements
β':	**Amplitude Error/Conditional Bias** Tendency of the model prediction and observation to vary in the same (order of) magnitude
b':	**The correlation (regression) slope** shows if model prediction overestimates smaller observed values and underestimates larger observed values.
γ':	**Systemic Bias** Indication that model predictions are overestimates (underestimates) the observed morphological changes (i.e. sediment-budget mismatch)
ϵ':	**Normalisation Error** Indication that model predictions are becoming more skillful when they move away from the reference prediction. (i.e. model prediction approaches observed morphological trend)
$\rho_{p'o'}$:	**Correlation Coefficient** Indication that the model predictions and observations are correlated (i.e. model prediction shows morphological change of the same magnitude and sign as observations)
$\sigma_{p'}/\sigma_{o'}$:	Normalised morphological variability of model prediction.

Table 6: Template pointwise Metric Assessment Table for Model Validation

Field Deformation Method

In the displacement-based error metrics, often approaches are employed to qualitatively discern between *skillful* model predictions and observations without incorporating quality mismatches as a consequence to location errors (i.e. spatial misplacements). Hereby, model predictions are deformed (i.e. warped) using image deformation algorithms such that an "optimal image resemblance" is obtained between model predictions and observations. Hence, the result of the latter image-matching method is an optimal deformation field which shows the smallest work necessary to transform the observation field into the *warped* field (i.e. location errors are minimised). Bosboom (2019) proposes the application of field deformation methods whereby the accuracy of the predictions is defined by two metrics that take into account (1) the minimised error in the displacements and (2) the combined effect of location and amplitude ("image intensity") errors. This method is referred to as the warping method.

Warping method

A warping method is a widely used and employed technique that measures the uniqueness (i.e. optical similarity) between model predictions ("images) and observation fields (i.e. Pennec *et al.* (1999),Kroon and Slump (2009),Vercauteren *et al.* (2009)). The objective hereby is to find an optimal transformation that maps each point of a static image (observed field) onto a corresponding point (with same intensity) in the moving image (predicted field). Best known in the coastal engineering discipline is the optical flow technique which estimates small displacements in time-varying image sequences. In the optical flow method, it is assumed that the intensity of the flow does not change significantly in the intermediate time interval. In the same analogy, a modified free-form deformation method is applied - the Demon's Registration method (e.g. Thirion (1998), Pennec *et al.* (1999)) [see Figure 34]. The Demon's Registration aims to minimise the squared image intensity between the model predicted and observed (image) field.

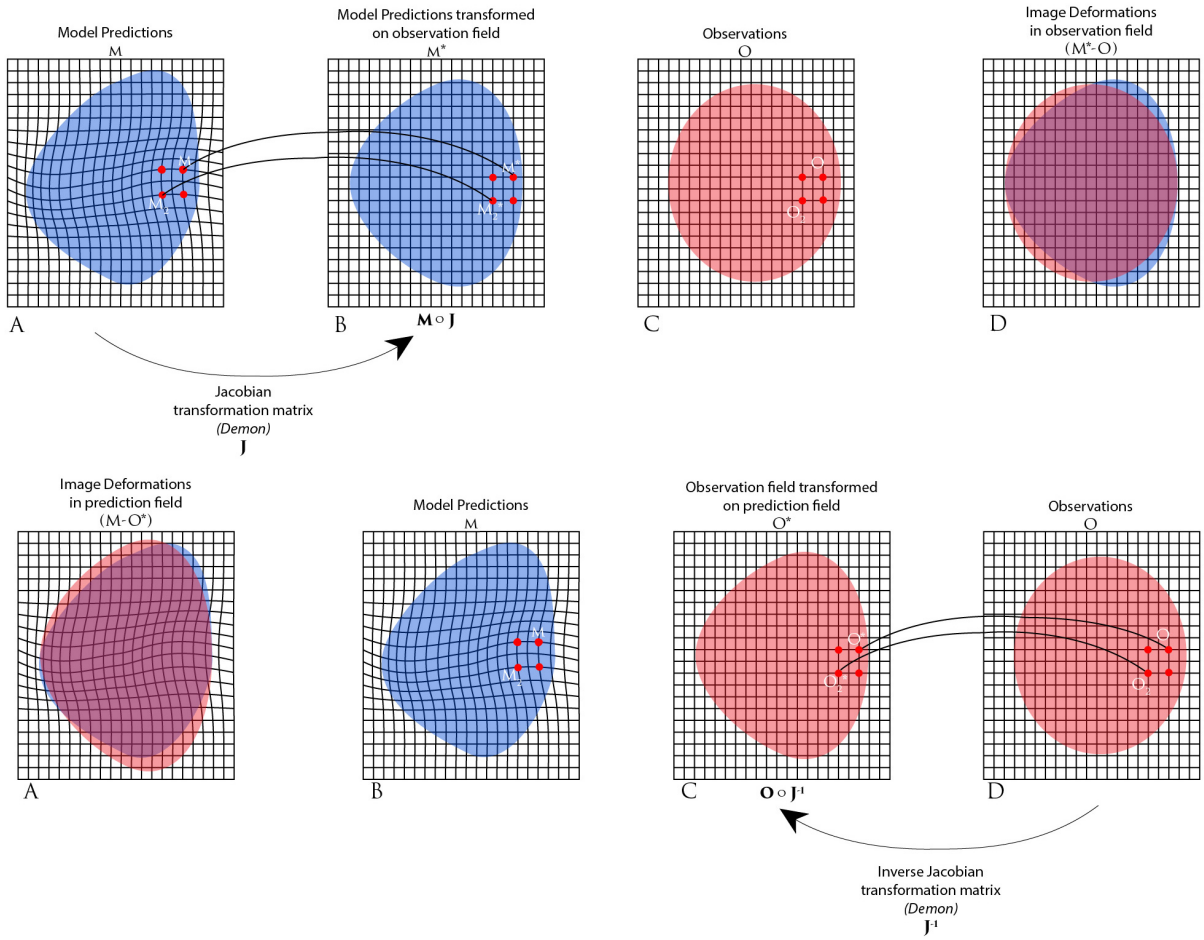

Figure 34: Schematic representation of the warping method (i.e. diffeomorphic demon registration method). The upper panel (from left to right) shows the process of mapping the model prediction onto the observation field. Here, the image of the model prediction is deformed as such that the location errors between the observations and predictions are minimised (i.e. minimisation of the image squared errors) [image A/B]. This removes the location error and gives one the possibility to analyse the differences in patterns between the model prediction and the observations - and that in the same field (i.e. the field of the observations) [image D]. The image of the predictions $\mathbf{M}$ is said to be mapped onto the observation field $\mathbf{O}$ by means of a set of instructions $\mathbf{J}$ that transforms $\mathbf{M}$ in to $\mathbf{M}^*$. The latter is also known as Forwards image transformation. In the case of a Backwards image transformation (i.e the lower panel), the same process takes place, yet only in reversed direction (i.e. from right to left). Here, the observations are mapped onto the prediction field by means of $\mathbf{J}^{-1}$ and are then compared with the model predictions $\mathbf{M}$ in the prediction field.

Hence, the Demon's registration ensures that the optimal deformation field is found for the model predictions for which the pointwise RMSE is minimised. Hereby, the target of the minimisation is the sum of the square image intensities between the deformed predictions and observations such that,

$$0 \leq RMSE_1 \leq RMSE_0$$

The $RMSE_1$ is expected to measure the (dis)agreement in the predicted morphological feature if inevitable misplacements are avoided. Hence, for the two predictions with the same $RMSE_0$, the predictions that shows features - albeit misplace - will be granted a smaller $RMSE_1$ than the featureless prediction. Furthermore, Bosboom (2019) theorises that similarities in intensity and location between morphological patterns can be assessed using three quality measures: (1) the pointwise error $RMSE_0$, (2) the warping pointwise error $RMSE_1$, and a map-mean location error $\overline{D}$.

Map Mean Location Error $\overline{D}$

The map-mean location error describes the weighted-averaged displacement field between the observations and the predictions, and therefore, is a measure for the (averaged) structural dissimilarity in the system patterns. Meanwhile, the Demon's Registration method registers only morphological changes normal to the contour line as the method does not provide inherently a constraint for contour-parallel morphological changes (i.e. the Aperture Problem). Therefore, an extra provision must be installed to limit the allowable morphological displacement in the contour-parallel direction. This is provided by the *Gaussian-Smoothing procedure* which ensures that (for all grid points in close vicinity) morphological displacements are similar in magnitude to the registered contour-normal displacements. The implication of the latter is that for locations along the contour lines of the affected regions of interest where otherwise no morphological activity is observed, nonzero displacements are prevalent. To minimise the smoothing-effect of the Gaussian-filter, a weighted-averaged location error is defined to account for the relative contribution of individual points to the minimisation of the $RMSE_1$. Since, the areas negatively affected by the Gaussian smoothing procedure are locations that contributes the least to the minimisation of the *sum of the square images* they are filtered out rather effectively. Given the aforementioned, the map-mean location error is defined as a weighted mean error that weighs the backward displacement magnitude D based on their contribution to the minimisation of the *sum of the square images*, viz. eq. (138):

$$\overline{D} = \frac{\sum_{i=1}^{n} w_i D_i}{\sum_{i=1}^{n} w_i}, \qquad w_i = \frac{SE_{0,i} - SE_{1,i}}{\sum_{i=1}^{n} (SE_{0,i} - SE_{1,i})} \tag{138}$$

with:

- $\overline{D}$: The weighted map-mean error
- w_i: Weighing factor based on the SE_i
- $SE_{0,i} SE_{1,i}$: The squared location errors found in the predicted field before and after warping procedure, respectively

An Overarching single-point metric $RMSE_w$

The rather common desire of coastal morphologists to adhere information of regarding the quality of a morphodynamic model (model predictions) from one single-point measure has led to the development of the $RMSE_w$[2] (e.g. Bosboom (2019)). The weighted root mean squared error $RMSE_w$ is a measure defined on the basis of the *weighted squared errors* SE_w, which for each point in the domain weighs the errors SE_0, SE_1 obtained before and after the warping procedure. As such the $RMSE_w$ is bounded by the $RMSE_0$ and the $RMSE_1$, viz.

$$RMSE_1 \leq RMSE_w \leq RMSE_0$$

and is linearly weighted with respect to the "normalised" displacement amplitude $\delta_i = D_i / D_{max}$. Hence, the weighted root-mean squared error $RMSE_w$ may be defined as in eq. (139) below,

$$RMSE_w = \sqrt{\frac{\sum_{i=1}^{n} SE_{w,i}}{n}}, \qquad \text{with} \quad SE_w = SE_1 + \delta\,(SE_0 - SE_1) \tag{139}$$

from which can be inferred that a *linear* displacement penalty is applied to the difference between the *pre-* and *after-* warping RMSE. Consequently, the single-point measure accounts for the relative importance of the localised misplacement over the possible appearance of deformation errors. Locations which show large local displacement errors, compared to a user-defined upper bound D_{max}, should be penalised stricter for its misplacement than its possible shape error such that $RMSE_w \to RMSE_0$. Whereas for small D_i, relatively larger error reductions are permitted upon granting a $RMSE_w \to$

[2] the "w"-subscript indicates that is concerns a weighted root mean squared error

$RMSE_1$. If displacements D_i larger or equal than D_{max} are necessary to transpose *observed* points to the location of the *predicted* points then the $RMSE_w$ is set equal to the upper-bound $RMSE_0$.

Note that in the aforementioned, D_{max} could be seen as an upper-bound for which the coastal morphologist allow prediction errors on the morphological features still to be considered as meaningful (valid). D_{max} is often taken in the same order of magnitude as the length scale of the morphological feature.

Effective Transport Difference Method

In the previously reviewed warping method, the predicted morphological field was qualitatively evaluated by means of a comparison between the predicted morphological patterns and the observed patterns. The performance of the model prediction is thereby adhered from the amount of image manipulations (i.e. squeezing and compressing, stretching) that must be acquired to obtain the observed morphological field starting from the predicted morphological field. Metrics were assigned to measure the (dis)similarity between observations and predictions without penalising the model on its inevitable location errors. A map-mean error is thereby employed to define the weighted-averaged spatial misplacement between observations and (warped) predictions. The inherent disadvantage of image registration is that the sediment masses - in a 2DH field - are not conserved throughout the free-form deformation procedure which is essentially the consequence of the fact that while stretching and compressing the (3D) mass conservation balance is not guaranteed.

Conversely, the effective transport difference method considers morphological changes from the perspective of the driving force which initiates morphological changes - the sediment transport field. The sediment transport field is hereby used as indicator for structural resemblance and model accuracy. This (optimal) sediment transport field is symmetric in nature as opposed to the warping method such that the sediment mass balance is always pertained.

The Optimal Sediment Transport Field

The effective transport difference method measures the difference in the transport field between the observations and predictions as "the distance between the predicted and observed morphological fields in terms of the optimal sediment transport field. The optimal sediment transport field describes hereby the sediment volumes that are to be displaced in order for the *predicted* morphology to *reach* the observed morphology *with the least amount of work* (i.e. the shortest possible distance). This is also known as the *economic quadratic transportation cost*. Figure 35 gives an example for an idealised inlet (i.e. Bosboom (2019)). On the basis of this optimal sediment transport field a transport error may be derived by taking the root-mean summation of the squares of the optimal sediment transport - the so-called root mean squared sediment transport error RMSTE. Hence, it can be seen that for two predictions, the prediction that reproduces the observations with *the smallest amount of work* - the smallest quadratic transportation cost - is designated as the better performing model prediction (given its lower RMSTE). The latter minimisation problem may be defined by an elliptical partial differential equation and can be solved by consideration of the $\mathcal{L}^2$ Monge-Kantorovich transport optimisation problem in the euclidean space (e.g. $\mathbb{R}^3$). In light of the aforementioned, the minimisation of the optimal transport field may be proceeded by minimising the 2-norm of the transport difference between the observations and predictions and is defined in eq. (140) below as,

$$\underbrace{\text{minimise}}_{\text{minimisation condition}} \quad \underbrace{\mathbf{q}}_{\nabla \mathbf{q} = h_1 - h_2} \qquad \|\mathbf{q}\|_2 = \left\{ \int_\Omega |\mathbf{q}|^2 \, d\Omega \right\}^{1/2} \tag{140}$$

with:

- $\|\mathbf{q}\|_2$: The minimised 2-norm of the optimal sediment transport field, or conversely the Root Mean Squared Transport Error (in m^2)

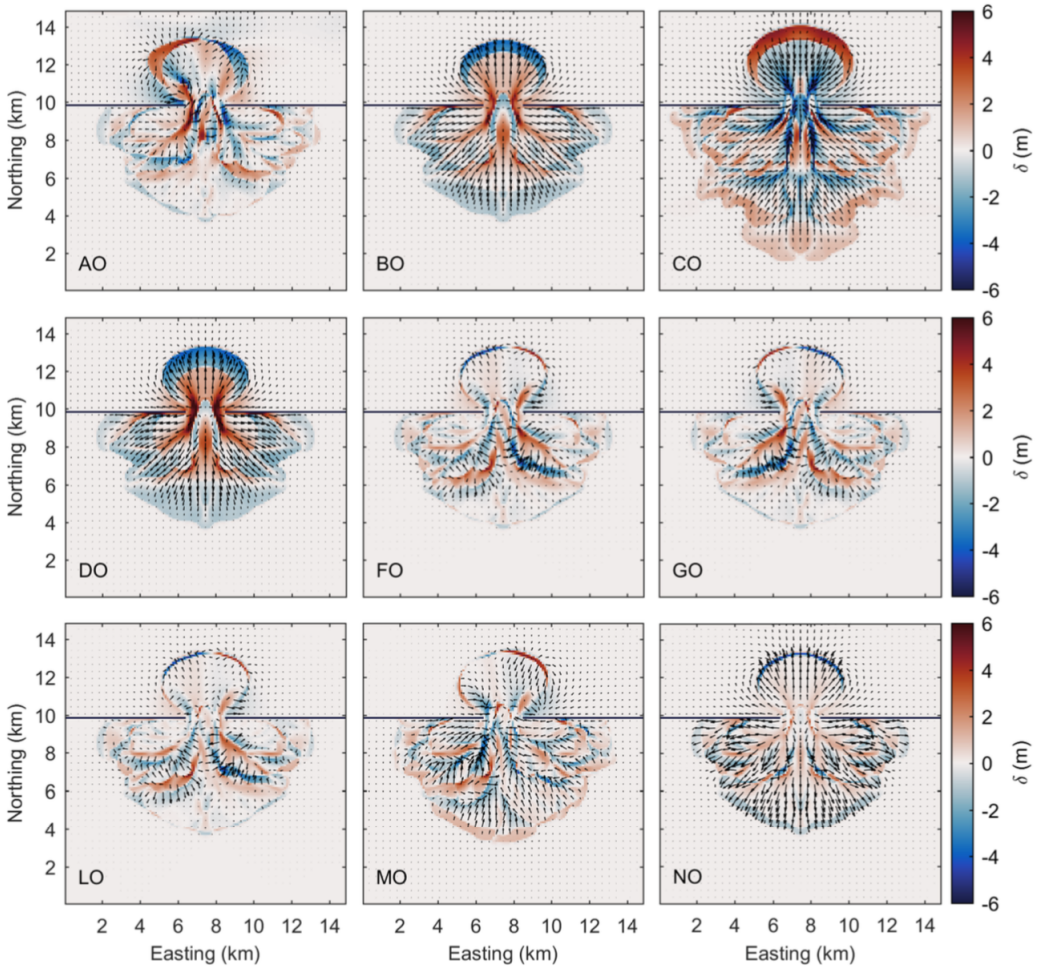

Figure 5.10: Bed level differences and transport fields, with the length and direction of the arrows indicative of the transport magnitude and direction, respectively, for predictions A through N compared to the "observations" O.

Figure 35: An example of the results following from an effective transport method assessment [courtesy of Bosboom (2019)]. In the 9 different panels difference plots are shown between (arbitrary) model results (*A* to *N*) and observation (*O*). The blue and red patches are indicative to sediment deficit (i.e. negative difference between prediction and observation) and sediment abundance (i.e. positive difference between prediction and observation) respectively. The differences in location and amplitude of the modelled features drive here a sediment transport from locations of sediment abundance (i.e. the red patches) towards locations of sediment deficit (i.e. the blue patches) along the shortest possible path. The black arrows in between show the magnitude and direction of this sediment transport. The effective transport method can as such be seen as a method to describe topological (miss)agreements between predictions and observations by means of the total volume of sediment that must be replaced to obtain the observation (*O*).

- h_1, h_2: The predicted and observed sediment mass budget conversely (in m^3)
- $|q|$: The amplitude of the transport field (in m^2)

Evaluation. of the latter $\mathcal{L}^2$ Monge-Kantorovich transport optimisation problem shows that by minimising the corrective transportation field, the root mean squared transport error (eq.(140)) may be rewritten as a scalar multiple of the squared of optimal sediment transport (i.e. the squared economic transportation cost) as is proceeded in eq.(141),

$$RMSTE = \frac{1}{\sqrt{A_\Omega}} \|\mathbf{q}_{L2}\|_2 \tag{141}$$

with:

- $RMSTE$: The root-mean sediment transport error (in m^2)
- $\|\mathbf{q}_{L2}\|_2$: The quadratic economic transportation cost or conversely the norm of the corrective sediment transport field (in m^3)
- A_Ω: The surface area of the computational domain (in m^2)

Hereby, it may be seen that the RMSTE represents the *least* amount of sediment mass that must be displaced from misplaced feature in h_1 to the observed location h_2 by means of the optimal sediment transport field to erode h_1 and supply H_2.

10.3 Scale-Selective Accuracy Metrics

Scale-selective accuracy metrics indicate the performance of a morphodynamic model on the relevant spatial scales. (High-resolution) morphodynamic models present model predictions on to the smallest scale of the computational grid size. Although with ever-increasing computational capabilities morphological models can be executed using smaller grid sizes, not always does a smaller grid size necessarily constitute higher-quality model predictions at the smallest scale features. It is regarded by Bosboom (2019) that the quality of the model predictions on the scale of the smallest features is rather limited in comparison with the skillfulness of the larger scale features in the same model prediction. In a more generic perception, morphodynamics models are characterised by presenting more skillful results on larger spatial scales than on smaller spatial scales - there is a scale-dependent skill prevalent in the model prediction. Hence, a quality dissimilarity might be evident on various spatial scales in present morphodynamic models. As a coastal morphologist, it may be of particular interest to evaluate and ensure that at the *target* feature level an acceptable (i.e. high-quality) prediction is prevalent from which skillful information can be derived. The scale-selective validation method is equipped to measure the performance of the model predictions not only by their location errors, structural and/or amplitude dissimilarity, but also by the scale at which these similarities prevail. Subsequently, scale-selective validation approaches are derived to investigate either the skill of the model prediction by evaluation of the amplitude similarity in *sliding window* of various window sizes (i.e. scale-dependent skill measure). Whereas the pooled skill measure proposes quality information by investigation of the amplitude and structural (dis)similarity based on a stochastic sampling of the *sliding window* quality parameters on the same range of window sizes. These model performance measures will be further elaborated in the following sections. It should be noted that scale-selective quality assessment metrics are compatible with other model quality assessments and could as such be applied in harmony with pointwise accuracy metrics, displacement-based error metrics, etc.

Scale-dependent Skill

In the scale-dependent skill approach the objective is to discriminate in the skillfulness of the model on the basis of the level at which the model predictions seem to properly mimic morphological variability whilst pertaining an acceptable resemblance in spatial (pattern) structures. With a set of localised statistics, the performance of the model prediction may be assessed from maps that capture the spatial variation of the structural and amplitude similarities within a *sliding window*.

Structural Similarity

As such, Bosboom (2019) proposes several measures that enables the monitoring of the tendency of the model predictions to vary in the same fashion (i.e. magnitude of displacements & direction) as the observations. Therefore, the Pearson product-moment correlation coefficient ρ_{po} and the ratio of the standard deviations $\hat{sigma} = \sigma_p/\sigma_o$ are taken into consideration as quality measures.

$$\rho_{po} = \frac{cov(\sigma_p, \sigma_o)}{\sigma_p \sigma_o}, \qquad \hat{\sigma} = \frac{\sigma_p}{\sigma_o}$$

If $\rho_{po} = 1$, the model predictions perfectly resemble the observed variability in the tendency, spatial structure and magnitude of the morphology. Moreover, if $\rho_{po} \in \langle 0, 1]$, the correlation coefficient may show dissimilarity in the magnitude of the displacements which are underestimated. With $-1 \leq \rho_{po} \leq 0$ the model predictions are ought to show morphological activity with opposing sign with respect to the observations.

The relative variability $\hat{\sigma}$ shows whether or not the model predictions have the tendency to overshoot (undershoot) observed morphological variability. Larger than 1, indicates overestimation and vice versa for underestimation.

Amplitude Similarity

A normalised measure that may be employed to assess the consistency of the local amplitude of the predicted morphology is the amplitude similarity measure η as defined below in eq. (142),

$$\begin{aligned} \eta &= \left(\frac{2}{\hat{\sigma} + \hat{\sigma}^{-1}} \right)^q \qquad \forall \quad 0 \leq \eta \leq 1 \\ &= \left(\frac{2\sigma_p \sigma_o}{\sigma_p^2 + \sigma_o^2} \right)^q \qquad \text{q is user-specified} \end{aligned} \tag{142}$$

In Bosboom (2019) a value of 2 is proposed for the coefficient q. It should be note that in this formulation η is shown to be insensitive to the cause of the amplitude dissimilarity (i.e. overshoot/undershoot). Both overestimation and underestimation of the same extent, receive the same penalty. Conversely, the latter may be derived from $\hat{\sigma}$ which shows the tendency of the model predictions while the ρ_{po} correctly states the nature of the dissimilarity.

Running Window Skill Score S

In an attempt to condense the quality information into a single-point measure that varies of the computational domain, a running window skill score S is established. Hereby, the measure indicates the skillfulness of the model prediction observed from a running window that moves across the domain.

One of the candidates for the definition of the window skill score S could be the RMSE. However, given the nature of the RMSE to penalise model predictions for its ability to produce features (albeit misplaced, i.e. double penalty effect), this may not seem to be the right candidate. Instead, a skill score is considered that discriminate in the performance of model predictions based on the accuracy of the predicted morphological variability and shape (i.e. magnitude and structural) similarity, hereby disregarding any possible location errors. As proposed by Bosboom (2019), the running window skill score S is given by eq. (143), viz.

$$S_i = \left(1 + \rho_{po,i}\right)^m \eta_i{}^n, \qquad 0 \leq S \leq 1 \tag{143}$$

It is thereby acknowledged that the skill score is uniquely defined for each window i in the computational domain for which the performance is assessed. Given a rectangular window W that is dissimilar to the grid size, a special weighing procedure is conducted to cast local *window-mean* measures for the statistical parameters. As such, the computational domain is divided into N windows W that covers the latter domain. Within the local domain W_i, the weighted mean observations $\bar{o}$, and

predictions $\overline{p}$ are found by a weighing of the local values o and p on the basis of their proximity to the window centre grid point i. Viz. eq.(144),

$$\overline{o_i} = \sum_j w_{ij} o_j, \qquad \overline{p_i} = \sum_j w_{ij} p_j \tag{144}$$

On the basis of the window *weighted mean* observations and predictions, the remaining set of arbitrary *window-averaged* statistical parameters can be derived - see eq. (145).

$$\begin{aligned} \sigma_{o,i} &= \sqrt{\sum_j w_{ij} \left(o_j - \overline{o_i}\right)^2} \\ \sigma_{p,i} &= \sqrt{\sum_j w_{ij} \left(p_j - \overline{p_i}\right)^2} \\ cov_i(p,o) &= w_{ij} \left[\left(o_j - \overline{o}_j\right)\left(p_j - \overline{p}_j\right)\right] \\ \rho_{po,i} &= \frac{cov_i(p,o)}{\sigma_{p,i}\sigma_{p,i}} \\ \eta_i &= \left(\frac{2}{\hat{\sigma}_i + \hat{\sigma}_i^{-1}}\right)^q \\ \hat{\sigma}_i &= \frac{\sigma_{p,i}}{\sigma_{o,i}} \end{aligned} \tag{145}$$

with:

- q: User-specified coefficient = 2
- w_{ij}: Weighing factor for grid point j in the vicinity of the window centre point j
- σ_i: The relative standard deviation between the model prediction and observation in window i
- $\sigma_{p,i}$: The standard deviation of the model prediction in window i
- $\sigma_{o,i}$: The standard deviation of the observation in window i
- $\overline{p}_j$: The map-mean error in the model prediction provided by grid point j in window i
- $\overline{o}_j$: The map-mean error in the observations provided by grid point j in window i
- p_j: Model prediction specified at grid point j in window i
- o_j: Observation specified at grid point j in window i
- $cov_i(p,o)$: The *window-averaged* covariance between the model prediction and observation in window i
- $cov_i(p,o)$: The *window-averaged* covariance between the model prediction and observation in window i
- η_i: The *window-averaged* amplitude similarity factor in window i
- $\rho_{po,i}$: The *window-averaged* value for the Pearson product-moment correlation coefficient in window i

Lastly, the spatial varying skill score S_i can be reviewed on the basis of maps that show the local similarities in structures and amplitude (i.e. maps of η_i and $\hat{\sigma}_i$ respectively - Figure 36), in harmony with a map that specifies the associated pattern skill score (i.e. maps of S_i) for a given window size W.

Pooled Skill

Another way to validate the quality of model predictions is by means of histograms for (1) the amplitude similarity η, (2) the correlation coefficient ρ_{po}, and (3) the pattern skill score S for the subset of arbitrary statistics (η, ρ_{po}, and S) for different window sizes W. Here, the tendency of the entire computational domain, resampled for all the sliding window sizes, can be observed and domain-averaged data on each scale can be fostered for the respective scales (see Figure 37 for an example for the case of the Bornrif). Evidently, it is shown in Bosboom (2019) that indeed the model predictions vary in skillfulness on respective spatial scales, giving better quality predictions at the larger scales than on the smaller scales.

The appearance of small-scale features thus reduces the overall performance of the model prediction. It can be argued that a possible smoothing of the smaller scale topography may constitute in better skilled predictions albeit at the expense of the high-resolution definition of the morphological features. Thereby, the optimal skill of model predictions is found at the spatial scale for which the model shows acceptable skill in model information (which differs from case to case). The morphologist has the freedom therein to assess the morphological prediction on the spatial scale for which he/she deems the information suitable (i.e. meaningful) for further analysis (i.e. analysis of small ripple formations requires skillful data on smaller scales). A balance should as such be found between the skill of the model predictions and the information richness.

10.4 Reference Prediction

In previous sections, it has been shown that various quality metrics measure and validate the accuracy of the model predictions hereby identifying the skillfulness of the model. The skill of the model is found by means of a comparison between the model predictions with respect to the presumed common reference of zero morphological change - the so-called reference prediction. Often coastal morphologists use an initial bathymetry as reference prediction. This reference prediction however has a particular topography consisting of possible (coherent) features and patterns, such that it may be seen that the reference prediction retains a certain reference skill. Quality measures fail to represent, therefore, the inherent relative complexity of the reference predictions when establishing scores for the skillfulness of the model predictions. A better fit as reference prediction in morphodynamic models for the purpose of quality measurement and model validation would be a skillful topography yet not unreasonable in the forecasted morphological setting. (i.e. avoid unrealistically large features amplitudes, or flatbed). This retains the ability of quality measures to capture the complexity of the reference prediction and prevailing absolute model skill. Depending on the target temporal scale of the model predictions, morphodynamic models should reflect the intrinsic complexity of the reference prediction in a larger or lesser apparent extent. The reference prediction can therefore be decomposed in a topography that changes under the effect of short-term processes and an underlying footprint that varies due to large-scale morphological adjustments both occurring on different temporal scales. For short-term model predictions it bears to assume that the large-scale morphodynamic features does not vary significantly. Such changes prevail at a larger temporal scale such that the reference prediction can be represented as a static topography from which morphological changes are issued within the model duration (i.e. freezing of large-scale topography/morphostatic substrate). For long-term predictions, the underlying footprint (i.e. substrate), evolutions in the large-scale morphodynamic features should be included in the reference prediction. The reference prediction is therefore ought to change over time showing the morphological adjustment of the underlying footprint under external (forcing) excitations which may also be inferred from the average morphodynamic change in historic data (i.e. trendline, regression line etc.).

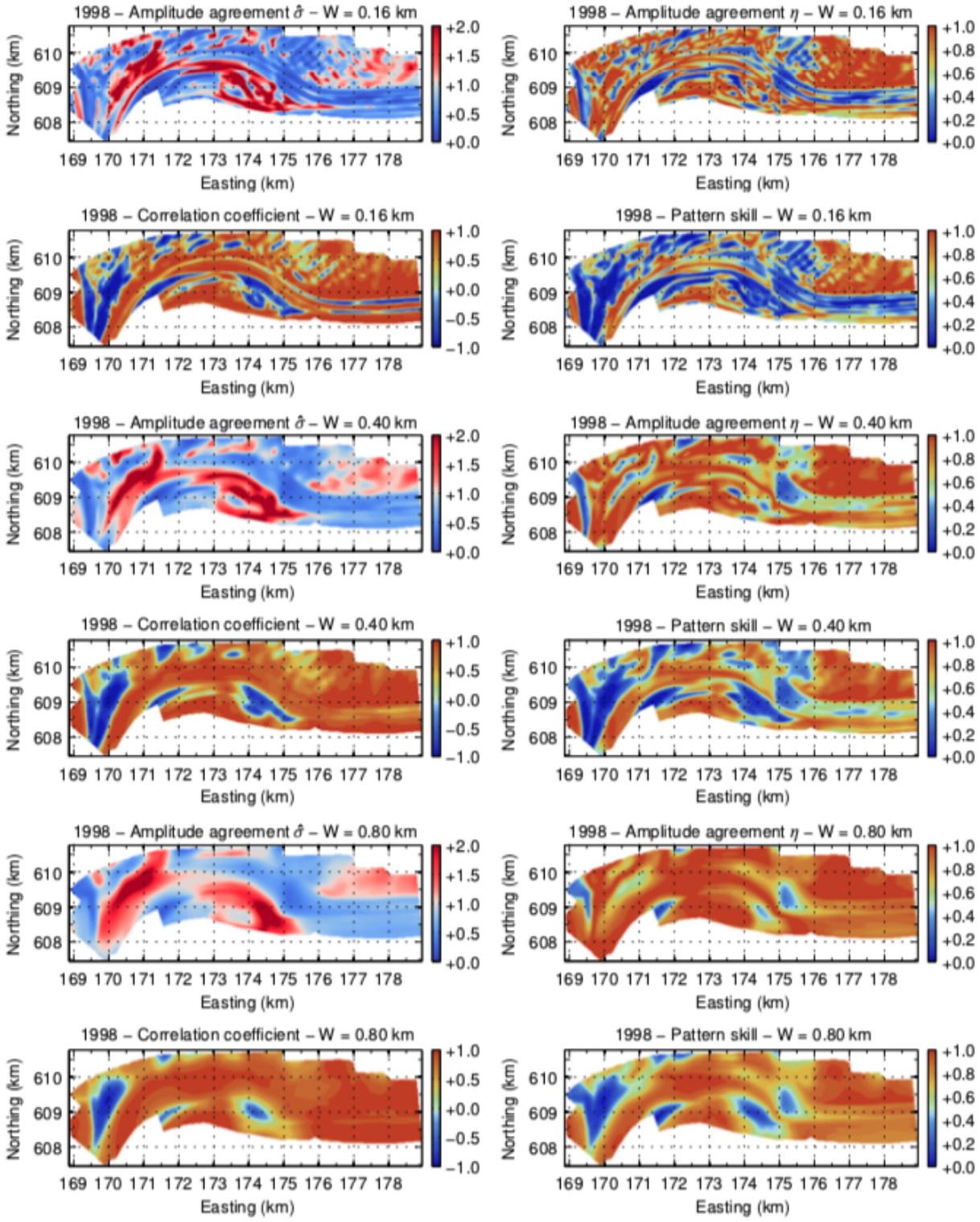

Figure 6.5: Normalized maps of structural and amplitude similarity and pattern skill for three different window sizes W = 0.16, 0.4 and 0.8 km. For all quality metrics a value of 1 represents perfect agreement.

Figure 36: Example of quality parameters for the morphodynamic model of the Bornrif (Bosboom *et al.* (2014)). The spatial maps show the spatial variation of the quality parameters ($\hat{\sigma}$, η, ρ and S) for the given areal size of focus W. (From Bosboom (2019))

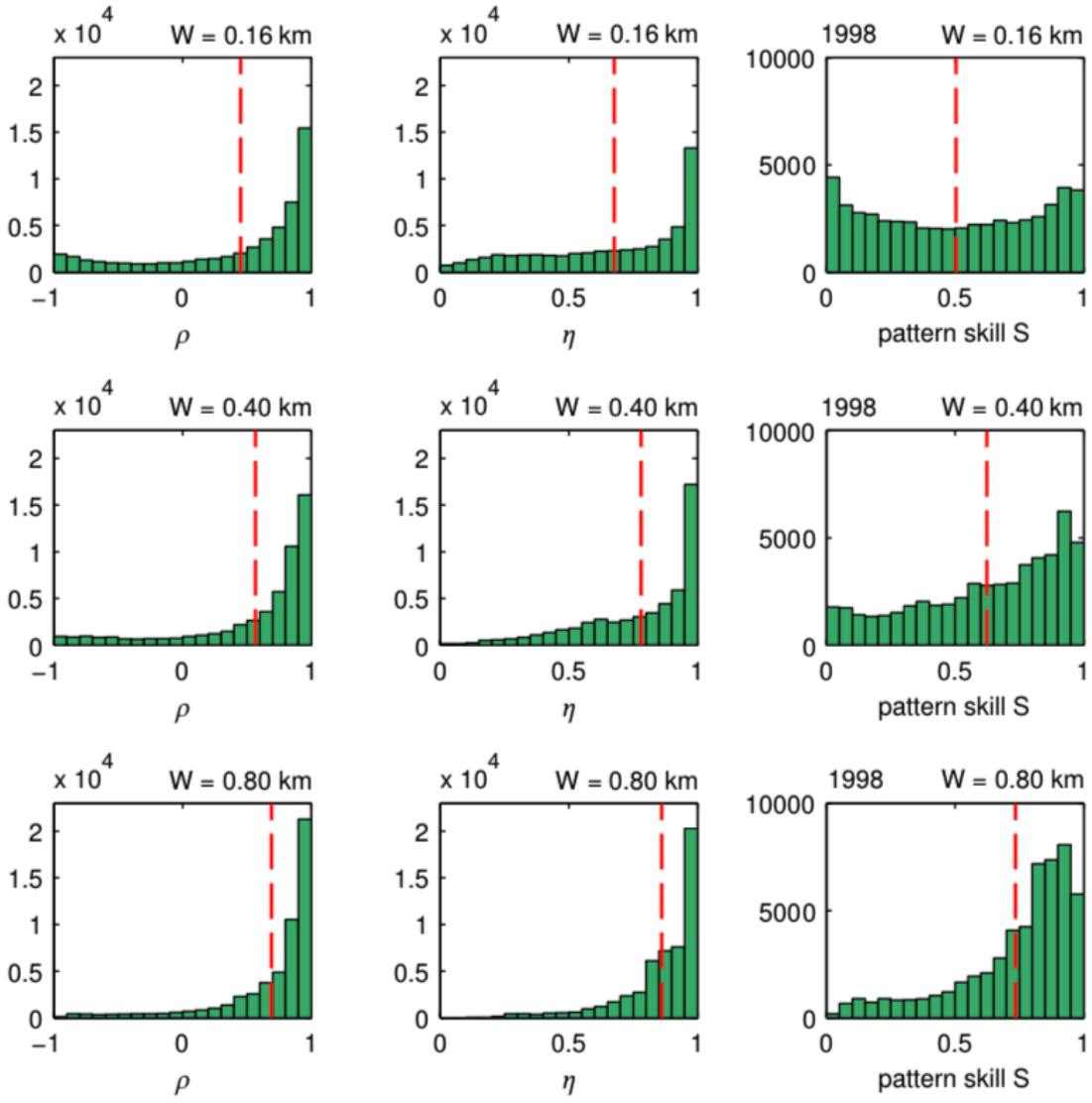

Figure 6.6: Histograms of the correlation, amplitude similarity and pattern skill for the three window sizes W = 0.16, 0.4 and 0.8 km. Note that the histograms correspond to the respective maps in Fig. 6.5. The red lines indicate the domain-averaged values which can be seen to increase with spatial scale.

Figure 37: Example of quality parameters for the morphodynamic model of the Bornrif (Bosboom *et al.* (2014)). The histograms show the spatial variation of the quality parameters (ρ, η and S) for the given areal size of focus W. This is obtained by defining quality parameters for the window sizes W and subsequent sampling of the associated results. (From Bosboom (2019))

11 CONCLUSION

The quality of morphodynamic predictions is often indicated by means of a quantitative validation measure - a *skill score*. This provides a standardised measure for morphologists to specify the accuracy of the model based on an overarching classification of *skill levels*, and a means to relate morphodynamic models of *equal skill*. The relative accuracy of a model prediction can be quantified by means of a *point-wise accuracy* metric. Quality measure stemming from such metrics (i.e. BSS, MSE, RMSE) compare the model predictions with the observations on a *grid point level*.
It has been shown that the BSS as point-wise metric is prone to the *double penalty effect*. Hereby, the BSS penalises (1) the model predictions for producing morphological features (albeit misplaced), and (2) for the presence of inevitable location errors between the position of the *predicted* and *observed* morphological feature. It is found that model predictions with features (only displaced) are granted a lower skill score than the reference prediction of zero morphological change. Inherently, morphologists are, therefore, encouraged to underestimate morphological variability in order to be rewarded with larger skill scores which seems odd in the morphologist's intuitive perception of *skill*. Hence, other metrics to measure the performance of morphodynamic models are reviewed.

Firstly, methods under the category displacement-based errors metrics are reviewed. Hereby, a method is introduced that only considers mismatches in the amplitude and shape of the morphological features when inevitable location errors are disregarded. This *field deformation method* uses free-form image warping techniques to map the deformed prediction field over the observation field and detects changes in the shape of the morphology. The skilfulness of the model is determined by the amount of work that must be proceeded to transform the deformed predicted field into the observational field.

Also, the *effective transport difference method* is discussed. This method shows the performance of the model by evaluation of *the amount of work that must be proceeded to recreate the observations starting from the predictions* by means of an optimal sediment transport field. This transport field enables the minimised transport of sediment volumes between the (mis)placed predicted morphological features and the observations.

Furthermore, the application of scale-selective accuracy metrics is assessed. The *scale-dependent skill approach* shows, here, the relative skill of the model by investigating window-averaged quality parameters (i.e. amplitude similarity, structural similarity and, pattern skill score) within an arbitrary areal size of focus (i.e. the sliding window). The *pooled skill approach*, introduces thereby a means to analyse *prediction quality* information using histograms to display the statistical distribution of the quality information for each window size.

From the different classes of quality metrics, the following aspects can be deduced. If the Brier Skill Score is applied as indicator for the model performance, it is highly recommended to accompany such scoring with a full statistical set of quality parameters (i.e. the Murphy and Epstein (1989)-decomposition). Incorporation of such quality parameters gives (coastal) morphologists an overview of the model decisions taken to target a certain *skill* or *performance*. The framework as specified in Table 6 provides a good starting point for such an undertaking.

The displacement-based error metrics provide tools that compare the structural and amplitude similarity in the model predictions without accounting for the appearance of any inevitable location error. These methods serve well in highly active morphological environment whereby complex topographies prevail (i.e. estuarine and tidal environments). Especially when the point-based metrics showed *skewed* results for the quality assessment (i.e. double penalty effect). It is a strong and widely assessed tool

that gives a qualitative framework of quality comparison. The downside is, however, that the sediment mass balance cannot be maintained due to the free-form image warping techniques (i.e. stretching, compressing). Nonetheless, this can be easily overcome by considering instead a mass-conservative displacement-based error measure such as the *effective transport difference method*.

The scale-selective model validation method provides a strong and robust tool for qualitative (i.e. amplitude & structural similarity) and quantitative (i.e. pattern skill score) assessment of the quality of model predictions. The methods are easy to be implemented. And since the *prediction quality* information is condensed in quality assessment plots for each parameter, the information is clear and relatively easy to be observed. The methods are also compatible with other metrics such that the validation of the model prediction may be supplemented with other skill metrics.

12 MORPHOLOGISTS' PERCEPTION OF SKILL – AN ASSESSMENT TO SKILLFUL MESOSCALE PREDICTIONS

Morphological Modelling Meso-scale Medium Term Coastal Features

In an investigation towards the best practice of modelling morphological developments in tidal and estuarine environments - with characteristic length scales of O(10km) and temporal scales of O(5 years) - the present-day modelling procedure is reviewed in order to find strategies that might enhance the production of better solutions in this complex domain of interest.

On short-term and long-term temporal scale, morphodynamic models seem to produce better model predictions. That is, on a short-term scale O(days - months) (i.e. individual tides and storm waves, episodic events), the short-term behaviour is governed by the dominance of small-scale interaction between the hydrodynamics and morphodynamics (i.e. ripple formations, overwash, dune erosion, breaching). Short-term small-scale morphodynamic models apply hereby formulations of the physical processes that are posed in such a way that it aligns with instantaneous nature of the short-term phenomenological events (i.e. implementation of the time series data).

On a long-term scale O(decades - centuries), the physical processes contributing to bed level evolution must be parameterised using schematised process descriptions that solve for the long-term sediment transport without having to deal with individual physical processes. Process-based morphodynamic models enable coastal modellers to incorporate the necessary model reduction to (only) capture the governing physical processes in a given domain of interest, thereby greatly reducing the computationally intensity of the model.

On a medium term scale, morphodynamic models have the disadvantage that the computational power is too limited to resolve for (1) the morphological development following from direct implementation of water level, wind and wave time series data and (2) the application of short term physical process descriptions for the larger time and spatial scale. The mutual dependence of such models to the short-term hydrodynamics as well as the morphodynamic changes on a larger temporal and spatial scale sets an extra complexity to model explorations on this scale. Water levels, tides, surges data series are carefully reduced in order to mimic the morphological changes on the scale of O(5 years). The wave and wind data are thereby also reduced to a set of individual conditions for which a representative littoral drift may be acquired. The application of morphological tides representing the sediment transport and bed level evolution of a characteristic hydrodynamic tidal climate (i.e. spring-neap tide, astronomical tide) enables thereby the possibility to calculate the morphological development on the basis of schematised forcing condition. The application of schematised forcing conditions with(out) morfac may predict, thereby, the qualitative shape of the large-scale coastal features correctly given that small to negligible errors are introduced by the input reduction but is in lesser degree capable of resolving individual smaller-scale morphological features.

Moreover, the imbalance between the initial conditions (i.e. schematised waves, tides, bathymetry & bed composition) in relation to the nature of the system (i.e. the state of the bed in relation to the magnitude of the physical processes) sets of spurious oscillations that steers the composition of the bed and bathymetry far away from the imposed initial conditions. Hence, the latter describes the necessity of high-resolution multi-modal data to instigate the system without the appearance of large initial oscillations.

Main Question and Interview objective

The intermediate temporal and spatial scale remains an active field of research where coastal modellers are eager to find an overarching strategy to increase the skill of morphodynamic models within the given spatial and temporal frame of reference (e.g. de Vriend *et al.* (1993), Lesser (2009)). Due to the multiple interdependence between the individual processes and the larger temporal scale morphodynamics, this has proven to be quite a challenge (e.g. Lesser (2009)). It is with the aforementioned at heart that a questionnaire is instigated in order to find a comprehensive and collaborative approach for model acquisitions in the scope of medium-term meso-tidal environments by interviewing *applied morphodynamics* experts that have dealt with many (alike) problems. Henceforth, the latter objectives are condensed into a set of interviews in which a general consensus is aimed to be found for the following research question:

- *What is the best modelling strategy to capture the behaviour of meso-scale features on a medium-term temporal scale (i.e. 5 - 10 years)?*

Therefore, particular interest is placed in the *systematic strategy* that (coastal) applied morphologists acquire to develop morphodynamic models in the broad scope of medium- to long-term temporal scales:

- Choice of Modelling Suite: Delft3D-4 or Delft3D-FM
- Grid Composition
- Physical Process Description and Schematisation
- Model Complexity versus Computation Time
- Bed Schematisation & Model Calibration

dr. ir. Victor Chavarrías Borrás

The investigation towards the best practice in medium-term meso-scale morphodynamic modelling started with an analysis towards the differences and similarities in the modelling endeavours throughout the field of *Applied Morphodynamics* - which is concerned with the morphological evolution of coastal and fluvial systems. Therefore, an interview was arranged with dr. ir. Victor Chavarrías Borrás of Deltares - Department *Freshwater Systems (Unit River dynamics and inland water transport)*. As a River engineer and researcher Victor has dealt in his career with the development of many morphodynamic models focused on riverine environments. Thereby, he is part of the software development team which continuously aims to find new codes for widely used software suites as SOBEK and Delft3D(4/FM) amongst others.

The first objective in the interview with Victor was to investigate the similarities and differences in the morphodynamic models composed for river engineering problems in comparison with models that were composed for the Tidal & Estuarine environment. Thereby, it was within the scope of the interview to find lessons-learned from the River *Morphodynamic* Modellers that may be transposed to the Coastal, Estuarine & Tidal Environment.

Physical Process Description

Discussion

It is known that in the River Engineering discipline state-of-the-art (quasi) 3D morphodynamic models prevail with sophisticated 3D-extensions to account for secondary flows, and widely applicable for complex 3D river problems (e.g. de Vriend *et al.* (1993), Lesser (2009)).

Question

Victor, given your experience in river morphodynamic models, what would you say are the similarities (differences) in the transport formulation of sediment transport?

Answer

There are not so many differences in the formulation of the sediment transport for rivers, coasts, estuaries, or tidal basins. As a matter of fact, we are using the same formulations as for the sediment transport in coastal & estuarine models.
The only difference is that in rivers the morphological evolution of the system is defined mainly by the transport of fine to coarse sand fractions. In estuaries and tidal environments there is a larger dependence on the transport and deposition of suspended load. Consequently, it is important to have a transport formulation that accounts for suspended sediment transport explicitly. Hence, in river morphodynamic models, one can apply the Engelund and Hansen (1967)-formulation and MPM-formulation which solves for the *bulk sediment transport*, or for the van Rijn (1984b)-formulation (e.g. van Rijn (1984a)) which accounts for bedload and suspended sediment transport separately. The latter is therefore better suitable in models that investigate the morphodynamic evolution of coastal & estuarine systems. Moreover, in the tidal & estuarine environment the appearance of cohesive materials in the model may be equally as important as the non-cohesive materials such that - in the formulation of the available sediment fractions in the bed - the cohesive fractions should also be specified.

Active Layer Models

Discussion

Furthermore, the efficacy of bed composition generation models and the formulation of the bed in morphodynamic models is assessed in the interview. Hereby, the objective was to find a systematic strategy to compose a multi-grain size graded bed.

For the formulation of a multi-fraction bed, the Hirano (1972) model is often used. Hereby, the bed is decomposed in an active layer and a substrate layer. In the active layer, the volume fractions are considered of each (non)cohesive sediment fraction specified. Thereby, the transport is governed by the formulation of (1) the mass conservation balances for each fraction (Hirano), (2) the unsteady flow equations and (3) the Exner equation. Consequently, changes in the bed level are associated with changes in sediment composition (and vice versa).

Question

What is the right strategy as it comes to the formulation of the bed composition by means of an active layer model (i.e. bed composition generation model)?

Answer

Considering estuarine & tidal environments, it is firstly important to specify the cohesive and non-cohesive sediment fractions at the bed if from prior analysis it follows that cohesive sediment fractions are important for the morphological development of the tidal (estuarine) system.
Then an *active layer* may be defined as the part of the bed that is continuously mixed. This is a physical parameter and is given by means of available data of the bed (i.e. historic bathymetry, stratigraphic data). From this data may be inferred up to which depth, the bed appears to be well-mixed (i.e. graded bed). The *active layer thickness* in the model is specified by the keyword argument *"ThTrLyr"*. It is hereby recommended to relate the active layer thickness to the timescale of interest (i.e. make sure that the model shows an active layer thickness related to the depth of the graded bed that is in reality occupied over the course of the 5-year model duration). On the basis of the proposed bed, the active layer model then accounts for the processes that drive vertical mixing over the bed layers (i.e. active layer towards the deeper substrate layers).

Another indication for the thickness of the active layer could be the variability in the bed elevation over the model duration. Hereby, the maximum bed excursion (as observed in data) might give an idea of the minimum allowable thickness that may be applied in the model for the timeframe of interest. If the characteristic dune height becomes significant within the timeframe of interest (i.e. $h_d \approx 0.04h$ and dunes around $0.4m$ (van Rijn (2007))), the characteristic dune height can also be used as an indicator for

the active layer thickness.

Next, it is important to consider the amount of bed fractions that are specified at the bed - this has a twofold bearing. The first is that the initial conditions for the bed (always) create initial noise with respect to the considered system (i.e. morphological spin). The more sediment fractions are incorporated, the more degrees of freedom the system has to vary in and will only increase the morphological spin up.

On the other hand, the data available for model validation dictates the amount of - and which - fractions considered. For instance, for the Rijn river high-resolution data has been present where up to O(10) grain sizes are specified. The modeller may therefore specify the amount of grain sizes (s)he wishes to incorporate in the model. The only limitation that the modeller may experience is that the D3D model only allows up to 4 (non)cohesive fractions in the model (i.e. 4 cohesive + 4 non-cohesive sediment fractions). Nevertheless, it should be noted that it is more efficient to apply the size fractions that contribute the largest to the morphological adjustment that the modeller aims to predict in the model.

Furthermore, it may be wise to process the bed composition data outside the D3D environment (i.e. pre-processing) before importing the bed composition data in the model. Hereby, the modeller has the opportunity to align the data with the modelling objective. By means of smoothing or refining, the data can be processed such that it fits with the grid schematisation. Also, the bed composition data can be aligned to only specify the considered fractions for which the modeller aims to forecast the (particular) morphological development with.

The initial morphological spin up is hereby an important modelling aspect to consider. The effect of the initial spin up must be minimised in the model simulation in order to obtain acceptable results. Therefore, it is recommended to measure the extent of the spin up in one or two preliminary test runs. To do so, fix the bed in the first runs such that only the bed composition varies (i.e. in time and space). Estimate subsequently the duration of the transient (i.e. the duration until slow development is observed).

Another interesting feature to see is whether the bed composition itself generates spin up [1]. Here, the bed composition is fixed, and the bed level is permitted to vary (in time and space). Next, measure the duration of the transient to see if there is any difference. The largest duration is thereby used to define the time duration for which the model is prohibited to vary the bed level.

Dry cell erosion

Discussion

Moreover, the next objective concerns the implementation and the efficacy of dry cell erosion in river morphodynamic models. The objective here was to research how the dry cell erosion is performing in river models and to synthesis what river modellers are doing to overcome possible related challenges.

In order to model planform changes on a long-term temporal scale the erosion of river banks becomes an important aspect of the model. Even on smaller temporal scale, where rivers form bends in which point bars are created, erosion of the banks play an important role. Both are important if the morphodynamic evolution of rivers is investigated.

Question

How would you normally deal with bank erosion and instability considering the drying and flooding of computational cells?

[1] this has not been tested yet

Answer

River models are quite good in computing the formation of point bars. The reason for this is that the point bars are fully submerged (i.e. the formation of the bars and sediment transport takes place below the water line). Hence, the erosion of the point bar follows from the prevailing hydrodynamic field and sediment transport.
Bank erosion is however quite difficult to model correctly. One of the reasons is that the available data present for model verification of the bank erosion is rather limited. These datasets may entail registration of the bank position every 10 years with a resolution of 500 metres (along the bank). For medium-term models, this dataset is rather limited to accurately verify bank erosion. The question thereby also prevails whether it is important to have the bank erosion well-verified and highly detailed which depends on the case at hand.

Modelling of erosion in river morphodynamic models is a rather challenging endeavour. Even though the point bars are fully submerged the sediment transport calibrations remains a timely and sensitive task. In the channels, for instance, it could occur that the sediment transport field creates too small tangential transport vectors close to the bank such that the bank slope becomes too pronounced. Or it could also occur that channel excursions are overestimated. To reduce this, modellers often (overly) increase the transverse bed slope effects so that locally larger (tangential) sediment transport rates prevail. This should always be avoided. A too-large transverse bed slope factor may have a diffusive influence on the banks which therefore ensure that the banks become smoother (i.e. less pronounced). Consequently, one would obtain "a nice picture without any physical substance".

Modelling Strategy

Discussion

Lastly and in conclusion of this interview, it is in line with the objective of this interview to propose a systematic strategy of modelling morphodynamic features on a timescale of 5 - 10 years in estuarine and tidal environments.

Question

What is in your opinion that best strategy to model meso-scale morphodynamic features on a temporal scale of 5-10 years?

Answer

Modelling morphodynamic evolution constitutes ultimately that the right physical behaviour is observed in the model. This means that the modeller has to take many modelling aspects into account. Start with a simple model encompassing the essential physical process(es) and increase afterwards the complexity of the model layer for layer. Hence, start with:

1. **Modelling Software D3D-(4/FM)**
    - D3D-Flexible Mesh[2] has an updated hydrodynamics code that has the ability to run the model in parallelisation mode (i.e. multiple independent cores).
    - This will greatly reduce the computational time of the model and gives the possibility to run in brute forcing mode within a fraction of the original computation time (i.e. model simulation times decreases from originally O(1 month) to up to +/- O(2 weeks)).
2. **Type of model 2DH/3D**
    - If flow structures are present and important (i.e. salinity, temperature and density structures), consider a 3D model
    - Otherwise, a 2DH model

[2] The morphological code is in beta version.

3. **Bathymetry**
   - **Start with a flat bed**
     (a) Are the locations of the channels correctly predicted?
     (b) Is the transport field correctly predicted?
     (c) Are there any locations or spots that does not align so well (i.e. off spots)?
       – Highlight these locations (i.e. "regions of extra attention")
   - **Add complexity by considering a sloping bed**
     (i.e. in the context of a river, modelling a river course with an arbitrary sloping bed. In the context of a tidal inlet, modelling the inlet with an outer sloping bed and a flat back barrier basin or a back barrier basin with prevailing morphology).
     (a) Are the locations of the channels correctly predicted?
     (b) Is the transport field correctly predicted?
     (c) Is the bank erosion correctly predicted?
     (d) Are the bed shear stresses well represented?

4. **Bank Erosion, Drying and Flooding**
   - **The grid composition is highly important for the drying & flooding procedure**
     (a) To accurately model the slopes within the grid, make sure that the computational grid has high resolution close to the banks and close to the characteristic features such as in tidal environments:
       – The terminal lobe
       – The shoal and chute formations
       – The adjacent shorelines
       – The main ebb channel
   - **Is the banks erosion correctly predicted?**
   - **Are the locations of erosion and deposition correctly predicted?**
   - **How well are the characteristic prevailing features predicted?**

5. **Secondary Flows** (if considered in the model)
   - **How well are the locations of the channel bends predicted?**
   - **How well is the (cross-sectional) shape of the channel bend predicted?**
   - **Are erosion and deposition volumes properly given?**
   - **Is the sediment transport field correctly predicted?**
     (a) Order of magnitude
     (b) The right directions

6. **Bed Composition Model**
   - **How well does the predicted bed composition aligns with the observations?**
   - **Is the sediment transport field correctly predicted?**
     (a) Order of magnitude
     (b) The right directions
   - **Does the predicted bed level change follow the observed morphological trend?**
   - **Is the bed over-coarsening during the model simulation? (i.e. formation of coarser active layer than substrate)**
     (a) Substitute the instantaneous substrate with the initial composition which will restart the composition model only with a stable bed structure (instead of the instable formation).

- **Is the bed composed of consolidated cohesive or rock material (that is unlikely to erode)?**
  (a) Consider the implementation of a non-erodible bed
- **How well is the bed shear stress field calculated at the grid cells?**
- **How well are the total dissipation rates computed?**
  (a) Order of magnitude
  (b) The right directions
- **How well are the turbulent kinetic energy rates computed?**
  (a) Order of magnitude
  (b) The right directions

Closing Remark

Lastly, it should be emphasised that

" Modelling at this temporal scale is in essence an art form" .

Prof. (Assoc.) dr. ir. Mick van der Wegen

The next step in the investigation towards the best practice in Estuarine and Tidal environments was to find a systematic strategy to reduce dissimilarities in the model predictions starting from the implementation of the (initial) bed. Prof. (Assoc.) dr. ir. Mick van der Wegen is with his extensive knowledge and fast experience in Estuarine (morpho)dynamics an expert as it comes to the morphodynamic modelling in Estuarine environments on temporal scales ranging from decades to centuries. It is with the latter at heart that an interview was arranged with Prof. (Assoc.) dr. ir. Mick van der Wegen of IHE Delft - Department *Estuarine Dynamics* & Deltares - Department *Sea & Coastal Systems (Unit Applied Morphodynamics)*. Amongst others his extensive research on the Western Scheldt Estuary, the Netherlands (e.g. van der Wegen (2010), Dam *et al.* (2016)) and the San Pablo Bay, San Francisco (e.g. van der Wegen *et al.* (2011a), van der Wegen *et al.* (2011b)) gives plenty of latitude from which lessons-learned may be transposed and a systematic strategy could be derived to model medium-term meso-scale morphodynamic features.

The first objective in the interview with Mick van der Wegen was to investigate whether or not certain strategies (methods) prevail that are applied by (Estuarine) modellers to tackle challenges concerning apparent dissimilarities in the model predictions with respect to the observed morphological features (i.e. misplaced channel formation, overestimation of scour in main channel, predictability of channel migration).

Amplitude and Structural Dissimilarities in channel prediction

Discussion

Often (Estuarine) morphodynamic models tend to overestimate the scouring effects in the channel formations predicting unrealistically large channel incisions (e.g. Lesser (2009), Baar *et al.* (2019), Murshid and Mariotti (2021)). Thereby, these models tend to underestimate bank erosion such that channel migration is not captured properly in the model predictions.

Question

Mick, what methods can and should (estuarine) modellers apply in your opinion to overcome the aforementioned challenges in the predictability of the channel formation (and migration) in morphodynamic models?

Answer

One of the main model aspects to consider is the bed shear stress field. D3D models enables modellers to specify either a constant bed roughness or a bed roughness map. However, both are limited in the ability to capture the interactions between the time varying roughness height (due to changes in

the active layer composition) and the local flow field. The application of a *good* roughness predictor could thereby increase the model's predictability in a sense that the refined bed shear stress field enables better computation of the local flow field (in and around the channel). And subsequently less likely situations of overestimated channel erosion.
The recent study of Brakenhoff *et al.* (2020) on the Ameland ebb-tidal delta may therefore be a good start. Here, Brakenhoff *et al.* (2020) researched the efficacy of different small-ripple predictors in capturing the time and spatial variation of small-scale wave- and current-related ripples on the bed. Moreover, she came to the conclusion that the application of Soulsby *et al.* (2012)'s formulation for time-varying formation of small-scale ripples (i.e. ripple bedform height) slightly outperforms van Rijn (2007)'s roughness model.

Considering the channel migration, it might be interesting to calibrate the dry cell factor θ_{SD} (i.e. 0-1) which assigns a fraction of the wet cell erosion to the adjacent dry cell. The critical slope parameter is a threshold above which the slope is prohibited to vary, and calibration of this parameter might possibly give better results. However, it should be noted that these changes effect all slopes in the entire model domain.
Also, the formulation of the bed slope effects could be changed in order to observe if better predictions prevail with other formulations. Often the formulation of Ikeda (1982) and Bagnold (1966) are used, but other formulations exist too and are available in the D3D-environment (i.e. Koch and Flokstra (1980), Parker and Andrews (1985)).

Also, it may be wise to give the active layer as minimum a thickness that is related to the characteristic roughness height. Use the (mega)ripple bedform height - which prevails within the temporal scale at which the forcing condition is defined - as indicator for the layer thickness. If for instance, forcing conditions are defined based on the annual sediment transport, make sure that ripple heights are considered which are characteristic within the annual timeframe. Often as an indication, the active layer has a maximum thickness in the order of 0.5 m - order of the largest mega ripples (e.g. van Rijn (2007))- with 1 m as strict upper bound.

Bed Composition Generation Model

Discussion

The bed composition generation model (i.e. active layer model) may be a powerful tool for geomorphologists to cast the composition of the initial bed when the associated data is scarce or unavailable. The efficacy of a bed composition model depends thereby also on the amount (and extent) of the spin up that it generates in relation to the number of fractions considered.

Question

In this regard, can bed composition generation (BCG) models contribute here to better prediction of estuarine and tidal systems? And what is, in your opinion, the best strategy to configure these models?

Answer

Bed composition generation models could be applied to incorporate the temporal and spatial varying bed sorting processes in the well-mixed, graded bed (i.e. active layer). The amount of incorporated sediment fractions in the BCG model depends on the data availability for the region of interest. If the data is available, well-defined and encompasses a wide-grading of sediment size fractions, then the modeller has the freedom to specify more fractions (up to the limits of the D3D environment). The question always remains if there is particular necessary to specify more fractions. The downside of using more fractions is that the time interval necessary to obtain stable solutions (i.e. slowly natural development) increases with the addition of sediment fractions. Consider therefore in the order of 3 (sand/mud) fractions as maximum.
Moreover, the validation of the BCG model is of utmost importance. Make sure that a sufficient dataset is present (if available) of the bed and bed composition for the region of interest. Hence, the distribution

of the specified size fractions in the domain of interest (i.e. stratigraphy) as well as the (initial) bed topography could be calibrated to align with reality in the best way possible.

Question

In the realm of 5-10 years meso-scale modelling, what is in your opinion the largest challenges to tackle as it comes to the design of BCG models?

Answer

In the realm of 5 to 10 years meso-scale modelling, the largest constraint is that the morphological spin up may live within the given timeframe of interest. A way to minimise the amount of spin up is to let the initial bed composition vary until slow natural development is to be observed. This time interval may be subsequently used to restrict the initial bed from varying at the start of the model simulation [3]. Hence, the duration wherein the bed composition is spun up is very important regarding the efficacy of the BCG models.
If the BCG run is stopped to early, the modeller allows for unprecedented morphological spin up to emit into the (final) model simulation which is inconvenient.
Conversely, if the BCG run is proceeded for too long all the natural variability in the morphological development is alleviated from the initial bed. The bed is then overstrained and will not be able to show any desired natural variability in the morphological development. Hence, the time instances should be monitored for which the bed composition shows slow and steady variations.

San Pablo Bay, San Francisco

Discussion

In your research on the morphological development on the San Pablo Bay, San Francisco (i.e. van der Wegen *et al.* (2011a)) you investigated the effect of multiple size fractions (i.e. 3 sand + 3 mud fractions) on the morphological spin up. Hereby, the sand fractions needed approximately 15 - 20 morphological days to stabilise whereas the mud fractions roughly needed 10 - 15 morphological days. It should be note that the determination of these values is based on subjective observations of the research results.

Question

One would reckon that sand fractions take longer to stabilise (i.e. show slower development) than mud fractions. If a time instance must be accounted for in which the morphological spin up is most likely to occur, on which fraction should this interval be tuned at?

Answer

There is no exact strategy or science as it comes to the precise interval of morphological spin up. On the basis on figures describing the variability of the composition, one would infer a time instance until slow development in the broad scope of its objective to reduce the spin up. Take for instance the San Pablo Bay, in the previous study, a spin up of around the 10 - 20 days would fit all in the scope of acceptable durations of morphological spin up and that is irrespective of the individual spin up per size fraction.

Western Scheldt Estuary, the Netherlands

Discussion

In your research on the Western Scheldt estuary (i.e. Dam *et al.* (2016), van der Wegen (2010)), the morphological development was assessed of the estuary which mainly constituted the development and migration of the main channels and the formation of flood embankments within the boundaries of the system (i.e. fixed boundaries). In order to make sure that the channel position and migration was correctly predicted - amongst others - the bed sloping effect where calibrated in the model (e.g. van der Wegen (2010)) and an associated value of $\alpha_{BN} = 10$ was considered. (It should be noted that in recent (to this date) modelling studies of the Western Scheldt $\alpha_{BN} = 100$ are applied).

[3] An investigation into the morphological spin up of the bed composition self has thereby not (yet) been conducted

Question

What is the best factor for the bed sloping effects to consider in meso-scale morphodynamic models of Estuarine environments? And what strategy did you apply to determine the magnitude of which bed sloping effects are accounted for in the model?

Answer

Based on model calibrations, the transverse bed slope factor is chosen. $\alpha_{BN} = 10$ was the value for which the sediment transport close to the embankments showed acceptable values. But this slope parameter is dependent on the system at hand, and therefore no strict guideline prevails for dealing with the calibration of this parameters. Nevertheless, do no use too-large α_{BN} values in your model. An indication for this is when the sediment transport rates and patterns starting to deviate too significantly from reality with increasing slope factor. The slopes in the entire domain has then become overly diffusive.
In Dam *et al.* (2016), the Western Scheldt estuary is run in FINEL2D, which is a diffusive model that has the capabilities to attenuate numerical-induced diffusion. Therefore, larger bed slope effect can be applied before the slopes become overly diffusive. There is as such more freedom to finely tweak the sloping factor.

Final Remarks

Discussion

In conclusion, the last objective of this interview concerns the derivation of a systematic strategy to model morphological features over a period of 5 - 10 years. Therefore, an approach is ought to be found that ensures that the channel formation and migration, but also (flood) embankments and erosion holes are modelled correctly.

Question

What is, in your opinion, the best practice to capture the right morphological behaviour over the course of a model simulation for 5 - 10 years development?

Answer

To make sure that the model predicts the right morphological changes, a broad scope of modelling aspects must be reviewed to do so. Therefore, consider the following aspects:

1. **Bed Composition Generation Model**
   - **Consider no more than 3 fractions (sand/mud). Otherwise the initial morphological spin up may become too large. And note that extra fractions do not necessarily bring better results**
   - **Make sure that a preliminary run is proceeded to measure the duration of the initial spin up**
     (a) Run a preliminary model wherein the bed level changes are restricted, and the bed composition is permitted to vary in time and space
       – too long and the bed is overstrained (i.e. no natural variability)
       – too small and the bed inherit unintended morphological spin up
   - **Validate the bed composition model with well-defined data of the bed and bed composition**
     (a) Is the predicted morphological development in line with the observed morphological development?
     (b) Is the predicted bed composition consistent with the observations?
   - **Stable Stratigraphy (well-posedness of the bed)**
     (a) Regulate the bed if the bed structure becomes ill-posed
     That is, when coarser sediment in the active layer covers a relatively finer substrate

(b) Firstly, inspect the natural (i.e. observed) stratigraphy of the bed on the basis of historic data, and seek for signs that may indicate the origin of the ill-posed problem
  - The appearance of deep embedded coarser layers that are next to deep embedded fine layers
  - Make sure that, for instance, the active layer is not eroded completely in one timestep.
  - Another measure could be to limit the availability of sediment in the active layer
  - The most stringent measure is to stop the calculations and replace the instantaneous substrate (and/or active layer) with the initial conditions

2. **Channel Formation and Migration**

- **Are the erosion and deposition volumes correctly predicted?**
- **Are the locations of channel bends correctly predicted?**
- **Is the sediment transport field correctly represented?**
  (a) Order of magnitude
  (b) The right directions
- **Are the bed shear stresses correctly predicted?**
  (a) Use a roughness predictor that updates the timely and spatially varying bed shear stresses such that it aligns with the timely formation of bedforms and the flow field
  (b) Consider the calibration of the dry cell factor θ_{SD} and the critical slope formulation (i.e. use different slope formulations)
  (c) Consider the calibration of the bed slope factor α_{BN} such that the sediment transport aligns better

3. **Bathymetry**

- **Make sure that the morphological spin up is effectively reduced**
- **Start with flat bed and extent the level of complexity afterwards**
  (a) Be aware not to put too much effort in this (preliminary) study as it tends to become quite consuming
  (b) Use the flat bed to identify *"troublesome locations"* and check in runs with a realistic bathymetry if those locations still prevail.
  (c) From the latter, identify the (remaining) *regions of further improvement* and propose methods to resolve the prevailing challenges.

ir. João Dobrochinski

The investigation towards the best practice in medium-term mesoscale modelling continued further with an analysis on the intricacies of the Coastal and Tidal environment which is characterised by a complex interplay between hydrodynamic processes and morphodynamic development. As a Coastal engineer & Researcher, ir. João Dobrochinski has a wide experience and witted knowledge on the morphodynamic modelling of Coastal and Fluvial systems. He has dealt with the development of numerous models to assess the effects of human interventions on coastal systems in a wide variety of projects. In light of the aforementioned, an interview was arranged with ir. João Dobrochinski of Deltares - Department *Hydraulic Engineering (Unit Harbour, Coastal and Offshore engineering)* with the objective to identify lessons-learned from his wide experience in the latter field of interest. Next, it is aimed to condense these lessons into a (systematic) strategy to capture the morphodynamic behaviour of coastal systems & tidal environments on a temporal scale of 5 - 10 years.

The Case of Ameland Ebb-tidal Delta

Discussion

The first objective is to find a best practice in modelling morphodynamic features on a temporal scale of 5 - 10 years for tidal environments. Hereby, the Ameland ebb-tidal delta is considered (i.e. Elias (2006)). On the foundation of extensive research of Elias (2018), it has been concluded that the benchmark models, that aim to describe the morphodynamic development of the Ameland ebb-tidal delta, show a reasonable qualitative resemblance with the observations (e.g. Bosboom (2019), Bosboom *et al.* (2014), Elias (2018)). The present-day models however prevail that the erosion and deposition volumes are not perfectly reproduced - instead, they are overestimated:

Some of the observed tasks for further improvement

- The westward migration of the main ebb-channel in the inlet gorge shows (slight) inconsistencies with the observations
- The chute formations are observed, yet the volumes do not align with reality
- The (cyclic) shoal attainment to the adjacent downdrift beach is observed, but shows deviations in the shape and amplitude of erosion and deposition volumes (i.e. Bosboom *et al.* (2014), Bosboom (2019))
- The position of the shoals and the shape of (small-)features (e.g. strandhaak, Bornrif Bankje) does not completely align with the observations

Question

João, given such model validation challenges, what would be in your opinion the best strategy to obtain medium-term meso-scale morphological features for which the amplitude and structural (dis)similarity is enhanced (minimised) ?

Answer

First of all, if the model predicts the overall features that are found in the observations, but it seems to be (almost) impossible to calibrate the model correctly such that the patterns and volumes align, perhaps it is wise to go for a 3D simulation. If from the calibrated 3D model, it follows that the patterns are favourably changing with respect to the 2DH model, then that is the solution and the way to go forward. Hereby, a vertical grid size distribution must be specified (i.e. σ-layers).
In the layers where wave-breaking effects and local dissipation are resolved (e.g. near-bed, free surface), try to increase the resolution locally. Hence, it is recommended to create layers near the bed with a relative layer thickness of 3-4% ideally.
Then for the layers distant from the free-surface and the bed, a factor of 1.5 may be considered for the relative layer thickness giving approximately 4.5% - 6%.

At the free surface- especially in the surf zone - apply a finer resolution of 3% - 4% (or 5% at most). Lastly, make sure to add ar least around the 10 - 12 layers.

Overall, coastal morphodynamic models are characterised by their tendency to push sediment towards shore. Hereby, the models create steeper cross-shore profiles such that the waves do not break at the right location and the longshore transport is incorrectly predicted. In a 2DH-model, the f_{sus} and f_{bed} is therefore often reduced to reduce the migration rate of the morphological features. However, while doing so, the beach becomes too erosive (i.e. less sediment supply rates) and the cross-shore profile is shifted towards the bars.

In a 3D-model, start with a f_{sus} and f_{bed} equal to 1 and observe the predicted morphological changes. Furthermore (if necessary), change the latter values on the basis of a model calibration procedure. So, if the morphological features are migrating too rapidly, try reducing f_{sus} and f_{bed}.

Also consider the tuning parameters f_{susw} and f_{bedw} which primarily effect the cross-shore distribution of the sediment. If the cross-shore profiles are improperly predicted, try reducing the f_{susw} and f_{bedw} from 1 to an arbitrary small number (upon calibration). This has an effect on the extent to which wave-related effects are considered in the formulation of the (suspended) sediment transport.

Question

What is in your opinion the best way to ensure that the transport patterns and predicted volume amplitudes (i.e. erosion & deposition volumes) align better?

Answer

One of the aspects of the aforementioned morphodynamic model is that it shows an overestimation of sediment transport in the channels (i.e. channel incisions). This is generally overcome by adding a bed roughness predictor to the model which updates the models' bed shear stress field with the changes in bed roughness (through bedform formations). This works overall well for channels but for shoals, bed roughness predictors do not seem to properly work. Channels are naturally maintained by mixed-graded transport of various sediment fractions ranging from fine to coarse sediment. Shoals are generally characterised by a narrow-sorting distribution which mainly consists of coarse-graded sediment. Hence, a smaller variability of sediment size fractions may be observed at shoals over time and space which dictates in turn the efficacy of the bed roughness predictors at shoals.

In order to make the predicted channel formation and the migration align with the observations, make sure that the sediment transport close to the channel slopes is correctly predicted. The model has the tendency to underestimate the local sediment transport at these locations, so common practice is to increase the transverse bed slope effects with a factor of 10 compared with the default value (i.e $\alpha_{BN} = 1.5$). Hence, consider $\alpha_{BN} = 10 - 15$).
Moreover, it may be wise to include a bed composition generation (BCG) model. Hereby, it would suffice to include 3-4 fractions in the formulation of the BCG model. The sediment size fractions are found from data on the bed and bed composition for the region of interest. Sometimes, it helps to deviate from the observed sediment fractions (found in the dataset) and use coarser material at locations where it is known that the model overpredicts erosion volumes (e.g. channels). Then, in the deepest part of the channels a coarser grain size fraction is implemented which will decrease the local erosive rate of the sediment transport.
To make sure that these coarser grains do not travel through the model domain and immobilise other morphological features consider setting the local active layer thickness to zero (or zero sediment availability).

Morphological Spin Up

Discussion

Often morphodynamic models require at the start of the simulation morphological spin up. At the temporal scale of 5 - 10 years this spin up may have a considerable effect on the model performance.

Question

Considering the aforementioned, what are methods that you would propose to minimise the morphological spin up?

Answer

The effect of the natural imbalance between the physical footprint of the system and the physical footprint of the model is the cause of the so-called "morphological spin up", which rather should have been called "Natural model imbalance". This initial disturbance can be reduced by proposing input conditions that align better with reality. If the input conditions are perfect, and the natural imbalances still prevail then the complexity of the model needs to be increased.
Improving the model input may concern the quality of the bathymetry data that is applied. If the data is not available or scarce, then a bed composition model can be applied to guide the morphological development of the bed towards the observed morphology.
Increasing the complexity of the model concerns an intricate process that involves a wide range of model aspects. That is:

1. **Start with an inspection of the initial condition of the bed**
   - Is the proposed initial bathymetry consistent with the observations of the bed and bed composition?
   - Is the data used for the verification of the bed composition and bathymetry reliable and high-detailed? Or is it scarce and does it provide coarse data on bed level changes and bed composition?
     (a) Use a bed composition generation model to bridge the gap between scarce field data and required model data, and to minimise the associated spin up.
2. **Define trachytopes for the computational domain**
   - Use a bed-roughness predictor
   - Inspect if the shear stresses are correctly defined
3. **Calibration**
   - Calibration of $f_{sus(w)}$ and $f_{bed(w)}$
   - Is the sediment transport field correctly predicted?
4. **Forcing Conditions**
   - Are the physical processes properly represented by the schematised forcing conditions?
     – Schematisation of wind, tide, waves, etc.
     – Is the (variable) *morfac* properly defined?
       * Are there any (significant) errors in the deposition and erosion volumes due to the proposed *morfac(s)*?

Forcing Conditions

Question

Given the Ameland tidal inlet environment, what strategy would you apply to derive a sound schematisation of the local forcing conditions?

Answer

Depending on the scale of the tidal inlet, it may be recommended to apply a time sequence brute forcing method, rather than a schematised forcing condition. If the scale of the inlet is small $\mathcal{O}(100m)$, the inlet may be rather sensitive for individual wave events (i.e. episodic events). Storm events could create for instance the breaching or widening of the inlet, of which the changes are irreversible. The presence of individual wave events in the forcing condition is thereby important. Hence, a sequential brute forcing method would serve the intricacies of the system better, and the necessity to implement the chronology of the wave events may as such be implicitly fulfilled.

When the scale of the inlet is large $\mathcal{O}(10km)$ which is the case for the Ameland ebb-tidal delta, the inlet is sufficiently large to be less sensitive to individual wave events. The basin has more inertia such that the morphological evolution is less dependent on the chronology of the wave conditions. Hence, a force schematisation would be more relevant. With respect to the latter, a MorMerge would be rather suitable to enable swift computations of the bed level changes.

Final Remarks

Discussion

The overarching objective is to find a systematic strategy to model meso-scale medium-term morphological features in Tidal & Estuarine environments.

Question

What would you say is a right strategy to capture such dynamic behaviour?

Answer

The most important aspect to consider is the implemented physics. Make sure that the physics align with reality. That is, always monitor if the physical processes are correctly implemented in the model and the model predictions are in close coherence with the observed morphology. Questions for which an answer should be found throughout the cycle of model conceptualisation & optimisation (i.e. iterative process):

- Make sure that the flow patterns are properly defined
- Make sure that the sediment transport patterns are properly defined in order of magnitude and location
- Make sure that the bed shear stresses are properly predicted in magnitude and at the right location
- Make sure that the energy dissipation is modelled correctly
  - Use for instance a breaker model such as the variable γ-roller model which enables the incorporation of the complex breaking processes in the model

ir. Pieter Koen Tonnon

The investigation towards the best practice in morphodynamic modelling of medium-term meso-scale features is concluded with a final analysis of the modelling intricacies of the Ameland ebb-tidal delta. Therefore, an interview was arranged with ir. Pieter Koen Tonnon. As a senior advisor & researcher in Coastal morphology, ir. Pieter Koen Tonnon has vast experience and extensive knowledge in morphodynamic models for a wide variety of research projects concerning mega-nourishments and coastal system analysis - amongst others the Ameland Ebb-tidal delta. He has also dealt with a numerous amount of morphodynamic model on a wide range of temporal scales. It is with the latter at heart, that an interview was arranged with ir. Pieter Koen Tonnon of Deltares - Department *Sea & Coastal Systems (Unit Applied Morphodynamics - Coastal Morphology)*.

The Case of Ameland Ebb-tidal Delta

Question

Pieter Koen, given the model validation challenges for the Ameland Ebb-tidal Delta model (i.e. page 124), what would in your opinion be the best approach to model meso-scale morphological features on a temporal scale of 5-10 years for the Ameland Ebb-tidal Delta?

Answer

In an recent, extensive study regarding the Ameland ebb-tidal delta - Kustgenese 2.0 - it is found that the one of the main model challenges for the delta is the position of the adjacent shorelines of the Islands Ameland and Terschelling (i.e. Elias and Tonnon (2016)). The position of these shorelines is of utmost importance for the import of sediment to the delta. It is a vital part of the system. Thereby, it is essential that the cross-shore profile does not become too steep, because otherwise the longshore transport will be off-predicted. The importance of the right cross-shore profile is related to the location where wave breaking takes place. As the model has the tendency of producing steeper cross-shore profiles, waves are ought to break further offshore which renders the longshore transport smaller than actually observed. Hence, the cross-shore processes influence the longshore processes.
To make sure that the wave-breaking is correctly represented in the model at the right location along the shoreline, the grid resolution should be locally increased. For instance, if the grid size in the model is usually $\mathcal{O}(50m)$ then reduce the grid size to $\mathcal{O}(25m)$.
In order to ensure that the pace at which the morphological features are migrating is not too fast, the f_{sus} and $f_{bed} = 0.5$. For this value, it is seen that the pace at which the elements in the system migrate is in line with the observations. In order to ensure reasonable predicted cross-shore profiles the f_{susw} and $f_{bedw} = 0.2$.

Coupling of Models

Discussion

It is know that the numerical codes of 1D-line models are better capable of predicting the timely coastline position (i.e. Huisman (2014)).

Question

Do you see any added benefit in coupling the morphodynamic 2DH-model with a 1D-line model (e.g. Unibest, Xbeach) which is known to predict the coastline position more accurately ?

Answer

An option could be to couple a D3D model with a 1D line model. However, it is a very computationally intensive task that is also rather complex and time-consuming. Especially the intermittent communication between the complex D3D model and the line model is a rather critical step for the efficacy of such coupling yet could be quite challenging to implement. Instead, a big step forward may yet to be made if the relevant physical processes contributing to the formation of small-scale features are

incorporated in the morphodynamic model which already predicts the large-scale features. Following from the conclusions of the Kustgenese 2.0 project, it appears that the formation of small-scale features influences the behaviour and formation of the larger-scale features. This should be incorporated in future models.
To do so, one clue lies in the way the forcing is schematised. Perhaps, small-scale processes could be incorporated in the model by capturing wave and tide forcing schematisations that are closer to reality. That is, morphological tide is composed of one specific amplitude wave with one specific period that is processed in a cyclic recurrent manner. By using such a morphological tide we miss out on the morphological development which is caused by the seasonal variation of the free surface elevation. It may be wise to incorporate a spring-neap tidal cycle in the model. This makes also sure that the cross-shore profile is becoming smoother given that the spring-neap wave reaches higher (lower) elevations on the cross-shore profile than the morphological tide. Sand is being displaced with the spring tide up in the profile whereas with neap tide sand is deposited in the lowest section of the profile. A spring-neap cycle ensures that the tide-related water level variation is incorporated in the model.

Moreover, a wave climate must be applied that also (naturally) varies in time. A *wave-averaged* calculation results in *wave-averaged* morphological evolutions. Maybe, the incorporation of seasonal variations in the tide and wave climate would be a step forward. Hereby, the tide and wave climate may be decomposed in schematised forcing conditions for the respective seasons. These wave conditions can also be accelerated with the (variable) factor of *morfac*. Promptly, the schematised morphological tides should be calibrated (in amplitude) such that the predicted currents are consistent with the observed current patterns within the (seasonal) timeframe of interest. Considering the *morfac*, a maximum allowable *morfac* of 100-150 may be applied in the D3D-4 giving its robust and stable cyclic scheme. D3D-FM applies a stable but less robust scheme such that the maximum permissible *morfac* is 30. Nonetheless, it is always recommended to take a conservative value of *morfac* (i.e. < 50) unless otherwise necessary. Notice that there would not be a great need for large *morfac* if seasonal forcing conditions were considered. In the case of seasonal forcing, observe that with a *morfac* of 12 (i.e. 1/2-month spring-neap x **12** $\longrightarrow$ 6 months development) one can compute 10 *summers* and 10 *winters* if the morphological development for over 10 years is requested.

Model Performance

Discussion

The Ameland ebb-tidal delta is a morphological active environment that consists of many features (i.e. channels, chutes, shoals). Prediction of these large-scale features often is accompanied by inevitable location errors. In point-based metrics where the (dis)similarity between model predictions and observations is evaluated on the grid point scale, this can easily introduce *double-penalty effects*. The Brier skill score may therefore be not suitable for model quality assessments of a dynamic environment as the Ameland ebb-tidal delta.

Question

What is, in your opinion, the best method to assess the accuracy of model predictions concerning the Ameland ebb-tidal delta?

Answer

Always, consider that the computations may not align perfectly - deviations will always occur. Therefore, in an attempt to measure the performance of the model predictions, use a *qualitative* measure such as the MKL (Periodically observed coastal position/ *dutch: Momentane kustlijn*). The MKL is a (roughly) quantitative norm indicating the yearly measured shoreline position and sediment volume. Keep an eye on the predicted annual deposition and erosion volumes along the coast and acknowledge the order of magnitude - that is more than sufficient.
An analysis on the performance using the BSS score or alike quantitative measure would be too complex for the region of interest and a rather time-consuming effort.

Model Software D3D(4/FM)

Discussion

Nowadays, morphodynamic models can be designed in both Delft3D4 and Delft3D-FM[4]. Each of the modelling suites have their own particularities and strength. D3D-4 uses a robust and stable scheme which gives more flexibility in morphological accelerated computations, whereas D3D-FM enables the modeller to compute morphological development using parallelised computing and the ability to create composed grid schematisations.

Question

In your opinion, which modelling suite would you choose for the morphodynamic model assessment of the Ameland ebb-tidal delta?

Answer

The advantage of Flexible Mesh (FM) is that it runs on a new code that enables parallelised computations on multiple workers (i.e. individual cores). This will decrease the computation time drastically. Thereby, the Flexible Mesh suite has the ability to integrate various models such as a SWASH model, an aeolian transport model (i.e. AeoLis) or coupling between various projects. Coupling of SWASH could be beneficial for the derivation of the transport field in and around the main ebb-channel to account for wave actions averaged on the wave-group scale. However, such a coupling is highly computational intensive and complex. Also, since the sediment transport should be calibrated to align with the observed transport field the true objective is the calibration procedure of the sediment transport and not necessarily the underlying transport field. It should be noted that the parallelisation of the computation process only works for the *online morphology* simulations. With MorMerge this feature is not (yet) available.

Calibration

Discussion

A critical part for proper estimation of the sediment transport close to the shoreline, banks, and channel slopes is the calibration of the transverse bed slope parameter α_{BN}. Too large, and the slopes become overly diffusive. Too small and the slopes are too steep.

[4] The morphology module is currently in beta version

Question

How would you calibrate the bed slope factors and what is in your opinion a proper value for this parameter?

Answer

To make sure that the adjacent coastline profiles have reasonable cross-shore profiles, the transverse bed slope factor should be set to $\alpha_{BN} = 15 - 20$ with a strict maximum of $\alpha_{BN} = 50$. Lastly, to prevent the occurrence of channel incisions, it might be wise to incorporate bed roughness predictors and a bed composition model.

13 CONCLUSION AND SYNTHESIS OF INTERVIEWS

Modelling morphodynamic evolution constitutes ultimately that the right physical behaviour is observed in the model. This means that the geomorphologist has to account for many modelling decisions. Start with a simple model encompassing the essential physical process(es) and increase afterwards the complexity of the model layer for layer. Hence, start with:

1. **Modelling Software D3D-(4/FM)**

   - D3D-Flexible Mesh[1] has an updated hydrodynamics code that has the ability to run the model in parallelisation[2] mode (i.e. multiple independent workers)
   - This will greatly reduce the computational time of the model and gives the possibility to run in brute forcing mode with model simulation times up to +/- O(2 weeks)
   - D3D-FM also offers the flexibility in grid composition, and has the ability to integrate multiple models (i.e. AeoLis for aeolian transport) and couple multiple projects
   - D3D-4 uses a robust and stable scheme which gives more flexibility in morphodynamic accelerated computations (i.e. large *morfac*)
   - Both modelling suites are capable of predicting the morphodynamic advancements on a 5 - 10 years temporal scale. Hence, irrespective of the choice of suite the modelling results will be equally as *skilled* for both models

2. **Choice of Discretisation (3D/2DH)**

   - The choice of discretisation depends primarily on the importance of flow structures in the model domain
   - This may be the case in areas where strong stratification is observed, and omission of these effect would misestimate the observed behaviour.
   - If flow structures are present and important (i.e. salinity and temperature structures), consider a 3D model
   - Otherwise, a 2DH model

3. **Bathymetry**

   - **Start with a flat bed and extend the level of complexity afterwards**
     (a) Are the locations of the channels correctly predicted?
     (b) Is the transport field correctly predicted?
     (c) Are there any locations or spots that does not align so well (i.e. off spots)?
         – Highlight these locations (i.e. "regions of extra attention")
     (d) Be aware not to put too much effort in this (preliminary) study as it tends to become quite consuming
     (e) Use the flat bed to identify *"troublesome locations"* and check in runs with a realistic bathymetry if those locations still prevail.
   - **Add complexity and consider the real bathymetry**

[1] The morphological code is in beta version.
[2] It should be noted that the parallelised computation feature is only available for "online morphology" - MorMerge is not (yet) available.

(a) Identify the (remaining) *regions of further improvement* and propose methods to resolve the prevailing challenges.
  - Are the locations of the channels correctly predicted?
  - Is the transport field correctly predicted?
  - Is the banks erosion correctly predicted?
  - Are the bed shear stresses well represented?

- **Make sure that the morphological spin up is effectively reduced**

4. **Bed Composition Generation Model**

- **Consider no more than 3 fractions (sand/mud).**
  Otherwise the initial morphological spin up may become too large. And note that extra fractions do not necessarily bring better results
- **Make sure that a preliminary run is proceeded to measure the duration of the initial spin up**
  (a) Run a preliminary model wherein the bed level changes are restricted, and the bed composition is permitted to vary in time and space
    - *too long and the bed is overstrained (i.e. no natural variability)*
    - *too small and the bed inherit unintended morphological spin up*
- **Stable Stratigraphy (well-posedness of the bed)**
  (a) Is the bed composed of consolidated cohesive or rock material (that is unlikely to erode)?
    - Consider the implementation of a non-erodible bed
  (b) **Regulate the bed if the bed structure becomes ill-posed**
  (i.e. that is, when coarser sediment in the active layer covers a relatively finer substrate)
    - Firstly, inspect the natural (i.e. observed) stratigraphy of the bed on the basis of historic data, and seek for signs that may indicate the origin of the ill-posed problem
      * *Notice the locations where deep embedded coarser layers are located next to deep embedded fine layers*
    - **Measure 1:** *Make sure that the active layer is not eroded completely in one timestep.*
    - **Measure 2:** *Another measure could be to limit the availability of sediment in the active layer*
    - **Measure 3:** *The most stringent measure is to stop the calculations and replace the instantaneous substrate (and/or active layer) with the initial conditions*
- **Validate the bed composition model with well-defined data of the bed and bed composition**
  (a) How well does the predicted bed composition aligns with the observations?
  (b) Is the predicted morphological development in line with the observed morphological development?
  (c) Is the sediment transport field correctly predicted?
    - Order of magnitude
    - The right directions
  (d) How well is the bed shear stress field calculated at the grid cells?
  (e) How well are the total dissipation rates computed?
    - Order of magnitude
    - The right directions
  (f) How well are the turbulent kinetic energy rates computed?
    - Order of magnitude
    - The right directions
- **Channel Formation and Migration**

(a) Are the erosion and deposition volumes correctly predicted?
(b) Are the locations of channel bends correctly predicted?
(c) Is the sediment transport field correctly represented?
  - Order of magnitude
  - The right directions
(d) Are the bed shear stresses correctly predicted?
  - Use a roughness predictor that updates the timely and spatially varying bed shear stresses such that it aligns with the timely formation of bedforms and the flow field
  - Consider the calibration of the dry cell factor θ_{SD} and the critical slope formulation (i.e. use different slope formulations)
  - Consider the calibration of the bed slope factor α_{BN} such that the sediment transport aligns better
(e) Sometimes, it helps to use coarser material at locations where erosion volumes are overpredicted.
Specify, a coarser grain size fraction in the deepest part of the channels. To make sure that these coarser grains do not travel through the model domain set the local active layer thickness to zero (or zero sediment availability).

5. **Bank Erosion, Drying and Flooding**

- **The grid composition is highly important for the drying & flooding procedure**
  (a) To accurately model the slopes within the grid, make sure that the computational grid has high resolution close to the banks and close to the characteristic features such as in tidal environments:
    - The terminal lobe
    - The shoal attainment (close to adjacent shorelines)
    - The adjacent shorelines
    - The main ebb channel
- For tidal environments use a $\alpha_{BN} = 5 - 10$ in combination with $\theta_{SD} = 0.3 - 1$ to obtain structural resemblance with observations (if van Rijn (2007)'s formulation is applied)[3]
- In interviews with the morphodynamic experts, an indicative value of $\alpha_{BN} = 10 - 15$ is found to provide good resemblance with observations[4]
- Is the bank erosion correctly predicted?
- Are the locations of erosion and deposition correctly predicted?
- How well are the characteristic prevailing features predicted?

6. **Secondary Flows**

- **How well are the locations of the channel bends predicted?**
- **How well is the (cross-sectional) shape of the channel bend predicted?**
- **Are erosion and deposition volumes properly given?**
- **Is the sediment transport field correctly predicted?**
  (a) Order of magnitude
  (b) The right directions

7. **Calibration of Sediment transport**

[3] It should be noted that the exact value for these perimeters is decided upon calibration and is dependent on the geomorphological setting at hand.
[4] It should be noted that the exact value for these perimeters is decided upon calibration and is dependent on the geomorphological setting at hand.

- Start with a factor of 1 for $f_{sus(w)}$ and $f_{bed(w)}$ and then reduce the parameter, if necessary, based upon further model calibrations
- From the interviews, it is found that the ideal value for the f_{sus} and $f_{bed} = 0.5$
  For this value, it is seen that the pace at which the elements in the system migrate is in line with the observations.
- In order to ensure reasonable predicted cross-shore profiles the f_{susw} and $f_{bedw} = 0.2$
- Validation of Sediment transport
  (a) How well is the (cross-sectional) shape of the channel bend predicted?
  (b) Are erosion and deposition volumes properly given?
  (c) Is the sediment transport field correctly predicted?
    - Order of magnitude
    - The right directions

" Morphodynamic Modelling of Meso-scale Medium-term Features is in essence..."
An Art Form .

Part IV

BEST STRATEGY FOR MEDIUM-TERM MESO-SCALE MORPHODYNAMIC MODEL PREDICTIONS

14 CONCLUSIONS & RECOMMENDATIONS

The overarching aim of this research is to contribute towards a best practice in modelling meso-scale $\mathcal{O}(10km)$, medium-term $\mathcal{O}(5yrs.)$ morphological features in Tidal & Estuarine environments. Therefore, several modelling aspects are discussed throughout the 3 proposed pillars. The first pillar argues the need for numerical models in the geomorphological Engineering discipline on the basis of a brief overview of the historic advances in numerical modelling (Sect.1.2). Next, the foundation of a numerical model has been considered by means of a brief overview of numerical discretisation techniques and their characteristics (Sect.1.3). The representation of the physical processes in present-day morphodynamic models is assessed, and a comparison is proceeded between two models that have been composed by means of two different numerical discretisation techniques (Sects.2.1, 2.2). The second pillar gives an overview of the methods that a geomorphologists may employ to reduce the model input, and methods to accelerate the morphological computations (Ch.6 & Ch.7). The last pillar provides an overview of the methods that could be employed to quantitatively validate model predictions (Ch. 10). Lastly, this research is concluded with a set of interviews wherein esteemed *applied morphodynamics'* experts were asked about their perception on a possible best practice in modelling skilful meso-scale features in the timeframe of reference. This research hints towards an overarching systematic strategy that could be applied by geomorphologists to acquire accurate model predictions for the scale of 5-10 years.

Conclusions

The overarching research objective builds upon the 3 interrelated pillars which aim to answer the following research questions:

"What is the best modelling strategy to capture the behaviour of an ebb-tidal delta on a medium-term temporal" scale (i.e. 5 years) for meso-scale morphological adjustments?

Research Question 1 - Formulation of physical processes

"Which physical processes are accounted for in the morphodynamic model and how are they to be mathematically" described?

In Ch.2, the numerical foundation of two morphodynamic models are discussed: (1) D3D-4 and (2) FINEL3D. The D3D model is a model based on *finite difference*, and divided in a (1) flow module, (2) wave module and (3) morphodynamics module. The *flow* module solves for the unsteady shallow water wave equations eqs.(3), (4), (5) & (6) whereby the hydrostatic pressure assumption is implemented in the vertical momentum equation. This means that the flow solver is in essence hydrostatic. However, a separate non-hydrostatic solver is implemented to correct for significant deviations in the hydrostatic computations. The flow and transport of waterborne constituents is defined by eq.(7) and also governs the suspended sediment transport. Characteristic for D3D models is its robust and stable scheme (i.e. the ADI-method or cyclic scheme) that enables stable solutions up to courant numbers $\sigma < 10$.
The *wave* module is a separate module and accounts for the wave-induced forces and currents. In summary, the processes that the wave module solves for are: (1) *wave forcing due to wave breaking*, (2) *enhanced bed shear stresses due to wave-current interaction*, (3) *wave-induced mass transport due to residual motion*, (4) *Wave-induced currents (i.e. streaming)*, and (4) an *additional dissipation of turbulence-related energy dissipation*. The derivation of these processes is discussed in Sect. 2.1. The morphodynamic module ensure that bed level evolution take place on the basis of the accumulation or erosion of sediment volumes in the computational grid. For the transport of sediment, van Rijn (1993)'s formulation is taken

into consideration given its frequent use in coastal settings. The van Rijn (1993) formulation considers separately the bedload transport and suspended sediment transport by means of eqs.(73),(74). On the basis of a model calibration procedure for transverse and longitudinal bed slope factor α_n & α_s, and the calibration parameters for currents- or wave-effects $f_{sus(w)}$, $f_{bed(w)}$, the sediment transport can be attuned to the geomorphological setting at hand.

FINEL3D is a model based on *finite elements*, and is also divided in (1) a flow part, (2) a morphodynamics part and (3) a energy dissipation part. Furthermore, FINEL3D solves for the three-dimensional (3D) Navier-Stokes equations for non-hydrostatic flows. It should be noted that the 3D-implementation of the sediment transport and morphology is currently not operational in FINEL3D, but it is available in FINEL2D. Hence, in the 2D-setting the depth-averaged flow equations are considered eqs.(110),(111), (112 & (113)). Discretisation of the computational domain in discrete elements by the (Discontinuous) Galerkin method gives the discretised flow state eqs.(117),(118). The Discontinuous Galerkin has an attractive property to stabilise convective-dominated flow and to minimise the artificial diffusion generated at the interfaces between elements. This may be rather beneficial during model calibration as it dampens the diffusivity of the slopes. The sediment transport is, here, described by the Engelund and Hansen (1967)-formulation of bulk sediment transport eq.(120) and bed level evolution is implemented by means of the *Exner equation* eq.(119).

It is emphasised that irrespective of the choice of numerical discretisation technique, the final numerical results are very much the same. Nonetheless, each of the respective methods have attractive properties which may be beneficial in later modelling stages as is noted in Ch.4.

Research Question 2 - Model Methodologies and Schematisation

"Which modelling methodologies exist to accelerate the computations of morphological development in an efficient and accurate manner?"

In Ch.6, the notion of morphological evolution is discussed whereby multiple methods are described that may be applied to accelerate morphological computations. For medium-term meso-scale morphological features, it is important that the instantaneous interaction between morphodynamics and hydrodynamics is captured appropriately in the D3D model. To do so, the morphodynamic module must be engaged in the flow module. Therefore, it is shown in Ch.8 and Ch.9 that *online* morphological evolution techniques are best suitable for the aforementioned objective. It is seen in Ch.6.3 that the MorMerge approach is rather efficient due to its ability to compute morphology parallelised. The Brute Forcing Merged approach is also reviewed in Sect.6.5 and interpreted as a promising evolution scheme that bears the advantages of the (sequential) online method (i.e. incorporation of time series, seasonality, and the chronology of wave events), yet implemented in an efficient *merging* scheme.

Ch.7 outlines the methods that may be employed by geomorphologist to reduce the relevant physical processes into (a set of) schematised forcing conditions. For the tidal residual components, the improved morphological tide is discussed in Sect.7.1. Here, the tidal residual (TR) time series is schematised on the basis of a selection of a particular tidal wave in the TR time series as the morphological tide. To ensure that the actual tidal residual transport is captures, an artificial tidal constituent is cast and implemented in the tide schematisation. Another, promising method for the model assessment of meso-scale features is the astronomic decomposition method as seen in Sect.7.1. Here, the TR time series is decomposed in the relevant tidal constituents which establishes a schematised tide that closely resembles the actual tide-related variation of the free surface.

Also, in Sect.7.3 a method has been outlined the employ a variable *morfac* to efficiently speed up the morphodynamic computations. In the aforementioned, the case is described in which the value of *morfac* should vary with the seasonality of the wave conditions. It is seen that the variable morfac is, in this respect, related to the period of the morphological tide, the season duration per wave condition and the probability of occurrence. Thereby, a strict procedure is reviewed that ensures that

the suspended sediment concentrations do not unrealistically grow during the transition of one state of *morfac* towards another. Moreover, in Ch.9 it is argued that the application of a *Brute Forcing Merge* approach with *seasonal varying wave conditions* and an *astronomical tide decomposition* as schematisation, renders a promising candidate for the model assessment of meso-scale morphological features.

Research Question 3 - Model Accuracy and Efficiency

"Which methods exist to discern the quality of model predictions, and how should geoscientists document this?"

Methods to validate the performance of model predictions based on a quantitative (qualitative) measure for *skill* is discussed in Ch.10. Firstly, the well-known and often applied BSS skill score was introduced in Sect.10.1. It is shown that these (and alike) *point-wise accuracy metrics* penalises models that predict morphological features, albeit misplaced, more than models which did not predict morphological changes (i.e. the reference prediction) (i.e. *double penalty effect*). Inherently, morphologists are, therefore, encouraged to underestimate morphological variability in order to be rewarded with larger skill scores which seems odd in the morphologist's intuitive perception of *skill*. Hence, other metrics to measure the performance of morphodynamic models are reviewed. It should be noted that if the Brier Skill Score is applied as indicator for the model performance, it is highly recommended to accompany such scoring with a full statistical set of quality parameters (i.e. the Murphy and Epstein (1989)-decomposition). Incorporation of such quality parameters gives (coastal) morphologists an overview of the model decisions taken to target a certain *skill* or *performance*. The framework as specified in Table 6 provides a good starting point for such an undertaking.

Sect.10.2, highlights two qualitatively (quantitatively) strong displacement-based error metrics: (1) the field deformation method and (2) the effective transport difference method. Both methods describe the performance of a model prediction by the amount of work necessary to transform the displacement field into the observational field. However, the effective transport difference method is sole mass-conservative such that the *quality measure* has a physical interpretation and is related to the amount of displaced sediment volumes.

Sect.10.3 elaborates on an overarching method to quantify the performance of a model on the basis of its ability to produce skilful predictions on each scale within the prediction field. As seen in Ch.10.3, the scale-selective model validation method provides a strong and robust tool for qualitative (i.e. amplitude & structural similarity) and quantitative (i.e. pattern skill score) assessment of the quality of model predictions. The quality of the model prediction is found by assessment of the quality parameters on a *window-averaged* scale. This method is easy to implement and to apply and can be augmented with other quality metrics considered.

Research Question 4 - Expert Assessment: Strategy towards medium-term meso-scale predictions

In an investigation towards the best practice of modelling morphological developments in tidal and estuarine environments - with characteristic length scales of O(10km) and temporal scales of O(5 years) - the present day modelling procedure is reviewed in order to find strategies that might enhance the production of better solutions in this complex domain of interest. It is with the aforementioned at heart that a questionnaire is instigated in order to find a comprehensive and collaborative approach for model acquisitions in the scope of medium-term meso-tidal environments by interviewing *applied morphodynamics* experts that have dealt with many (alike) problems. Henceforth, the latter objectives are condensed into a set of interviews in which a general consensus is aimed to be found for the following research question:

"What is the best modelling strategy to capture the behaviour of an ebb-tidal delta on a medium-term temporal scale $\mathcal{O}(5yrs.)$ for meso-scale morphological adjustments?"

Based on the assessments, there are several aspects that must be considered to obtain such a systematic strategy.

Choice of Modelling Suite

Firstly, the **choice of modelling suite** shall be considered. Nowadays, morphodynamic models can be designed in both D3D-4 as in D3D-FM. D3D-4 uses hereby a robust and stable scheme which gives more flexibility in morphodynamic accelerated computations (i.e. large *morfac*). Whereas, the D3D-FM enables modellers to execute parallelised computations on multiple workers (i.e. processor cores). Thereby D3D-FM also offers the flexibility in grid composition and has the ability to integrate multiple models (i.e. AeoLis for aeolian transport) and couple multiple projects to the morphodynamic model at hand. It should be noted that the parallelised computation feature is only available for "online morphology" - MorMerge is not (yet) available. Both modelling suites are capable of predicting the morphodynamic advancements on a 5 - 10 years temporal scale. Hence, irrespective of the choice of suite the modelling results will be equally as *skilled* for both models. Lastly, added value was seen in the coupling of a SWASH model (or XBeach) with the morphodynamic D3D. Note that for this coupling it is not dependent on the GUI of the D3D-FM. Such a coupling can also be proceeded in D3D4 but then as an extension (build-in) of the SWASH code in the hydrodynamic module. For Xbeach, a more integrated process is necessary which is dependent on the GUI of D3D-FM (e.g. van Ormondt *et al.* (2020)). Such objectives, if prompted, may have an effect on the choice of modelling suite.

Choice of Discretisation (3D/2DH)

The choice of discretisation depends primarily on the importance of flow structures in the model domain. This may be the case in areas where strong stratification is observed, and omission of these effect would misestimate the observed behaviour.
Thereby, the argument is also been raised in the interviews that while condensing origin 3D (geo)morphic settings in a 2DH model, schematisations are implemented to account for processes that originally are 3D in nature. If 2DH-models are difficult or almost impractical to calibrate and validate, maybe it would suit to derive a 3D-model. While duly noted, the application of 3D models is seen to be overly computational intensive for its purpose in this regard. Contrarily, the objective should be to review & update the 3D-extensions in 2DH models to align better with such processes. Hence, it is argued that a more elaborate implementation of physical processes in the D3D numerical code will address the general challenges of 2DH models in an efficient manner. Areas of further improvement are, yet not limited to:

- A variable breaker model that accounts for both wave asymmetry and wave skewness
- An accurate description for bank avalanching and bank erosion processes
- A more detailed sediment transport formulation such that $f_{sus(w)}$, $f_{bed(w)}$ and α_{BN} does not need to be overly calibrated to account for physical, yet undefined processes
- The calibration *paradox* of the α_{BN} which comprises that the gravitational slope effects can only be attuned to cater a geometrical resemblance, or can be tweaked to provide transport resemblance yet not both (e.g. Baar *et al.* (2019))

Bathymetry and Bed Composition models

The initial bathymetry is the starting topography on which further morphodynamic development is to be derived. An imperfection in the configuration of the initial bed may cause natural system imbalances (i.e. morphological spin up) and have consequences on the predictability of the observed morphological evolution. Therefore, the morphological spin up must be effectively reduced to avoid any unrealistic morphological variability - stemming from the schematisation of the initial bed - from being emitted in the final morphodynamic computations.

A bed composition generation model can be applied if the reference data is scarce. This bed composition model should acquire at most 3 fractions (e.g. sand/mud) to make sure that the initial spin up does not become too large. In the BCG model run, bed level changes should be restricted, and the bed composition may vary during this preliminary run. Observe the time until slow (natural) development prevails - this is an indication for the morphological spin up. If during the model run an ill-posed bed structure prevails, it is important that the model the following is considered:

1. Regulate the bed if the bed structure becomes ill-posed
   That is, when coarser sediment in the active layer covers a relatively finer substrate

2. Firstly, inspect the natural (i.e. observed) stratigraphy of the bed on the basis of historic data, and seek for signs that may indicate the origin of the ill-posed problem

   - The appearance of deep embedded coarser layers that are next to deep embedded fine layers
   - Make sure that, for instance, the active layer is not eroded completely in one timestep.
   - Another measure could be to limit the availability of sediment in the active layer (or substrate)
   - The most stringent measure is to stop the calculations and replace the instantaneous substrate (and/or active layer) with the initial conditions

Channel Incisions (overestimation of erosion)

Moreover, it might be the case that the model overestimates the (local) erosion volumes (e.g. channel incisions). The application of roughness predictors may be rather beneficial as it updates the timely and spatial varying trachytopes. Hence, the transport field is adjusted accordingly. For the choice of bed roughness formulation, it has been found that for the Ameland ebb-tidal delta Soulsby *et al.* (2012)'s formulation gives slightly better results than van Rijn (2007)'s formulation.

Sometimes, it helps to deviate from the observed sediment fractions (found in the dataset) and use coarser material at locations where it is known that the model overpredicts erosion volumes (e.g. channels). Then, in the deepest part of the channels a coarser grain size fraction is implemented which will decrease the local erosive rate of the sediment transport.
To make sure that these coarser grains do not travel through the model domain and immobilise other morphological features consider setting the local active layer thickness to zero (or zero sediment availability).

Drying and Flooding

The drying and flooding of computational cells in a morphodynamic model is an important process. At locations where the erosion of a feature does not entirely take place below the water line (i.e. at the submerged bed), extra parameters are necessary to ensure that the slopes are modelled correctly. This may be relevant at the interface where land and water meet (e.g. dry beach predictions, bank erosion, avalanching).

In the model, dry cell erosion is defined as the fraction of the wet cell erosion that may be designated to the adjacent dry cell. This dry cell erosion is governed by the parameter $\theta_{SD} \in (0-1)$ of which its value is determined on the basis of model calibration. A water level threshold is also implemented such that the model can discern between dry cell and wet cell throughout the morphodynamic computations. Thereby, the calibration of the transverse bed slope factor α_{BN} also dictates the efficacy of the dry cell erosion. It is acknowledge that α_{BN} is dependent on the grid size resolution for small values of α_{BN} (i.e. 10 - 15 for van Rijn (2007)'s formulation). For large values of the bed slope factor ($\alpha_{BN} = \mathcal{O}(100)$ for van Rijn (2007)'s formulation) the transverse bed slope factor is independent on the grid size resolution. Conversely, the danger of applying large values of α_{BN} is that the slopes in the computational domain becomes too diffusive in character (i.e. Baar *et al.* (2019)). Hence, it is advised not to consider too large values for α_{BN}. That is, it is found by Murshid and Mariotti (2021) that for tidal environments

an $\alpha_{BN} = 5 - 10$ in combination with $\theta_{SD} = 0.3 - 1$ is necessary to obtain the best resemblance with observations. In interviews with the morphodynamic experts, an indicative value of $\alpha_{BN} = 10 - 15$ is found to provide good resemblance with observations. Thereby, it is advised to apply a finer grid resolution closer to shore and closer to the tidal inlet. It should be noted that the exact value for these perimeters is decided upon calibration and is dependent on the (geo)morphological setting at hand.

Calibration

From the interviews, it is found that in order to ensure that the pace at which the morphological features are migrating is not too fast, the f_{sus} and $f_{bed} = 0.5$. For this value, it is seen that the pace at which the elements in the system migrate is in line with the observations. In order to ensure reasonable predicted cross-shore profiles the f_{susw} and $f_{bedw} = 0.2$. Overall, the recommendation is to start with a factor of 1 for $f_{sus(w)}$ and $f_{bed(w)}$ and then reduce the parameter, if necessary, based upon further model calibrations.

Forcing Condition

For the Ameland ebb-tidal delta it is found that the formation of small-scale features influences the behaviour and formation of the large-scale features. The efficacy of morphodynamic model concerning the ebb-tidal delta is dependent on the extend towards which the model is capable to produce these small-scale features. The forcing conditions play an important role in this regard. It is advised that in order to capture the small-scale features in the model predictions, forcing schematisations should be applied that are closer to reality. That is, the forcing conditions should account for natural (seasonal) variability in the water level which is alleviated from the present-day models by employing morphological tides with constant cycles. Hence in the interviews, a spring-neap cycle was proposed as boundary condition. Notice, that also a morphological tide based on the decomposition of the relevant astronomical constituents could be an appropriate candidate for the schematised tide. That is because it also comprises the natural variation of the tide-related water level oscillations.

Furthermore, for the wave climate, it was advised to employ wave conditions that are encompassing the seasonal variability of wave-related water level variations (i.e. seasonal wave conditions). To obtain such results, the OPTI method can be applied to reduce the wave climate in a set of wave conditions that cater the same seasonal target sediment transport as the observations.

Depending on the scale of the tidal inlet, it may be recommended to apply a time sequence brute forcing method, rather than a schematised forcing condition. If the scale of the inlet is small $\mathcal{O}(100m)$, the inlet may be rather sensitive for individual wave events (i.e. episodic events). Storm events could create for instance the breaching or widening of the inlet, of which the changes are irreversible. The presence of individual wave events in the forcing condition is thereby important. Hence, a sequential brute forcing method would serve the intricacies of the system better, and the necessity to implement the chronology of the wave events may as such be implicitly fulfilled.

If the scale of the inlet is large $\mathcal{O}(10km)$ which is the case for the Ameland ebb-tidal delta, the inlet is sufficiently large to be less sensitive to individual wave events. The basin has more inertia such that the morphological evolution is less dependent on the chronology of the wave conditions. Hence, a force schematisation would be more relevant. With respect to the latter, a MorMerge would be rather suitable to enable swift computations of the bed level changes. Notice that a convenient combination of the "online morphology" and the "MorMerge" method - the brute forcing merged approach - may also be seen as a suitable candidate for the model since it combines the need for seasonal varying forces and the application of a computational efficient updating scheme.

15 MEDIUM-TERM MESO-SCALE MODELLING OF EBB-TIDAL DELTAS - AN OVERARCHING STRATEGY

The complexity of morphodynamic modelling assessments on a medium-term meso-scale temporal is largely dependent on the coastal setting at hand and the associated dominant physical processes. In the case of a coastal section, the morphodynamic behaviour is particularly defined by the presence of waves, whereas in the case of an estuary the behaviour is governed by river discharges and the strength of the tidal flow. For tidal inlets, the morphodynamic behaviour is primarily governed by the presence of tides and waves, which increases the complexity of the model calibration procedure. In order to show this inherent intricacy, the calibration of morphodynamic models is broadly displayed by zooming in on three different sections of the Dutch Coast - the Delfland Coast, the Western Scheldt Estuary and the Ameland Ebb-Tidal Delta.

15.1 The Delfland Coast

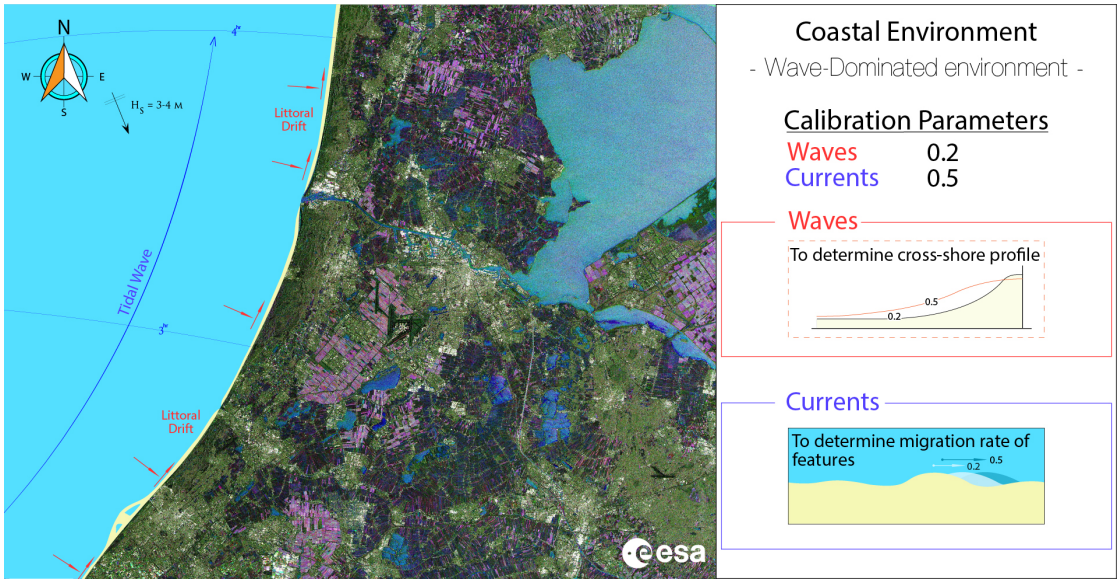

Figure 38: Schematic representation of the coastal environment along the Dutch Coast.

The Delfland coast is part of the southern section of the Dutch coastline and located between Scheveningen and Hoek van Holland. The coastline is in the order of 20 kilometres long and appears to be in a dissipative beach state (i.e. fairly uniform beach with here and there a shore parallel bar formation and gently sloping cross-shore profile) (Wijnberg and Terwindt (1995)). The Defland coast is a wave-dominated environment - The physical processes driving this coastal setting are primarily governed by tides and waves of which waves are dominating the morphodynamic behaviour of the coast.

Wind-generated surface gravity waves - originating from distant storms at the North Sea - reach the Holland Coast from the southwest-northwest direction(Luijendijk (2019)). Under mild conditions, waves of 0.5 - 1.5 metres are coming in under a favourable direction of west-northwest, whereas under normal conditions wave heights up to 3.5 metres are observed with a wave direction from south-southwest. Under storm conditions, waves up to 4.5 metres reach the coast with a dominant wave direction of

west-northwest.

Given the presence of two amphidromic points in the North sea and the confinement of the tidal wave by the coastal boundary, the tide is propagating northwards along the Dutch coastline as a coastally trapped Kelvin wave. The tidal wave is characterised by a spring/neap cycle with an amplitude of 1 - 2 metres (**see Figure** 38). Consequently, the tides are providing here an alongshore current, while the waves enable the redistribution of sediment along coastal sedimentary features and also shape the cross-shore profile.

In order to model the meso-scale morphodynamic behaviour of the Delfland Coast - for instance the Sand Engine - a similar notion could be applied in the calibration procedure of the sediment transport. Here, the van Rijn (2007)-parameterisation is considered given the relative importance of the suspended and bedload transport to the observed morphodynamic response:

- The order of magnitude of the alongshore sediment transport may be targeted by calibration of the underlying alongshore current. This is handled by the current-induced sediment transport and the current-related calibration parameter in the van Rijn (2007)-parameterisation.
- The transport patterns and magnitude of transport could be further assessed by tweaking the effects of the incident waves. The latter is handled by the wave-related sediment transport and the wave-related calibration parameter in the van Rijn (2007)-parameterisation.

Following this modelling strategy, one inherently used the currents as a *pivot point* for *amplitude similarity* whereas the waves are used to create *structural similarity*.

An example of the latter could be found in one of the morphodynamic assessments of the Sand Engine (i.e. Luijendijk (2019)). In this study, the current-related sediment transport was set to 50 % of the total (current-related) transport capacity while the wave-related sediment transport was set to 20 % of the total (wave-related) transport capacity [1] in order to model the migration of the local shoal platform correctly. Figure 38 gives an schematic overview of the aforementioned showing the effect of the calibration parameters to the modelled morphological response.

[1] It should be noted that in the van Rijn (2007)-parameterisation often calibration parameters smaller than 1 are found, since otherwise (i.e. uncalibrated) unrealistically large sediment transport magnitudes are created.

15.2 Western Scheldt Estuary

Figure 39: A schematic overview of the Western Scheldt Estuary, illustrating hereby the important physical processes and the associated modelling strategy.

As discussed in Sec.3.1, The Western Scheldt Estuary is a meso-scale and tide-dominated system located at the southern part of the Dutch coast. The estuary has characteristic length and width scales of 50 kilometres and 5 kilometres respectively, and consists of a series of meandering channels separated by the onset of shoals and bars in between. As a consequence to the boundary confinement, the morphodynamic behaviour of the estuary entails the migration of the main channel alongside the continuous formation and closure of secondary channels.

Furthermore, the physical processes governing this morphodynamic behaviour are the upstream river outflow and the downstream tidal inflow (See Figure 39). Therefore, in order to model the meso-scale morphodynamic behaviour of the estuary solely the current-driven transport should be considered. The importance of wave-related effects may only prevail when the adjacent coastlines are added to the model - otherwise waves may be omitted in such modelling studies. The advantage of the latter is that for the Western Scheldt Estuary and alike environments different sediment transport parameterisations can be applied:

- The Engelund and Hansen (1967)-parameterisation could be applied when the decomposition in the sediment transport into bedload and suspended transport is not necessary (i.e. when the suspended-sediment transport is small compared to the bedload transport). This means that the calibration of the sediment transport is proceeded over the bulk transport instead of over the components individually. For instance, in Dam *et al.* (2016) the Engelund and Hansen (1967)-parameterisation was applied because the river inflow was found to be nil compared to the tidal prism thereby limiting the availability of suspended sediment from upstream.
- The van Rijn (2007)-parameterisation may also be considered in estuarine modelling.

For the latter van Rijn (2007)-parameterisation, the calibration procedure of the model entails the adjustment of the strength of the tidal current in the estuary and its associated transport. By tweaking the current-related calibration parameter, the latter transport can be set to meet the order of magnitude of the observed bed level changes and to ensure that the tidal prism is accurately represented in the model.
Given the relatively larger influence of currents on the observed morphodynamic changes, it is argued by the author that the current-related calibration parameter must be set to 0.5 - 0.8 to predict the morphological development correctly. Figure 39 illustrates the coastal system at hand and the different model calibration options.

15.3 Ameland Ebb-Tidal Delta

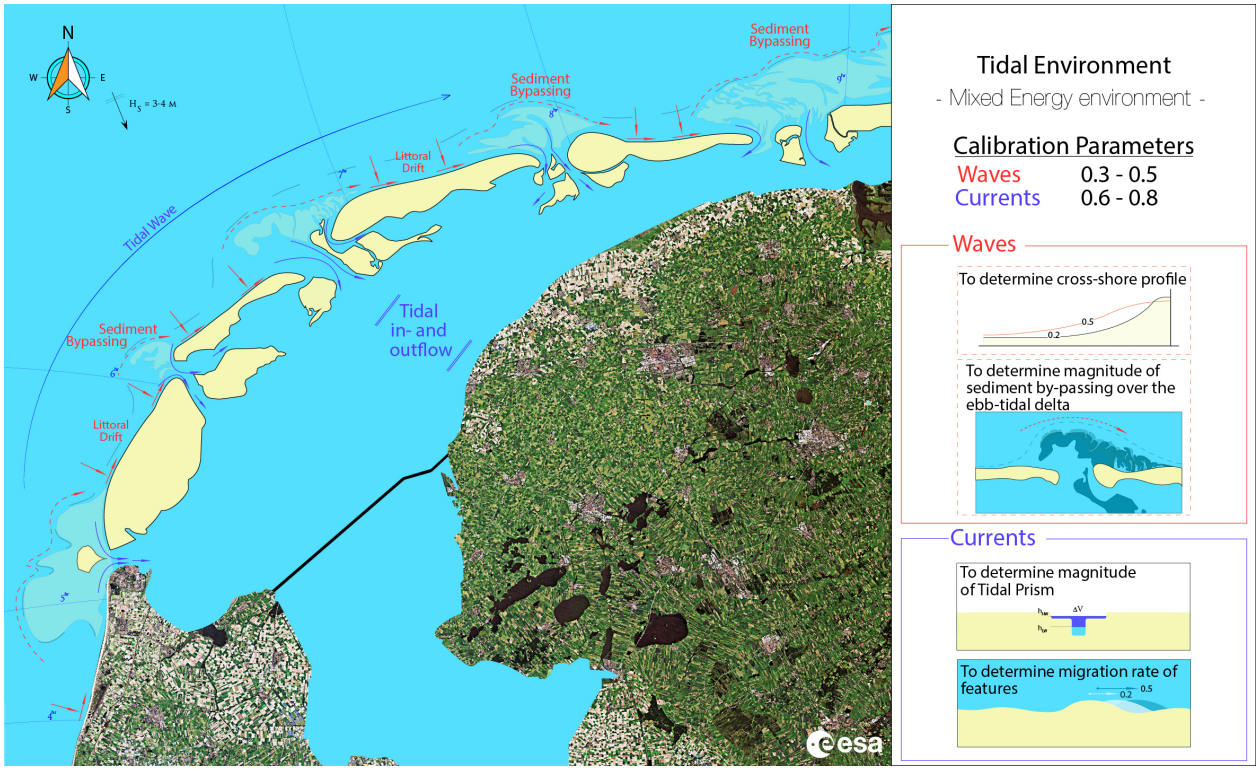

Figure 40: A schematic overview of the tidal inlet environment around the northern section of the Dutch Coast, showing the 5 Dutch Barrier Islands (From left to right, Texel, Vlieland, Terschelling, Ameland and Schiermonnikoog). The important physical processes describing the development of the individual tidal inlets and ebb-tidal deltas are depicted as well as the connection to the sediment transport calibration process.

The Ameland Ebb-Tidal Delta (ETD) is a meso-scale mixed-energy coastal system located at the northern section of the Dutch coastline with length and width scales of 15 kilometres and 10 kilometres respectively. The ETD is characterised by the formation of chutes, migration of the main ebb-channel and cyclic attainment of shoal platforms on the Ameland Coast. Hereby, the physical processes determining this morphodynamic behaviour are governed by the presence of tides and waves which make the calibration of associated morphodynamic models a challenging exercise.

Fortunately, on the foundation of extensive research a benchmark model for the ETD has been constructed (i.e. Elias (2018)), which shows qualitative resemblance of the model results in comparison with the observations. The model is able to capture the formation of chutes over the timescale of interest provided that the bathymetry already inherently shows signs of such an emergence. Furthermore,

the model correctly predicts the main ebb-channel which extends towards the main ebb-shield via the Akkepollegat and shows the eastward migration of the Akkepollegat over the last decades. Also, the formation of the main shoal platform and the attainment of the shoal to the downdrift Ameland coastline is captured.

However, it has been concluded that the model also shows dissimilarities in the order of magnitude of the morphodynamic changes. The model tends to overestimate the erosion and deposition volumes, and underestimates the migration rate of the meso-scale features within the medium-term timescale of interest.

Some of the observed tasks for further improvement

- The westward migration of the main ebb-channel in the inlet gorge shows a slower development than the observations
- The chute formations are observed, yet the amplitude of the morphodynamic change does not align with the measured changes
- The (cyclic) shoal attainment to the adjacent downdrift beach is observed, but shows deviations in the shape and amplitude of erosion and deposition volumes (i.e. Bosboom *et al.* (2014), Bosboom (2019))
- The position of the shoals and the shape of (small-)features (e.g. strandhaak, Bornrif Bankje) does not completely align with the observations

The benchmark model is calibrated using the parameter settings as found in the Delfland Coast setting (i.e. Currents = 0.5 and Waves = 0.2) - see Figure 38. It is hypothesised that the appearance of these amplitude and structural inconsistencies may inherently be ascribed to an imbalance in the representation of the physical processes in the model. Hence, in order to provide a better agreement in the amplitude and structure of the morphodynamic development, the model must be recalibrated. Hereby, the current and wave-driven transport should be enhanced.

As such, it is acknowledge that the morphodynamic response is highly sensitive to changes in the current- and wave-related transport. That is, in the model the wave-related sediment transport governs:

1. the position and slope of the adjacent shoreline,
2. and the magnitude of the sediment by-passing over the terminal lobe of the ETD complex.

Whereas on the other hand, the current-related sediment transport accounts for:

1. the order of magnitude of the sediment transport along the adjacent shoreline (i.e. amplitude similarity)
2. the prediction of the tidal prism in the back barrier basin of the Amelander inlet.

The objective to resolve the latter current-related tasks at ones in a calibration procedure is unfortunately impossible. Targeting the *amplitude similarity* along the adjacent shorelines, will not ensure the right prediction of the tidal prism (i.e. determination of tidal inlet and secondary channels) and vice versa. Hence, the choice is either to model the migration of the shoals and chutes in the ETD complex or to model the formation and onset of the main ebb-channel, however not both. Consequently, an underlying dependency prevails between the calibration parameters for the case of the Ameland ETD. Using the current-related sediment transport as *pivot point* to target the *order of magnitude* so that the transport patterns may be further fine-tuned with the wave-related transport is here unfortunately not an option (i.e. see the Delfland coast approach).

Providing, therefore, the best possible model prediction for the Ameland ETD means that another method must be acquired to obtain comparable morphodynamic behaviour. In light of the aforementioned, a decoupling of the calibration procedure into *two quasi-independent calibration domains* is proposed

as a solution procedure. Hereby, the objective of this method is to decompose the morphological setting of the Ameland ETD into an *outer delta part* and an *tidal inlet part* for which the previous established calibration strategies can be applied. The solution is then found in twofold - the decomposition of the morphological setting leads to two fairly independent regions:

1. **A outer delta domain** which can be resolved by means of a Delfland Coast-type Approach
   - set the order of magnitude with the current-related transport
   - and recreate the observed sediment patterns by fine-tuning the wave-related sediment transport.
2. and **A tidal inlet domain** which is resolved by means of a Western Scheldt-type Approach (and an *additional requirement*)
   - set the strength of the currents and its associated transport to match the order of magnitude of the observed bed level changes by means of the current-related transport
   - *hold the morphology of the back barrier basin steady over the medium-term timescale.*

The latter procedure is depicted in Figure 41 below. The grey area 1^A coincides with the **tidal inlet domain** and the green area 1^B coincides with **outer delta domain**. The solution procedure for the calibration of the Ameland Ebb-Tidal Delta may henceforth be concluded with the following steps.

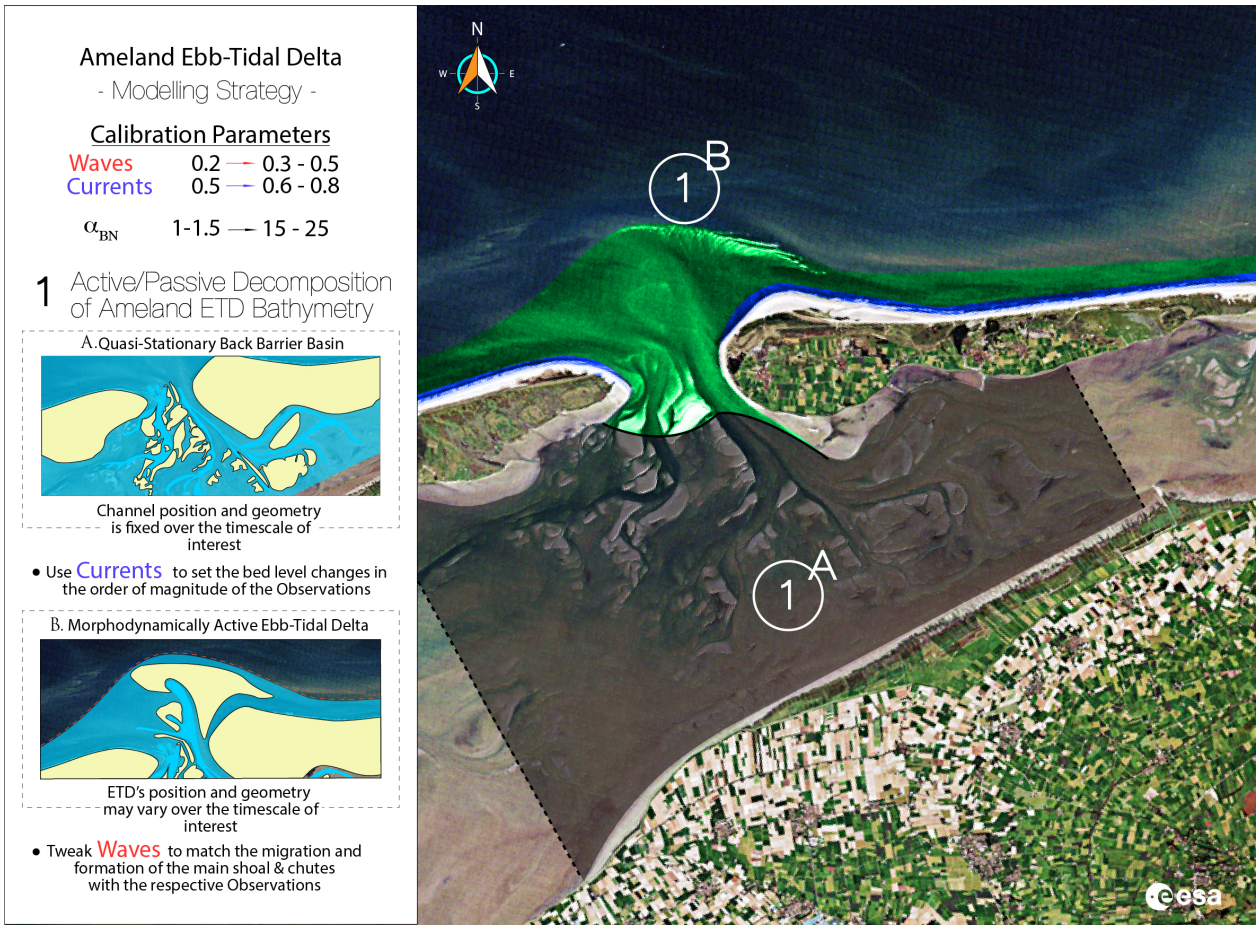

Figure 41: Overview of the model calibration strategy and its underlying steps.

1 - Active/Passive Decomposition of the Ameland ETD

- ***Step 1 - Freeze the back barrier basin and designate an active part of the bathymetry***

  In the first step, the morphological setting is decomposed in a stationary back barrier basin and a morphodynamically active ebb-tidal delta. The back barrier basin may be considered stationary over a medium term timescale since the geometry and position of the secondary channels do not vary significantly over the timescale of interest. The back barrier basin can then be fixed during the morphodynamic computation by limiting the sediment availability over the entire basin so that locally no erosion can occur. Conversely, another option is to change the sediment composition of the back barrier basin to a very coarse (almost non-erodible) composition (i.e. rock or boulder clay). The most stringent option is to model the back barrier basin as non-erodible bed.

- ***Step 2 - Set the Current-related sediment transport***

  Next, the current-related sediment transport is increased to ensure that the order of magnitude of the bed level changes aligns with the observed morphodynamic response. Consequently, the volume of the shoals and chutes in the ebb-tidal delta is set in the right ballpark.

- ***Step 3 - set the Wave-related sediment transport***

  Moreover, the wave-related sediment transport is subsequently increased to make sure that the sediment by-passing over the terminal lobe of the ETD as well as the cross-shore profile of the adjacent coastlines is modelled correctly.

- ***Step 4 - increase the transverse bed slope parameter***

  Present-day morphodynamic models are to a lesser degree able to erode submerged slopes and banks due to the absence of the required mechanism in the transport formulation. It was noted that the westward migration of the main ebb-channel was developing slower in the benchmark model compared with observations. So, to enhance the migration rate of the main ebb-channel, the transverse bed slope parameter (α_{BN}) is increased. This enables the gravitation-induced erosion of the channel slopes which in turn supports the migration of the main ebb-channel.

  Increasing the transverse bed slope parameter, however, has the main disadvantage that all slopes in the modelling domain may become steep. Hence, it may be expected that the adjacent coastal profiles and channel slopes tend to oversteepen. Meanwhile, as a consequence to the increased current-related transport, the main ebb-channel is ought to create channel incisions. To mitigate these effects, two measures are considered (see Figure 42):

  - a maximum slope criterion for the cross-shore profile
  - and and active depth criterion for the main ebb-channel.

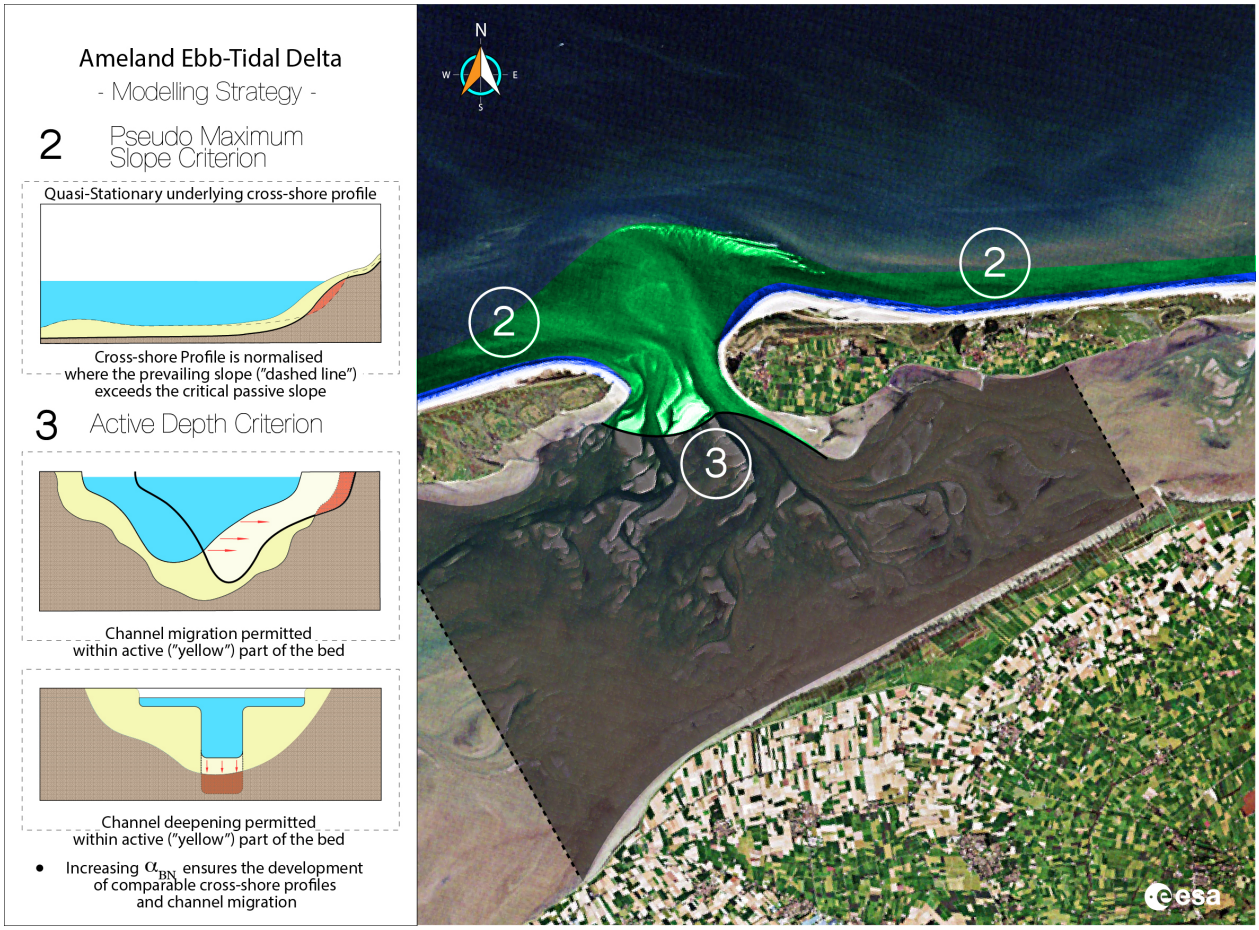

Figure 42: Overview of the proposed mitigation measures to limit the oversteepening of slopes and the local deepening of channels (i.e. channel incisions).

2 - Pseudo Maximum Slope Criterion

In the pseudo maximum slope criterion, the oversteepening process of the adjacent shorelines is counterbalanced employing an underlying normal slope. This normal slope is determined based on the average shoreline profile over the timescale of interest. If during the computations the instantaneous slope retreats beyond the limits of this maximum slope then the cross-shore profile is locally set to the profile of the underlying maximum slope. A pseudo maximum slope could be obtained by specifying a local maximum depth after which the sediment availability is limited and no erosion is longer permitted.

3 - Active Depth Criterion

The active depth criterion prevents the overdeepening of the main ebb-channel. Based on the observed variations of the channel position and depth measurements within the region of the inlet gorge, an active part of the bed may be discerned. In the region of the bed, the channel is allowed to migrate within the timescale of interest. This could be realised by providing a maximum depth beyond which no erosion is longer permitted over the cross-section of the inlet gorge.

16 RECOMMENDATIONS FOR FUTURE RESEARCH

The benchmark model for the Ameland Ebb-Tidal Delta is able to predict morphodynamic development of the meso-scale features in the ebb-tidal complex. The main ebb-shoal, the main-ebb channel and the migration of the Akkepollegat are hereby to a large extent captured in the model prediction. Modelling the chute formation and subsequent migration is however contingent on its pre-existence in the underlying bathymetry.

For recent years the Ameland ebb-tidal model shows better agreement with the observed morphological changes than for the model predictions for the past bathymetries. This is mostly contributed to the development of updated monitoring and measuring techniques, and the enhanced resolution of the measurement data. Overall, the model shows on the larger scale a reasonable resemblance with the observed morphodynamic changes on a medium term temporal scale.

In Chapter 15, a method is also proposed to enhance the agreement in morphological development with the observations using the benchmark model. This model uses schematised boundary and wave conditions. Although suited for a quantitative analysis on the morphodynamic behaviour of the Ameland ETD, in order to predict the migration and development of the ebb-tidal shoals and chutes more accurately, a different modelling approach should be considered. For the Ameland Ebb-Tidal Delta, the interaction between the small-scale processes and the larger scale hydro- & morphodynamics is imperative to obtain a good understanding of the observed morphological behaviour of the ebb-tidal system (e.g. Lenstra *et al.* (2019)). Therefore, a 2DH model using realtime observations of the wave height and water level to enforce the system - a quasi-realtime approach - may be better equipped for such a modelling assessment. The Brute Forcing Merge approach (i.e. Sec. 6.5) is thereby an highly recommended candidate for the modelling procedure.

BIBLIOGRAPHY

A. Luijendijk, *Crossing borders in coastal morphodynamic modelling*, Delft University of Technology, Repository , 13 (2019).

P. Wong, I. Losada, J. Gattuso, J. Hinkel, A. Khattabi, K. McInne, Y. Saito, and A. Sallenger, *Coastal systems and low-lying areas*, Climate Change 2014: Impacts, Adaptation, and Vulnerability. Part A: Global and Sectoral Aspects. Contribution of Working Group II to the Fifth Assessment Report of the Intergovernmental Panel on Climate Change , 361 (2014).

J. Blew, K. Günther, B. Hälterlein, R. Kleefstra, K. Laursen, J. Ludwig, and G. Scheiffarth, *Wadden sea quality status report 2017*, Netherlands Journal of Sea Research **22 Issue 1** (2017), https://qsr.waddensea-worldheritage.org/species.

E. P. Elias, A. J. Van der Spek, S. G. Pearson, and C. Jelmer, *Understanding sediment bypassing processes through analysis of high-frequency observations of ameland inlet, the netherlands*, Marine Geology **415**, 1 (2019).

A. J. Van der Spek and D. J. Beets, *Mid-holocene evolution of a tidal basin in the western netherlands: a model for future changes in the northern netherlands under conditions of accelerated sea-level rise?* Sedimentary Geology **80 Issues 3-4**, 185 (1992).

B. Huisman, *Modelling Coastal Evolution* (Deltares, 2014) pp. 2–3.

G. Lesser, *An approach to medium-term coastal morphological modelling*, Delft University of Technology, Repository , 2 (2009).

J. Syvitski, R. Slingerland, P. Burgess, E. Meiburg, A. B. Murray, P. Wiberg, G. Tucker, and A. Voinov, *Morphodynamic models: An overview,* River, Coastal and Estuarine Morphodynamics, RCEM 2009 , 3 (2010).

M. van der Wegen, *Modeling morphodynamic evolution in alluvial estuaries: UNESCO-IHE PhD Thesis*, Ph.D. thesis, Delft University of Technology (2010).

T. Duong, R. Ranasinghe, A. Luijendijk, D. Walstra, and D. Roelvink, *A qualitative assessment of climate change impacts on the stability of small tidal inlets via schematised numerical modelling*, (2014) 34th International Conference on Coastal Engineering, ICCE 2014 ; Conference date: 15-06-2014 Through 20-06-2014.

G. Lesser, J. Roelvink, J. van Kester, and G. Stelling, *Development and validation of a three-dimensional morphological model*, Coastal Engineering **51**, 883 (2004), coastal Morphodynamic Modeling.

Z. B. Wang, I. Townend, and M. Stive, *Aggregated morphodynamic modelling of tidal inlets and estuaries*, Water Science and Engineering **13**, 1 (2020).

W. Froude, *On the rolling of ships*, Read at the second session of the Institution of Naval Architects,March 1, 1861, the Rev. Canon Moseley, M.A. (1861).

J. T. Thijse, *Scale models in hydraulic engineering*, Nature **161**, 219 (1948).

O. Reynolds, *On certain laws relating to the regime of rivers and estuaries, and on the possibility of experiments on a small scale,* The British Association for the Advancement of Science **57th. Meeting, Manchester** (1887).

J. Allen, *British hydraulic engineering and research*, Delft University of Technology, Repository (1963).

H. Lorentz, H. Wortman, E. van Everdingen, and W. Stoel, *Report of commission lorentz Verslag van de commissie Lorentz (gevolgen afsluiting Zuiderzee op het getij)*, Hydraulic Engineering Reports (1926).

J. Dronkers, *Tidal computations in rivers and coastal waters*, The British Association for the Advancement of Science (1964).

J. Dronkers, J. Schönfeld, and A. Waalewijn, *Tidal computations in shallow water - report on hydrostatic levelling across the westerschelde*, Rijkswaterstaat Communications 01 (1958).

J. van Veen, *Analogie entre marées et courants alternatifs*, La Houille Blanche **5 (Septembre-Octobre 1947)**, 401 (1947).

D. Aten, H. Buijks, P. van Dam, H. van Engen, A. de Klerk, J. Kuys, J. Pilon, H. Toussaint, and W. Wolters, *Tijdschrift voor waterstaatsgeschiedenis 10e jaargang 2001*, Tijdschrift voor Waterstaatsgeschiedenis **10(5-2001)**, 16 (2001).

E. D. De Goede, *Historical overview of 2d and 3d hydrodynamic modelling of shallow water flows in the netherlands*, Ocean Dynamics **70**, 521 (2020).

J. J. Leendertse, *Aspects of a computational model for long-period water-wave propagation*, Research Memoranda (1967).

R. Labeur, *Finite element modelling of transport and non-hydrostatic flow in environmental fluid mechanics*, Delft University of Technology, Repository (2009).

J. Nicholson, I. Broker, J. Roelvink, D. Price, J. Tanguy, and L. Moreno, *Intercomparison of coastal area morphodynamic models*, Coastal Engineering **31**, 97 (1997).

H. de Vriend, J. Zyserman, J. Nicholson, J. Roelvink, P. Péchon, and H. Southgate, *Medium-term 2dh coastal area modelling*, Coastal Engineering **21**, 193 (1993), special Issue Coastal Morphodynamics: Processes and Modelling.

P. Péchon and C. Teisson, *Numerical modelling of bed evolution behind a detached breakwater*, Coastal Engineering 1996 **25th International Conference on Coastal Engineering, September 2-6, 1996; Orlando, Florida, United States**, 2050 (1996).

D. Gessler, B. Hall, M. Spasojevic, F. Holly, H. Pourtaheri, and N. Raphelt, *Application of 3d mobile bed, hydrodynamic model*, Journal of Hydraulic Engineering **125**, 737 (1999).

D. Logan, *First Course in the Finite Element Method*, Vol. 6^{th} Edition (Cengage Learning, Inc, 2017).

C. Grossmann, H. Roos, and M. Stynes, *Numerical Treatment of Partial Differential Equations* (Springer, January 2007, 2007).

G. Dam, M. van der Wegen, R. J. Labeur, and D. Roelvink, *Modeling centuries of estuarine morphodynamics in the western scheldt estuary*, Geophysical Research Letters **43**, 3839 (2016).

J. Roelvink, *Coastal morphodynamic evolution techniques*, Coastal Engineering **53**, 277 (2006).

Deltares, *Deflt3D-FLOW: Simulation of multi-dimensional hydrodynamic flows and transport phenomena, including sediments* (Deltares, 2020).

J. Groeneweg, *Wave-current interactions in a generalized lagrangian mean formulation*, Institutionary Repository (1999).

M. Dingemans, *Water wave propagation over uneven bottoms*, Institutionary Repository (1994).

J. Fredsøe and R. Deigaard, *Mechanics of Coastal Sediment Transport* (WORLD SCIENTIFIC, 1992).

R. Soulsby, L. Hamm, G. Klopman, D. Myrhaug, R. Simons, and G. Thomas, *Wave-current interaction within and outside the bottom boundary layer*, Coastal Engineering **21**, 41 (1993), special Issue Coastal Morphodynamics: Processes and Modelling.

R. Deigaard, J. Fredsøe, and I. B. Hedegaard, *Suspended sediment in the surf zone*, Journal of Waterway, Port, Coastal, and Ocean Engineering **112**, 115 (1986).

D. J. R. Walstra, J. A. Roelvink, and J. Groeneweg, *Calculation of wave-driven currents in a 3d mean flow model*, 27th International Conference on Coastal Engineering (ICCE) July 16-21, 2000; Sydney, Australia , 1050 (2000).

D. Swart, *Offshore sediment transport and equilibrium beach profiles*, Institutionary Repository (1974).

L. van Rijn, *Principles of sediment transport in rivers, estuaries, and coastal seas* (Aqua Publications, Amsterdam, the Netherlands, 1993).

C. Eckart, *Properties of water: Part ii. the equation of state of water and sea water at low temperatures and pressures*, American Journal of Science **256**, 225 (1958).

L. van Rijn, *Sediment transport, part ii: Suspended load transport*, Journal of Hydraulic Engineering **110**, 1613 (1984a).

L. van Rijn, *General view on sand transport by currents and waves: Data analysis and engineering modelling for uniform and graded sand (transpor 2000 and crosmor 2000 models)*, Hydraulic Engineering Reports, Repository (2001).

R. A. Bagnold, *An approach to the sediment transport problem from general physics*, Geological Magazine **104**, 409 (1966).

S. Ikeda, *Incipient motion of sand particles on side slopes*, Journal of the Hydraulic Engineering **108**, 95 (1982).

R. J. Labeur and G. N. Wells, *A galerkin interface stabilisation method for the advection–diffusion and incompressible navier–stokes equations*, Computer Methods in Applied Mechanics and Engineering **196**, 4985 (2007).

F. Engelund and E. Hansen, *A monograph on sediment transport in alluvial streams*, TEKNISKFORLAG Skelbrekgade 4 Copenhagen V, Denmark. (1967).

R. Galappatti and C. Vreugdenhil, *A depth integrated model for suspended sediment transport*, Communications on hydraulics, 1983-07 (1983).

G. Dam, A. Bliek, R. Labeur, S. Ides, and Y. Plancke, *Long term process-based morphological model of the western scheldt estuary*, River, Coastal and Estuarine Morphodynamics: RCEM 2007, Two Volume Set **2**, 1077 (2008).

J. Sutherland, A. Peet, and R. Soulsby, *Evaluating the performance of morphological models*, Coastal Engineering **51**, 917 (2004).

B. Latteux, *Techniques for long-term morphological simulation under tidal action*, Marine Geology **126**, 129 (1995).

J. Bosboom and M. Stive, *Coastal Dynamics I - Lecture Notes CIE4305*, Vol. 0.5 (Delft University of Technology, Delft Academic Press, 2005).

A. P. Luijendijk, R. Ranasinghe, M. A. de Schipper, B. A. Huisman, C. M. Swinkels, D. J. Walstra, and M. J. Stive, *The initial morphological response of the sand engine: A process-based modelling study*, Coastal Engineering **119**, 1 (2017).

J. Stark, *The influence of dredging activities on the morphological development of the Columbia River mouth*, Master's thesis, Delft University of Technology (2012).

J. Bosboom, *Quantifying the quality of coastal morphological predictions*, Ph.D. thesis, Delft University of Technology (2019).

J. Bosboom, A. Reniers, and A. Luijendijk, *On the perception of morphodynamic model skill*, Coastal Engineering **94**, 112 (2014).

K. J. H. Lenstra, S. R. P. M. Pluis, W. Ridderinkhof, G. Ruessink, and M. van der Vegt, *Cyclic channel-shoal dynamics at the ameland inlet: the impact on waves, tides, and sediment transport*, Ocean Dynamics **69**, 409 (2019).

P. Bougeault, *The wgne survey of verification methods for numerical prediction of weather elements and severe weather events*. World Climate Research Programme (WCRP) **13th session of WMO/Commission for Atmospheric Science, january 2003** (2003).

A. H. Murphy, *Skill scores based on the mean square error and their relationships to the correlation coefficient*, Monthly Weather Review **116**, 2417 (01 Dec. 1988).

A. H. Murphy and E. S. Epstein, *Skill scores and correlation coefficients in model verification*, Monthly Weather Review **117**, 572 (01 Mar. 1989).

X. Pennec, P. Cachier, and N. Ayache, *Understanding "the demon's algorithm": 3d non-rigid registration by gradient descent*, in *Medical Image Computing and Computer-Assisted Intervention – MICCAI'99*, edited by C. Taylor and A. Colchester (Springer Berlin Heidelberg, Berlin, Heidelberg, 1999) pp. 597–605.

D. Kroon and C. H. Slump, *Mri modalitiy transformation in demon registration*, in *2009 IEEE International Symposium on Biomedical Imaging: From Nano to Macro* (2009) pp. 963–966.

T. Vercauteren, X. Pennec, A. Perchant, and N. Ayache, *Diffeomorphic demons: Efficient non-parametric image registration*, NeuroImage **45**, S61 (2009), mathematics in Brain Imaging.

J.-P. Thirion, *Image matching as a diffusion process: an analogy with maxwell's demons*, Medical Image Analysis **2**, 243 (1998).

L. van Rijn, *Sediment transport, part i: Bed load transport*, Journal of Hydraulic Engineering **110**, 1431 (1984b).

M. Hirano, *Studies on variation and equilibrium state of a river bed composed of nonuniform material*, Proceedings of the Japan Society of Civil Engineers **1972**, 51 (1972).

L. C. van Rijn, *Unified view of sediment transport by currents and waves. i: Initiation of motion, bed roughness, and bed-load transport*, Journal of Hydraulic Engineering **133**, 649 (2007).

M. van der Wegen, A. Dastgheib, B. Jaffe, and D. Roelvink, *Bed composition generation for morphodynamic modeling: case study of san pablo bay in california, usa*, Ocean Dynamics **61**, 173 (2011a).

M. van der Wegen, B. E. Jaffe, and J. A. Roelvink, *Process-based, morphodynamic hindcast of decadal deposition patterns in san pablo bay, california, 1856–1887*, Journal of Geophysical Research: Earth Surface **116** (2011b), https://doi.org/10.1029/2009JF001614.

A. W. Baar, M. Boechat Albernaz, W. M. van Dijk, and M. G. Kleinhans, *Critical dependence of morphodynamic models of fluvial and tidal systems on empirical downslope sediment transport*, Nature Communications **10**, 4903 (2019).

S. Murshid and G. Mariotti, *Geometry of natural and engineered tidal inlets*, Coastal Engineering **164**, 103 (2021).

L. Brakenhoff, M. Kleinhans, G. Ruessink, and M. van der Vegt, *Spatio-temporal characteristics of small-scale wave–current ripples on the ameland ebb-tidal delta*, Earth Surface Processes and Landforms **45**, 1248 (2020).

R. Soulsby, R. Whitehouse, and K. Marten, *Prediction of time-evolving sand ripples in shelf seas*, Continental Shelf Research **38**, 47 (2012).

F. Koch and C. Flokstra, *Bed level computations for curved alluvial channels*, in *In Proceedings of the XIXth congress of the International Association for Hydraulic Research, 2-7 Feb. 1981, New Delhi, India*, Vol. 2 (Delft Hydraulics Laboratory, 1980) pp. 357–364.

G. Parker and E. D. Andrews, *Sorting of bed load sediment by flow in meander bends*, Water Resources Research **21**, 1361 (1985).

E. Elias, *Morphodynamics of texel inlet, The Netherlands*, Ph.D. thesis, Delft University of Technology (2006).

E. Elias, *Bench-mark morphodynamic model ameland inlet - kustgenese 2.0 (zg-c2)*, Deltares - Kustgenese 2.0 (ZG-C2) **1** (2018).

E. Elias and P. Tonnon, *Beschrijving kennisbasis modellering van zeegaten t.b.v. kustgenese2*, Deltares - Kustgenese 2.0 **1** (2016).

M. van Ormondt, T. R. Nelson, C. J. Hapke, and D. Roelvink, *Morphodynamic modelling of the wilderness breach, fire island, new york. part i: Model set-up and validation*, Coastal Engineering **157**, 103 (2020).

K. M. Wijnberg and J. H. Terwindt, *Extracting decadal morphological behaviour from high-resolution, long-term bathymetric surveys along the holland coast using eigenfunction analysis*, Marine Geology **126**, 301 (1995).


Deltares
Enabling Delta Life
TU Delft